# ASSESSING THE ROLE OF THE TRANSIENT RECEPTOR POTENTIAL A1 CHANNEL IN METHYLMERCURY-INDUCED NEUROTOXICITY

By

Heidi Elise Hannon

#### A DISSERTATION

Submitted to
Michigan State University
in partial fulfillment of the requirements
for the degree of

 $\label{lem:comparative} \begin{tabular}{l} Comparative Medicine and Integrative Biology-Environmental Toxicology-Doctor of Philosophy \\ \end{tabular}$ 

2016

#### ABSTRACT

## ASSESSING THE ROLE OF THE TRANSIENT RECEPTOR POTENTIAL A1 CHANNEL IN METHYLMERCURY-INDUCED NEUROTOXICITY

By

#### Heidi Elise Hannon

Methylmercury (MeHg) is an environmental contaminant which bioaccumulates in aquatic food chains and, because fish and piscivorous animal species are global commodities, the potential for human exposure to this toxicant knows no geographic boundary. Human populations exposed to MeHg, either acutely or chronically, present with severe neurologic symptoms, with the preeminent clinical sign being distal paresthesia. The definitive mechanisms by which this pathologic state arises remains elusive, though the penultimate event is widespread degeneration somatosensory neurons of the dorsal root ganglia (DRG). Moreover, following in vivo MeHg exposure, a significant reduction in the size and number of large-fiber mechanoreceptive afferents is measurable, with a relative sparing of small-fiber nociceptive afferents and motor efferents. MeHg-induced cytotoxicity has been attributed to unregulated increase in intracellular Ca<sup>2+</sup> concentration ([Ca<sup>2+</sup>]<sub>i</sub>); this perturbation arises in kinetically distinct phases, with sources of Ca<sup>2+</sup> including efflux from intracellular storage organelles, and influx through Ca<sup>2+</sup>-permeable ion channels. The transient receptor potential (TRP) family of ion channels has been implicated as potential targets for MeHg due to their Ca<sup>2+</sup> permeability, high expression in DRG neurons, and polymodal means of activation. The objective of this study was to determine whether the ankyrin 1 TRP channel isoform (TRPA1) selectively confers MeHg sensitivity on large-fiber DRG, and to characterize the contribution of TRPA1 to MeHg-induced [Ca<sup>2+</sup>]<sub>i</sub> dysregulation; TRPA1 was selected as a putative target for its role as a mechanoreceptor and potential for activation via cysteine-reactive compounds. Recombinant TRPA1, when

acutely exposed to MeHg *in vitro*, contributed to MeHg-induced [Ca<sup>2+</sup>]<sub>i</sub> dysregulation and cell death in an extracellular Ca<sup>2+</sup> (Ca<sup>2+</sup><sub>e</sub>)-dependent manner. MeHg-induced [Ca<sup>2+</sup>]<sub>i</sub> elevations and neurotoxicity was also Ca<sup>2+</sup><sub>e</sub>-dependent in acute dissociations of primary DRG, however the definitive contribution of TRPA1 as a mediator of Ca<sup>2+</sup> influx could not be confirmed. Rather, whole-cell current recordings of large-fiber DRG revealed Na<sup>+</sup> as the primary charge carrier in agonist-induced activation of TRPA1, and the onset of [Ca<sup>2+</sup>]<sub>i</sub> disruption was dependent upon extracellular Na<sup>+</sup>. This work contributes to our understanding of the actions of MeHg on TRP channels and implicates a role for other cations in mediating MeHg-induced [Ca<sup>2+</sup>]<sub>i</sub> dysregulation.

Copyright by HEIDI ELISE HANNON 2016 to Mom, Dad, Char, Kevin, and the girls for their encouragement, strength, and unending love

#### **ACKNOWLEDGEMENTS**

Thank you to my mentor, Dr. William D. Atchison, for his continued support and patience; members of my guidance committee, Drs. Susan M. Barman, Patricia E. Ganey, Michael T. Flink, and Yukun Yuan, for their consideration of my experiments, thoughtful suggestions, and time; Drs. Vilma Yuzbasiyan-Gurkan, and Robert Roth of the Comparative Medicine and Integrative Biology program and Institute for Integrative Toxicology, respectively, for providing me the opportunity to pursue my interests and present my work. Dr. Peter J.R. Cobbett for his open door and willingness to help me troubleshoot; Dr. Colleen C. Hegg for access to her lab and osmometer, without which my electrophysiology experiments would have been markedly more frustrating.

I am grateful to have had the opportunity to build lasting, professional relationships with the staff and students of the Atchison lab, many of whom contributed to my dissertation research in immeasurable ways. Thank you, again, to Dr. Yukun Yuan for teaching me every aspect of patch-clamp electrophysiology, from the logistics of setting up a rig, technical skills, and conceptual aspects of experimental design. Thank you to Dr. Ravindra K. Hajela for, quite simply, everything—the lab would be lost without your omniscience; Dr. Sara M. Ciotti and Dawn Autio for their tutelage in standard operating procedures and general guidance when I first joined the lab; Alexandra Colón-Rodriguez for her help in establishing an animal colony for my studies in primary neurons, and sharing her knowledge on animal husbandry and primary cell culture; Mónica Ríos-Cabanillas, Chelsea Giese, Kia Z. Pérez-Vale, Shadae Sutherland, Ivelisse Cruz-Torres, and Erin Formiller, the six undergraduate researchers I have had the pleasure of mentoring, for their technical assistance and contributions to my doctoral research project.

#### **PREFACE**

A portion of the introduction has been submitted for publication as part of a review article; sections included in this dissertation are those which I authored. Additionally, some of the data contained in this dissertation have been prepared for submission for publication with contributions from Dr. Erica M. Sparkenbaugh and Mónica Ríos-Cabanillas. Erica is recognized for her contribution to the experimental design, collection of preliminary data, and assistance with manuscript revisions; Mónica Ríos-Cabanillas is recognized for her technical assistance and help with manuscript preparation:

Colón-Rodríguez A., **Hannon H.E.**, and Atchison W.D. (2015) Effects of methylmercury on spinal cord afferents and efferents—a review. *Neurotoxicology*. Submitted.

**Hannon H.E.**, Ríos-Cabanillas M., Sparkenbaugh E.M., and Atchison W.D. (2015) Comparative contribution of recombinant voltage-gated Ca<sup>2+</sup> channels to methylmercury-induced Ca<sup>2+</sup> dysregulation and cytotoxicity in human embryonic kidney cells. *J Pharmacol Exp Ther*. In progress.

## TABLE OF CONTENTS

| LIST OF TABLES   | хi  |
|--|-----|
| LIST OF FIGURES  | xii |
| KEY TO ABBREVIATIONS   | XV  |
| CHAPTER ONE: INTRODUCTION  | 1   |
| 1.1. Background  | 2   |
| 1.1.1. Mercury species: sources and potential for human exposure                               | 2   |
| 1.1.2. A historical perspective on methylmercury poisoning in humans                           | 5   |
| 1.1.3. Effects of methylmercury on calcium homeostasis   | 6   |
| 1.1.4. Structure and biodiversity of voltage-gated calcium channels                            | 9   |
| 1.1.5. Actions of mercurials on neurotransmitter release and voltage-gated                     |     |
| calcium channels   | 12  |
| 1.1.6. The somatosensory system and methylmercury neurotoxicity                                | 16  |
| 1.1.7. The transient receptor potential channel superfamily                                    | 26  |
| 1.1.8. Actions of mercurials on transient receptor potential channels                          | 29  |
| 1.2. Research objective and rationale  | 31  |
| 1.2.1. Hypothesis  | 31  |
| 1.2.2. Aims  | 33  |
| 1.3. Model systems   | 34  |
| 1.3.1. Heterologous expression in human embryonic kidney cells                                 | 34  |
| 1.3.2. Primary culture of murine dorsal root ganglia neurons                                   | 35  |
| 1.4. Techniques  | 37  |
| 1.4.1. Ratiometric calcium imaging   | 37  |
| 1.4.2. Patch-clamp electrophysiology   | 38  |
| CHAPTER TWO: COMPARATIVE CONTRIBUTION OF RECOMBINANT   |     |
| VOLTAGE-GATED CALCIUM CHANNELS TO METHYLMERCURY-INDUCED  |     |
| CALCIUM DYSREGULATION AND CYTOTOXICITY IN HUMAN EMBRYONIC                                      |     |
| KIDNEY CELLS   | 41  |
| 2.1. Abstract  | 42  |
| 2.2. Introduction  | 44  |
| 2.3. Methods   | 47  |
| 2.3.1. Materials   | 47  |
| 2.3.2. HEK cell culture and transfection   | 48  |
| 2.3.3. Single-cell microfluorimetry  | 49  |
| 2.3.4. Measurement of cell viability   | 50  |
| 2.3.5. Statistics  | 51  |
| 2.4. Results   | 52  |
| 2.4.1. Characteristics of MeHg-induced Ca <sup>2+</sup> <sub>i</sub> dysregulation mediated by |     |
| recombinant transiently-expressed α <sub>1</sub> subunits in HEK cells                         | 52  |

|         | 2.4.2.              | Contribution of Ca <sup>2+</sup> <sub>e</sub> to MeHg-induced Ca <sup>2+</sup> <sub>i</sub> dysregulation in                    |
|---------|---------------------|---|
|         | 2 4 2               | untransfected HEK cells.  |
|         | 2.4.3.              | Effect of the VGCC $\alpha_1$ subunit on the rate of onset of MeHg-induced  |
|         | 2.4.4               | Ca <sup>2+</sup> <sub>i</sub> dysregulation and concomitant cytotoxicity in transfected HEK                                     |
|         | 2.4.4.              | Contribution of endogenously expressed LVA VGCCs on   |
| 2.5     | Diamai              | MeHg-induced Ca <sup>2+</sup> i dysregulation and cell viability  |
| 2.3.    | Discussi            | .011  |
| CH A DT | ЕР ТИРІ             | EE: ASSESSING THE SENSITIVITY OF RECOMBINANT  |
|         |                     | CEPTOR POTENTIAL ANKYRIN 1 CHANNELS TO THE  |
|         |                     | FECTS OF METHTHYLMERCURY  |
|         |                     | LC13 OF WILTHTH EWILKCOKT   |
|         |                     | tion  |
|         |                     | S   |
| 3.3.    |                     | Materials   |
|         |                     | HEK cell culture and transfection.  |
|         |                     |   |
|         | 3.3.3.<br>3.3.4.    | Immunocytochemistry   |
|         |                     | · · · · · · · · · · · · · · · · · · ·   |
|         |                     | Measurement of cell viability Statistics  |
| 2.4     |                     |   |
| 3.4.    |                     | Characteristics & M. II. in 1-1 Co. 2+ 1-1-1-1 (1.4-11)   |
|         | 3.4.1               | Characteristics of MeHg-induced Ca <sup>2+</sup> <sub>i</sub> dysregulation mediated by recombinant TRPA1 channels in HEK cells |
|         | 3 1 2               | Role of Ca <sup>2+</sup> <sub>e</sub> in MeHg-induced Ca <sup>2+</sup> <sub>i</sub> elevations in TRPA1-HEK                     |
|         | 3.4.3.              | <u> </u>  |
|         | J. <del>4</del> .J. | channels to MeHg-induced Ca <sup>2+</sup> <sub>i</sub> dysregulation  |
|         | 3 1 1               | Characterization of phase 0 in AITC-sensitive TRPA1-HEK   |
|         | 3.4.4.              |   |
|         | 3.4.3.              | $\mathcal{E}$   |
| 2.5     | D:                  | MeHg exposure   |
| 3.3.    | Discussi            | ion   |
| CHADT   | ED EOLII            | R: TRANSIENT RECEPTOR POTENTIAL ANKYRIN 1 CHANNEL   |
|         |                     | E MEDIATOR OF METHYLMERCURY-INDUCED CALCIUM   |
|         |                     | ON AND CYTOTOXICITY IN JUVENILE MOUSE DORSAL ROOT   |
|         |                     | RONS  |
|         |                     |   |
|         |                     | #ion  |
| 4.2.    |                     | tion  |
| 4.3.    |                     | S   |
|         |                     | Materials   |
|         | 4.3.2.              | Animals   |
|         | 4.3.3.              | Isolation of primary dorsal root ganglia  |
|         | 4.3.4.              | Single-cell microfluorimetry  |
|         | 4.3.5.              | Measurement of cell viability   |
|         |                     | Double-fluorescence immunocytochemistry   |
|         | 437                 | Whole-cell voltage-clamp  |

|        | 4.3.8.   | Statistics  |
|--------|----------|---|
| 4.4.   | Results. |   |
|        |          | Assessing the viability of DRG following acute in vitro MeHg  |
|        | 4.4.2    | exposure  |
|        | 4.4.2.   | Distribution of TRPA1 in heterogeneous populations of acutely dissociated DRG   |
|        | 4.4.3.   | Contribution of Ca <sup>2+</sup> <sub>e</sub> and TRPA1 to MeHg-induced Ca <sup>2+</sup> <sub>i</sub>                         |
|        |          | dysregulation in DRG.   |
|        | 4.4.4.   | Involvement of Na <sup>+</sup> <sub>e</sub> in MeHg-induced elevation of Ca <sup>2+</sup> <sub>i</sub> in AITC-sensitive DRG. |
| 4.5.   | Discussi | on  |
| СНАРТ  | ER EIVE  | : SUMMARY AND CONCLUSIONS   |
|        |          | ry of experiments   |
| J.1.   |          | Differential VGCC expression alone does not confer unique   |
|        | 512      | sensitivity to MeHg  TRPA1 rapidly contributes to [Ca <sup>2+</sup> ] <sub>i</sub> dysregulation at sub-µM                    |
|        | J.1.2.   | MeHg  |
|        | 5.1.3.   | Na <sup>+</sup> <sub>e</sub> influx contributes to phase 2 Ca <sup>2+</sup> <sub>i</sub> disruption in AITC-                  |
|        |          | sensitive DRG   |
| 5.2.   | Propose  | d mechanism of TRPA1-mediated MeHg neurotoxicity  |
| 5.3.   | Conclud  | ing remarks   |
| APPEN. | DIV      |   |
| AFFEN. | DIA      |   |
| REFERI | ENCES    |   |

## LIST OF TABLES

| Table 1.1. | Classification of VGCC subtypes by pharmacologic and electrical properties                  | 10  |
|------------|---|-----|
| Table 1.2. | Properties of somatosensory neurons   | 21  |
| Table A.1. | Classification of DRG subtypes by C <sub>m</sub> and characteristics of whole-cell current. | 163 |

## LIST OF FIGURES

| Figure 1.1. | Subunit composition of VGCCs   | 11 |
|-------------|--|----|
| Figure 1.2. | The human dermatome: divisions of the spinal cord  | 17 |
| Figure 1.3. | Organization of spinal nerves at the spinal cord   | 19 |
| Figure 1.4. | Schematic of TRPA1 channel structure   | 28 |
| Figure 1.5. | Hypothesized role of TRPA1 in mediating MeHg neurotoxicity   | 32 |
| Figure 2.1. | HEK cells exposed to MeHg display a multiphasic elevation in Ca <sup>2+</sup> <sub>i</sub> that is independent of VGCC expression and Ca <sup>2+</sup> <sub>e</sub>  | 53 |
| Figure 2.2. | Comparative effects of Ca <sup>2+</sup> <sub>e</sub> on times-to-onset of MeHg-induced Ca <sup>2+</sup> <sub>i</sub> elevations in untransfected HEK   | 56 |
| Figure 2.3. | Application of MeHg alters the times-to-onset of phase 1 and 2 Ca <sup>2+</sup> <sub>i</sub> elevations in VGCC-HEK in both a concentration- and VGCC subtype-dependent manner.                            | 58 |
| Figure 2.4. | Changes in viability of VGCC-HEK are VGCC subtype-dependent at an early timepoint following acute <i>in vitro</i> MeHg exposure  | 60 |
| Figure 2.5. | The multiphasic rise of Ca <sup>2+</sup> <sub>i</sub> in untransfected HEK cells induced by MeHg is not apparently dependent upon endogenous T-type VGCCs  | 62 |
| Figure 2.6. | Mibefradil has contrasting effects on the times-to-onset of MeHg-induced Ca <sup>2+</sup> <sub>i</sub> elevations in untransfected HEK   | 63 |
| Figure 2.7. | Mibefradil improves viability of untransfected HEK at both early and late timepoints following acute <i>in vitro</i> MeHg exposure   | 64 |
| Figure 2.8. | Mibefradil pretreatment produces contrasting effects on the times-to-onset of MeHg-induced Ca <sup>2+</sup> <sub>i</sub> elevations in untransfected HEK, despite removal of Ca <sup>2+</sup> <sub>e</sub> | 66 |
| Figure 2.9. | Mibefradil has little effect on improving viability of untransfected HEK following acute <i>in vitro</i> MeHg exposure under Ca <sup>2+</sup> <sub>e</sub> -free conditions                                | 67 |
| Figure 3.1. | Representative micrographs depicting endogenous and heterologous expression of TRPA1 in HEK cells  | 85 |

| Figure 3.2.  | MeHg induces a multiphasic Ca <sup>2+</sup> <sub>i</sub> elevation in TRPA1-HEK  | 86 |  |  |  |
|--------------|--|----|--|--|--|
| Figure 3.3.  | TRPA1 expression hastens the time-to-onset of phase 2 at sub-µM MeHg concentrations  |    |  |  |  |
| Figure 3.4.  | Removal of Ca <sup>2+</sup> <sub>e</sub> slows the time-to-onset of phase 2 in TRPA1-HEK   | 89 |  |  |  |
| Figure 3.5.  | In the absence of Ca <sup>2+</sup> <sub>e</sub> , TRPA1 expression hastens the times-to-onset of phases 1 and 2 at sub-µM MeHg                 |    |  |  |  |
| Figure 3.6.  | AITC-induced Ca <sup>2+</sup> <sub>i</sub> elevation in TRPA1-HEK is blocked by pretreatment with 100 nM A-967079                              | 92 |  |  |  |
| Figure 3.7.  | Block of endogenous TRPA1 channels slows the time-to-onset of phase 2 in untransfected HEK   | 93 |  |  |  |
| Figure 3.8.  | Block of recombinant TRPA1 does not alter the time-to-onset of phase 1 nor 2 in TRPA1-HEK  | 94 |  |  |  |
| Figure 3.9.  | Recombinant TRPA1 expression hastens the time-to-onset of phase 2 despite pretreatment with A-967079   |    |  |  |  |
| Figure 3.10. | .10. Representative tracings of TRPA1-HEK illustrating occurrence of phase (coincides with response to AITC                                    |    |  |  |  |
| Figure 3.11. | The presence of phase 0 in AITC-sensitive TRPA1-HEK is inversely related to MeHg concentration and occurrence is unaltered with block of TRPA1 | 98 |  |  |  |
| Figure 3.12. | Pretreatment with A-967079 slows the time-to-onset of phase 0 in TRPA1-HEK exposed to 2 µM MeHg  | 10 |  |  |  |
| Figure 3.13. | TRPA1 expression increases MeHg-mediated cytotoxicity in a Ca <sup>2+</sup> e-dependent manner at 1 h post-exposure                            | 10 |  |  |  |
| Figure 4.1.  | .1. Viability of DRG is reduced within 4 h of <i>in vitro</i> exposure to low μM MeHg  |    |  |  |  |
| Figure 4.2.  | DRG viability is restored 4 h following <i>in vitro</i> exposure to MeHg under Ca <sup>2+</sup> <sub>e</sub> -free conditions                  |    |  |  |  |
| Figure 4.3.  | AITC-induced Ca <sup>2+</sup> <sub>i</sub> elevations in acutely dissociated DRG is blocked by pretreatment with 500 nM A-967079               |    |  |  |  |
| Figure 4.4.  | Block of TRPA1 improves DRG viability 4 h following <i>in vitro</i> MeHg exposure  | 12 |  |  |  |

| Figure 4.5.  | TRPA1 immunoreactivity is detected in Aβ DRG   |     |  |
|--|--|-----|--|
| Figure 4.6.  | DRG exposed to MeHg display a multiphasic elevation in Ca <sup>2+</sup> <sub>i</sub> that is insensitive to block of TRPA1, but dependent upon Ca <sup>2+</sup> <sub>e</sub> |     |  |
| Figure 4.7.  | Removal of Ca <sup>2+</sup> <sub>e</sub> delays time-to-onset of phase 2, while block of TRPA1 has no effect on phase 1 nor phase 2  | 128 |  |
| Figure 4.8.  | $Na^+$ is the primary charge carrier in AITC-induced current in $A\beta$ DRG   | 130 |  |
| Figure 4.9.  | The MeHg-induced multiphasic elevation inCa <sup>2+</sup> <sub>i</sub> in AITC-sensitive DRG is diminished with the reduction of Na <sup>+</sup> <sub>e</sub>                | 131 |  |
| Figure 4.10. Low Na <sup>+</sup> <sub>e</sub> delays the time-to-onset of phase 2 in AITC-sensitive DRG, while AITC-insensitive DRG are unaffected |  | 132 |  |
| Figure 5.1.  | Proposed mechanism of TRPA1-mediated MeHg toxicity in Aβ DRG   | 154 |  |
| Figure 5.2.  | Hypothesized protection from TRPA1-mediated MeHg toxicity in small-fiber DRG   | 155 |  |
| Figure A.1.  | Mean current-voltage relationships are similar among DRG subtypes  | 160 |  |
| Figure A.2.  | Representative current tracings in naïve DRG   | 162 |  |
| Figure A.3.  | Relationship between I <sub>Peak</sub> roughly corresponds with C <sub>m</sub> and, in turn, cell size   | 164 |  |
| Figure A.4.  | Timecourse of reduction in the amplitude of I <sub>Peak</sub> , I <sub>End</sub> , and I <sub>Tail</sub> in all DRG subtypes under standard recording conditions             | 166 |  |
| Figure A.5.  | Whole-cell Ca <sup>2+</sup> currents in Aδ and Aβ DRG are unaffected by exposure to 500 nM MeHg  | 167 |  |
| Figure A.6.  | $I_{Tail}$ duration in both A $\delta$ and A $\beta$ DRG is unaltered with exposure to 500 nM MeH $\alpha$   | 168 |  |

#### **KEY TO ABBREVIATIONS**

AITC allyl isothiocyanate

ANOVA analysis of variance

ATP adenosine 5'-triphosphate

Ba<sup>2+</sup> barium

BAPTA 1,2-Bis(2-aminophenoxy)ethane-N,N,N',N'-tetraacetic acid

tetrakis(acetoxymethyl ester)

BSA bovine serum albumin

<sup>45</sup>Ca<sup>2+</sup> radiolabeled calcium

Ca<sup>2+</sup> calcium

Ca<sup>2+</sup>e extracellular calcium

Ca<sup>2+</sup>i intracellular calcium

[Ca<sup>2+</sup>]<sub>e</sub> extracellular calcium concentration

[Ca<sup>2+</sup>]<sub>i</sub> intracellular calcium concentration

CaCl calcium chloride

Calcein-AM calcein acetoxymethylester

Cd<sup>2+</sup> cadmium

cDNA complementary deoxyribonucleic acid

Choline-HBS choline-containing HEPES-buffered saline

Cl<sup>-</sup> chloride

C<sub>m</sub> membrane capacitance

CMF-HBS calcium- and magnesium-free HEPES-buffered saline

CO<sub>2</sub> carbon dioxide

CsCl cesium chloride

CsOH cesium hydroxide

DAPI 4',6-diamidino-2-phenylindole

DMEM Dulbecco's modified eagle medium

DMSO dimethyl sulfoxide

DNA deoxyribonucleic acid

DRG dorsal root ganglia

 $\frac{dV_m}{dt}$  rate of change of membrane potential

EC<sub>50</sub> half maximal response concentration

EGTA ethylene glycol-bis(2-aminoethylether)-N,N,N',N'-tetraacetic acid

EGTA-HBS EGTA-containing HEPES-buffered saline, calcium omitted

EPP end-plate potential

EthD-1 ethidium homodimer-1

F-12 Ham's F-12 nutrient mixture

F<sub>340</sub> Fura-2 fluorescence signal at 340 nm excitation

F<sub>380</sub> Fura-2 fluorescence signal at 380 nm excitation

F<sub>340/380</sub> Fura-2 fluorescence ratio

FBS fetal bovine serum

FITC fluorescein isothiocyanate

Fura-2 AM Fura-2 acetoxymethylester

g force of gravity

g<sub>i</sub> ionic conductance

GABA gamma-aminobutyric acid

GFP green fluorescent protein

GluR glutamate receptor

h hour

HBS HEPES-buffered saline

HCl hydrochloric acid

HEK human embryonic kidney-293 cells

HEPES (4-(2-hydroxyethyl)-1-piperazineethanesulfonic acid)

HERG Human ether-a-go-go-related gene

Hg<sup>0</sup> elemental mercury

HgCl<sub>2</sub> mercuric chloride

HVA high voltage-activated

I<sub>c</sub> capacitive current

IC<sub>50</sub> half minimal inhibitory concentration

I<sub>Ca</sub> calcium current

I<sub>End</sub> end current; non-inactivating current remaining in final 20 ms of

voltage step

I<sub>i</sub> ionic current

I<sub>m</sub> membrane current

IP<sub>3</sub> inositol 1,4,5-trisphosphate

I<sub>Peak</sub> peak current; maximum current measured within first 20 ms of

voltage step

I<sub>Tail</sub> tail current; current induced upon return to holding potential

K<sup>+</sup> potassium

KCl potassium chloride

kDa kilodalton

kg kilogram

KH<sub>2</sub>PO<sub>4</sub> monopotassium phosphate

kHz kilohertz

LVA low voltage-activated

μg microgram

μL microliter

μM micromolar

M molar

 $M\Omega$  megaohm

MeHg methylmercury

MEPP miniature end-plate potential

mg milligrams

 $Mg^{2+}$  magnesium

MgCl<sub>2</sub> magnesium chloride

MgSO<sub>4</sub> magnesium sulfate

min minute

mL milliliter

mm millimeter

mM millimolar

mOsm milliosmole

mRNA messenger ribonucleic acid

ms millisecond

mV millivolt

nA nanoampere

Na<sup>+</sup> sodium

Na<sup>+</sup>e extracellular sodium

Na<sub>2</sub>ATP adenosine 5'-triphosphate disodium salt

Na<sub>2</sub>HPO<sub>4</sub> disodium phosphate

nAChR nicotinic acetylcholine receptor

NaCl sodium chloride

NaHCO<sub>3</sub> sodium bicarbonate

NF-200 neurofilament of 200 kilodaltons; heavy-chain neurofilament

NGS normal goat serum

Ni<sup>2+</sup> nickel

nm nanometer

nM nanomolar

pA picoampere

PBS phosphate-buffered saline

 $P_{Ca}/P_{Na}$  membrane permeability ratio

pF picofarad

PLC phospholipase C

PKA protein kinase A

PKC protein kinase C

ppm parts per million

pS picosiemen

s second

SEM standard error of the mean

siRNA small interfering ribonucleic acid

TD<sub>50</sub> median toxic dose

TEACl tetraethylammonium chloride

TPEN N,N,N',N'-tetrakis(2-pyridylmethyl)ethane-1,2-diamine

TRP transient receptor potential channel

TRPA1 transient receptor potential ankyrin 1 channel

TRPA1-HEK transient receptor potential ankyrin 1 channel-transfected human

embryonic kidney cells

TRPC transient receptor potential canonical

TRPM transient receptor potential melastatin

TRPV transient receptor potential vanilloid

TTX tetrodotoxin

TTX-R tetrodotoxin-resistant

TTX-S tetrodotoxin-sensitive

U enzyme unit

v/v volume per volume

VGCC voltage-gated calcium channel

VGCC-HEK voltage-gated calcium channel-transfected human embryonic

kidney cells

VGSC voltage-gated sodium channel

V<sub>h</sub> holding potential

V<sub>i</sub> ionic reversal potential

V<sub>m</sub> membrane potential

w/v weight per volume

Zn<sup>2+</sup> zinc

## CHAPTER ONE

## INTRODUCTION

#### 1.1. Background

#### 1.1.1. Mercury species: sources and potential for human exposure

In its elemental form, mercury (Hg<sup>0</sup>) exists as a silver-colored liquid at ambient temperatures. The chemical symbol for mercury, Hg, was adopted from the Latin and Greek translations of "liquid silver", hydraygyrum and hydragyros, respectively. Liquid Hg<sup>0</sup> is highly volatile and readily releases a monoatomic gas, Hg<sup>0</sup> vapor. Practical applications of Hg<sup>0</sup> are numerous due to unique physical properties of the metal, which include an exceptional ability to conduct electricity and its reflective surface. In the industrial era, liquid and vaporous Hg<sup>0</sup> could be found in barometers and thermometers, catalytic electrodes for the production of chemicals, electrical switches in automobiles, and incandescent lightbulbs. The propensity for liquid Hg<sup>0</sup> to amalgamate with other metals, namely silver and gold, also led to its use in mining to effectively separate the precious metals from ores (Clarkson and Magos, 2006, Bernhoft, 2012). Hg<sup>0</sup> is present in the crust of the earth at approximately 0.5 parts per million (ppm), thus release of Hg<sup>0</sup> into the environment can be either naturally-occurring or anthropogenic. In fact, it is estimated that the magnitude of Hg<sup>0</sup> released from natural versus anthropogenic sources is roughly equal, making environmental Hg<sup>0</sup> a persistent concern despite any regulatory intervention to limit Hg<sup>0</sup> emissions from the burning of fossil fuels, municipal incinerators, and automobile waste (Fitzgerald and Clarkson, 1991). While liquid Hg<sup>0</sup> presents minimal hazard, history has revealed Hg<sup>0</sup> is particularly toxic when in the vaporous state; inhaled Hg<sup>0</sup> vapor is readily absorbed and distributes widely throughout the body to elicit toxicity on several organ systems (Clarkson and Magos, 2006, Bernhoft, 2012).

Hg<sup>0</sup> vapor is a stable and persistent form of the heavy metal, capable of remaining in the atmosphere for up to a year. Residence in the atmosphere permits global distribution of Hg<sup>0</sup> vapor,

meaning the potential for exposure extends beyond its origin. During this time in the atmosphere, Hg<sup>0</sup> vapor can undergo oxidative reactions in a process which is not fully understood. Mercurous mercury is produced when Hg<sup>0</sup> has lost one electron, and is commonly found in the form of mercurous chloride, or calomel. Mercurous mercury is used as a laxative in some regions of the world, as it has low solubility and is not readily absorbed into the bloodstream. The second oxidative state of Hg<sup>0</sup> is mercuric mercury; this form of mercury is a component of nearly all inorganic and organic mercurials. Inorganic mercuric chloride (HgCl<sub>2</sub>) has been used a preservative and in the processing of photographic film, while organic mercury compounds, particularly methyl- and ethylmercury, have been exploited for their potent antifungal properties. The distinction between inorganic and organic mercuric chloride is important, as the two mercurial forms have distinct toxicological profiles. Whereas the mercuric cation Hg<sup>2+</sup> generally targets the gastrointestinal tract and kidneys, the organomercuric cation elicits toxicity specifically in the nervous system (Clarkson and Magos, 2006, Bernhoft, 2012). Methylmercury (MeHg) is a form of organic mercuric mercury of contemporary concern due to its presence in aquatic food chains, placing at risk the human populations across the globe that rely on fish and piscivorous mammals as a dietary mainstay (Clarkson, 1995, Mergler et al., 2007).

Following oxidation in the atmosphere, mercuric mercury falls to the earth in rainwater, and accumulates in sediment and bodies of water. Though it is believed that a fraction of mercuric mercury is reduced and returned to the atmosphere as vapor, the primary focus remains on the conversion of mercuric mercury into MeHg by aquatic microorganisms (Mason et al., 2005, Clarkson and Magos, 2006). Virtually all forms of mercury which reach salt or freshwater systems are substrates for methylation by sulfate-reducing bacteria in what is apparently a protective mechanism for the microorganisms (Jensen and Jernelöv, 1969, Jernelöv, 1969, Hamdy and

Noyes, 1975). Following conversion into the methylated species, MeHg can be readily taken up by phytoplankton (Pickhardt and Fisher, 2007, Wu and Wang, 2011), and bioaccumulates in the aquatic food chain, with larger predatory fish and sea mammals containing highest MeHg concentrations (Clarkson, 1995, Clarkson and Magos, 2006).

Approximately 95% of ingested MeHg is absorbed into the blood and subsequently distributed to body tissues (Clarkson and Magos, 2006). The fact that MeHg binds to thiol groups with high affinity (Kostyniak and Clarkson, 1981, Rabenstein et al., 1982, Harris et al., 2003), and thus targets cysteine groups in proteins, is a critical component in its distribution throughout the body following exposure; the MeHg-cysteine complex resembles the structure of methionine, and thereby is able to employ the large neutral amino acid transporter to gain entry into cells and cross the blood-brain barrier (Kerper et al., 1992, Simmons-Willis et al., 2002). Within the liver, MeHg forms a complex with reduced glutathione, and is subsequently secreted into bile via glutathione carriers for elimination (Ballatori and Clarkson, 1985, Ballatori et al., 1995). The MeHgglutathione complex is then broken down to release a MeHg-cysteine complex, which can either be reabsorbed into the bloodstream (Dutczak et al., 1991, Dutczak and Ballatori, 1992, 1994) or further metabolized to inorganic mercuric mercury by the flora of the gastrointestinal tract (Suda and Hirayama, 1992, Suda et al., 1993, Clarkson and Magos, 2006). The half-life for elimination of MeHg is estimated to be 44 days following exposure to a low dose (about 0.2 - 0.7 parts per billion) of MeHg (Smith et al., 1994), with the primary route of elimination being via the feces. The primary mercurial excreted by those exposed to MeHg is inorganic mercuric mercury, thus metabolism is critical in the clearance of MeHg (Rowland et al., 1984, Rowland et al., 1986). Evidence suggests in situ metabolism of MeHg also occurs in the brain (Magos et al., 1985, Vahter et al., 1995), though the resulting inorganic species is inert in the central nervous system and does not contribute to toxicity associated with MeHg exposure (Magos et al., 1985, Davis et al., 1994).

#### 1.1.2. A historical perspective on methylmercury poisoning in humans

Much of what is known about MeHg poisoning in humans is derived from two accidental exposures. The first mass poisoning occurred in Minamata, Japan, a small fishing village, throughout the 1950s and 1960s. The source of pollution was traced back to a chemical plant which utilized inorganic mercury as a catalyst in the manufacturing of acetaldehyde; MeHg is generated as a byproduct of this catalytic reaction. The chemical plant had been releasing the mercurycontaining industrial waste into Minamata Bay since acetaldehyde production began in 1932, though the first cases of human poisoning associated with environmental MeHg did not come until 1953. During this period, the population unknowingly consumed fish with MeHg concentrations in excess of 20 ppm (McAlpine and Araki, 1958, Irukayama, 1977, Harada, 1995). The second outbreak occurred in Iraq in 1971 and 1972 when farmers received a shipment of seed grain from Mexico after a failed crop season. The seed was covered with MeHg fungicide and, rather than planting the seed, the MeHg-treated grain was used to prepare bread and feed livestock (Bakir et al., 1973). Since the mass poisonings in Minamata and Iraq, measures have been taken to regulate mercury pollution and limit human exposure to MeHg (WHO, 1976, 1990). However, because Hg<sup>0</sup> also arises from natural sources, the global cycling of mercury and potential for human exposure to MeHg through the consumption of fish remains a concern.

The clinical signs of MeHg poisoning in Japan and Iraq did not differ despite the vastly different lengths of exposure. Thus, the distinction between acute versus chronic exposure is not meaningful (Clarkson and Magos, 2006). In both episodes, pathological studies revealed the

nervous system to be the primary site of damage by MeHg, with the first clinical sign of poisoning observed at a hair-mercury concentration of 50 – 100 ppm (Bakir et al., 1973, Eto et al., 2002a). Whole blood and hair are the media of choice when estimating the absorbed dose of MeHg in adults (Cernichiari et al., 1995a, Rice et al., 2003). Whole blood mercury measurements account for non-transportable, protein-bound mercurial species bound to hemoglobin at a single instance (Ancora et al., 2002). In contrast, total mercury concentration in hair more accurately reflects exposure to MeHg, as other mercuric mercury species tend not to aggregate in hair, and timecourse of exposure can be obtained (Cernichiari et al., 1995b, Lindberg et al., 2004). Paresthesia is the preeminent sign of MeHg poisoning, with ataxia, dysarthria, and loss of vision following in succession as the body burden of MeHg increases (Clarkson and Magos, 2006, Takaoka et al., 2008). Clinical signs of MeHg exposure have been attributed to irreversible damage to and degeneration of discrete neuronal populations in the peripheral and central nervous systems through complex mechanisms (Takeuchi et al., 1962, Bakir et al., 1973, Al-saleem, 1976, Eto, 1997, Eto et al., 2002a). While the definitive events preceding MeHg-induced cell death are not fully understood, disruption of intracellular Ca2+ (Ca2+i) regulation appears to contribute significantly.

#### 1.1.3. Effects of methylmercury on calcium homeostasis

Studies by Komulainen and Bondy (1987) were some of the first to link MeHg exposure with elevated intracellular  $Ca^{2+}_{i}$  concentration ( $[Ca^{2+}]_{i}$ ); exposure of rat cerebral synaptosomes to MeHg (2.5 – 30  $\mu$ M) dose-dependently increased the intrasynaptosomal  $[Ca^{2+}]_{i}$  by 100 – 800 nM. It was concluded that extracellular  $Ca^{2+}$  ( $Ca^{2+}_{e}$ ) is the primary source of  $Ca^{2+}$  contributing to the disruption in homeostasis, as  $^{45}Ca^{2+}$  from the extracellular preparation accumulates in

synaptosomes following MeHg exposure. However, MeHg exposure also marginally increases [Ca<sup>2+</sup>]<sub>i</sub> in nominally Ca<sup>2+</sup><sub>e</sub>-free conditions. Because MeHg alters mitochondrial functions (Verity et al., 1975, Cheung and Verity, 1981) and depolarizes the mitochondrial membrane potential (Kauppinen et al., 1989), it was suggested that MeHg interacts with the mitochondria to disrupt Ca<sup>2+</sup><sub>i</sub> regulation. Indeed, MeHg-induced [Ca<sup>2+</sup>]<sub>i</sub> elevations are reduced when synaptosomes are pretreated with rotenone, an inhibitor to complex I of the mitochondrial electron transport chain, or oligomycin A, an inhibitor of ATP synthase (Komulainen and Bondy, 1987).

Since these preliminary findings, elevation of  $[Ca^{2+}]_i$  throughout MeHg exposure (0.5-5)uM) has been demonstrated in multiple primary and immortalized cell lines (Denny et al., 1993, Hare et al., 1993, Marty and Atchison, 1997, Marty et al., 1997, Edwards et al., 2005, Ramanathan and Atchison, 2011); this disruption in [Ca<sup>2+</sup>]<sub>i</sub> occurs in at least 2 kinetically distinct phases. In neonatal rat cerebellar granule cells, the occurrence of the first phase of [Ca<sup>2+</sup>]<sub>i</sub> increase is independent of Ca<sup>2+</sup><sub>e</sub>, indicating an internal source of Ca<sup>2+</sup> contributes to MeHg-induced [Ca<sup>2+</sup>]<sub>i</sub> disruption (Marty and Atchison, 1997). The contribution of mitochondrial Ca<sup>2+</sup> to phase 1 [Ca<sup>2+</sup>]<sub>i</sub> increases is indisputable; brief exposure (10 s) of isolated rat forebrain mitochondria to MeHg (10  $-100\,\mu\text{M}$ ) results in stimulated  $^{45}\text{Ca}^{2+}$  efflux and reduced or blocked reuptake by the mitochondrial Ca<sup>2+</sup> uniporter (Levesque and Atchison, 1991). This MeHg-induced efflux of mitochondrial Ca<sup>2+</sup> is ample enough to increase spontaneous release of acetylcholine in rat brain synaptosomes (Levesque et al., 1992). Pretreatment with cyclosporine A, an inhibitor of the mitochondrial permeability transition pore, slows the initial rise in [Ca<sup>2+</sup>]<sub>i</sub> and mitochondrial membrane depolarization induced by MeHg (0.2 - 0.5 µM) in rat cerebellar granule cells (Limke and Atchison, 2002). Cyclosporine A is also effective in protecting cells against MeHg-associated cytotoxicity, implicating mitochondrial Ca<sup>2+</sup> efflux via the permeability transition pore as a significant contributor to MeHg neurotoxicity.

Interestingly, depletion of mitochondrial  $Ca^{2+}$  prior to MeHg exposure does not abolish the MeHg-induced rise in  $[Ca^{2+}]_i$  in rat cerebellar granule cells. Furthermore, cells exposed to  $0.5 \,\mu\text{M}$  MeHg display a biphasic elevation in mitochondrial  $[Ca^{2+}]$  in a manner which is  $Ca^{2+}e^{-}$  independent, indicating mitochondrial  $Ca^{2+}$  is not the only internal source of  $Ca^{2+}$  contributing to MeHg-induced  $[Ca^{2+}]_i$  elevations (Limke et al., 2003). Findings in the neuroblastoma-derived cell line NG108-15 (Hare and Atchison, 1995a) and rat cerebellar granule cells (Limke et al., 2003, Limke et al., 2004) demonstrate  $Ca^{2+}$  release from the smooth endoplasmic reticulum via the inositol 1,4,5-trisphosphate (IP<sub>3</sub>) receptor contribute to phase 1  $[Ca^{2+}]_i$  perturbations induced by MeHg exposure. Generation of IP<sub>3</sub> is increased in cerebellar granule cells, but not glial cells, following exposure to 5  $\mu$ M MeHg (Sarafian, 1993) in a M3 muscarinic receptor-linked mechanism (Limke et al., 2004). Thus,  $Ca^{2+}$  release from the mitochondria and endoplasmic reticulum appear to be inextricably linked; although the mitochondria first attempt to buffer  $Ca^{2+}$  released from the smooth endoplasmic reticulum, mitochondrial overload ensues and  $Ca^{2+}$  is released back into the cytosol by the mitochondria themselves (Limke et al., 2003).

The second phase of MeHg-induced [Ca<sup>2+</sup>]<sub>i</sub> is attributed to Ca<sup>2+</sup> influx, as this response is abolished in the absence of Ca<sup>2+</sup><sub>e</sub> (Hare et al., 1993, Marty and Atchison, 1997). The time-to-onset of this second phase is slowed in cerebellar granule cells and primary spinal neurons with the block of specific Ca<sup>2+</sup>-permeable ion channels, namely voltage-gated Ca<sup>2+</sup> channels (VGCCs). Voltage-dependent Na<sup>+</sup> channels are not apparently involved in activation of VGCCs, as block of Na<sup>+</sup> current with tetrodotoxin (TTX) does not alter phase 2 [Ca<sup>2+</sup>]<sub>i</sub> (Marty and Atchison, 1997, Ramanathan and Atchison, 2011).

Cerebellar granule cells exposed to MeHg  $(0.5-1~\mu\text{M})$  display a concentration-dependent reduction in cell viability within 1 or 3.5 h of exposure. The loss of cell viability is attributed to elevated  $[\text{Ca}^{2+}]_i$ , as pretreatment with a membrane-permeable form of the  $\text{Ca}^{2+}$  chelator BAPTA prevents MeHg-induced cytotoxicity. Block of discrete VGCC isoforms with either nifedipine or  $\omega$ -conotoxin MVIIC also protects against cell death following MeHg exposure, indicating  $\text{Ca}^{2+}$  influx through  $\text{Ca}^{2+}$ -permeable ion channels as a mechanism which contributes to MeHg cytotoxicity (Marty and Atchison, 1998).

#### 1.1.4. Structure and biodiversity of voltage-gated calcium channels

VGCCs are ionotropic channels which mediate Ca<sup>2+</sup> flow into the neuron following depolarization of the plasma membrane. They are divided into two classes based upon the degree of depolarization required for their activation; the high voltage-activated (HVA) VGCCs include the L-, N-, P/Q-, and R-type channels (*Cav*1.2, 2.2, 2.1, and 2.3, respectively), and low voltage-activated (LVA) VGCCs include only T-type channels (Table 1.1). Ca<sup>2+</sup> influx through VGCCs mediates intracellular events, such as contraction, secretion, synaptic transmission, and gene expression, in addition to propagating electrical signals (Catterall, 1998).

Neuronal VGCCs are comprised of up to five subunits ( $\alpha_1$ ,  $\beta$ ,  $\alpha_2$ ,  $\delta$ , and occasionally  $\gamma$ ) which impart distinct biophysical and pharmacological properties (Fig. 1.1) (Tsien et al., 1991). The  $\alpha_1$  subunit, encoded for by Cav, contains both the channel pore and pharmacologic binding sites, whereas the auxiliary subunits influence channel assembly and kinetics (Ertel et al., 2000, Catterall et al., 2003, Benarroch, 2010). The process of discriminating among extracellular cations is due in part to a selectivity filter present at the mouth of the VGCC pore. A region of four negatively-charged glutamic acid residues projects into the lumen outside the pore; the ability of

| Туре | Channel<br>subtype | Antagonists   | Conductance<br>/τ  | α1-coding<br>gene   | Cell/tissue-<br>specific<br>expression             | Function  |            |            |            |                        |   |
|------|--------------------|---|--|---|--|---|------------|------------|------------|------------------------|---|
|      | L                  | Phenylalkylamines,<br>duhydropyridines,<br>benzothiazapines,<br>ω-agatoxin IIIA | 25 pS/<br>20 – 50 ms   | $\alpha_{1S}$ (Cav1.1)  | Skeletal muscle                                    | Excitation-<br>contraction<br>coupling                                  |            |            |            |                        |   |
|      |                    |   |  | α <sub>1C</sub> (Cav1.2)                                      | CNS (dendrites,<br>cell bodies),<br>cardiac muscle | Plasticity, cardiac<br>muscle<br>contraction                            |            |            |            |                        |   |
|      |                    |   |  |   | Cochlea  | Sensory<br>transduction   |            |            |            |                        |   |
|      |                    |   |  |   | Striatal medium                                    | Neurotransmitter  |            |            |            |                        |   |
|      |                    |   |  | $\alpha_{1D}$   | spiny neurons                                      | release   |            |            |            |                        |   |
|      |                    |   |  | ( <i>Cav</i> 1.3)   | Substantia nigra pars compacta                     | Pacemaker activity  |            |            |            |                        |   |
|      |                    |   |  |   | Retina   | Sensory<br>transduction   |            |            |            |                        |   |
| HVA  | P/Q                | P-type: ω-agatoxin<br>IVA<br>Q-type: ω-conotoxin<br>MVIIC                       | P-type: 9-20 pS/>100 ms  |   | Presynaptic terminals                              | Neurotransmitter<br>release in<br>neuromuscular<br>junctions and<br>CNS |            |            |            |                        |   |
|      |                    |   | Q-type: ω-conotoxin  | Q-type: 9 –<br>20 pS/<100<br>ms                               | 20 pS/<100   | 20 pS/<100  | 20 pS/<100 | 20 pS/<100 | 20 pS/<100 | $\alpha_{1A}$ (Cav2.1) | Purkinje<br>neurons,<br>cerebellar<br>granule cells |
|      |                    |   |  |   | Thalamus   | Depolarization of thalamic neurons                                      |            |            |            |                        |   |
|      | N R                |   | 13 pS/50 –<br>110 ms (500 – 800 ms in<br>sympathetic<br>neurons) | $\alpha_{1B}$ $(Cav2.2)$ $\alpha_{1E}$ $(Cav2.3)$             | Only expressed in neurons                          | Neurotransmitter release  |            |            |            |                        |   |
|      |                    |   |  |   | Nociceptive<br>DRG neurons                         | Depolarization  |            |            |            |                        |   |
|      |                    |   |  |   | Presynaptic terminals                              | Neurotransmitter release  |            |            |            |                        |   |
|      |                    |   |  |   | Hippocampus  | Depolarization  |            |            |            |                        |   |
| LVA  | Т                  | Kurtoxin,<br>mibefradil,<br>amiloride   | 5 – 11 pS/?  | $\alpha_{1G}, \alpha_{1H}, \\ \alpha_{1I} \\ (Cav 3.1 - 3.3)$ | Dendrites, somas<br>of some CNS<br>neurons         | Rhythmic burst firing, pacemaker activity                               |            |            |            |                        |   |

Table 1.1. Classification of VGCC subtypes by pharmacologic and electrical properties. VGCC subtypes are determined by the  $\alpha_1$  subunit which is encoded for by specific genes; these channels may be further characterized by  $Ca^{2+}$  conductance, pharmacologic sensitivities, and expression in distinct tissues or brain regions. From Marrero-Rosado et al. (2013) with permission from Springer. *Copyright* © 2013 by Springer.

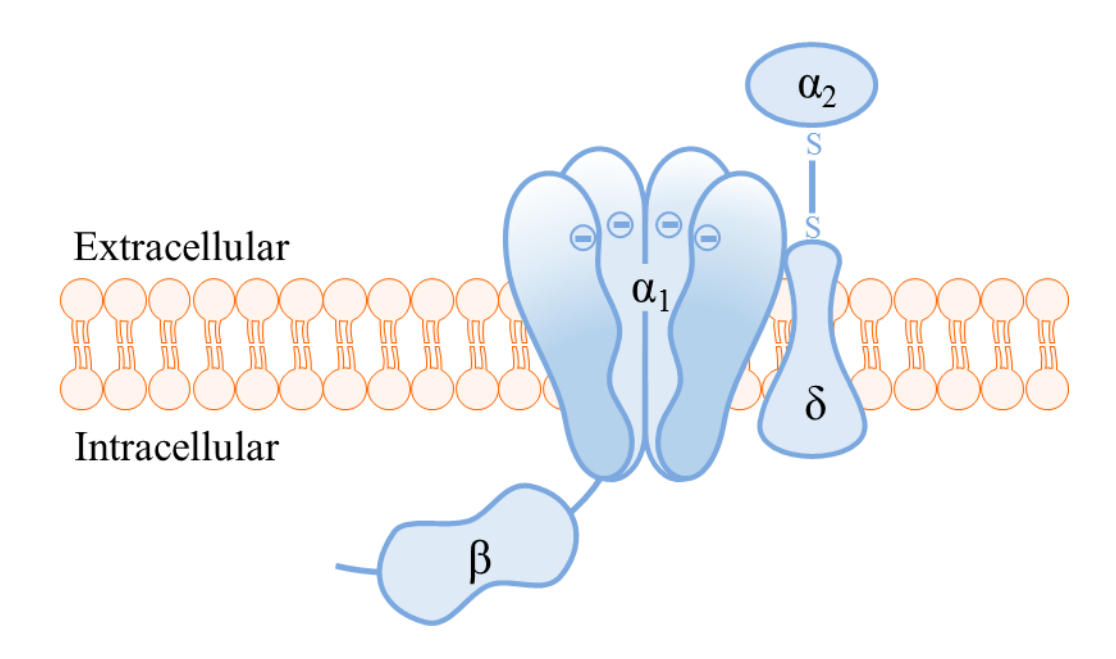


**Figure 1.1. Subunit composition of VGCCs.** VGCCs are heteromeric protein complexes. The primary subunit,  $\alpha_1$ , forms the pore of the channel and provides unique pharmacologic binding sites. Negatively charged glutamate residues within the mouth of the pore serve as a cation selectivity filter. The activity of the  $\alpha_1$  subunit can be modulated by auxiliary subunits  $\beta$ ,  $\alpha_2\delta$ , and, in some instances,  $\gamma$ . The  $\beta$  subunit has no transmembrane segments and interacts with  $\alpha_1$  through specific interaction domains to promote trafficking and insertion of the pore-forming subunit into the plasma membrane. Additionally, the  $\beta$  subunit modulates kinetics of activation and inactivation. The  $\alpha_2\delta$  subunit consists of 2 distinct subunits joined by a disulfide bond; a single transmembrane segment and heavy glycosylation suggests this subunit is primarily extracellular. Co-expression of  $\alpha_2\delta$  enhances  $\alpha_1$  expression and alters inactivation kinetics. Within skeletal muscle,  $\gamma$  subunits confer further modification of the biophysical properties of  $\alpha_1$  subunits.

these residues to bind Ca<sup>2+</sup> is believed to be crucial for ion discrimination (Kim et al., 1993, Yang et al., 1993, Heinemann et al., 1994, Ellinor et al., 1995). This selectivity is so efficient that, even though extracellular sodium ions are found in greater concentrations, VGCCs are still more permeable to Ca<sup>2+</sup>. Because Ca<sup>2+</sup> and some divalent metals share chemical properties, including ionic radius and charge, VGCCs are particularly susceptible to perturbations in function through interactions with heavy metals, including lead and mercury (Audesirk, 1993, Atchison, 2003).

#### 1.1.5. Actions of mercurials on neurotransmitter release and voltage-gated calcium channels

Initial studies of actions of MeHg relied upon use of in vitro models at amphibian and mammalian neuromuscular junction due, in part, to the fact that an increased incidence of myasthenia gravis-like syndromes was observed in the Iraqi exposure to MeHg, (Bakir et al., 1973). In these preparations, bath application of MeHg (20 – 400 µM) disrupts patterns of nerveevoked and spontaneous transmitter release in a similar manner to that of Hg<sup>2+</sup>; there is a decrease in end-plate potential (EPP) amplitude and an initial increase, then decrease of miniature end-plate potential (MEPP) frequency to complete block. EPPs are measured as a graded amplitude depolarization of the postsynaptic membrane in response to nerve-evoked release of neurotransmitter, whereas MEPPs are measured as a small and random depolarization of the postsynaptic membrane as a result of spontaneous vesicle release. These effects of MeHg on EPPs and MEPPs are time- and concentration-dependent, however, in contrast to inorganic Hg<sup>2+</sup>, they are also irreversible (Juang, 1976, Atchison and Narahashi, 1982, Traxinger and Atchison, 1987). Iontophoresis of acetylcholine elicits EPPs with unaltered amplitudes throughout MeHg exposure, indicating MeHg-induced disruption of nerve-evoked neurotransmitter release occurs presynaptically (Atchison and Narahashi, 1982).

Because the rate of spontaneous neurotransmitter release is related to presynaptic [Ca<sup>2+</sup>]<sub>i</sub> (Kavalali, 2015), the MeHg-induced increase in MEPP frequency reflects an intracellular effect and is suggestive of movement of the neurotoxicant across the plasma membrane. Increase in MEPP frequency occurs more rapidly in the presence of Ca<sup>2+</sup>e, though magnitude is unaltered (Atchison and Narahashi, 1982, Atchison, 1986). Treatment of the neuromuscular junction preparation with Bay K 8644, an L-type VGCC agonist, reduces the latency of MeHg-induced increases in MEPP frequency (Atchison, 1987). These experiments suggest, albeit indirectly, that MeHg may utilize VGCCs to cross the cell membrane into the nerve terminal. However, a main attribute that distinguishes methylated forms of Hg<sup>2+</sup> from inorganic Hg<sup>2+</sup> is the ability of the former to disrupt VGCC function when the channel is at rest (Shafer et al., 1990, Shafer and Atchison, 1991, Szücs et al., 1997). Another important difference is the fact that MeHg acts in a non-competitive manner, whereas higher concentrations of Ca<sup>2+</sup>e can interfere with block of VGCC current caused by Hg<sup>2+</sup> (Atchison et al., 1986, Hewett and Atchison, 1992). Therefore, it has also been hypothesized that MeHg interacts with the channel in additional ways, most likely due to its relatively higher lipophilicity.

The  $Ca^{2+}$ -dependence of neurotransmitter release in conjunction with the dominant role of VGCCs in regulating  $Ca^{2+}$  entry into the nerve terminal shifted subsequent studies towards more direct examination of effects of mercurials on VGCCs. Forebrain synaptosomes briefly exposed (1-10~s) to MeHg  $(2.5-250~\mu\text{M})$  reveal  $Ca^{2+}$  influx occurs in two kinetically-distinct phases: the fast phase, which is associated with neurotransmitter release and inactivates within 1-2~s, and the slow phase, which persists for 20-90~s following depolarization and is perhaps the product of a non-inactivating  $Ca^{2+}$  channel or reversal of the  $Na^+/Ca^{2+}$  exchanger (Shafer and Atchison, 1989). MeHg reduces VGCC-mediated  $^{45}Ca^{2+}$  uptake in both phases, though the block is more

pronounced in the slow phase; block is just minimally overcome by increasing [Ca<sup>2+</sup>]<sub>e</sub>, suggesting a non-competitive mode of action. This is in contrast to the VGCC blocking effect of inorganic Hg<sup>2+</sup> which is highly hindered by an increase in [Ca<sup>2+</sup>]<sub>e</sub> (Atchison et al., 1986, Shafer and Atchison, 1989). Even though increasing the extracellular concentration of  $K^+$  concurrently with 100 μM MeHg exposure results in an increased percentage block of synaptosomal <sup>45</sup>Ca<sup>2+</sup> influx, VGCC current block occurs irrespective of channel configuration (e.g. closed, activated, inactivated). Prior VGCC activation is not required for MeHg to induce a decrease in Ca<sup>2+</sup> influx (Atchison et al., 1986, Shafer et al., 1990). MeHg also inhibits <sup>45</sup>Ca<sup>2+</sup> uptake in synaptosomes isolated from rat cerebellum. Pretreatment with ω-conotoxin GVIA or ω-conotoxin MVIIC blocks the MeHg-induced inhibition of synaptosomal <sup>45</sup>Ca<sup>2+</sup> uptake (Yan and Atchison, 1996). These data suggest MeHg interacts with N- and P/Q-type VGCCs in the cerebellum.

Electrically neutral mercurials, such as *p*-chloromercuribenzoate (PCMB) and dimethylmercury, or the negatively charged *p*-chloromercuribenzene sulfonate (PCMBS), do not block synaptosomal <sup>45</sup>Ca<sup>2+</sup> uptake, even at high [K<sup>+</sup>]<sub>e</sub>, indicating that mercurial lipophilicity is not the sole determinant which accounts for blocking capabilities (Hewett and Atchison, 1992). However, the ability of MeHg to noncompetitively block VGCCs despite channel configuration suggests lipophilicity is an important factor which contributes to its blocking actions (Atchison et al., 1986, Shafer et al., 1990). In contrast to negatively charged or neutral mercurials, those with a positive charge, such as ethylmercury, MeHg, and Hg<sup>2+</sup>, block synaptosomal <sup>45</sup>Ca<sup>2+</sup> influx through VGCCs in a voltage-dependent manner, indicating these ions may interact with or pass through the channel's pore (Atchison et al., 1986, Shafer et al., 1990, Hewett and Atchison, 1992).

The synaptosomal model has also been used for studies of receptor occupancy involving competition-binding experiments due to its endogenous expression of multiple subtypes of

VGCCs. In these experiments, synaptosomes were pre-incubated with radiolabeled ligands with specificity for distinct VGCC subtypes and mercurials were introduced as unlabeled "cold" competitors. Results show MeHg reduces the specific binding of <sup>3</sup>[H]-nitrendipine, an L-type VGCC antagonist, at a concentration (100 μM) that also inhibited <sup>45</sup>Ca<sup>2+</sup> influx. Specific binding of <sup>125</sup>I-ω-conotoxin GVIA in the rat pheochromocytoma cell line PC12 is also reduced by MeHg (Shafer et al., 1990). Together, these data suggest that MeHg may interact with L- and N-type VGCCs. In particular, mercurials bind with sulfhydryl groups within proteins. Therefore sulfurcontaining residues in the pore of an ion channel represent potential sites for mercurial action. In contrast to Hg<sup>2+</sup>, which has the ability to bind two sulfhydryl groups, MeHg only binds one (Rabenstein et al., 1982); interactions with sulfur-containing groups in VGCCs may directly alter activation/inactivation of the channel, or disrupt overall channel function indirectly through effects on membrane fluidity. Differences among the physiochemical properties of mercurials could contribute to the differential effects on VGCCs previously discussed.

Electrophysiological studies aiming to determine how mercurials alter VGCC currents reveal MeHg (1 – 20  $\mu$ M) completely and irreversibly blocks whole cell Ba<sup>2+</sup> current through L-and N-type VGCCs in PC12 cells; onset of current block occurs at a rate which is concentration-dependent. As observed in synaptosomes, block by MeHg is not determined by the state of the VGCCs (Shafer and Atchison, 1991). Similar effects on Ba<sup>2+</sup> current are observed in the highly-sensitive cerebellar granule cell following *in vitro* exposure to MeHg (0.25 – 1  $\mu$ M) (Sirois and Atchison, 2000), though it appears that primary cell cultures are more sensitive to the effects of MeHg than are transformed cell cultures.

The potency of MeHg as a VGCC blocker is indisputable, as complete block of current often occurs in the low  $\mu M$  range. However, VGCC subtype-specificity of MeHg has not been

studied extensively in native currents. Previous studies report rat hippocampal HVA currents as being more resistant to MeHg (block at 5 and 10  $\mu$ M), whereas LVA currents are more sensitive with a marked current reduction by 2  $\mu$ M MeHg (Szücs et al., 1997). Using heterologous expression of human neuronal VGCC subunits in HEK cells, the effects of mercurials on single VGCC isoforms have been examined. MeHg (0.125 – 5.0  $\mu$ M) causes a concentration- and time-dependent reduction in current through the L-type VGCC, though this block is incomplete with approximately 25% current remaining in the presence of 5  $\mu$ M MeHg. Nimodipine, an L-type VGCC antagonist, completely blocks current through the recombinant channel on its own and blocks residual current which remained following 5  $\mu$ M MeHg exposure (Peng et al., 2002). MeHg also induces a concentration- and time-dependent block of current through recombinant N- and R-type VGCCs; this block is complete at the upper range of concentrations examined (Hajela et al., 2003). In contrast to the native hippocampal currents, recombinant LVA currents are less sensitive to block by MeHg (IC<sub>50</sub> = 13.0  $\pm$  5  $\mu$ M) (Tarabová et al., 2006).

## 1.1.6. The somatosensory system and methylmercury neurotoxicity

The spinal cord consists of nerves that transmit information between the brain and the body. Nervous tissue is protected by the vertebral column, which can be divided into 4 morphologically distinct regions: cervical, thoracic, lumbar, and sacral (Fig. 1.2A). Nerves emanating from the spinal column service distinct regions of the body, or dermatomes, corresponding to the level from which they exit the vertebral column. (Fig. 1.2B). Nerves residing in the spinal cord include cutaneous and visceral afferents, motor efferents, and neurons of the sympathetic and parasympathetic systems. While each fiber type has a precise source or destination within the spinal column, all neurons enter or exit the spinal cord via spinal nerves. Spinal nerves are formed

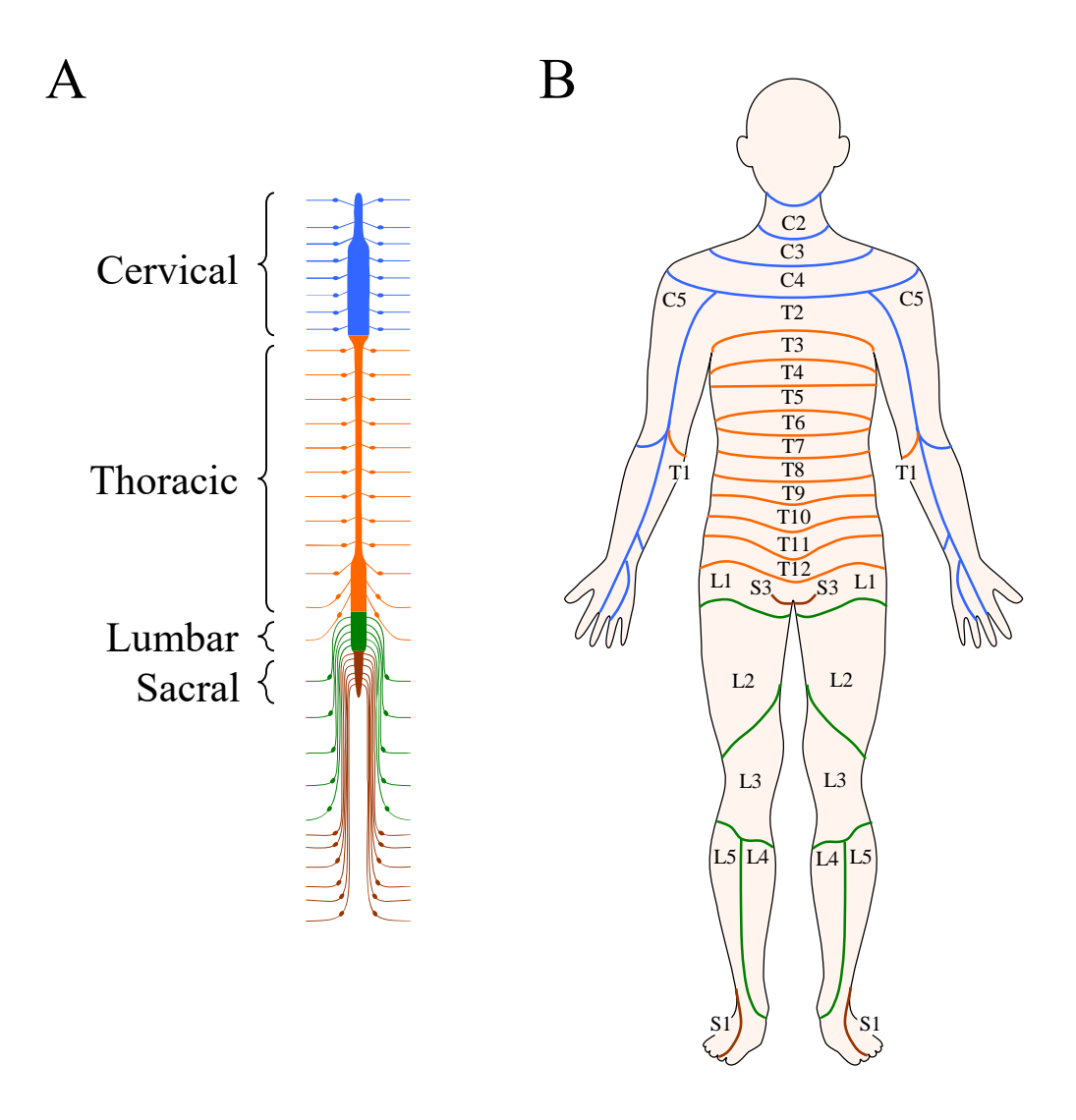
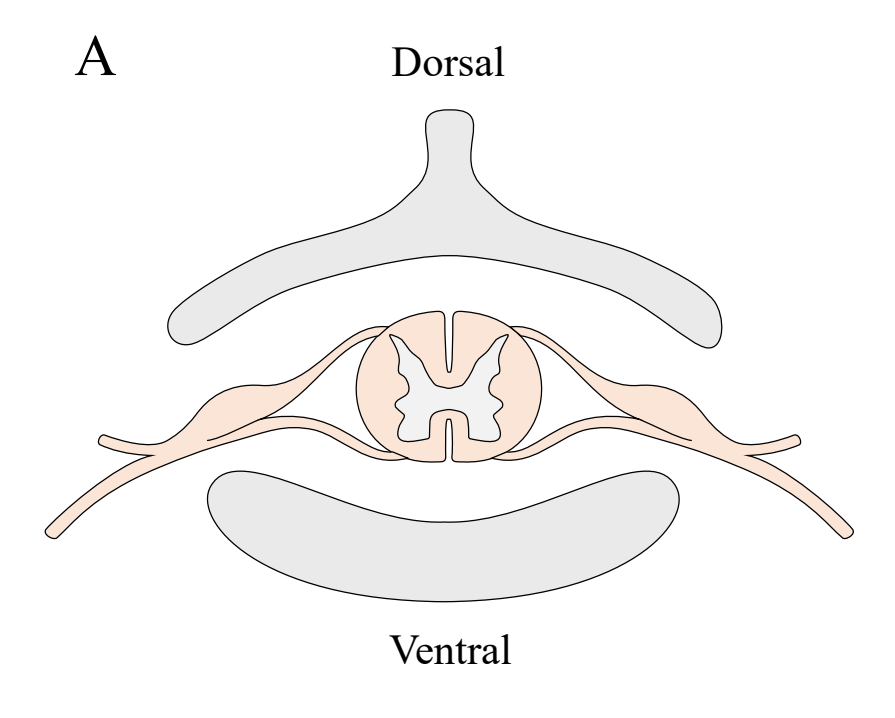


**Figure 1.2. The human dermatome: divisions of the spinal cord.** (A) The spinal cord is divided into 4 segments: cervical, thoracic, lumbar, and sacral. At each level, spinal nerve roots emanate bilaterally from the spinal cord between vertebral segments. (B) Spinal roots serve distinct regions of the body, as mapped out in the human dermatome, providing organization to the somatosensory and motor systems.

by the convergence of dorsal and ventral nerve roots, and emanate bilaterally from the vertebral column via intervertebral foramina (Fig. 1.3A–B). The human spinal cord has 31 pairs of spinal nerves: 8 cervical, 12 thoracic, 5 lumbar, 5 sacral, and 1 coccygeal (Boron and Boulpaep, 2009, Watson et al., 2009). The adult human spinal cord is approximately 20% smaller than the vertebral column, extending to about the first lumbar vertebra. Whereas cervical spinal nerves are nearly level with their corresponding vertebrae, the extension of lower spinal nerves becomes increasingly oblique towards corresponding intervertebral foramina (Ranson and Clark, 1953).

Transverse sections of the spinal cord reveal a composition of both gray and white matter. Gray matter is arranged in the form of a butterfly, with dorsal and ventral projections, or horns; intermediate gray matter connects dorsal and ventral horns (Fig. 1.3A). Spinal gray matter is comprised of neuronal cells bodies, dendrites, axons, and glial cells. Upon microscopic analyses, gray matter can be divided into successive layers, or laminae, on the basis of cytoarchitecture (Rexed, 1952, 1954). The first nine laminae are arranged sequentially from dorsal to ventral, and the tenth surrounds the central canal of the spinal cord. Function of nerve fibers can be loosely categorized based upon the laminae in which they reside. Spinal gray matter is notably enlarged in the brachial and lumbosacral regions from which nerves of the upper and lower limbs arise (Ranson and Clark, 1953). Surrounding white matter consists of longitudinal axon projections and glial cells. Nerve fibers in spinal white matter are bundled into funiculi and fasciculi, and follow pathways with discrete functional connotations (Watson et al., 2009).

Somatosensory information is carried from the periphery to the brain via sensory afferents, or dorsal root neurons. The cell bodies of these sensory fibers are aggregated in ganglia residing just outside the dorsal spinal cord. Dorsal root ganglia (DRG) are unique in that they are pseudounipolar; soma do not give rise to dendrites, but rather short axon projections bifurcate to



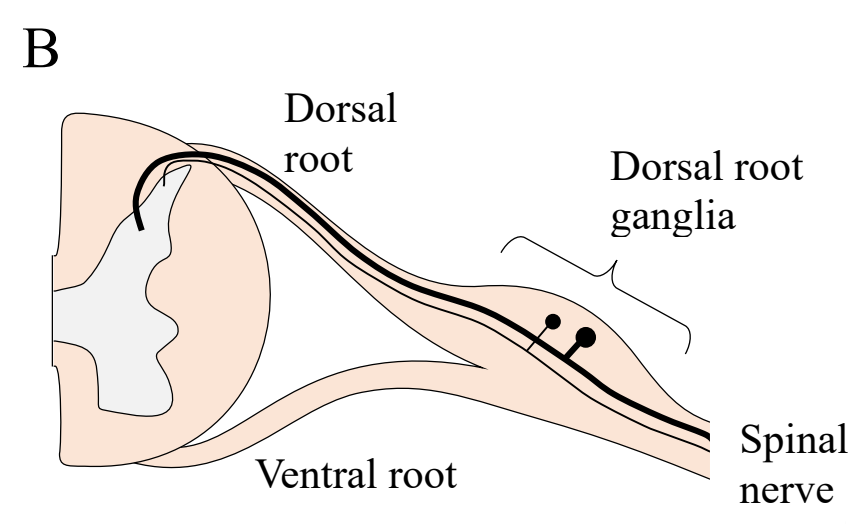


**Figure 1.3. Organization of spinal nerves at the spinal cord.** (A) Spinal nerves diverge within the spinal cord, giving rise to dorsal and ventral nerve roots. (B) Neurons of the dorsal root transmit somatosensory information from the periphery to the somatosensory cortex. Cell bodies of these nerves reside in the dorsal root ganglia, proximal to the entry point of the nerves on the dorsal side of the spinal cord. Neurons of the ventral root transmit motor information from the motor cortex to peripheral muscle tissue.

send processes to both the periphery and spinal cord (Fig. 1.3B). Four somatosensory modalities (mechanoreception, proprioception, thermoreception, nociception) are differentially transmitted by four distinct DRG neuron types (Aa, Ab, Ab, C) (Boron and Boulpaep, 2009). These neurons can be generally characterized by fiber diameter (Lee et al., 1986, Scroggs and Fox, 1992a), immunoreactivity (Hökfelt et al., 1976, Dodd et al., 1983, Hjerling-Leffler et al., 2007), action potential duration (Villière and McLachlan, 1996, Djouhri et al., 1998, Fang et al., 2005), and various other electrical properties (Scott and Edwards, 1980, Harper and Lawson, 1985, Lawson, 2002, Murali et al., 2015). It is these unique physical and electrical attributes of afferent neurons, in addition to diverse expression of specialized peripheral receptors, localization within the dorsal horn, ascending spinal pathways, and central targets, which contribute to modality segregation (Uddenberg, 1966, 1968, Wall and Dubner, 1972, Willis and Coggeshall, 2004). Consequently, somatosensory modalities can be loosely related to discrete DRG neuron types (Table 1.2). Aδ and C fibers are the smaller of the DRG neurons and canonically categorized as nociceptive. Both  $A\delta$ and C DRG extend quite shallowly into the dorsal horn, residing within the first two laminae. While A $\delta$  fibers transmit sharp, pricking pain sensations, C fibers mediate dull and burning pain; the distinct quality of pain carried by these neurons can be specifically attributed to conduction velocity and receptor expression. Aα and Aβ are the larger of the DRG neurons and transmit mechanoreceptive and proprioceptive signals. Aβ reside deeper within the dorsal horn, laminae III -VI, whereas A $\alpha$  can be found in laminae VI - IX in the intermediate gray matter and ventral horn (Rexed, 1952, 1954, Zigmond et al., 1999, Boron and Boulpaep, 2009).

Clinical assessment and nerve biopsies of MeHg-poisoned adults suggest MeHg-related paresthesia is associated with degeneration of DRG (Eto, 1997, Eto et al., 2002a), though experimental studies demonstrate distinct changes in cell morphology and electrical properties

|           | Sensory modality       | Axon diameter<br>(μm) | Myelinated? | Conduction velocity (m/s) | Central<br>projection |
|-----------|------------------------|-----------------------|-------------|---------------------------|-----------------------|
| Αα        | Proprioception, reflex | 12 - 20               | Yes         | 72 - 120                  | Laminae VI – IX       |
| $A\beta$  | Touch, proprioception  | 6 - 12                | Yes         | 36 - 72                   | Laminae III – VI      |
| $A\delta$ | Pain, temperature      | 1 – 6                 | Yes         | 4 - 36                    | Laminae I – II        |
| С         | Pain, temperature      | 0.2 - 1.5             | No          | 0.4 - 2.0                 | Laminae I – II        |

**Table 1.2. Properties of somatosensory neurons.** DRG may be loosely categorized by size, conduction velocity, and location of projections in the spinal cord. These features, along with peripheral receptors and ascending pathways contribute to modality segregation. Adapted from Zigmond et al. (1999), Boron and Boulpaep (2009).

precede cell death. Interestingly, severe perturbations in DRG function and neurodegeneration have been reported in only  $A\alpha$  and  $A\beta$ , placing an onus on not only understanding the mechanisms preceding DRG degeneration, but also why large-fiber afferents are uniquely susceptible to MeHg neurotoxicity.

To better understand the mechanisms of MeHg neurotoxicity in DRG, rodent models are commonly used in conjunction with *in vivo*, subacute and subchronic exposure paradigms; findings under these conditions align with spinal nerve biopsies and autopsies of patients poisoned with MeHg. Adult rats administered with 5 mg/kg/day MeHg present with severe changes in afferent morphology in as little as 8 days. Earliest signs of MeHg toxicity in the DRG of these animals include loss of Nissl staining, cytoplasmic vacuolization, swelling of cisternal organelles, and proliferation of satellite cells. These morphologic changes are predominantly present in large-diameter DRG neurons, corresponding to the Aα and Aβ fiber types, with only occasional degeneration of myelinated neurons (Cavanagh and Chen, 1971, Delio et al., 1992).

In a separate set of experiments, adult rats were administered 2 mg/kg/day MeHg for 19 days followed by a 32 day recovery period. Despite the lower dose and opportunity for recovery and repair, a marked reduction in the number and mean soma volume of large-fiber DRG is measurable, whereas small-fiber DRG are relatively spared from MeHg-related damage (Schiønning et al., 1998). Wallerian degeneration is observed at both the level of the dorsal roots and spinal cord fasciculus gracilis, and is thought to be related to MeHg-induced microtubule disruption in these neurons (Abe et al., 1975, Miura et al., 2000). This widespread degeneration of DRG neurons precedes any detectable morphologic alterations in motor afferents or the cerebellum (Eto, 1997, Schiønning et al., 1998, Cao et al., 2013). Autopsy and biopsy material from poisoned patients show consequences of MeHg exposure at protracted timepoints, up to 11 years following

onset of sensory disturbances; samples from MeHg poisoned patients show endoneurial fibrosis, Büngner's bands, and proliferation of fibroblasts and Schwann cells in the sural nerve tissue, suggesting an attempt to repair the damaged nerve tissue, albeit an abnormal and incomplete regeneration (Eto, 1997, Eto et al., 2002a). Thus, it has been suggested that early-stage ataxia, muscle weakness, and abnormal reflexes coinciding with MeHg-induced paresthesia are more so related to degeneration of proprioceptive  $A\alpha$  and  $A\beta$  neurons rather than central lesions (Yip and Riley, 1987).

Damage at the somatosensory cortex is not as well defined. A proteomic study of the somatosensory cortices of juvenile rats reveals 40 µg/kg/day MeHg for 12 weeks induces a state of metabolic deficit through downregulation of essential metabolic proteins and components of neurotransmission (Freire et al., 2007, Kong et al., 2013). Though the impact of MeHg-induced damage to the somatosensory cortex may not be as immediately detectable as damage to peripheral afferents, it seems alterations in this brain region may contribute to persistent paresthesia long after cessation of exposure to MeHg. When assessed 30 years following MeHg exposure in Minamata, poisoned patients perceive sensations of touch, though the threshold for sensation is elevated at both distal and proximal sites. This indicates that long-lasting sensory dysfunction caused by MeHg may not be due to direct injury of peripheral nerves alone, but also central mechanisms (Ninomiya et al., 2005).

In addition to morphologic abnormalities, MeHg-induced paresthesia may be explained by electrical changes to DRG neurons. Studies in isolated neonatal rat DRG revealed MeHg (0.25 – 50  $\mu$ M) blocks current voltage-activated ion channels to varying extents; potency of MeHg at voltage-activated Ca<sup>2+</sup> and K<sup>+</sup> channels (IC<sub>50</sub> = 2.6 and 2.2  $\mu$ M, respectively) is much higher than at voltage-activated Na<sup>+</sup> channels (IC<sub>50</sub> = 12.3  $\mu$ M) (Leonhardt et al., 1996a, Leonhardt et al.,

1996b). Despite the inhibitory action of MeHg on voltage-activated ion channels *in vitro*, DRG from adult rats administered MeHg (5 mg/kg/day for 10 days) do not show any significant alteration in resting membrane potential, or action potential duration, amplitude, or kinetics. However, conduction velocity of A $\beta$  and A $\delta$  afferents are slowed by 150 – 200%, resulting in a significant delay in action potential onset following nerve stimulation. A $\beta$  and A $\delta$  afferents from MeHg-treated rats also display ectopic repetitive action potential discharge from single nerve stimulation in approximately 25% of cells sampled, whereas repetitive discharge in A $\alpha$  and C is a rare occurrence (Delio et al., 1992). Similar action potential trains are present in organotypic slices of the somatosensory cortex from rats exposed to MeHg *in utero* through weaning, where the dam received 0.375  $\mu$ g MeHg/kg/day; the increase in the number of action potential spikes evoked from single nerve stimulation may be related to the reduced spike threshold in MeHg-treated animals (Világi et al., 2000).

Inorganic mercury also alters ion channel functions and, in turn, electrical properties in sensory afferents. HgCl<sub>2</sub> (1  $\mu$ M), when applied acutely to neonatal rat DRG, blocks peak and sustained currents carried through VGCCs to the same extent as 5  $\mu$ M MeHg (Leonhardt et al., 1996b). A comparative study of the action of mercurial compounds on  $\gamma$ -aminobutyric acid (GABA)-induced currents in neonatal rat DRG found comparable results in that HgCl<sub>2</sub> had a higher potency than MeHg. However, the discrete actions of HgCl<sub>2</sub> and MeHg on GABA-induced currents are opposite; acute application of 10  $\mu$ M HgCl<sub>2</sub> greatly enhances GABA currents to nearly 140% of control, whereas 100  $\mu$ M MeHg reduces GABA currents to approximately 80% of control (Arakawa et al., 1991). The mechanism for HgCl<sub>2</sub> potentiation of GABA-induced currents includes G protein and protein kinase A (PKA)-coupled pathways, while the mechanism of MeHg reduction of these currents has not been elucidated (Huang and Narahashi, 1997a, b). When applied alone,

both organic and inorganic mercury induce a slow, inward current in afferents which is not mediated by voltage-activated cation channels or GABA-mediated Cl<sup>-</sup> channels, suggesting the mercurials also act upon non-specific cation channels (Arakawa et al., 1991, Narahashi et al., 1994, Huang and Narahashi, 1997a, b). Given the importance of ion gradients in maintaining membrane excitability and propagating action potentials, the distinct effects of both MeHg and HgCl<sub>2</sub> on ion channels may contribute to abnormal electrical properties observed in afferents exposed to mercurials.

Ionic balance is not only important for maintaining electrical homeostasis in afferents, but also biochemical homeostasis. Although MeHg blocks current carried through VGCCs (Shafer and Atchison, 1991, Leonhardt et al., 1996b, Sirois and Atchison, 2000, Peng et al., 2002, Hajela et al., 2003, Tarabová et al., 2006), it also disrupts [Ca<sup>2+</sup>]<sub>i</sub> homeostasis. Regulation of [Ca<sup>2+</sup>]<sub>i</sub> is critical given the central role of this cation in basic neuronal functions, including protein synthesis and synaptic transmission. Indeed, protein synthesis is reduced by 60% in the DRG of animals treated with MeHg for 7 days (10 mg/kg/day). The reduction in protein synthesis persists beyond cessation of MeHg treatments and into the symptomatic period, or approximately day 15 of exposure (Omata et al., 1982). However, the reduction in protein synthesis is not uniform and depends upon the gene product, where production of a majority of proteins is suppressed, though some are upregulated (Kasama et al., 1989). Alterations protein synthesis within MeHg-exposed DRG can lead to phenotypic changes of these neurons. Primary adult mouse DRG cultures exposed to  $0.1 - 1 \mu M$  MeHg for 24 h display a rise in the percentage of substance P and calcitonin generelated peptide immunoreactivity (Baxter and Smith, 1998), both of which are immunologic markers for discrete subtypes of small-fiber nociceptive neurons (Otten et al., 1980, Jeftinija and Jeftinija, 1990). It is suggested that these alterations in DRG immunoreactivity may contribute to

abnormal nociceptive responses in MeHg poisoning (Baxter and Smith, 1998). Additionally, neurite outgrowth is inhibited in both chick ( $TD_{50} = 2 \mu M$ ) (Nakada et al., 1981) and embryonic rat DRG cultures ( $TD_{50} = 0.5 \mu M$ ) (Wilke et al., 2003).

Disruption of electrical and biochemical homeostasis in sensory afferents leads to apoptosis (Wilke et al., 2003), and eventual neurodegeneration (Chang and Hartmann, 1972). Putative cellular targets through which MeHg exerts neurotoxicity include mitochondria (Levesque et al., 1992, Hare et al., 1993, Limke and Atchison, 2002, Limke et al., 2003), IP<sub>3</sub>-sensitive stores (Hare and Atchison, 1995a, Limke et al., 2003), and ion channels (Shafer et al., 1990, Arakawa et al., 1991, Shafer and Atchison, 1991, Hare and Atchison, 1995b, Peng et al., 2002, Hajela et al., 2003, Yuan and Atchison, 2003, 2005, Ramanathan and Atchison, 2011), though none of these targets are exclusive to DRG, let alone large-fiber DRG. Mechanistic studies indicate a complexity in the actions of MeHg, and dysfunction at multiple cellular targets may concertedly elicit toxicity. However, the fact that  $A\beta$  afferents are uniquely susceptible to MeHg suggests a molecular feature of these neurons may also be involved in events leading to cell death and neurodegeneration.

### 1.1.7. The transient receptor potential channel superfamily

The transient receptor potential (TRP) family of ion channels is organized into 6 distinct subgroups and consists of at least 30 known gene products. These nonspecific cation channels have permeability to Ca<sup>2+</sup> which varies across channel subtypes. Roles of TRPs in cellular physiology differ as widely as the range of chemical, mechanical, and thermal stimuli which activate the channels; in some cases, channel function or means of activation are unknown. Because of their high expression in DRG and sensory organs, TRPs have been implicated as critical components of sensory transmission. Within DRG, TRP expression is localized to the peripheral and central

terminals, as well as the soma. (Liedtke and Heller, 2007, Islam, 2011). Therefore, if a target of MeHg, dysfunction of TRPs may lead to perturbations in receiving, integrating, and transmitting sensory information. An isoform of the ankyrin family of TRPs, TRPA1, is of particular interest for its polymodal means of activation.

TRPA1 channels are tetrameric proteins, with each subunit consisting of consisting of 6 membrane-spanning segments and 14 – 19 characteristic N-terminal ankyrin repeats (Fig. 1.4) (Story et al., 2003, Nilius and Owsianik, 2011, Nilius et al., 2011). The ankyrin repeats interact with the cell's cytoskeleton and serve as a molecular spring, tranducing mechanical force into changes in gating at the channel pore (Zaytas et al., 2013). An EF-hand located among ankyrins on the N-terminus promotes TRPA1 activation by binding Ca<sup>2+</sup>, thus TRPA1 current is potentiated by [Ca<sup>2+</sup><sub>i</sub>] elevation (Doerner et al., 2007, Nilius et al., 2011, Zaytas et al., 2013). The pore of the channel is formed by the linker region between transmembrane segments 5 and 6; two negatively charged aspartic acid and glutamic acid residues residing in this linker region are believed to serve critical roles in determining the Ca<sup>2+</sup> permeability of the channel (Karashima et al., 2010, Bobkov et al., 2011, Nilius et al., 2011).

TRPA1 is widely expressed in DRG, and nodose and trigeminal ganglia (Story et al., 2003, Liedtke and Heller, 2007), though an increasing number of studies are finding TRPA1 in numerous other organs, including the brain (Koch et al., 2011, Shigetomi et al., 2011, Yokoyama et al., 2011), heart (Pozsgai et al., 2010, Early, 2012), lung (Mukhopadhyay et al., 2011, Nassini et al., 2012), and bladder (Du et al., 2007, Streng et al., 2008, Skryma et al., 2011). Within DRG, TRPA1 is localized in the soma, and both the peripheral and central terminals, and is involved in glutamatergic excitatory transmission (Uta et al., 2010, Inoue et al., 2012). A number of chemical

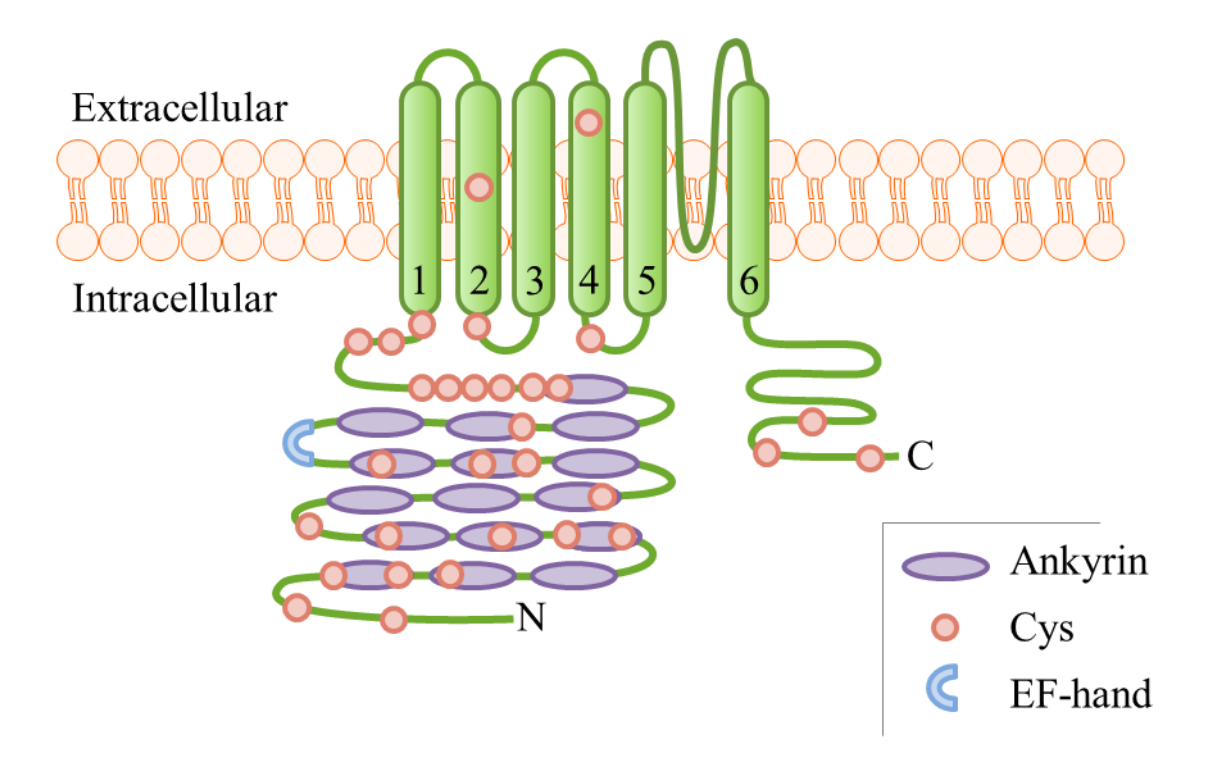


**Figure 1.4. Schematic of TRPA1 channel structure.** TRPA1 is a tetrameric protein, with each subunit consisting of 6 membrane-spanning domains. The channel is characterized by the 14-19 ankyrin-repeat domain at the N-terminus which tethers the membrane-bound channel to the cell's cytoskeleton. Mechanical force at this domain is propagated to the pore and gate to control TRPA1 activity. Over 30 critical cysteine residues, many at the N-terminus, interact with cysteine-reactive chemical irritants to increase the channel's probability of opening. Furthermore, TRPA1 activity can be modulated in a Ca<sup>2+</sup>-dependent manner at the EF-hand. Adapted from Takahashi and Mori (2011).

irritants and inflammatory mediators are agonists for TRPA1(Bandell et al., 2004, Jordt et al., 2004, Sadofsky et al., 2011, Komatsu et al., 2012), activating the channel through covalent modification of N-terminal cysteine residues (Macpherson et al., 2007, Takahashi et al., 2008, Cvetkov et al., 2011, Wang et al., 2012). Thus, the role of TRPA1 as a chemosensor and transducer of inflammatory pain is well characterized. However, the numerous N-terminal ankyrin repeats on TRPA1 implicates another critical role for the channel in mechanosensation. This function of TRPA1 is more enigmatic, though early studies demonstrate *trpa1* loss-of-function mutant invertebrates and *trpa1*-/- mice display altered or abolished mechanotransduction (Walker et al., 2000, Kindt et al., 2007, Kwan et al., 2009).

## 1.1.8. Actions of mercurials on transient receptor potential channels

The only investigation into the action of mercurials on TRPs was performed using heterologously-expressed TRPC isoforms, of the "canonical" TRP family. TRPC channels are store-operated channels, and activated directly by phospholipase C and diacylglycerol (Liedtke and Heller, 2007). TRPC channels were transfected into HEK cells and acutely exposed to either MeHg or HgCl<sub>2</sub> ( $0.1-10~\mu M$ ). Studies reveal the influx of  $Ca^{2+}$  through TRPC4 and TRPC5 is increased by both MeHg ( $EC_{50}=2.03~\mu M$ ) and HgCl<sub>2</sub> ( $EC_{50}=3.07~\mu M$ ) through interaction at two critical cysteine residues within the channel pore. The interaction between the channel and mercurials is believed to be specific, as other divalent heavy metals, such as  $Cd^{2+}$  and  $Zn^{2+}$  had no effect on  $Ca^{2+}$  influx. Similarly, mercurials did not elicit a stimulatory effect on all TRPs; TRPC3, TRPC6, TRPV1, and TRPM2 are among the TRP isoforms (from the canonical, vanilloid, and melastatin subfamilies) for which exposure to either MeHg or HgCl<sub>2</sub> does not enhance nor abolish  $Ca^{2+}$  entry through the channel. MeHg-induced cell death of TRPC5-expressing cells is reduced following treatment with specific channel blockers or siRNA against TRPC5 (Xu et al., 2012).

Though this provides reasonable evidence that this emerging class of ion channels may be a target of MeHg, studies need to be performed in primary tissues in which the full population of receptors and ion channels are available to interact with and modulate one another.

# 1.2. Research objective and rationale

# 1.2.1. Hypothesis

My central hypothesis is that nonspecific, Ca<sup>2+</sup>-permeable ion channels highly expressed in DRG are sensitive molecular targets of MeHg and contribute to MeHg-induced Ca<sup>2+</sup>i dysregulation, altered electrophysiologic properties, and DRG neurotoxicity. The basis for this hypothesis is three-fold. First, MeHg induces a slow, irreversible inward current insensitive to pharmacologic block of the GABA<sub>A</sub> receptor and voltage-gated Ca<sup>2+</sup>, Na<sup>+</sup>, and K<sup>+</sup> and channels, but sensitive to chelation of Ca<sup>2+</sup>, by BAPTA (Arakawa et al., 1991, Narahashi et al., 1994). Second, antagonists of VGCCs, and ionotropic glutamate (GluR) and Ca<sup>2+</sup>-permeable nicotinic acetylcholine (nAChR) receptors slow, but do not obviate, MeHg-induced increases in [Ca<sup>2+</sup>]<sub>i</sub> and cytotoxicity (Marty and Atchison, 1997, Ramanathan and Atchison, 2011). Finally, non-excitable HEK cells lacking endogenous expression of VGCCs, GluRs, and nAChRs exhibit a Ca<sup>2+</sup>edependent multiphasic increase in Ca<sup>2+</sup><sub>i</sub> in response to MeHg (Hannon and Atchison, 2011). Expression of TRPA1 in HEK cells (Tanner et al., 2007, Buber et al., 2010, Lin et al., 2014) and Aβ DRG (Walker et al., 2000, Kindt et al., 2007, Kwan et al., 2009) could indicate that not only is this channel contributing to Ca2+ dysregulation observed in HEK cells, but this class of ion channels may be integral to the heightened susceptibility of AB DRG. Given the potential for TRPA1 to conduct Ca<sup>2+</sup> current following activation by cysteine-reactive chemical irritants (Bandell et al., 2004, Jordt et al., 2004, Macpherson et al., 2007, Sadofsky et al., 2011, Komatsu et al., 2012), TPRA1 may serve a critical role in mediating Ca<sup>2+</sup> influx and contributing to MeHginduced Ca<sup>2+</sup><sub>i</sub> dysregulation when VGCCs are otherwise blocked by the neurotoxicant (Fig. 1.5).

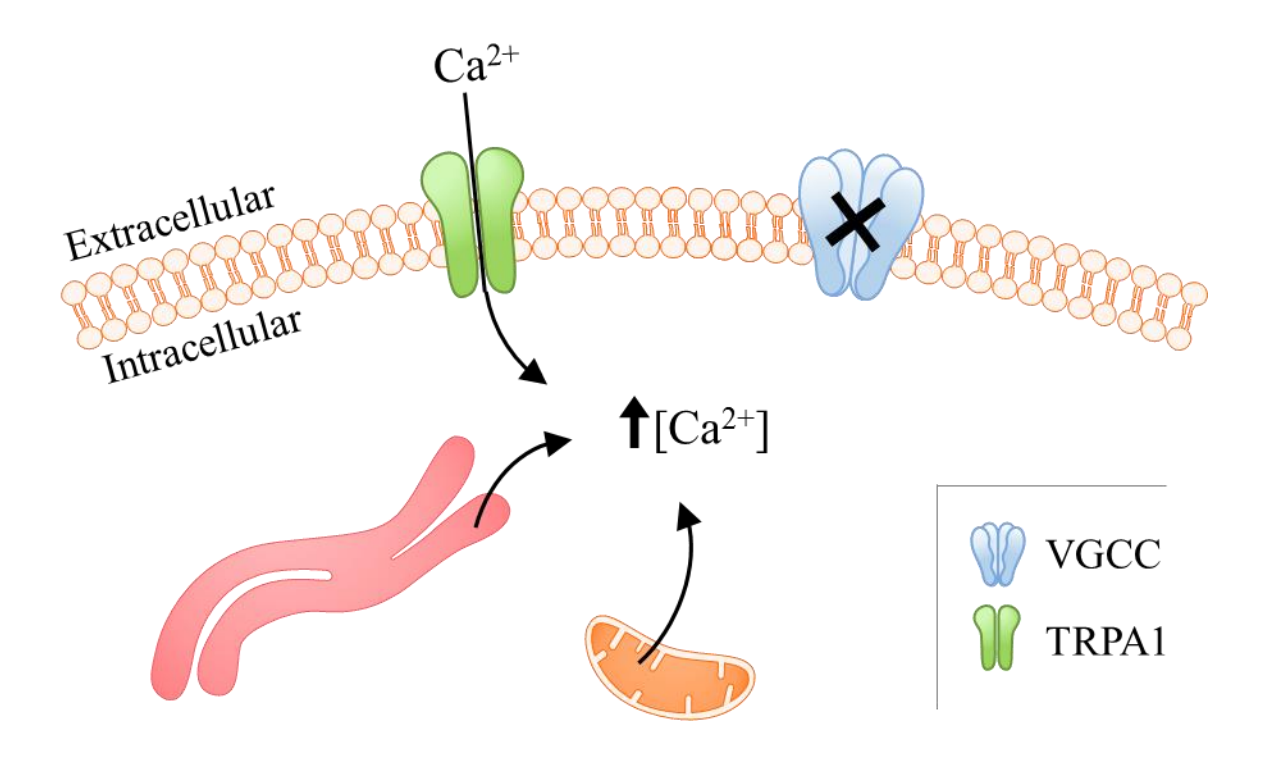


Figure 1.5. Hypothesized role of TRPA1 in mediating MeHg neurotoxicity. Because VGCCs are readily blocked by MeHg, I hypothesize there must exist another  $Ca^{2+}$ -permeable ion channel which readily contributes to MeHg-induced  $Ca^{2+}$  dysregulation. TRPA1 is a probable mediator of MeHg neurotoxicity due to its  $Ca^{2+}$  permeability, activation properties, and functional expression in Aβ DRG.  $Ca^{2+}$  influx via TRPA1, in combination with well-characterized MeHg-induced  $Ca^{2+}$  release from storage organelles, may give rise to neurotoxicity following exposure to MeHg.

### 1.2.2. Aims

The effects of MeHg on discrete  $Ca^{2+}$  entry pathways was assessed in a set of three studies. In the first, the differential sensitivity of VGCC isoforms was examined to understand whether expression of specific  $\alpha_1$  subunits would confer heightened susceptibility to MeHg-induced  $Ca^{2+}_i$  dysregulation and cell death. The second study probed the sensitivity of TRPA1 to MeHg; experiments were conducted in a heterologous expression system to isolate any TRPA1-associated changes in  $Ca^{2+}_i$  regulation and cell viability in MeHg-exposed cultures. Finally, I assessed the vulnerability of primary DRG neurons to MeHg-induced perturbations in  $Ca^{2+}_i$  regulation and subsequent cytotoxicity, as well as to determine the extent to which TRPA1 mediated these effects of MeHg exposure. Together, these studies characterize the sensitivity of discrete  $Ca^{2+}$ -permeable ion channels in a movement toward identifying molecular entities which make  $A\beta$  DRG sensitive to MeHg.

### 1.3. Model systems

### 1.3.1. Heterologous expression in human embryonic kidney cells

HEK cells were notably one of the first human cells to be transformed with a human adenovirus. The HEK-293 strain commercially available today is the product of kidney epithelial cells transformed with human adenovirus type 5 (Graham et al., 1977). This transformation results in insertion of a 4 kilobase pair DNA fragment into chromosome 19 (Louis et al., 1997), encoding for E1A and E1B proteins which disrupt the cell cycle and counteract apoptosis (Berk, 2005, Sha et al., 2010). Though adenovirus transformation was widely sought after in cells of human lineage to study adenoviruses, the application of HEK cells extends far beyond that today.

HEK cells are used extensively as model for heterologous expression studies. The endogenous biochemical components of these cells permit the complex post-translational processing required to generate mature, functional proteins with high efficiency and reproducibility (Thomas and Smart, 2005). Despite their epithelial lineage and, generally, less-sophisticated cellular architecture, there is evidence that adenovirus 5-transformed HEK cells possess properties found in cells of neuronal lineage. This includes 61 mRNAs normally expressed exclusively in neurons, such as ligand-gated and G protein-coupled receptors (see Thomas and Smart (2005) for a comprehensive list). Immunoreactivity of neurofilament subunits normally present in neurons has also been reported in native HEK (Shaw et al., 2002). Even more recently, Lin et al. (2014) sequenced the full HEK genome, permitting better informed studies of recombinant proteins. It has been hypothesized that upon transformation with adenovirus 5, genes canonically associated with a neuronal lineage and otherwise quiescent in kidney epithelial cells are turned on.

Although HEK cells share certain properties with cells of neuronal lineage, they are relatively non-excitable; small, transient inward currents (0.24 – 0.88 pA/pF) activated with a depolarizing step to -40 mV in native HEK cells have been attributed to current carried through endogenous T-type VGCCs (Berjukow et al., 1996). Given that the only endogenous VGCC channels carry small, rapidly inactivating currents (Soong et al., 1993), HEK cells have been widely used to study assembly, activation, and modulation of recombinant VGCC isoforms in isolation (Brust et al., 1993, Williams et al., 1994, Pérez-García et al., 1995, Bangalore et al., 1996, Jones et al., 1997, McCool et al., 1997). Similar molecular studies have been conducted in HEK cells expressing recombinant TRPA1 (Takahashi et al., 2008, Buber et al., 2010), among other TRP isoforms. Although native HEK cells are less sensitive to MeHg-induced cell death, as compared neuronal-derived cell lines (Vidal et al., 2011), heterologous expression in HEK cells has been powerful in understanding the manner in which MeHg alters the function of discrete ion channel isoforms (Peng et al., 2002, Hajela et al., 2003, Tarabová et al., 2006). This model was used to express recombinant VGCCs (Chapter 2) and TRPA1 (Chapter 3) to determine how these ion channels mediate MeHg-induced Ca<sup>2+</sup><sub>i</sub> dysregulation and cell death.

## 1.3.2. Primary culture of murine dorsal root ganglia neurons

Culture of DRG has been widely used, particularly in the field of neuropathic pain, for the study of molecular mechanisms of responses to mechanical (McCarter et al., 1999), chemical (Wood et al., 1988, Jordt et al., 2004), and thermal (Cesare and McNaughton, 1996, Reid et al., 2002) stimuli. The use of primary neuronal culture permits exceptional control of the extracellular environment, allowing for physiologic and pharmacologic manipulation to probe electrical and biochemical properties of DRG in response to sensory stimuli (Malin et al., 2007).

The mouse spinal cord gives rise to 34 pairs of spinal nerves (8 cervical, 13 thoracic, 6 lumbar, 4 sacral, and 3 coccygeal) (Cook, 1965); DRG can be readily identified at discrete levels of the spinal cord based upon vertebral structure and position in relation to the rib cage (Malin et al., 2007, Harrison et al., 2013). The primary DRG model is advantageous because the composition of DRG is stereotyped, with little variation from animal to animal in cell number, activation properties, and target innervation within a particular ganglion. Thus, the population of isolated cells remains consistent across parallel studies with multiple animals. Because maintenance of DRG in culture extending beyond 24 h can result in alterations of membrane electrical properties (Scott and Edwards, 1980), acutely dissociated DRG are a common alternative.

DRG can be easily removed from embryonic animals following differentiation from the neural crest in development (approximately embryonic day 10 – 13 in mice) (Lawson and Biscoe, 1979, Fariñas et al., 2002), as well as neonatal and adult animals. Whereas embryonic and neonatal cultures require trophic factors for survival, particularly nerve growth factor, DRG isolated from adults can be maintained in standard culture media (De Koninck et al., 1993, Snider and Silos-Santiago, 1996). *In vitro* studies of the actions of mercurials on primary DRG (reviewed in Chapter 1.1.3) have thus far used neonatal preparations (Arakawa et al., 1991, Huang and Narahashi, 1996, Leonhardt et al., 1996a, Leonhardt et al., 1996b). However, because the TRP expression profile develops from embryonic stages through at least post-natal day 30 (Hjerling-Leffler et al., 2007, Zhu and Oxford, 2011), these studies may not accurately reflect the response of adult DRG to mercurials. Therefore, the studies presented in Chapter 4 employed DRG isolated from juvenile (7 – 8 weeks old) to explore Ca<sup>2+</sup><sub>i</sub> perturbation and neurotoxicity associated with MeHg exposure.

## 1.4. Techniques

### 1.4.1. Ratiometric calcium imaging

Regulated increases in [Ca<sup>2+</sup>]<sub>i</sub> are critical for basic neuronal function, including protein synthesis and synaptic transmission. Conversely, when elevated [Ca<sup>2+</sup>]<sub>i</sub> is not appropriately cleared from the cytoplasm, cells can undergo metabolic rundown and cell death (Berridge, 1998). Thus, monitoring changes in [Ca<sup>2+</sup>]<sub>i</sub> throughout exposure to MeHg permits a better understanding of the timecourse of discrete events preceding cell death. Single-cell microfluorimetry, in combination with the Ca<sup>2+</sup> fluorophore Fura-2 acetoxymethylester (Fura-2 AM), allows for such real-time measurements to be made and has been used extensively in assessment of MeHg-induced [Ca<sup>2+</sup>]<sub>i</sub> disruption (Denny et al., 1993, Hare et al., 1993, Hare and Atchison, 1995a, Marty and Atchison, 1997, Limke et al., 2003, Limke et al., 2004, Edwards et al., 2005, Ramanathan and Atchison, 2011).

Fura-2 AM is a high affinity Ca<sup>2+</sup> fluorophore. The AM group makes Fura-2 lipid soluble, permitting diffusion across cell membranes. Upon reaching the cytosolic side of the plasma membrane, endogenous intracellular esterases cleave the AM group, effectively trapping Fura-2 in the cytoplasm. An advantage of using Fura-2 is the ability to make ratiometric measurements using dual-excitation and single emission; Fura-2 emits fluorescence at 505 nm following excitation at wavelengths of 340 and 380 nm, corresponding to its Ca<sup>2+</sup>-bound and unbound states, respectively. The ratio of fluorescence emissions following the dual excitation (F<sub>340/380</sub>) corresponds with relative changes in [Ca<sup>2+</sup>]<sub>i</sub>. Ratiometric measurements performed in this manner obviate differences in loading efficiency or Fura-2 concentration across the sample population (Grynkiewicz et al., 1985).

In some instances, it is possible to correlate the change in  $F_{340/380}$  with  $[Ca^{2+}]_i$  (Grynkiewicz et al., 1985). However, studies presented here will only refer to relative changes in  $[Ca^{2+}]_i$ , rather than absolute and quantifiable concentrations. Although Fura-2 has a high affinity for  $Ca^{2+}$ , other divalent cations, including zinc  $(Zn^{2+})$ , also readily bind the fluorophore and alter fluorescence. Denny et al. (1993) demonstrated MeHg induces release of intracellular  $Zn^{2+}$  and, thus, alters estimation of  $[Ca^{2+}]_i$  using Fura-2. Thus, without correcting for this  $Zn^{2+}$  component of  $F_{340/380}$ , quantification of  $[Ca^{2+}]_i$  would be inaccurate.

## 1.4.2. Patch-clamp electrophysiology

Neher and Sakmann (1976) were the first to record single channel ionic currents through the use of a new technique, patch-clamp electrophysiology. The patch-clamp technique permits real-time measurement of ion channel conductance through single channels or the whole cell, depending upon the patch orientation. Thus, this technique is useful in the study of pharmacological and toxic agents which modulate or interfere with ion channel function (Liem et al., 1995). Prior to patch-clamp, studies examining ionic current through discrete channel populations were limited to radiotracer flux studies (Tasaki et al., 1967) or microelectrode recordings (Hodgkin and Huxley, 1945). The use of large, intracellular recording electrodes in the latter precluded recording in most mammalian cells due to damage associated with electrode impalement. In contrast, patch-clamp recordings can be performed in smaller cells, and even excised membrane patches, with improved time resolution and signal-to-noise ratio (Hamill et al., 1981). This approach has been widely used to study the interaction of MeHg with native (Shafer and Atchison, 1991, Sirois and Atchison, 2000, Yuan et al., 2005) and recombinant (Peng et al., 2002, Hajela et al., 2003, Tarabová et al., 2006) VGCCs, as well as to characterize the electrical

alterations in DRG following MeHg exposure (Arakawa et al., 1991, Huang and Narahashi, 1996, Leonhardt et al., 1996a, Leonhardt et al., 1996b). The whole-cell configuration was used in the studies presented here to determine how MeHg alters function of the entire population of Ca<sup>2+</sup>-permeable ion channels through measurement of the macroscopic Ca<sup>2+</sup> current.

The voltage clamp method of patch-clamp recording is most widely used. In this approach, the membrane voltage is held at a specified potential while current across the membrane is measured. Total membrane current  $(I_m)$  is the sum of two components, ionic current  $(I_i)$  and capacitive current  $(I_c)$ :

$$I_{\rm m} = I_{\rm i} + I_{\rm c}$$

 $I_i$  is a measure of current conducted through ion channels, and is described by the following equation, where  $g_i$  is the ionic conductance,  $V_m$  is the membrane potential, and  $V_i$  is the ionic reversal potential:

$$I_i = g_i(V_m - V_i)$$

 $I_c$  is a measure of current distributed across the membrane, and is described by the following equation:

$$I_{c} = C_{m} \frac{dV_{m}}{dt}$$

 $C_m$  is membrane capacitance, and  $\frac{dV_m}{dt}$  is the rate of change in membrane potential (Hodgkin and Huxley, 1952). Because voltage is held constant  $\left(\frac{dV_m}{dt} = 0\right)$ , the  $I_m$  measured under voltage clamp is directly related to  $I_i$ . To measure current, a glass pipette filled with a conductive salt solution is positioned against the cell membrane to form a seal of gigaohm resistance. This high resistance gigaseal between the cell membrane and pipette minimizes the amount of leak current and improves the noise level of recordings. To obtain the whole-cell configuration, gentle negative

pressure is applied following formation of the gigaseal and the membrane located within the tip of the pipette is ruptured. Within minutes of obtaining the whole-cell configuration, contents of the internal pipette solution freely distribute throughout the intracellular space. Thus, the composition of both the bath and internal pipette solutions can be controlled under this patch-clamp configuration. With strategic formulation of recording solutions, specific ionic currents can be isolated or eliminated from the macroscopic current (Sigworth and Neher, 1980, Hamill et al., 1981).

## **CHAPTER TWO**

COMPARATIVE CONTRIBUTION OF RECOMBINANT VOLTAGE-GATED CALCIUM CHANNELS TO METHYLMERCURY-INDUCED CALCIUM DYSREGULATION AND CYTOTOXICITY IN HUMAN EMBRYONIC KIDNEY CELLS

#### 2.1. Abstract

In vitro MeHg exposure induces a characteristic biphasic elevation in Ca<sup>2+</sup>, which is, in part, dependent upon Ca<sup>2+</sup> influx through VGCCs. To determine whether distinct VGCC subtypes confer differential susceptibility to MeHg, cDNA clones of the pore-forming all subunit, along with accessory  $\beta_{3-a}$  and  $\alpha_{2B}\delta$  subunits, were transfected into HEK cells to produce either L-, P/Q-, N-, or R-type VGCCs. Fura-2 based microfluorimetry was used to monitor relative [Ca<sup>2+</sup>]<sub>i</sub> changes throughout exposure to MeHg (1, 2 or 5 µM). The onset of MeHg-induced Ca<sup>2+</sup><sub>i</sub> dysregulation occurred in a concentration-, VGCC subtype-, and phase-dependent manner. The onset of phase 1 differed among VGCC subtypes most significantly at 1 and 2 µM MeHg, where phase 1 was slowed in L-type-transfected HEK and hastened in all other subtypes; all VGCC-transfected cells were comparably susceptible to phase 1 Ca<sup>2+</sup><sub>i</sub> disturbances at 5 µM MeHg. N-type-transfected cells were the only to display a shortened time-to-onset of phase 2, as compared to untransfected HEK. In a separate set of experiments, cell viability was assessed after acute in vitro MeHg exposure. Viability of L-type-transfected HEK was reduced 1 h post-exposure at all tested MeHg concentrations, whereas only 5 µM MeHg reduced cell viability in P/Q-, N-, and R-typetransfected cells, as compared to untransfected HEK. Only cells transfected with R-type VGCCs were more susceptible to MeHg-induced cytotoxicity, compared to untransfected HEK, at 24 h. To determine the role of endogenously-expressed T-type VGCCs in altering Ca<sup>2+</sup>; with MeHg exposure, untransfected cells were pretreated with mibefradil, a T-type VGCC antagonist. Mibefradil treatment resulted in hastening of phase 1 and a slowing of phase 2 only at low µM MeHg, and was able to improve cell viability at both the acute and delayed timepoints. Similar results were observed in Ca<sup>2+</sup>e-free conditions. Together, these results indicate the actions of MeHg on VGCCs are more complex than simply stimulating or blocking  $Ca^{2+}_{e}$  entry through the channel pore, and endogenous VGCCs are not the sole contributors to  $Ca^{2+}_{e}$  influx in untransfected HEK.

### 2.2. Introduction

VGCCs play a critical role in intracellular signaling and have been implicated as targets for MeHg (Atchison and Narahashi, 1982, Atchison et al., 1986). In vitro studies in NG108-15 (Hare et al., 1993, Denny and Atchison, 1994) and rat cerebellar granule cells (Marty and Atchison, 1997) demonstrated that MeHg disrupts cellular Ca<sup>2+</sup> homeostasis through two temporally distinct phases, with phase 1 corresponding to Ca<sup>2+</sup> release from intracellular stores, including those which were IP<sub>3</sub>-sensitive (Hare and Atchison, 1995a, Limke et al., 2004). Phase 2 was attributed to influx of Ca<sup>2+</sup><sub>e</sub>; the onset of phase 2 is slowed in part by nifedipine, ω-conotoxin GVIA, and Ni<sup>2+</sup>, suggesting that individual VGCC subtypes uniquely contribute to MeHg-induced Ca<sup>2+</sup> dysregulation (Marty and Atchison, 1997). Moreover, there is a delay in the onset of Ca<sup>2+</sup>i disruption in cells that do not express VGCCs, indicating that the channel's pore may provide MeHg a route of entry into the cell (Edwards et al., 2002). Together, phase 1 and 2 disruptions in Ca<sup>2+</sup>; homeostasis contribute to MeHg-induced neurotoxicity, as application of Ca<sup>2+</sup> channel blockers improves survival of cerebellar granule cells exposed to MeHg (Sakamoto et al., 1996, Marty and Atchison, 1998). Paradoxically, whereas blocking VGCCs slows the phase 2 Ca<sup>2+</sup><sub>i</sub> response to MeHg, suggesting a stimulatory action of MeHg on VGCCs and Ca<sup>2+</sup>e influx, parallel electrophysiological studies produced apparently conflicting results. Extensive electrophysiological recordings in both isolated nerve terminals and cultured cells demonstrated MeHg rapidly and potently blocks current carried through VGCCs; low µM MeHg irreversibly blocks current carried through multiple VGCC subtypes in PC12 cells (Shafer and Atchison, 1991), and primary cultures of dorsal root ganglia (Leonhardt et al., 1996b) and cerebellar granule cells (Sirois and Atchison, 2000). Electrophysiological studies of the effects of MeHg on individual VGCC isoforms heterologously expressed in HEK cells suggest differential

susceptibility of the ion channel; current through N- and R-type recombinant channels is irreversibly reduced by MeHg in a time- and concentration-dependent manner (Hajela et al., 2003), while a MeHg-resistant current component persists through L-type channels following acute exposure (Peng et al., 2002).

Since MeHg blocks current through recombinant VGCCs in HEK cells when applied acutely, I sought to determine if the presence of these channels in isolation could facilitate the ability of MeHg to disrupt Ca<sup>2+</sup>; regulation. A model of heterologous expression was selected because primary cell cultures contain multiple potentially susceptible targets to MeHg, including multiple VGCC subtypes. Although HEK cells possess non-excitable properties, the absence of HVA VGCCs expression and ability to readily translate exogenous genetic material makes the system advantageous for heterologous expression of discrete VGCC isoforms (Thomas and Smart, 2005). HEK cells were transfected with human VGCC cDNA, keeping the  $\beta_{3-a}$  and  $\alpha_{2B}\delta$  subunits constant while varying the α<sub>1</sub> subunit, to produce cells expressing the L-, N-, P/Q- and R-type HVA VGCCs. Although in their native form, distinct VGCC subtypes consist of specific  $\alpha_1$  and  $\beta$ subunit combinations, the auxiliary subunit composition was kept constant to focus directly on the role of the pore-forming  $\alpha_1$  subunit. I investigated the role of the different  $\alpha_1$  VGCC subunits in mediating MeHg-induced Ca<sup>2+</sup> dysregulation and, because MeHg-induced Ca<sup>2+</sup> dysregulation and cell viability have been causally linked (Marty and Atchison, 1998), I also investigated whether differential expression of the  $\alpha_1$  subunit contributes to MeHg-induced cytotoxicity. HEK cells endogenously express low levels of LVA VGCCs (Berjukow et al., 1996), therefore untransfected cells in combination with an LVA VGCC antagonist were used to probe the susceptibility of Ttype VGCCs to MeHg. These LVA VGCCs are activated with very small membrane depolarizations and rapidly inactivate, implicating their role in mediating low-threshold Ca2+

spikes (Soong et al., 1993, Perez-Reyes, 2003). Despite the transient current carried through T-type channels, MeHg potently inhibits current through these channels (Tarabová et al., 2006).

The response of VGCC-transfected HEK cells (VGCC-HEK) to *in vitro* MeHg exposure was examined using single-cell microfluorimetry with continuous perfusion of environmentally-relevant MeHg concentrations significantly lower than whole-blood mercury concentrations in acutely poisoned individuals (Bakir et al., 1973). Monitoring changes in  $Ca^{2+}$  with this method permits the observation of a time course of toxicant-induced effects and may contribute to our knowledge of events leading up to MeHg-induced cell death (Limke and Atchison, 2009). Susceptibility of different VGCC subtypes to MeHg was also examined using a cell viability assay, allowing for a better understanding of how differential expression of the  $\alpha_1$  subunit contributes to the definitive consequences of exposure to MeHg.

#### 2.3. Methods

#### 2.3.1. Materials

HEK-293 cells (ATCC number CRL-1573) were purchased from American Type Culture Collection (Manassas, VA). Cell culture supplies, including Dulbecco's modified Eagle's medium (DMEM), antibiotics, and fetal bovine serum (FBS), were purchased from Gibco BRL (Invitrogen, Grand Island, NY). Plasmids containing expression cDNA clones of human neuronal  $Ca^{2+}$  channel subunits were provided by Dr. Kenneth A. Stauderman of SIBIA Neurosciences (San Diego, CA), now Merck Research Laboratories.  $\alpha_{1E-3}$  (Williams et al., 1994),  $\alpha_{1C-1}$ , and  $\beta_{3-a}$  clones (Mark Williams, Merck Research Laboratories, personal communication) were isolated from hippocampus;  $\alpha_{1A-2}$  was isolated from cerebellum (Hans et al., 1999),  $\alpha_{1B-1}$  was isolated from the IMR cell line (Williams et al., 1992a), and  $\alpha_{2B}\delta$  was isolated from brainstem and basal ganglia (Williams et al., 1992b).

All reagents were pure, laboratory-grade and purchased from Mallinckrodt Baker (Phillipsburg, NJ), unless otherwise noted. A 10 mM methylmercuric chloride (ICN Pharmaceuticals, Costa Mesa, CA) stock solution was prepared in double-distilled water from which test solutions were prepared daily at working concentrations. Experimental solutions were prepared in 4-(2-hydroxyethyl)piperazine-1-ethanesulfonic acid (HEPES)-buffered saline solution (HBS) containing (in mM): 150 NaCl, 5.4 KCl, 1.8 CaCl<sub>2</sub>, 0.8 MgCl, 20 D-glucose, and 20 HEPES (Sigma-Aldrich, St. Louis, MO) (pH 7.3 to with Tris). Ethylene glycol-bis(β-aminoethylether)N,N,N',N'-tetraacetic acid (EGTA)-containing solutions (EGTA-HBS) were prepared similarly to HBS solutions with the omission of CaCl<sub>2</sub> and addition of 20 μM EGTA (Sigma-Aldrich) for use in Ca<sup>2+</sup><sub>e</sub>-free experiments. Mibefradil-containing solutions were prepared daily, as needed, from a 10 mM mibefradil dihydrochloride (Santa Cruz Biotechnology, Dallas,

TX) stock solution for select experiments. Fura-2 AM was obtained from Sigma-Aldrich, and calcein acetoxymethylester (calcein AM) and ethidium homodimer-1 (EthD-1) were obtained from Molecular Probes (Invitrogen, Eugene, OR) as part of a commercial fluorometric viability assay.

### 2.3.2. HEK cell culture and transfection

HEK cells were cultured at 37°C and 5% CO<sub>2</sub> in DMEM containing 10% (v/v) FBS, 100 U/mL penicillin, 100 μg/mL streptomycin, and 250 ng/mL amphotericin B; cell passages 32 – 50 were used in experiments. Cells were plated on 35 mm polystyrene culture dishes at a density of  $6 \times 10^5$  cells/mL 24 h prior to gene transfer. During the log-growth phase, cells were transfected with a 1:1:1 M plasmid mixture of  $\alpha_{1X}$ ,  $\alpha_{2B}\delta$ , and  $\beta_{3-a}$  subunits of human neuronal VGCC cDNA, where " $\alpha_1 x$ " denotes the  $\alpha_1$  subunit that was varied to produce L-, N-, P/Q- and R-type VGCC isoforms, corresponding to  $\alpha_{1C}$ ,  $\alpha_{1B}$ ,  $\alpha_{1A}$  and  $\alpha_{1E}$  subunits, respectively. Jellyfish green fluorescent protein (GFP) cDNA was co-transfected into cells as a marker of transfection efficiency. The transfection solution was prepared in a reduced serum medium (Opti-MEM, Gibco BRL) and contained: 4.4% (v/v) FuGene (Roche Applied Science, Indianapolis, IN), 1.7% (w/v) VGCC cDNA mixture, and 0.4% (w/v) GFP cDNA. Cells were examined for transient GFP expression 48 h following transfection, and dishes containing approximately 20% GFP-expressing cells were replated at low density  $(7 \times 10^4 \text{ cells/mL})$  on 25 mm borosilicate glass coverslips coated with 0.01% (w/v) poly-L-lysine (Sigma-Aldrich) (Peng et al., 2002, Hajela et al., 2003). 24 h were allowed for cell growth and adhesion prior to use for recording. GFP cDNA was omitted from the transfection mixture for preparations for viability measurements so that fluorescence emissions from calcein (515 nm) would be unopposed from potentially interfering GFP (509 nm). Measurements for all experiments were made using cells from three independent transfections.

## 2.3.3. Single-cell microfluorimetry

Microfluorimetric imaging was performed using Fura-2 AM, a ratiometric Ca<sup>2+</sup> fluorophore, to measure relative changes in [Ca<sup>2+</sup>]<sub>i</sub>, as previously described (Hare et al., 1993, Marty and Atchison, 1997, Edwards et al., 2005). In brief, cells were rinsed three times with HBS and incubated at 37°C in 3 µM Fura-2 AM with 3 µM pluronic acid (Molecular Probes) for 45 min, at which time cells were transferred to a heated perfusion system (37°C, 2 mL/min); cells were perfused with HBS for 10 mins to allow for complete de-esterification of the fluorophore and to clear the visual field of debris and non-attached cells. Imaging was performed on a Diaphot microscope (Nikon, Tokyo, Japan) coupled to an IonOptix cation fluorescence imaging system (IonOptix, Milton, MA). Changes in Fura-2 fluorescence at excitation wavelengths 340 nm and 380 nm were monitored simultaneously from the soma of multiple cells within the same microscopic field throughout the duration of the experiment. Once stable baseline fluorescence was obtained, the perfusion buffer was changed to MeHg (1, 2, or 5 µM), and perfusion with MeHg continued at 2 mL/min for the remainder of the experiment. For experiments performed in the absence of Ca<sup>2+</sup>e, cells were perfused with EGTA-HBS for 5 min prior to MeHg exposure, and MeHg solutions were prepared in EGTA-HBS. Previous studies have measured Ca<sup>2+</sup><sub>e</sub> at 60 nM under these conditions, making the experiments nominally Ca<sup>2+</sup><sub>e</sub>-free (Marty and Atchison, 1997). For experiments with mibefradil, cells were perfused with 1 µM mibefradil for 10 min prior to and continually throughout MeHg exposure; this concentration is consistent with the IC<sub>50</sub> reported at physiological [Ca<sup>2+</sup>]<sub>e</sub> and temperatures (2 mM, 35°C), providing block of more than 75% of Ttype channel current (Martin et al., 2000). In each experiment, 5-10 cells from a given dish were monitored for changes in Fura-2 fluorescence until the fluorescence ratio (F<sub>340/380</sub>) reached plateau. With the initial application of MeHg being designated as time = 0, times-to-onset of phase 1 and

phase 2 were measured manually following exposure, as previously described (Hare et al., 1993, Marty and Atchison, 1997). Time-to-onset of phase 1 was measured as the time at which the slope of  $F_{340/380}$  rose irreversibly above baseline, while the time-to-onset of phase 2 was measured as the time at which the slope of  $F_{340/380}$  rose irreversibly above that of phase 1. Time-to-onset was calculated for each cell in the experimental field, then mean time-to-onset was calculated for that field of cells (n = 1).

### 2.3.4. Measurement of cell viability

Changes in cell viability were measured through the use of the fluorophores calcein AM and EthD-1, as previously described (Marty and Atchison, 1998, Limke and Atchison, 2002, Limke et al., 2004). Briefly, cells were plated at low density ( $3 \times 10^4$  cells/mL) in 96-well plates and incubated at 37°C for 24 h, at which time culture medium was replaced with HBS containing 0, 1, 2 or 5  $\mu$ M MeHg. Cells were exposed to MeHg for 1 h at 37°C; the duration of exposure was based on results from the aforementioned microfluorimetry experiments in which MeHg induced a biphasic elevation in Ca<sup>2+</sup>; in untransfected and VGCC- HEK cells within 1 h. Following exposure, MeHg was replaced with conditioned growth medium and cells were returned to the incubator. A similar exposure paradigm was used for Ca<sup>2+</sup>e-free experiments, except that MeHg solutions were made in EGTA-HBS and cells were incubated in medium containing 20  $\mu$ M EGTA post-exposure. For experiments with mibefradil, 1  $\mu$ M mibefradil was applied to cells as a pretreatment (10 min) prior to MeHg, and was contained in the MeHg treatment solution and post-exposure conditioned growth medium.

Viability was assessed at acute (1 h) and delayed (24 h) timepoints immediately postexposure. Cells were washed three times with HBS prior to simultaneous staining with assay reagents according to the manufacturer's instructions; in this assay, green-fluorescent calcein AM labeled viable cells while red-fluorescent EthD-1 labeled dead cells (Papadopoulos et al., 1994). MeHg exposure disrupts microtubule stabilization and cell adhesion (Abe et al., 1975, Imura et al., 1980, Vogel et al., 1985), therefore gentle centrifugation (140 g, 3 min) was applied in between washes to minimize the loss of cells. Cells were incubated with 0.1 μM calcein AM and 0.5 μM EthD-1 for 45 min at 37°C, at which time cells were examined under a Nikon Eclipse fluorescence microscope. Percentage of viable cells was determined by counting the live and dead cells in 3 distinct regions within the same well; the average number of live and dead cells was used in calculating viability for the well as follows:

Mean percent viabilities from triplicate wells (n = 1) were then normalized to the viability of cells which were not exposed to MeHg, but underwent all the experimental manipulations in standard DMEM to account for changes in viability attributed to transfection or cell culture conditions.

### 2.3.5. Statistics

The design was one of repeated measures: each experiment was performed in replicates of nine with cells from a minimum of three independent transfections, and data are presented as mean  $\pm$  standard error of the mean (SEM). Data were analyzed using the GraphPad Prism® statistical program (GraphPad Software Inc., San Diego, CA). A two-way analysis of variance (ANOVA) was performed to compare responses produced in multiple Ca<sup>2+</sup> channel subtypes or with mibefradil treatment, and MeHg concentrations. A *post hoc* Tukey's test was used when significant differences between sample means were detected (Steel and Torrie, 1960). Values of p < 0.05 were considered to be statistically significant.

## 2.4. Results

2.4.1. Characteristics of MeHg-induced  $Ca^{2+}{}_{i}$  dysregulation mediated by recombinant transiently expressed  $\alpha_{l}$  subunits in HEK cells

In initial experiments probing the response to *in vitro* MeHg application in untransfected HEK cells, a 2 min exposure to 40 mM KCl was used to confirm cell viability and Ca<sup>2+</sup> buffering capabilities. Such a KCl pulse induces membrane depolarization and a subsequent rise in Ca<sup>2+</sup><sub>i</sub> in multiple primary and immortalized excitable cell lines (Dyer et al., 1992, Marty and Atchison, 1997, Edwards et al., 2005, Lu et al., 2006, Ramanathan and Atchison, 2011); this effect can be observed as a rise in F<sub>340/380</sub>, which promptly returns to baseline in viable cells when the perfusion buffer is switched back to HBS. However, untransfected HEK cells did not display KCl-induced depolarizations, likely due to expression of few endogenous voltage-gated channels (Thomas and Smart, 2005, Lin et al., 2014).

In every instance, acute exposure of untransfected or VGCC- HEK cells to MeHg caused the characteristic rise in F<sub>340/380</sub> (Fig. 2.1A). The response was always multiphasic and consisted of at least two temporally distinct phases. Phase 1 of this response presented as an initial, rapid rise in F<sub>340/380</sub> which typically, but not universally, returned to baseline fluorescence measurements after a few minutes. Those cells which did not recover to near-baseline fluorescence after the onset of phase 1 were excluded from the study, as this is indicative of a cell's inability to buffer adequately sudden changes in Ca<sup>2+</sup><sub>i</sub>. In every case, cells also exhibited a second rise in F<sub>340/380</sub> that was sharp and irreversible. In both untransfected and VGCC-HEK cells, the two "classic" phase responses were separated by an "intermediate phase" which consisted of a slow rise in baseline fluorescence preceding the onset of phase 2; this observation of an intermediate phase is a unique response of HEK cells to acute exposure to MeHg, as it has not been reported in other cell types

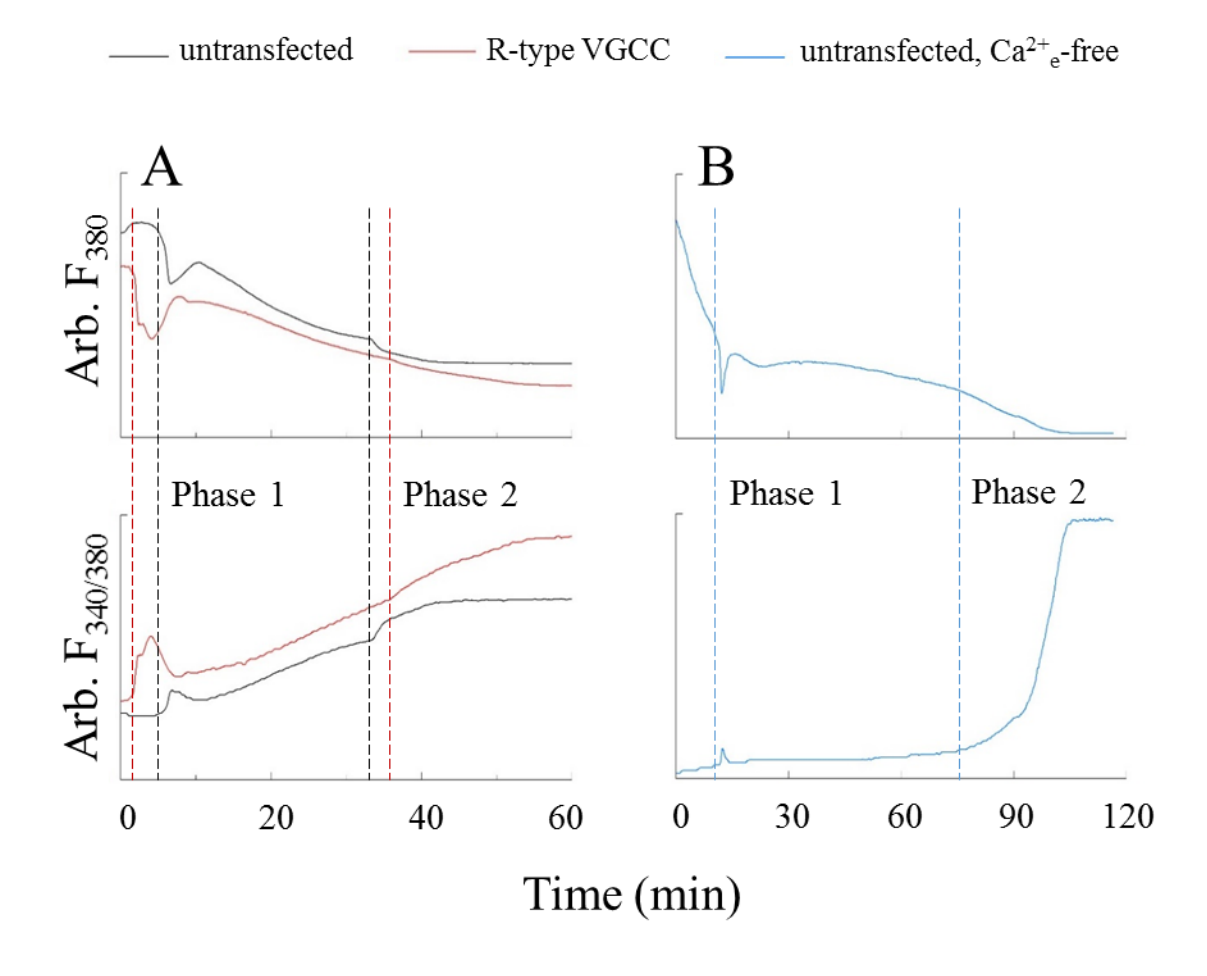


Figure 2.1. HEK cells exposed to MeHg display a multiphasic elevation in  $Ca^{2+}_i$  that is independent of VGCC expression and  $Ca^{2+}_e$ . (A) A multiphasic decrease in the  $F_{380}$  signal and increase in  $F_{340/380}$  was observed in all untransfected and VGCC-transfected cells with continuous perfusion of MeHg. Representative tracings from an untransfected (black) and R-type-transfected (red) HEK cell depict two clearly distinguishable phases and a steadily changing intermediate phase. (B) The multiphasic  $F_{340/380}$  response to MeHg application persisted in untransfected cells when  $Ca^{2+}_e$  was removed from the superfusion solution, though the intermediate phase was eliminated under this condition. Hashed lines indicate where the times-to-onset of phase 1 and 2 were lineated. All tracings are from cells exposed to 1  $\mu$ M MeHg, with application of MeHg beginning at t = 0.

in comparable studies (Hare et al., 1993, Marty and Atchison, 1997, Edwards et al., 2005, Ramanathan and Atchison, 2011).

A biphasic rise in  $F_{340/380}$  was also observed in untransfected HEK cells with the removal of  $Ca^{2+}_{e}$  (Fig. 2.1B), despite previous studies demonstrating the  $Ca^{2+}_{e}$ -dependent nature of phase 2 in neurons or synaptosomes (Denny et al., 1993, Hare et al., 1993, Marty and Atchison, 1997). Interestingly, the intermediate phase was obviated under these conditions. These results demonstrate the  $Ca^{2+}_{e}$ -dependence of the intermediate phase, suggesting there exists an endogenous  $Ca^{2+}$  entry pathway in untransfected HEK cells which participates in MeHg-induced  $Ca^{2+}_{i}$  elevations.

To better understand the intermediate phase observed in both untransfected and VGCC-HEK, tracings of the Fura-2 fluorescence at 380 nm excitation (F<sub>380</sub>) were examined (Fig. 2.1A–B). Because Fura-2 has affinity for other divalent cations and MeHg can increase cytosolic Zn<sup>2+</sup> (Denny and Atchison, 1994), it was not implausible that the intermediate phase could be a Ca<sup>2+</sup> independent effect (Grynkiewicz et al., 1985, Hare and Atchison, 1995a). Hare et al. (1993) reported F<sub>380</sub> was unaltered while F<sub>360</sub>, the isobestic point for Ca<sup>2+</sup>, displayed pronounced elevations in MeHg-exposed NG108-15 cells; increases in F<sub>360</sub> were subsequently blocked with the pretreatment of the Zn<sup>2+</sup> chelator N,N,N',N'-tetrakis(2-pyridylmethyl)ethane-1,2-diamine (TPEN). Thus, examination of the F<sub>380</sub> signal in these studies reasonably serve as an indicator of the divalent cation contributing to the steadily rising intermediate phase. The F<sub>380</sub> signal of all HEK cells, untransfected or VGCC-transfected, steadily decreased throughout the intermediate phase, revealing this component to be an effect of Ca<sup>2+</sup> from some undetermined source.

# 2.4.2. Contribution of $Ca^{2+}_{e}$ to MeHg-induced $Ca^{2+}_{i}$ dysregulation in untransfected HEK cells

Times-to-onset of phases 1 and 2 in untransfected HEK cells were inversely proportional to the concentration of MeHg at 1 and 2 µM MeHg. Exposure to 5 µM MeHg resulted in timesto-onset of both phase 1 and 2 similar to those measured with 2 µM exposures, indicating processes contributing to the biphasic elevation of Ca2+i in HEK cells may become saturated at low µM MeHg. Removal of Ca<sup>2+</sup>e from the perfusion buffer revealed a potentially complex interaction in phase 1; while Ca<sup>2+</sup>e-free conditions slowed the time-to-onset of phase 1 at 2 µM MeHg, the onset of phase 1 was hastened under the same conditions with exposure to 5 µM MeHg (Fig. 2.2A). Whereas phase 1-mediated Ca<sup>2+</sup><sub>i</sub> elevations have canonically been attributed to release of Ca<sup>2+</sup> from intracellular stores in other cell types (Hare and Atchison, 1995a, Limke et al., 2003, Limke et al., 2004), these results are the first to indicate a contribution of Ca<sup>2+</sup><sub>e</sub> in phase 1 Ca<sup>2+</sup><sub>i</sub> dysregulation in untransfected HEK cells, perhaps through Ca<sup>2+</sup>-induced Ca<sup>2+</sup> release. Removal of Ca<sup>2+</sup><sub>e</sub> slowed, but did not eliminate, the onset of phase 2 at all MeHg concentrations (Fig. 2.2B). Although this suggests Ca<sup>2+</sup>e influx contributes prominently to the onset of phase 2, the persistence of phase 2 under Ca<sup>2+</sup><sub>e</sub>-free conditions reveals alternative Ca<sup>2+</sup><sub>e</sub>-independent pathways also participate in phase 2 Ca<sup>2+</sup> disturbances.

# 2.4.3. Effect of the VGCC $\alpha_1$ subunit on the rate of onset of MeHg-induced $Ca^{2+}{}_i$ dysregulation and concomitant cytotoxicity in transfected HEK

While the times-to-onset in all VGCC-HEK exhibited concentration dependence, the responses varied in several surprising ways as a function of the type of VGCC expressed. The expression of either P/Q-, N-, or R-type VGCCs shortened the time-to-onset of phase 1 compared to untransfected cells. In contrast, cells transfected with the L-type channel exhibited a slower

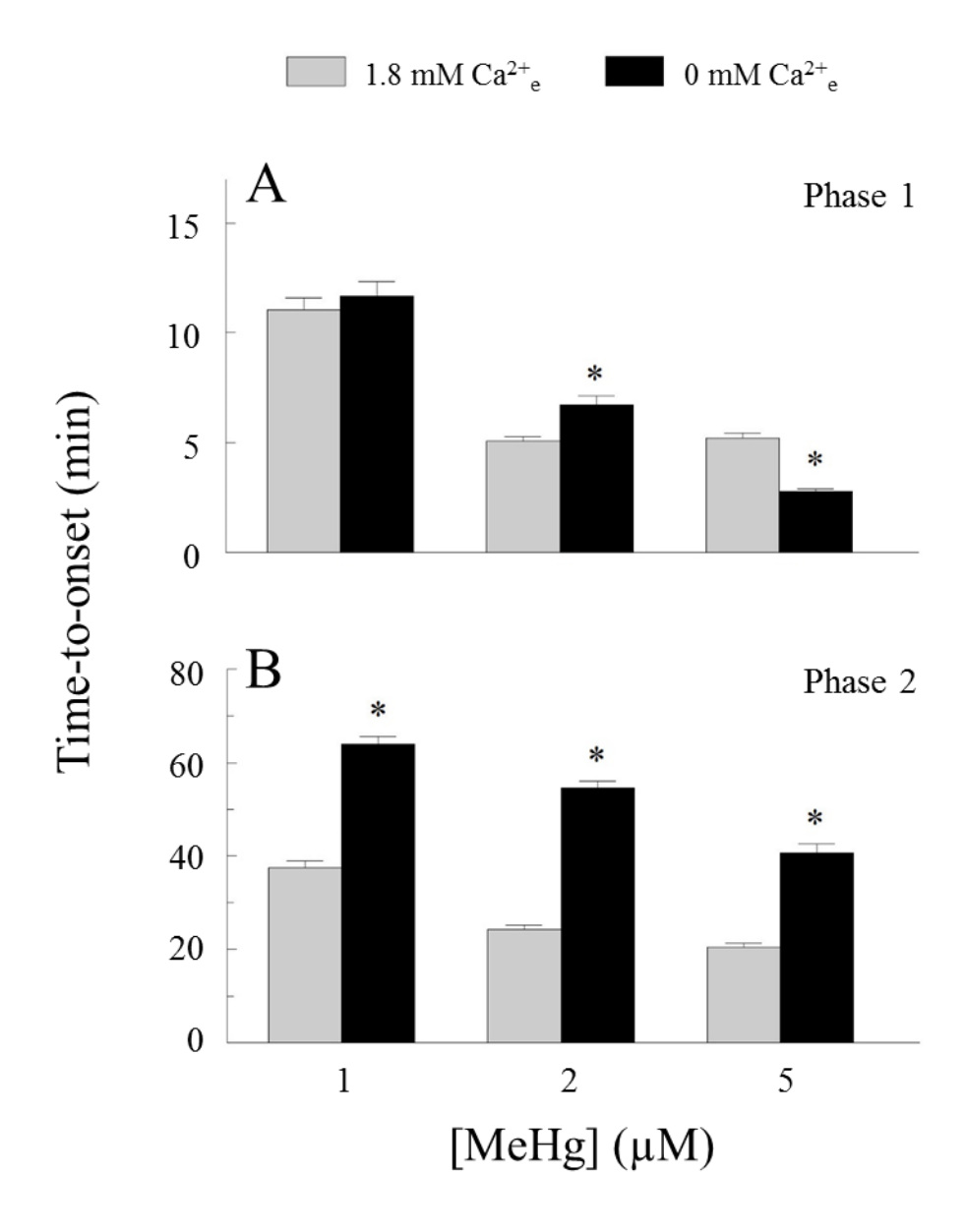


Figure 2.2. Comparative effects of  $Ca^{2+}_e$  on times-to-onset of MeHg-induced  $Ca^{2+}_i$  elevations in untransfected HEK. Untransfected HEK cells were superfused with MeHg in either standard HBS (1.8 mM  $Ca^{2+}_e$ ) or EGTA-HBS (0 mM  $Ca^{2+}_e$ ) while simultaneously monitoring changes in  $F_{340/380}$ . (A) Time-to-onset of phase 1 was hastened at 5  $\mu$ M MeHg in the absence of  $Ca^{2+}_e$ , but slowed at 2  $\mu$ M MeHg, as compared to exposures with 1.8 mM  $Ca^{2+}_e$  present. (B) Time-to-onset of phase 2 was delayed in a concentration-dependent manner in  $Ca^{2+}_e$ -free conditions for all tested MeHg concentrations. A significant difference from MeHg concentration-matched controls in 1.8 mM  $Ca^{2+}_e$  is denoted by \* (p < 0.05, n = 9).

onset of phase 1 at 1  $\mu$ M MeHg compared to all other VGCC-HEK and untransfected cells. Variations in the time-to-onset of phase 1 among the VGCC-HEK were more apparent at 1 and 2  $\mu$ M MeHg, whereas all VGCC-HEK were equally susceptible to more rapid Ca<sup>2+</sup><sub>i</sub> elevations at 5  $\mu$ M MeHg (Fig. 2.3A). These data indicate an important role for distinct VGCC subtypes in mediating phase 1 of MeHg-induced Ca<sup>2+</sup> dysregulation.

The time-to-onset of phase 2 was significantly shortened at all MeHg concentrations only in cells transfected with the N-type VGCCs. Phase 2 time-to-onset of N-type-transfected cells was also more rapid than any other VGCC subtype. L- and R-type-transfected cells varied from one another in the time-to-onset of phase 2 at all MeHg concentrations, though neither were consistently different from untransfected nor P/Q-type-transfected cells (Fig. 2.3B). With the exception of the N-type VGCC, these results demonstrate little variation in VGCC subtype sensitivity in the onset of phase 2, and are consistent with electrophysiological recordings of current carried through heterologously-expressed VGCCs in HEK cells; irreversible block of current carried through the recombinant L-, N- and R-type channels occurs in less than 10 min at MeHg concentrations between 1.25 and 5 µM (Peng et al., 2002, Hajela et al., 2003).

Because MeHg-induced cytotoxicity has been causally linked to unregulated elevations in [Ca<sup>2+</sup>]<sub>i</sub> (Marty and Atchison, 1998), I next determined whether expression of distinct VGCC subtypes influenced cell viability following acute *in vitro* MeHg exposure. VGCC-HEK cells were exposed to MeHg for 1 h, at which time cells were returned to normal growth medium. Because all cells, regardless of VGCC subtype expression, reached phase 2 in less than 1 h, this exposure time was expected to be sufficient to elicit the characteristic biphasic elevation in Ca<sup>2+</sup><sub>i</sub>. Acute and delayed viability measurements were made at 1 and 24 h, respectively, following MeHg

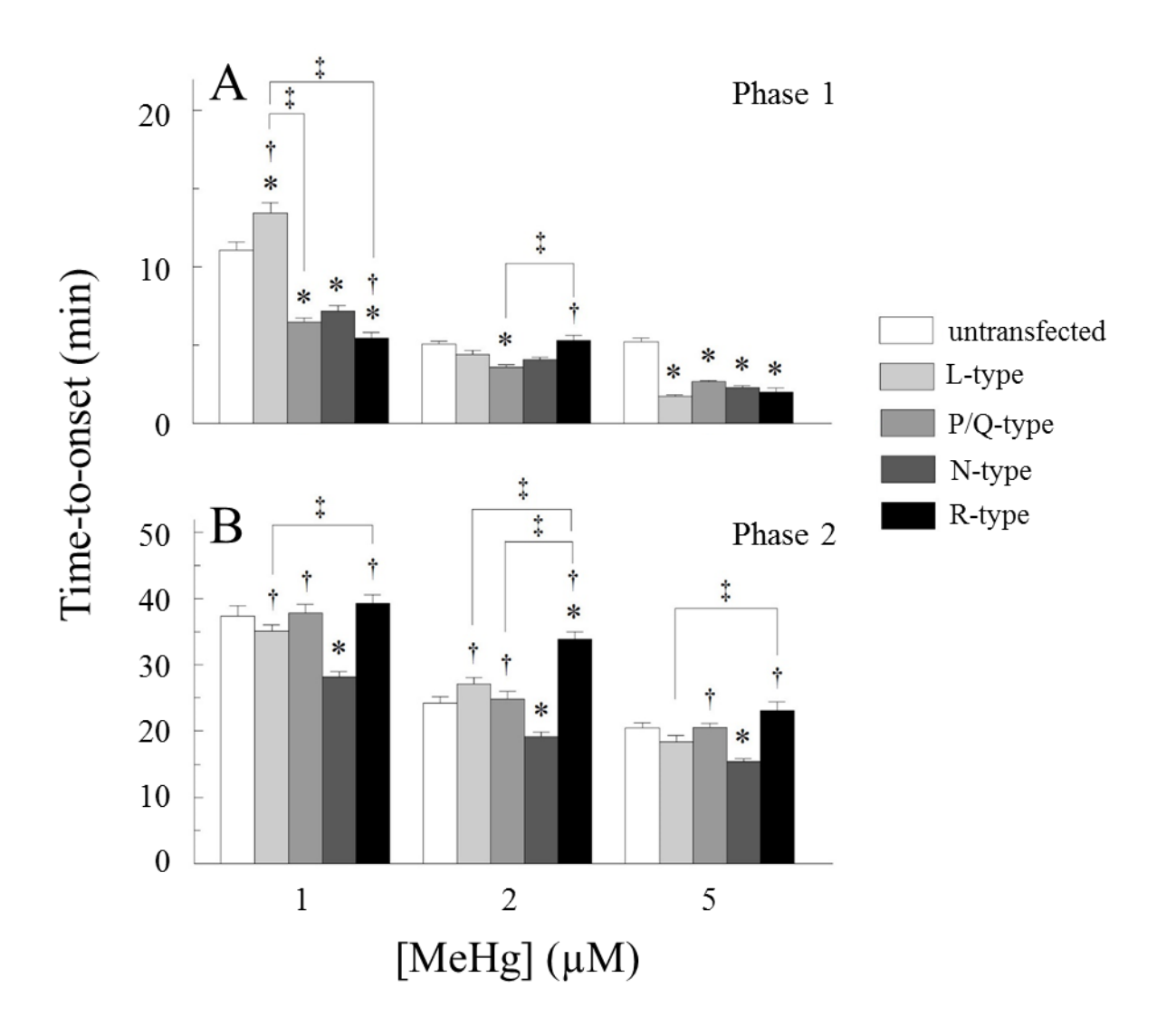


Figure 2.3. Application of MeHg alters the times-to-onset of phase 1 and 2  $Ca^{2+}i$  elevations in VGCC-HEK in both a concentration- and VGCC subtype-dependent manner. (A) Time-to-onset of phase 1 was hastened in VGCC-HEK, regardless of subtype, with more pronounced subtype specificity measured at lower [MeHg]. (B) Phase 2 time-to-onset was hastened in N-type-transfected cells at all [MeHg] and R-type-transfected cells at intermediate [MeHg], as compared untransfected HEK. Variations in phase 2 time-to-onset among VGCC subtypes, notably between L- and R-type-transfected cells, was measurable at all [MeHg]. A significant difference from concentration-matched untransfected cells is denoted by \*; significance from N-type-transfected cells is denoted by †. Additional significant differences between concentration-matched VGCC subtypes are denoted as ‡ for the indicated pair (p < 0.05, n = 9).

exposure. Acute viability of untransfected cells exposed to either 1 or 2  $\mu$ M MeHg was not significantly reduced, indicating that perturbations in Ca<sup>2+</sup><sub>i</sub> resulting from low  $\mu$ M MeHg exposure were not sizable enough to induce cytotoxicity in the absence of VGCC expression. Viability of L-type-transfected cells was significantly reduced across all concentrations of MeHg exposure at an acute timepoint, as compared to untransfected cells; P/Q-type-transfected cells were the only other subtype to display reduced viability at this timepoint, though only at 5  $\mu$ M MeHg. Cells transfected with either the N- or R-type VGCC were relatively resistant to acute cytotoxicity following MeHg exposure (Fig. 2.4A).

Cell viability was observed to be inversely related to the concentration of MeHg 24 h following exposure. R-type-transfected cells were susceptible to delayed cytotoxicity only at 1 µM MeHg, whereas viability of cells transfected with other VGCC subtypes did not vary from untransfected controls (Fig. 2.4B). Cytotoxicity at 24 h did not differ significantly from that at 1 h in untransfected HEK or L-type-transfected cells, suggesting the cytotoxic effects of MeHg are more immediate in these cells. In contrast, R-type-transfected cells display a time-dependence of cytotoxicity. Together, these viability findings are inconsistent with the pattern of MeHg-induced Ca<sup>2+</sup> dysregulation in VGCC-HEK, suggesting VGCC subtype-specific disruptions in Ca<sup>2+</sup><sub>i</sub> may not directly result in reduced viability at the assessed timepoints.

2.4.4. Contribution of endogenously expressed LVA VGCCs on MeHg-induced  $Ca^{2+}_{i}$  dysregulation and cell viability

Because untransfected HEK displayed a similar multiphasic rise in Ca<sup>2+</sup><sub>i</sub> as VGCC-HEK, I thought to examine the role of endogenously-expressed T-type channels in mediating MeHg-induced Ca<sup>2+</sup> dysregulation in untransfected cells (Berjukow et al., 1996). Cells were pretreated

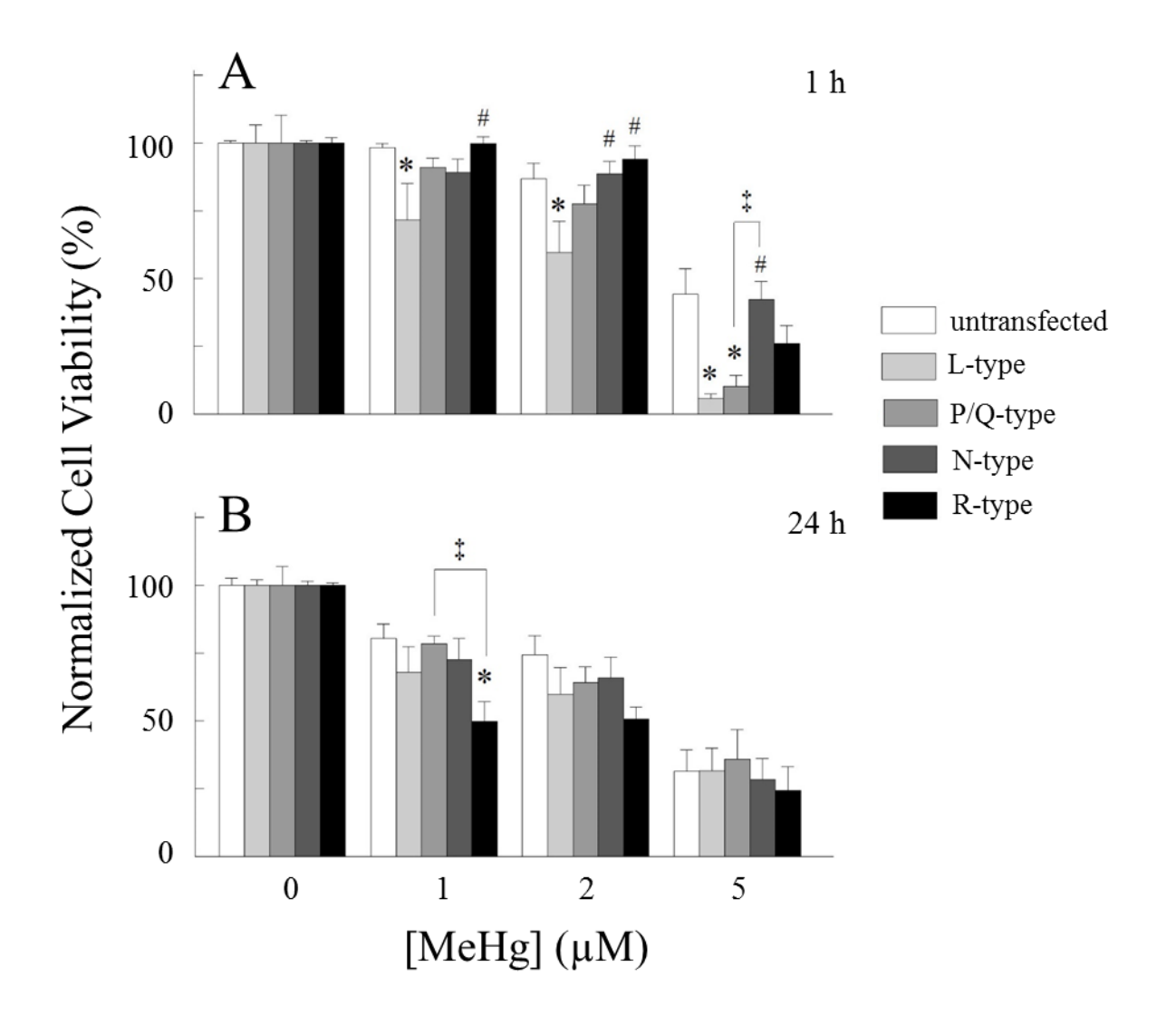


Figure 2.4. Changes in viability of VGCC-HEK are VGCC subtype-dependent at an early timepoint following acute *in vitro* MeHg exposure. VGCC-HEK were exposed to MeHg for 1 h, and cell viability was assessed at either 1 or 24 h immediately thereafter. (A) Viability 1 h post-exposure was most prominently reduced in L-type-transfected cells, as compared to untransfected HEK and cells transfected with other VGCC subtypes. Differences in viability among other VGCC subtypes were most noticeable at 5  $\mu$ M MeHg. (B) Viability 24 h post-exposure was concentration-dependent; R-type-transfected cells displayed the greatest reduction in viability, as compared to untransfected HEK and P/Q-type-transfected cells, though only at 1  $\mu$ M MeHg. A significant difference from concentration-matched untransfected cells is denoted by \*; significant differences between concentration-matched VGCC subtypes are denoted as ‡ for the indicated pair (p < 0.05, n = 9).

with 1  $\mu$ M mibefradil prior to and throughout MeHg exposures to ensure block of T-type VGCCs for the duration of the experiments (Martin et al., 2000). Untransfected HEK cells pretreated with mibefradil displayed a multiphasic elevation of Ca<sup>2+</sup><sub>i</sub> upon MeHg exposure, similar to that of the naïve cells (Fig. 2.5). Although mibefradil did not alter characteristics of the Ca<sup>2+</sup> response corresponding to phase 1 and 2, the intermediate phase appears to be less severe in the presence of mibefradil. This can be observed as a moderate return to baseline before a gradual rise in F<sub>340/380</sub>, both preceding a sharper increase in the fluorescence signal.

Interestingly, mibefradil treatment hastened the onset of phase 1 at 1 µM MeHg, suggesting a possible protective effect, through some unknown mechanism, of the endogenous T-type channel against phase 1 elevations in MeHg-induced Ca<sup>2+</sup> dysregulation. This effect was negated with higher concentrations of MeHg (Fig. 2.6A). In contrast, mibefradil slowed the time-to-onset of phase 2, indicating a contribution of T-type channels in Ca<sup>2+</sup> influx throughout MeHg exposure (Fig. 2.6B). The relationship between these perturbations in Ca<sup>2+</sup>, and viability of untransfected HEK was then explored. In addition to mibefradil pretreatment and co-exposure with MeHg, the T-type VGCC antagonist was added to the normal growth medium following MeHg exposure to negate any delayed contribution of T-type channels to cell death. Although mibefradil slowed the time-to-onset of phase 2 at low µM MeHg, there was no measurable improvement in cell viability 1 h post-MeHg exposure with pretreatment of the antagonist, likely because the viability of naïve untransfected cells at this acute timepoint was not significantly reduced. However, mibefradil improved the viability of cells exposed to 5 µM MeHg at this early timepoint (Fig. 2.7A). In contrast, mibefradil treatment increased the viability of untransfected cells 24 h following exposure to 1 and 2 µM MeHg, whereas the treatment was ineffective at improving the viability of cells exposed to 5 µM MeHg (Fig. 2.7B). These results indicate that the contribution of T-type channels

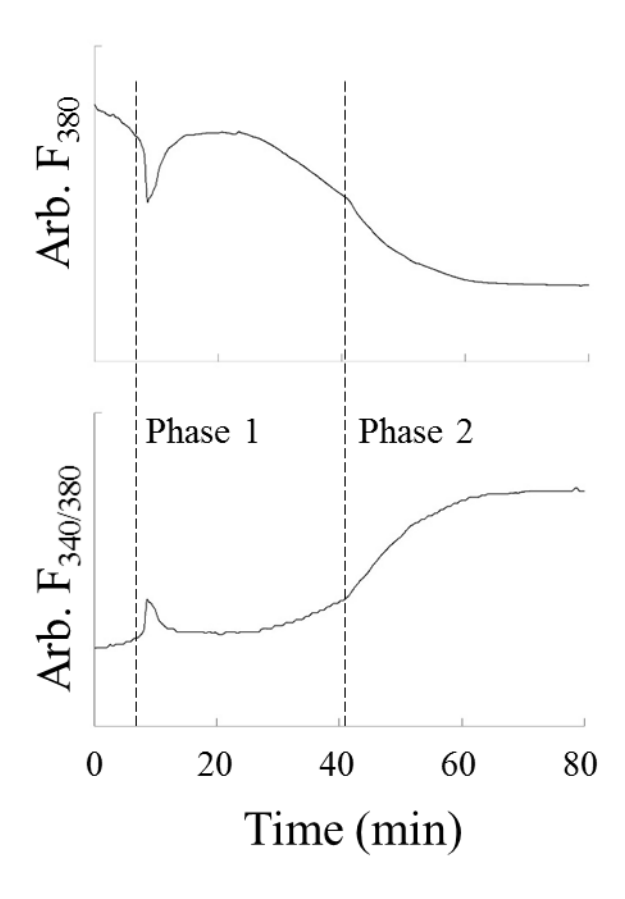


Figure 2.5. The multiphasic rise of  $Ca^{2+}$  in untransfected HEK cells induced by MeHg is not apparently dependent upon endogenous T-type VGCCs. Untransfected HEK cells were incubated in 1  $\mu$ M mibefradil 10 min prior to superfusion with MeHg. Despite pretreatment with mibefradil, MeHg-exposed cells presented marked phase 1 and phase  $Ca^{2+}$  elevations, and a steadily rising intermediate phase. Hashed lines indicate where the time-to-onset of phase 1 and phase 2 were determined. Representative tracing is from a cell co-exposed to 1  $\mu$ M mibefradil and 1  $\mu$ M MeHg, with application of MeHg beginning at t = 0.

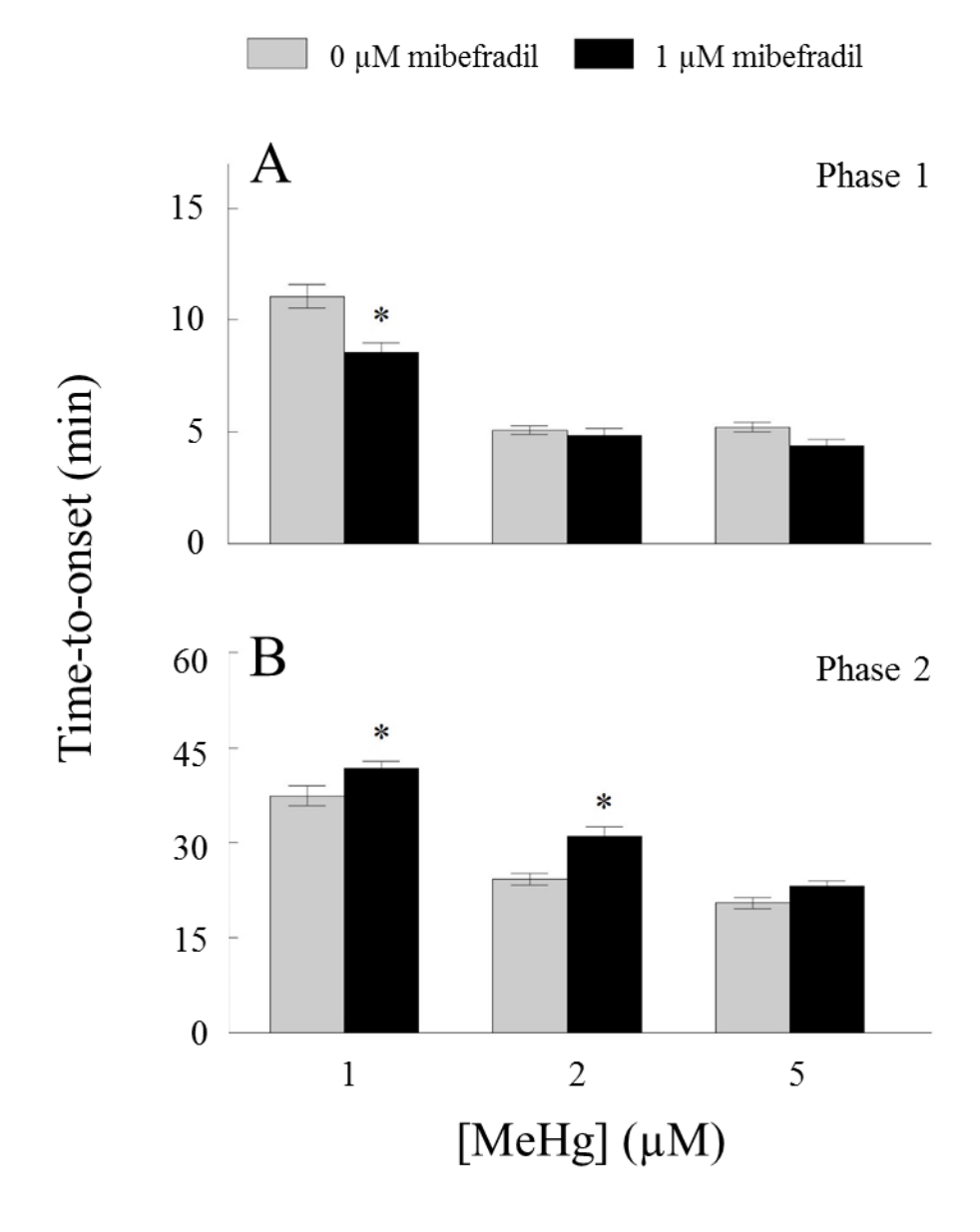


Figure 2.6. Mibefradil has contrasting effects on the times-to-onset of MeHg-induced Ca<sup>2+</sup>i elevations in untransfected HEK. Untransfected HEK cells were incubated in 1  $\mu$ M mibefradil 10 min prior to superfusion with MeHg while simultaneously monitoring changes in F<sub>340/380</sub>. (A) Time-to-onset of phase 1 was hastened with mibefradil treatment only at 1  $\mu$ M MeHg, whereas (B) phase 2 time-to-onset was slowed at both 1 and 2  $\mu$ M MeHg. A significant difference in time-to-onset resulting from mibefradil treatment is denoted by \* (p < 0.05, n = 9).

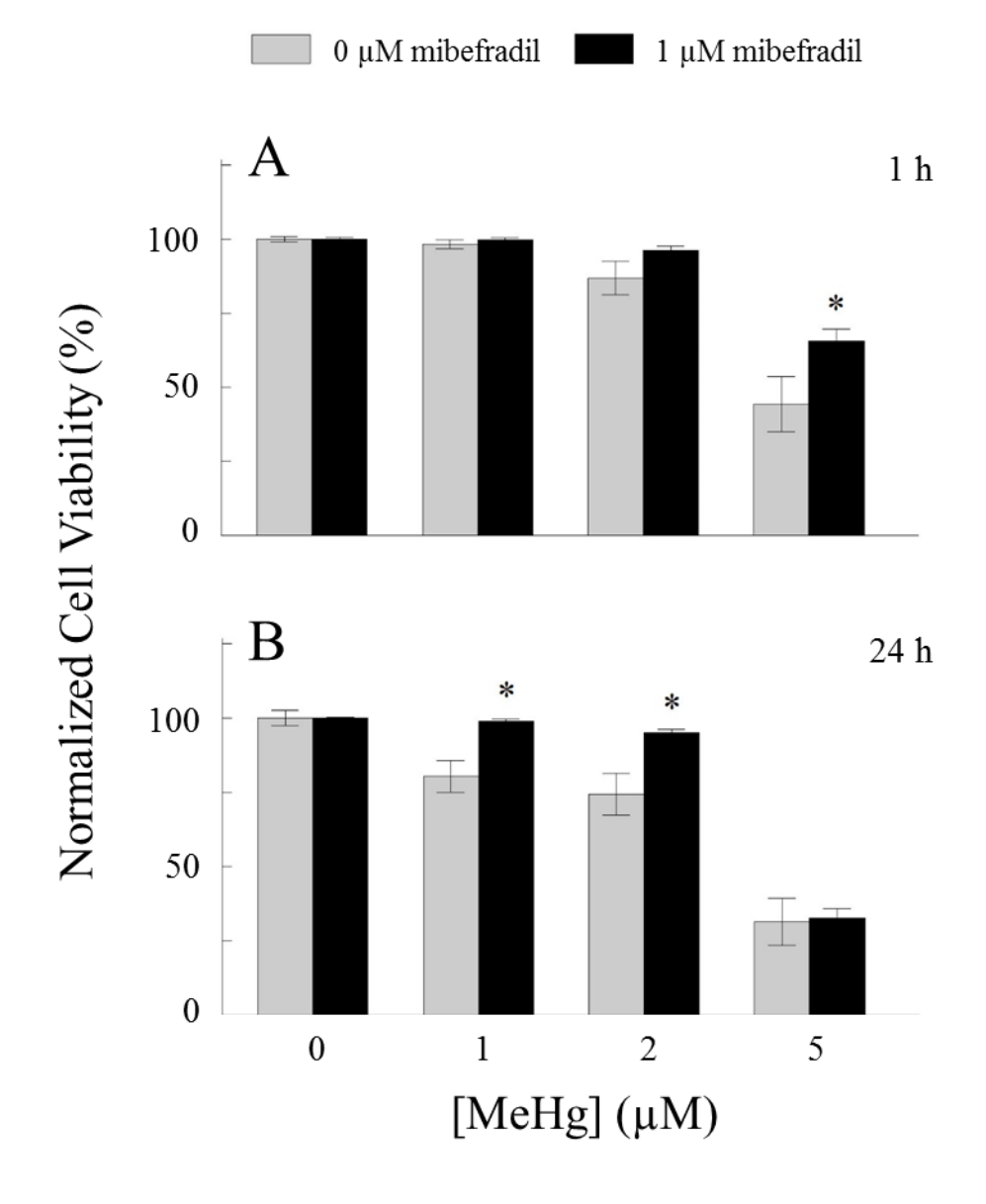


Figure 2.7. Mibefradil improves viability of untransfected HEK at both early and late timepoints following acute *in vitro* MeHg exposure. Untransfected HEK were incubated in 1  $\mu$ M mibefradil 10 min and then were exposed to MeHg for 1 h; cell viability was assessed at either 1 or 24 h following MeHg exposure. (A) Cell viability 1 h post-exposure was reduced only at 5  $\mu$ M MeHg and is partially restored with mibefradil pretreatment. (B) Viability of untransfected HEK 24 h post-exposure was improved with mibefradil pretreatment, though only when exposed to lower concentration of MeHg. A significant difference in viability resulting from mibefradil treatment is denoted by \* (p < 0.05, n = 9).

to MeHg-induced  $Ca^{2+}$  disruption is most noticeable at early timepoints and lower  $\mu M$  MeHg exposures, and effects mediated by T-type VGCCS may be masked by more sensitive or sizeable mechanisms for elevating  $Ca^{2+}{}_{i}$  as both exposure time and concentration of MeHg increase.

To better understand the actions of mibefradil, Ca<sup>2+</sup><sub>e</sub> was removed from external solutions in subsequent experiments. In doing so, I sought to determine whether the antagonist was serving simply to block Ca<sup>2+</sup> influx through the pore of the T-type channels or by some other mechanism independent of Ca<sup>2+</sup><sub>e</sub>. Cells were pretreated with mibefradil, as in previous experiments, in a Ca<sup>2+</sup>free buffer containing 20 µM EGTA. The effect of mibefradil treatment on the time-to-onset of phase 1 and 2 were similar to that of Ca<sup>2+</sup><sub>e</sub>-containing experiments in that it hastened the time at which an initial elevation in Ca<sup>2+</sup><sub>i</sub> was observed (Fig. 2.8A) and slowed the second (Fig. 2.8B). The presence of phase 2 in Ca<sup>2+</sup>e-free conditions is not consistent with previous studies of this nature which attribute Ca<sup>2+</sup>e influx as the predominant source of Ca<sup>2+</sup> in phase 2 (Denny et al., 1993, Hare et al., 1993, Marty and Atchison, 1997, Limke et al., 2003). Thus, these results reveal there may exist another Ca<sup>2+</sup>e-independent mechanism for elevating Ca<sup>2+</sup>i that may be masked in cells which highly express many distinct voltage-gated ion channels. This Ca<sup>2+</sup><sub>e</sub>-independent pathway appears to be negligible in mediating cell death, as viability of untransfected HEK is only marginally reduced at 1 h post-exposure with no effect from mibefradil pretreatment (Fig. 2.9A); viability at the 24 h timepoint is improved only at 2 µM MeHg exposure with mibefradil treatment (Fig. 2.9B).

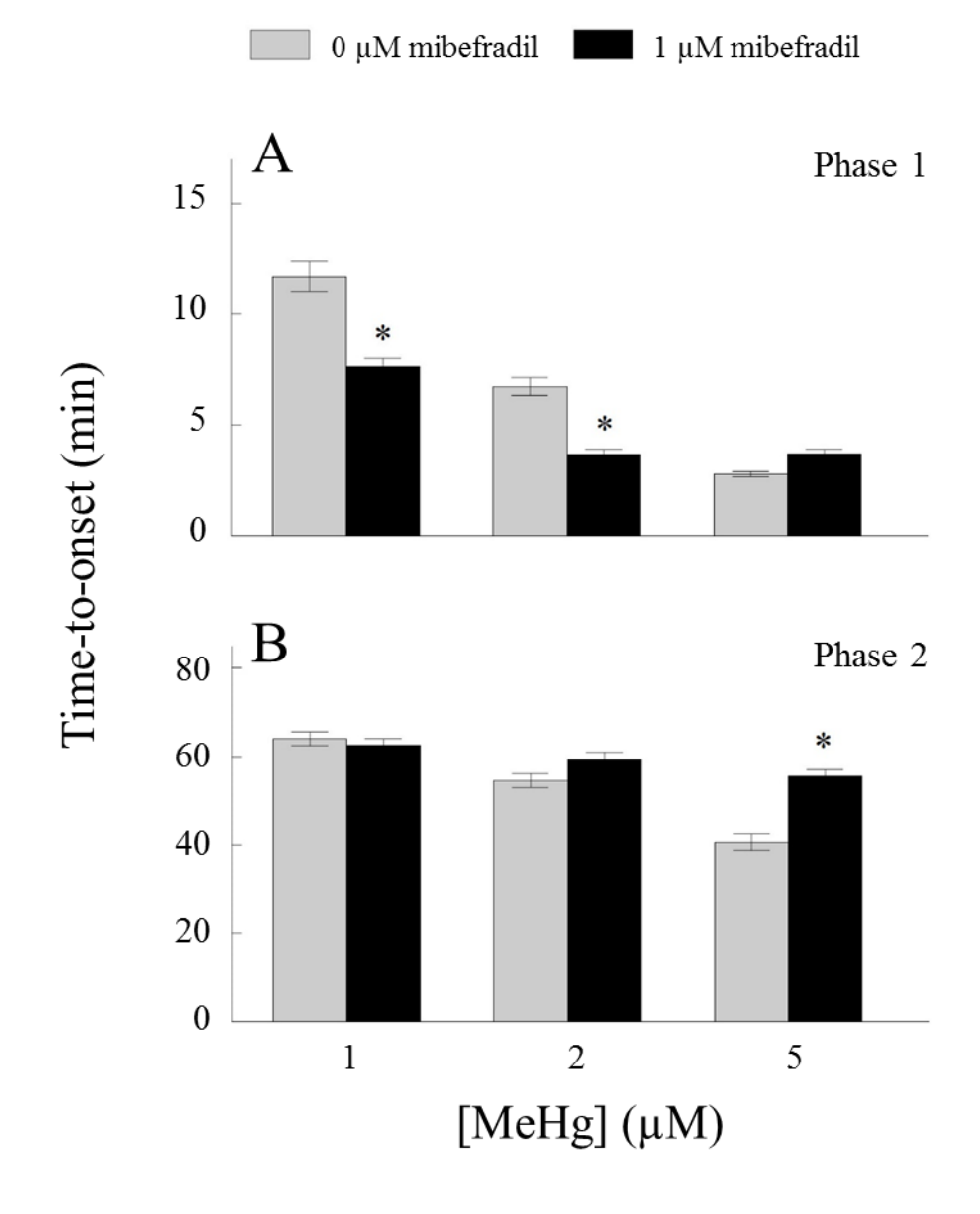


Figure 2.8. Mibefradil pretreatment produces contrasting effects on the times-to-onset of MeHg-induced Ca<sup>2+</sup><sub>i</sub> elevations in untransfected HEK, despite removal of Ca<sup>2+</sup><sub>e</sub>. Untransfected HEK cells were incubated in 1  $\mu$ M mibefradil 10 min prior to superfusion with MeHg in EGTA-HBS; changes in F<sub>340/380</sub> were simultaneously monitored throughout exposure. (A) Time-to-onset of phase 1 was quickened with mibefradil treatment at 1 and 2  $\mu$ M MeHg, whereas (B) the time-to-onset of phase 2 was slowed at 5  $\mu$ M MeHg. A significant difference in time-to-onset resulting from mibefradil treatment is denoted by \* (p < 0.05, n = 9).

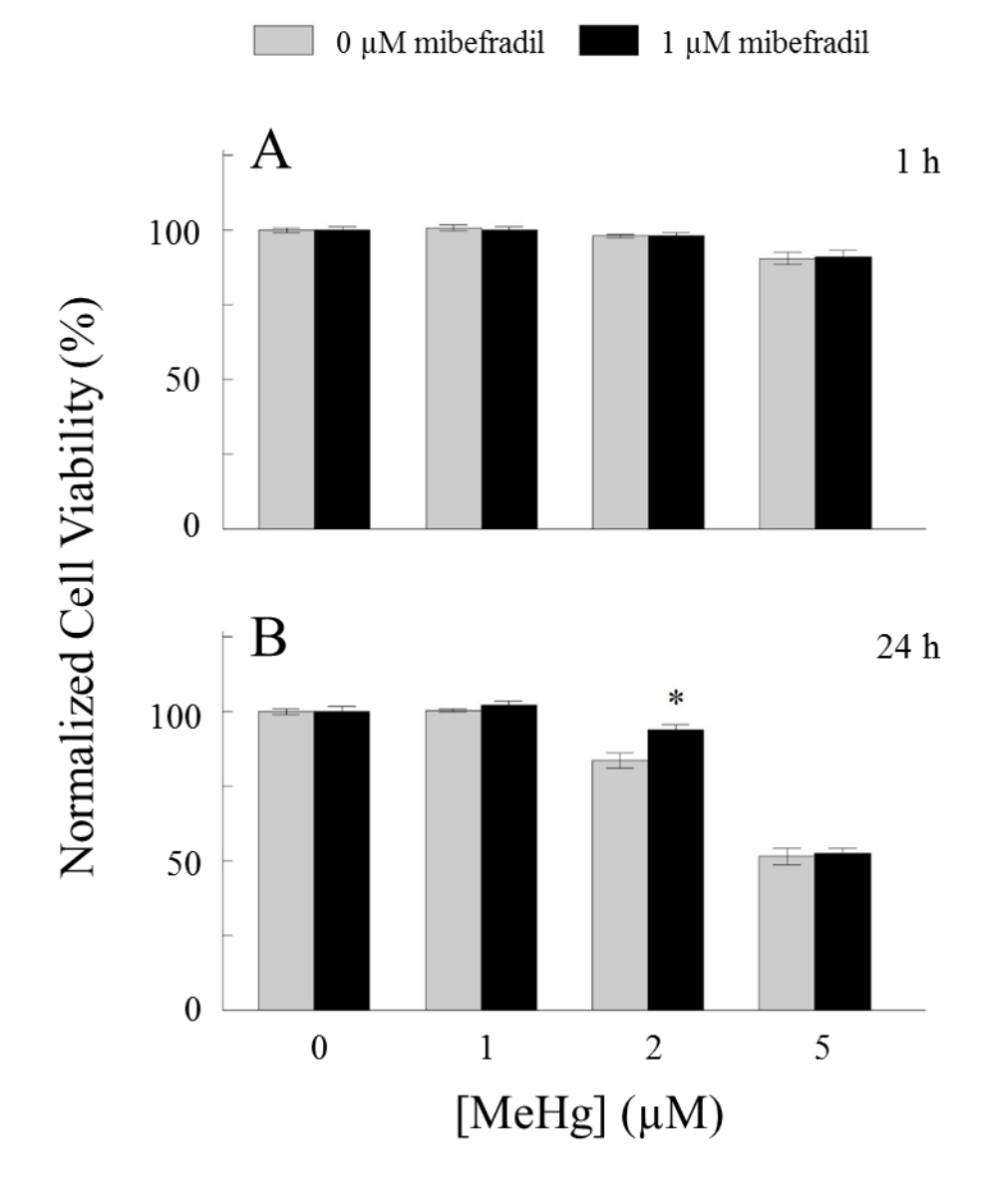


Figure 2.9. Mibefradil has little effect on improving viability of untransfected HEK following acute *in vitro* MeHg exposure under  $Ca^{2+}_{e}$ -free conditions. Untransfected HEK were incubated in 1  $\mu$ M mibefradil 10 min and then were exposed to MeHg in EGTA-HBS for 1 h; cell viability was assessed at either 1 or 24 h following MeHg exposure. (A) Cell viability at 1 h post-exposure was not reduced by MeHg when  $Ca^{2+}_{e}$  is removed, regardless of mibefradil treatment. (B) Mibefradil treatment improved viability of only the cells exposed to 2  $\mu$ M MeHg in  $Ca^{2+}_{e}$ -free conditions 24 h following MeHg exposure. A significant difference in viability resulting from mibefradil treatment is denoted by \* (p < 0.05, n = 9).

#### 2.5. Discussion

The results of this study demonstrate the actions of MeHg, particularly on Ca<sup>2+</sup><sub>i</sub> disruption, occur in a VGCC-subtype-dependent manner; this subtype dependence was more apparent in the times-to-onset of phase 1 than phase 2. Cells transfected with VGCCs, irrespective of subtype, exhibited a shortened time-to-onset of phase 1 as compared to untransfected cells. Moreover, differences in subtype sensitivity to a hastened onset of phase 1 began to occur at 1 µM MeHg. Interestingly, a shortening of the time-to-onset of phase 2 was only observed in HEK cells transfected with the N-type VGCC.

These results are contrary to what is currently known about the Ca<sup>2+</sup> sources that cause the increase in Ca<sup>2+</sup><sub>i</sub> in phases 1 and 2. Elevations in Ca<sup>2+</sup><sub>i</sub> contributing to phase 1 have been primarily attributed to the release of Ca<sup>2+</sup> from intracellular storage organelles, such as the mitochondria and smooth endoplasmic reticulum (Levesque and Atchison, 1991, Hare and Atchison, 1995a, Limke and Atchison, 2002, Limke et al., 2004). As such, it might be expected that expression of distinct surface proteins has little effect on the occurrence of phase 1 unless serving as a route of entry into the cell for MeHg. Thus, these results support the hypothesis that ion channels, notably VGCCs, provide a means of entry for MeHg into the cell (Shafer and Atchison, 1991, Edwards et al., 2002). Furthermore, it may be garnered that the ability of MeHg to traverse the membrane through the pore of a VGCC is dependent upon the channel subtype.

Previous studies showed that the onset of phase 2 can be slowed, in part, by the removal of Ca<sup>2+</sup><sub>e</sub> or pharmacologic block of Ca<sup>2+</sup>-permeable channels, demonstrating the important contribution of Ca<sup>2+</sup><sub>e</sub> influx in the time-to-onset of phase 2 (Denny et al., 1993, Hare et al., 1993, Hare and Atchison, 1995a, Limke et al., 2004). Because of this, it was hypothesized that the greatest VGCC-subtype specificity would be observed in the time-to-onset of phase 2. However,

there was little difference among the VGCC subtypes in the time-to-onset of phase 2, with the exception of the N-type VGCC which mediated a quicker onset of phase 2 in transfected cells. It may be that no subtype specificity was observed because *in vitro* application of MeHg induces a rapid and irreversible block, even in the absence of electrical stimulation (Shafer and Atchison, 1991, Sirois and Atchison, 2000). In the same heterologous expression system, application of low  $\mu$ M MeHg, reduced current carried through L-, N-, and R-type VGCCs to <20% of the control in fewer than 10 mins (Peng et al., 2002, Hajela et al., 2003). Because, at the fastest rate (N-type-transfected, 5  $\mu$ M MeHg), the onset of phase 2 occurred in 15.4  $\pm$  0.4 min, it is not implausible that a significant number of recombinant VGCCs were blocked prior to the onset of phase 2.

Although all cells had a reduction in viability 1 h following exposure to 5 µM MeHg, viability of L-type-transfected HEK cells was most immediately affected at lower MeHg concentrations. In contrast, N- and R-type-transfected cells were most resistant to acute cytotoxic effects. These results are in line with reported biophysical properties of VGCCs; L-type VGCCs carry large inward current with a slow rate of inactivation, whereas N- and R-type currents are more moderate both in size and rate of inactivation (Catterall, 2000). If MeHg is able to traverse the plasma membrane via VGCCs as hypothesized, it is logical that the measured cell viability at this early timepoint is congruent with kinetic properties inherent to distinct VGCCs.

Once inside the cell, MeHg elicits  $Ca^{2+}$  release from intracellular  $Ca^{2+}$  storage pools to effectively increase cytosolic [ $Ca^{2+}$ ] and depolarize the membrane (Hare and Atchison, 1992, Hare et al., 1993). With a sufficient amount of time to accumulate  $Ca^{2+}$ , it is not unreasonable that VGCC subtype-dependence was not observed 24 h following MeHg exposure. Though, a marked reduction in R-type-transfected cell viability was measured, it only occurred at 1  $\mu$ M MeHg. This may be due to differences in transcriptional or translational efficiency of VGCCs, resulting in

inconsistent channel densities among the transfected subtypes. It was also observed that MeHg caused some adherent cells to detach from the culture surface in a time-dependent manner. It is possible a VGCC subtype-dependence was not measurable at the later timepoint because cells were lost during critical wash steps prior to assessment of viability, despite application of gentle centrifugation in between washes to minimize loss of detached cells. This likely explains the apparent rise in viability when comparing the early onset and delayed cell viability datasets, since loss of dead and detached cells would make the measured viability deceptively high.

Previous studies have attributed the reduction of cell viability following MeHg exposure to MeHg-induced elevations in [Ca<sup>2+</sup>]<sub>i</sub> (Marty and Atchison, 1998, Limke et al., 2003, Edwards et al., 2005). The results from this study do not implicate a VGCC subtype-dependence in the correlation between increases in Ca<sup>2+</sup><sub>i</sub> and decreases in viability, as the recombinant VGCCs which resulted in the most rapid rises in Ca<sup>2+</sup><sub>i</sub> did not display the greatest amount of cytotoxicity. This may be due to the differences among the rat primary cerebellar granule cells used in previous studies and the HEK cell with non-excitable properties (Thomas and Smart, 2005). Presence of varying levels of  $\alpha_{1A}$ ,  $\alpha_{1B}$ ,  $\alpha_{1C}$ , and  $\alpha_{1E}$  mRNA and protein have been reported in cerebellar granule cells, with over 90% of whole-cell current in these cells attributed to current carried through the HVA VGCCs (Randall and Tsien, 1995, Tanaka et al., 1995, Volsen et al., 1995). The kinetics of the pore-forming all subunit are further modified by co-expressed auxiliary subunits, particularly the β subunits (Lacerda et al., 1991, Mori et al., 1991, Hullin et al., 1992, Williams et al., 1992a, Williams et al., 1992b, Ellinor et al., 1993). Although  $\beta_3$  is abundantly expressed in the brain and, of note, the internal granule cell layer,  $\beta_4$  and, to a lesser extent,  $\beta_{1b}$  and  $\beta_{1c}$ , are also expressed in the cerebellum (Hullin et al., 1992, Powers et al., 1992, Castellano et al., 1993b, a, Tanaka et al., 1995, Park et al., 1997). The diversity of subunits in this region gives rise to diversity in VGCC

composition. For example,  $\alpha_{1C}$  and  $\alpha_{1A}$  primarily co-localize with  $\beta_3$  and  $\beta_4$ , respectively, to produce the functional L- and P/Q-type VGCCs which contribute most significantly to VGCC-mediated current in cerebellar granule cells. While current carried through  $\alpha_{1A}$  is rapidly activated and slowly inactivated, co-expression with  $\beta_3$  results in acceleration of the inactivation (Stea et al., 1994). Thus, use of a constant  $\beta_3$  subunit in our recombinant channels may alter the activity of the channel beyond what is found endogenously in the cerebellum, making it difficult to correlate the actions of MeHg with any subtype specificity.

I went on to demonstrate endogenous T-type VGCCs appear to contribute to, but are not solely responsible for MeHg-induced elevations in Ca<sup>2+</sup><sub>i</sub> and reduced viability in untransfected HEK. Pretreatment with mibefradil prior to co-exposure with MeHg hastened the time-to-onset of phase 1 and slowed the time-to-onset of phase 2. The apparent stimulatory effect of mibefradil on the time-to-onset of phase 1 may be attributed to IP<sub>3</sub>-dependent Ca<sup>2+</sup> release induced by the drug itself, as first described in cardiac fibroblasts (Eberhard et al., 1995). This effect was reported by Eberhard et al. at >10 μM mibefradil, thus pretreatment with mibefradil may permit sufficient accumulation of the antagonist to elicit a stimulatory effect, whereas co-perfusion of MeHg and mibefradil may result in competition for binding sites and mibefradil washout. The slowing of the time-to-onset of phase 2 Ca<sup>2+</sup>i increases, presumably through block of T-type VGCCs, suggests these channels may contribute to Ca<sup>2+</sup>e influx. T-type VGCCs are not as readily blocked by MeHg as compared to HVA VGCCs, with a 13.0  $\pm$  5  $\mu$ M MeHg eliciting a 50% reduction in current through α<sub>1G</sub>-containing T-type channels (Tarabová et al., 2006). Thus, one may expect more channels to be available to mediate Ca<sup>2+</sup>e influx. Mibefradil pretreatment increased cell viability at high MeHg concentrations 1 h post-exposure and at low MeHg concentrations 24 h postexposure. These results indicate the inhibitory actions of mibefradil on Ca<sup>2+</sup><sub>i</sub> disturbances prevail

and are effective to reduce cytotoxicity following MeHg exposure. The differences in the efficacy of mibefradil among the MeHg concentrations and timepoints are likely due to the amount of Ca<sup>2+</sup><sub>i</sub> which has accumulated, and may suggest Ca<sup>2+</sup> sources other than influx through T-type VGCCs contribute more significantly to MeHg-induced Ca<sup>2+</sup><sub>i</sub> disruptions and concomitant cell death.

Although our results are indicative of a contribution from T-type VGCCs in MeHg toxicity, exposure of untransfected HEK to up to 100 µM MeHg does not induce any measurable wholecell Ca<sup>2+</sup> current (Tarabová et al., 2006). The reason for this may be supported by the biophysical properties of T-type channels, which consist of characteristic small conductance and fast inactivation at lower membrane potentials (Catterall, 2000). Though MeHg accelerates the rate of T-type VGCC inactivation and deactivation, and channels inactivate at more negative potentials in the presence of mibefradil, likely reducing the channel population available to mediate Ca<sup>2+</sup><sub>e</sub> influx (Gomora et al., 2000, Tarabová et al., 2006). Moreover, mibefradil (0.2 – 10 μM) has been reported to effectively inhibit HVA VGCCs, voltage-gated K<sup>+</sup> channels, HERG and ATP-activated K+ channels, and volume-activated Cl- channels, implicating mibefradil as a promiscuous antagonist (Bezprozvanny and Tsien, 1995, Nilius et al., 1997, Chouabe et al., 1998, Gomora et al., 1999, Liu et al., 1999, Hong et al., 2012). Distinct differences in biophysical properties have also been described among  $\alpha_{1G}$ -,  $\alpha_{1H}$ -, and  $\alpha_{1I}$ -containing recombinant T-type channels (Martin et al., 2000). The  $\alpha_1$  subunit subtype which produces the endogenous T-type current in HEK (Berjukow et al., 1996) has not yet been reported, making it difficult to understand the actions of both MeHg and mibefradil in these studies. Similarly, the  $\beta$  and  $\alpha_2\delta$  subunits endogenously expressed in HEK cells have not been fully elucidated. Because mibefradil pretreatment resulted in similar responses in the times-to-onset of phase 1 and 2 Ca<sup>2+</sup>i increases and improvement in cell viability under  $Ca^{2+}_{e}$ -free conditions, it is presumed that the protective action of mibefradil may be attributed to more than block of  $Ca^{2+}_{e}$  influx.

These results provide direct evidence for VGCC subtype-dependence of the time-to-onset of MeHg-induced  $Ca^{2+}_{i}$  dysregulation in HEK cells. However, the rise in  $Ca^{2+}_{i}$  attributed to transient expression of distinct VGCC subtypes could not be correlated with variations in cytotoxicity. This indicates that the mechanism for MeHg-induced  $Ca^{2+}_{i}$  elevation is more complex than what is currently known, and that there may exist a  $Ca^{2+}_{e}$ -independent mechanism for elevating  $Ca^{2+}_{i}$  in HEK cells.

# CHAPTER THREE

# ASSESSING THE SENSITIVITY OF RECOMBINANT TRANSIENT RECEPTOR POTENTIAL ANKYRIN 1 CHANNELS TO THE CELLULAR EFFECTS OF METHYLMERCURY

#### 3.1. Abstract

Untransfected HEK cells display a multiphasic increase in Ca<sup>2+</sup>; throughout in vitro MeHg exposure due, in part, to Ca<sup>2+</sup> influx. However HEK cells do not endogenously express HVA VGCCs and express only low levels of LVA VGCCs, suggesting another class of Ca<sup>2+</sup>-permeable ion channels may contribute to MeHg-induced Ca<sup>2+</sup><sub>i</sub> elevations. Endogenous TRPA1 expression has recently been reported in HEK cells. TRPA1 belongs to the Ca<sup>2+</sup>-permeable TRP ion channel superfamily, so it is possible TRPA1 may contribute to MeHg-induced Ca<sup>2+</sup><sub>i</sub> elevations. To determine the sensitivity of the TRPA1 channel in mediating MeHg-induced Ca<sup>2+</sup><sub>i</sub> dysregulation and corresponding cytotoxicity, HEK cells were transfected with TRPA1 cDNA; although HEK cells naturally express low levels of TRPA1, recombinant expression increased the channel density to better enable study of the sensitivity to MeHg. Single-cell microfluorimetry was used to record real-time changes in relative [Ca<sup>2+</sup>]; throughout exposure to MeHg (0.5, 1, 2 µM). Expression of TRPA1 did not alter the time-to-onset of phase 1, and only hastened phase 2 at 0.5 µM MeHg. Removal of Ca<sup>2+</sup><sub>e</sub> slowed the time-to-onset of phase 2 at all MeHg concentrations in TRPA1transfected HEK (TRPA1-HEK), while phase 1 was unaltered under these conditions. However, even under Ca<sup>2+</sup><sub>e</sub>-free conditions, the times-to-onset of phase 1 and 2 at 0.5 µM MeHg remained hastened by the expression of TRPA1, as compared to untransfected HEK cells. Pretreatment with the TRPA1 antagonist A-967079 did not alter the time-to-onset of phase 1 nor phase 2  $Ca^{2+}{}_{i}$ perturbations. Throughout microfluorimetry studies, a unique "phase 0" preceded the canonical phase 1 in TRPA1-HEK cells. The occurrence of this phase was: 1) dependent upon the cell's positive response to the TRPA1 agonist allyl isothiocyanate (AITC), 2) concomitant with the presence of Ca<sup>2+</sup>e in the treatment buffer, and 3) inversely proportional to MeHg concentration, such that phase 0 was observed less frequently in cells exposed to higher concentrations of MeHg.

Pretreatment with A-967079 did not alter the frequency with which phase 0 was observed in TRPA1-HEK, however the antagonist did slow the time-to-onset of phase 0 at 2  $\mu$ M MeHg. Viability of TRPA1-HEK was assessed 1 h following acute *in vitro* exposure to MeHg. Viability of TRPA1-HEK was significantly reduced at 1 h following exposure to either 1 or 2  $\mu$ M MeHg. Under Ca<sup>2+</sup><sub>e</sub>-free conditions, the viability of these cells was unaltered at all concentrations of MeHg, as compared to their untransfected counterparts. Together, these results indicate TRPA1 channels may contribute to MeHg-induced Ca<sup>2+</sup><sub>i</sub> disruptions, particularly phase 2, and cell death through Ca<sup>2+</sup><sub>e</sub>-depedent mechanisms.

#### 3.2. Introduction

The Ca<sup>2+</sup><sub>e</sub>-dependence of the multiphasic response in HEK cells indicates Ca<sup>2+</sup> influx is a probable contributor to the disruption in Ca<sup>2+</sup><sub>i</sub> regulation; the lack of expression of HVA VGCCs and low endogenous expression of LVA VGCCs (Berjukow et al., 1996, Lin et al., 2014) suggests another Ca<sup>2+</sup>-permeable ion channel or ion channel family must contribute to the response. The multiphasic Fura-2 response observed in untransfected HEK cells throughout MeHg exposure (Chapter 2.4.1. – 2.4.2.) is similar to that reported in type II cerebellar astrocytes cultures (Marty et al., 1997, Lundback et al., 2002). In this class of astrocytes, MeHg induced a triphasic rise in F<sub>340/380</sub> which was attributed to release of Zn<sup>2+</sup><sub>i</sub> and mitochondrial Ca<sup>2+</sup>. More recently, TRPA1, a Ca<sup>2+</sup>-permeable ion channel, has been implicated for its role in maintaining basal Ca<sup>2+</sup><sub>i</sub> (Shigetomi et al., 2011) and generating Ca<sup>2+</sup><sub>i</sub> spikes with the cooperation of co-localized mitochondria in hippocampal astrocytes (Jackson and Robinson, 2015). HEK cells express low levels of TRPA1 (Tanner et al., 2007, Buber et al., 2010, Lin et al., 2014) which may impart sensitivity to MeHg and confer a multiphasic Ca<sup>2+</sup><sub>i</sub> elevation in response to MeHg exposure.

TRPA1 has been extensively characterized in Aδ- and C-fiber DRG as a nociceptive ion channel (Gold et al., 1996, Numazaki and Tominaga, 2004, Kobayashi et al., 2005, Anand et al., 2008). Noxious stimuli, such as AITC, mustard oil, cinnemaldehyde, and primary alcohols activate TRPA1 through covalent modification of cysteine residues on the N-terminus (Bandell et al., 2004, Jordt et al., 2004, Macpherson et al., 2007, Sadofsky et al., 2011, Komatsu et al., 2012). However, TRPA1 expression has also been reported in the cardiovascular system (Pozsgai et al., 2010, Early, 2012), respiratory (Mukhopadhyay et al., 2011, Nassini et al., 2012) and urinary tracts (Du et al., 2007, Streng et al., 2008, Skryma et al., 2011), and auditory organs (Corey et al., 2004, Liedtke and Heller, 2007, Takumida et al., 2009). Alternative means of activation include mechanical force

(Walker et al., 2000, Kindt et al., 2007, Kwan et al., 2009), endogenous inflammatory mediators (Takahashi et al., 2008), and Ca<sup>2+</sup>i-mediated mechanisms (Doerner et al., 2007, Wang et al., 2008b). Upon activation, TRPA1 conducts a large, inward cationic current which results in an increase in Ca<sup>2+</sup>i (Kosugi et al., 2007, Maher et al., 2008, Kwan et al., 2009, Nilius et al., 2012). Given the ability of MeHg to covalently interact with cysteine residues (Bahr and Moberger, 1954), alter ionic currents (Quandt et al., 1982, Arakawa et al., 1991, Shafer and Atchison, 1991, Leonhardt et al., 1996a, Sirois and Atchison, 2000, Yuan and Atchison, 2003, 2007), and disrupt Ca<sup>2+</sup>i regulation (Kauppinen et al., 1989, Hare et al., 1993, Hare and Atchison, 1995a, Marty and Atchison, 1997, Limke and Atchison, 2002, Limke et al., 2004), it may be reasonably hypothesized TRPA1 is a molecular target of MeHg.

The actions of mercurials on the function of TRP-family ion channels is poorly characterized. Xu et al. (2012) described the differential susceptibility of TRPC channels to both HgCl<sub>2</sub> and MeHg. Both mercurials induced an inward current, increase in Ca<sup>2+</sup><sub>i</sub>, and concentration-dependent cytotoxicity in HEK cells expressing recombinant TRPC4 and TRPC5; cells expressing either TRPC3, TRPC6, TRPV1, or TRPM2 were relatively resistant to mercurials. Two cysteine residues located between transmembrane segments 5 and 6, near the mouth of the channel pore, were determined to be critical for the interaction of TRPC5 with mercurials (Xu et al., 2012). Whereas TRPC channels are canonically store-operated, the numerous cysteine residues on the N-terminus of TRPA1 (Nilius et al., 2012, Zaytas et al., 2013) could provide abundant potential for interaction with MeHg; Furthermore, MeHg-induced perturbation of TRP channel function, particularly those abundantly expressed in DRG, may explain sensory disturbances arising in poisoned individuals.

Because covalent modification of TRPA1 by thiol-reactive compounds results in elevations in Ca<sup>2+</sup><sub>i</sub>, I sought to determine whether expression of these channels contributes to MeHg-induced Ca<sup>2+</sup><sub>i</sub> perturbations. While distinct isoforms of TRPs are reported to modulate TRPA1 activity when co-expressed (Akopian et al., 2007, Patil et al., 2010, Staruschenko et al., 2010, Akopian, 2011, Fischer et al., 2014), a model of heterologous expression was chosen to first study the sensitivity of TRPA1 in isolation. HEK cells were selected for their apparently minimal contribution of Ca<sup>2+</sup> influx through endogenously-expressed LVA VGCCs (Chapter 2.4.4). HEK cells were transfected with human TRPA1 cDNA, and the role of TRPA1 in mediating MeHg-induced Ca<sup>2+</sup><sub>i</sub> elevations and subsequent cytotoxicity (Marty and Atchison, 1998) was assessed. Some studies were conducted in the absence of Ca<sup>2+</sup><sub>e</sub> to explore whether TRPA1 expression confers sensitivity to MeHg-induced Ca<sup>2+</sup><sub>i</sub> disruption via a mechanism other than mediating Ca<sup>2+</sup> influx through the channel.

#### 3.3. Methods

#### 3.3.1. Materials

Materials were obtained from sources and solutions prepared as described in Chapter 2.3.1., unless otherwise described here. Human TRPA1 cDNA was purchased from Origene Technologies (Rockville, MD). The TRPA1 agonist AITC and antagonist A-967079 were purchased from Sigma-Aldrich. A 1 M AITC stock was made fresh daily in dimethyl sulfoxide (DMSO), from which a 10 μM AITC solution was prepared in HBS. A 72 mM A-967079 stock was prepared in DMSO, and was diluted to a working concentration of 100 nM. Paraformaldehyde and bovine serum albumin (BSA) were both purchased from Sigma-Aldrich, and prepared as solutions in phosphate-buffered saline (PBS) containing (in mM): 135 NaCl, 2.7 KCl, 10 Na<sub>2</sub>HPO<sub>4</sub>, and 2 KH<sub>2</sub>PO<sub>4</sub> (pH to 7.4 with HCl).

### 3.3.2. HEK cell culture and transfection

HEK cells were cultured as described in Chapter 2.3.2. Cells were plated on 35 mm polystyrene culture dishes at a density of 2 × 10<sup>5</sup> cells/mL 24 h prior to gene transfer, at which time cells were transfected with TRPA1 cDNA. The transfection mixture was prepared in Opti-MEM, and contained: 6% (v/v) FuGene, 2% (w/v) TRPA1 cDNA, and 0.4% (w/v) GFP cDNA. 24 h following transfection, cells were replated at low density (5 × 10<sup>4</sup> cells/mL) on either 12 mm or 25 mm borosilicate glass coverslips coated with 0.01% (w/v) poly-L-lysine. An additional 24 h were allowed for gene expression and cell adhesion prior to use in experiments. Cells were examined for transient GFP expression immediately before use in immunocytochemistry assessment and microfluorimetry studies, and those coverslips with less than approximately 20% GFP-expressing cells were not used in experiments. GFP cDNA was omitted from the transfection

mixture in cell preparations for viability assessment. Measurements for all experiments were made using cells from three independent transfections.

## 3.3.3. Immunocytochemistry

TRPA1-HEK were immunolabeled to confirm effective transfection and expression of the TRPA1 channel. TRPA1-HEK were rinsed three times in ice-cold PBS, then fixed in 4% (w/v) paraformaldehyde for 15 min at room temperature. Cells were rinsed three more times with PBS prior to incubation in 1% (w/v) BSA blocking buffer for 30 min at room temperature. The blocking buffer was then replaced with a rabbit anti-TRPA1 primary antibody (Pierce Biotechnology, Rockford, IL) diluted 1:300 in 1% (w/v) BSA. Cells were incubated in the primary antibody for 2 h at room temperature, at which time cells were washed thrice more in PBS. Alexa Fluor 405-conjugated goat anti-rabbit antibody (Thermo Fisher Scientific, Waltham, MA) was diluted 1:200 in 1% (w/v) BSA, and cells were incubated in the mixture for 1 h at room temperature. TRPA1-HEK were then washed a final three times in PBS before coverslips were mounted on glass microscope slides using an aqueous hard-set mounting medium (Vector Laboratories, Burlingame, CA). Representative images of TRPA1-HEK were collected under a Nikon Eclipse fluorescence microscope equipped with a CoolSNAP EZ CCD camera (Photometrics, Tucson, AZ) and Nikon NIS-Elements software.

#### 3.3.4. Single-cell microfluorimetry

Fura-2 AM was used to monitor relative changes in  $[Ca^{2+}]_i$ , as described in Chapter 2.3.3. Briefly, cells were rinsed three times with HBS and incubated in 3  $\mu$ M Fura-2 AM with 3  $\mu$ M pluronic acid for 1 h at 37°C. Cells were then transferred to a heated perfusion system (37°C, 2

mL/min) and perfused with HBS for 30 min. Experiments began with a 40 s pulse of  $10 \,\mu\text{M}$  AITC to verify TRPA1 expression and cell viability; AITC induces large, reversible Ca<sup>2+</sup> currents and a concomitant rise in Ca<sup>2+</sup><sub>i</sub>, measurable by Fura-2, both of which are rapidly abolished when AITC is removed from the perfusion solution (Bandell et al., 2004, Jordt et al., 2004). Cells which either did not respond to AITC or did not return to baseline shortly following AITC exposure were omitted from further analyses. Once a stable baseline was reestablished, the perfusion buffer was changed to MeHg (0.5, 1, or 2  $\mu$ M) and perfusion continued at 2 mL/min for the duration of the experiment. In experiments performed with the TRPA1 antagonist, cells were first pulsed with 10  $\mu$ M AITC in standard HBS and, upon return to baseline, were incubated with 100 nM A-967079 for 10 min. Fura-2 recordings resumed and perfusion with MeHg began immediately following this incubation period. Time-to-onset was calculated for each cell responding to AITC within the experimental field, then mean times-to-onset of phases 1 and 2 were calculated for that population of cells (n = 1).

#### 3.3.5. Measurement of cell viability

TRPA1-HEK cell viability following acute *in vitro* MeHg exposure was assessed as described in Chapter 2.3.4.

#### 3.3.6. *Statistics*

Each experiment was performed in replicates of nine with cells from a minimum of three independent transfections; data are presented as mean  $\pm$  SEM. Data were analyzed using the GraphPad Prism® statistical program. A two-way ANOVA was performed to compare responses produced in TRPA1-HEK or with A-967079 treatment, and MeHg concentrations. A *post hoc* 

Tukey's test was used when significant differences between sample means were detected (Steel and Torrie, 1960). Values of p < 0.05 were considered to be statistically significant.

## 3.4. Results

3.4.1. Characteristics of MeHg-induced  $Ca^{2+}{}_{i}$  dysregulation mediated by recombinant TRPA1 channels in HEK cells

Although HEK cells express low levels of endogenous TRPA1 (Tanner et al., 2007, Buber et al., 2010, Lin et al., 2014), heterologous expression was used to facilitate the study of the channel MeHg-induced cytotoxicity. Transfection with human TRPA1 increased TRPA1 immunoreactivity beyond endogenous levels within 48 h (Fig. 3.1). Although a transfection efficiency of approximately 70 – 80% was routinely achieved, the TRPA1 agonist AITC was utilized to assess function of the channel. In microfluorimetric studies, the brief application of AITC served not only to identify those cells expressing functional TRPA1 channels, but also allowed for omission of the cells not healthy enough to buffer rapid changes in Ca<sup>2+</sup><sub>i</sub> induced by the agonist. TRPA1-HEK displayed a multiphasic F<sub>340/380</sub> signal comparable in shape to their untransfected counterparts (Fig. 3.2). Application of MeHg induced a rapid and reversible rise in F<sub>340/380</sub>, designated as phase 1, followed by a gradual and irreversible rise in the signal fluorescence. As with untransfected HEK cells, this intermediate phase which immediately follows phase 1 can be attributed to a steady rise in Ca<sup>2+</sup><sub>i</sub> rather than any other divalent cation, as it obviated with the removal of  $Ca^{2+}_{e}$ . Phase 2 is eventually reached when the rate of change in  $F_{340/380}$  further increases. Expression of functional TRPA1 channels does not alter the time-to-onset of phase 1, as compared to untransfected cells (Fig. 3.3A). This is result is not unexpected, as phase 1 is canonically attributed to the release of Ca<sup>2+</sup> from intracellular storage organelles (Levesque and Atchison, 1991, Hare and Atchison, 1995a, Limke and Atchison, 2002, Limke et al., 2004). The time-to-onset of phase 2 is hastened in TRPA1-HEK, however only at 0.5 µM MeHg (Fig. 3.3B). This effect may suggest that: 1) recombinant TRPA1 channels are susceptible to block by MeHg

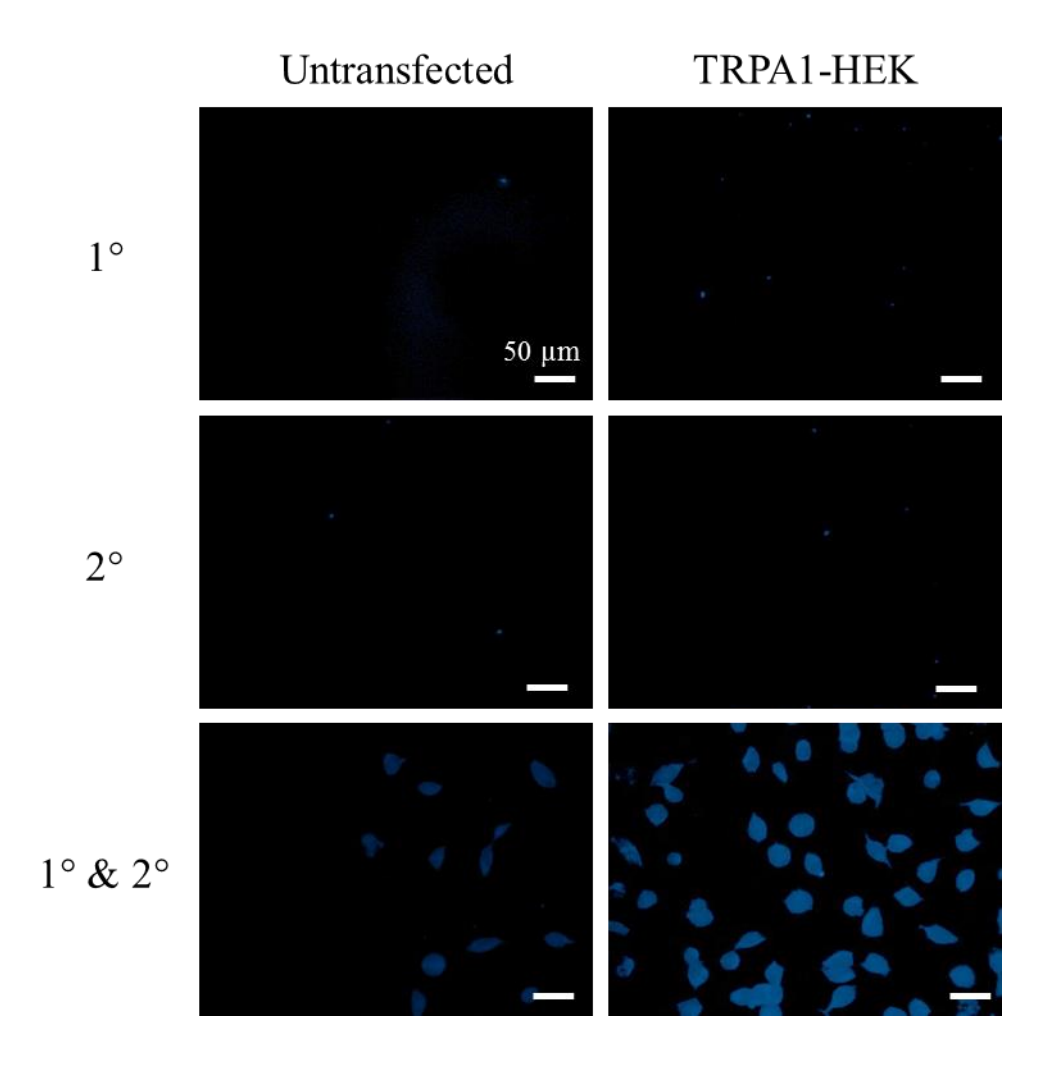


**Figure 3.1. Representative micrographs depicting endogenous and heterologous expression of TRPA1 in HEK cells.** Immunofluorescence of TRPA1 was enhanced beyond endogenous levels with heterologous expression of recombinant human TRPA1 in HEK cells. Cells were labeled with a human TRPA1 rabbit polyclonal antibody and detected with an Alexa Fluor 405-conjugated goat anti-rabbit secondary antibody. Images were taken under 20× magnification.

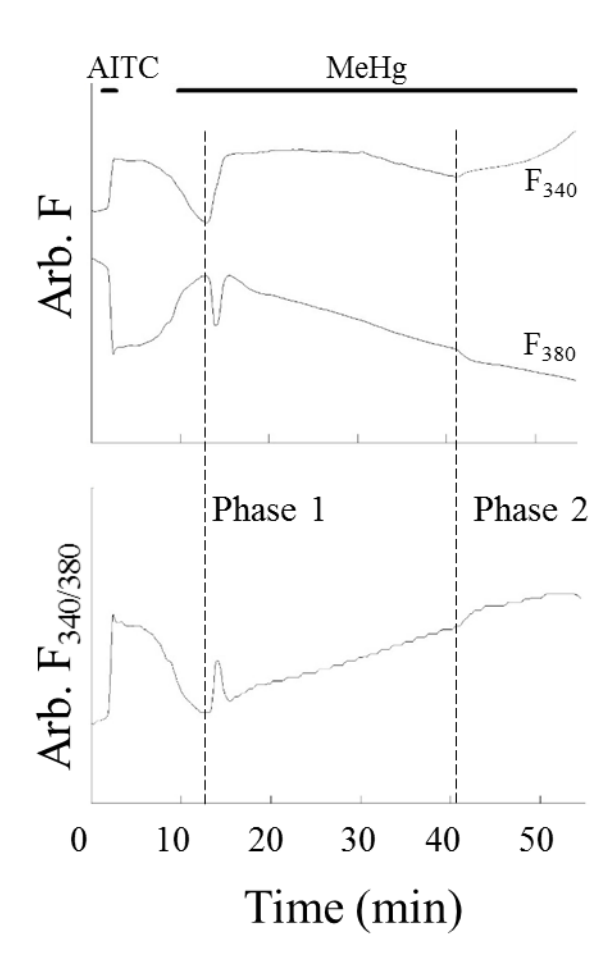


**Figure 3.2. MeHg induces a multiphasic Ca**<sup>2+</sup>i **elevation in TRPA1-HEK.** A multiphasic rise in the  $F_{340/380}$  signal was observed in all TRPA1-HEK throughout continuous MeHg exposure, with a steadily rising intermediate phase between the onset of phases 1 and 2; this response was typical in all cells regardless of response to AITC. Representative tracing is from a cell exposed to a 40 s pulse of 10  $\mu$ M AITC to determine TRPA1 response followed by 1  $\mu$ M MeHg, where indicated. Hashed lines indicate where the time-to-onset of phase 1 and phase 2 were determined.

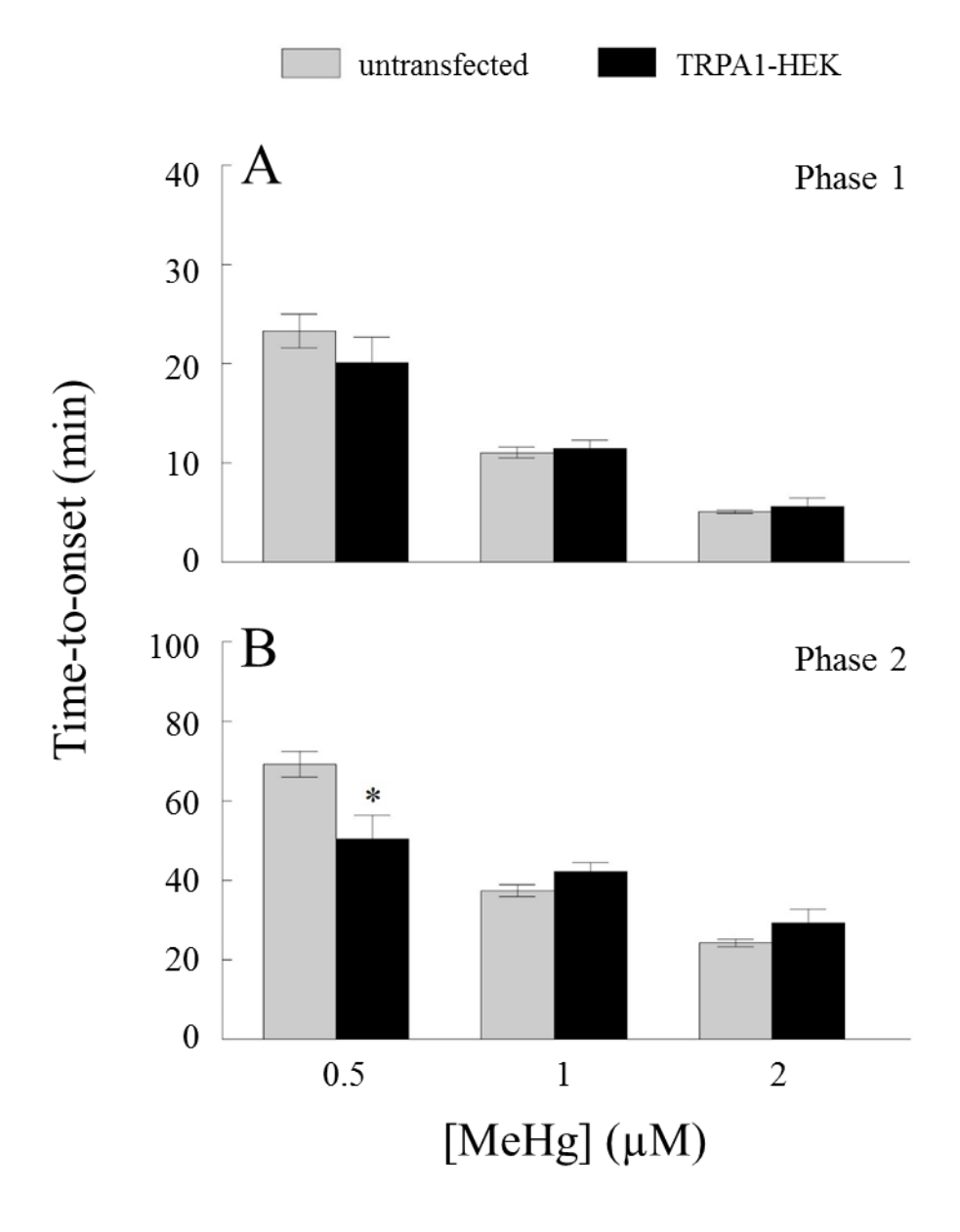


**Figure 3.3. TRPA1 expression hastens the time-to-onset of phase 2 at sub-μM MeHg concentrations.** Untransfected and TRPA1-HEK were superfused with MeHg while simultaneously monitoring changes in  $F_{340/380}$ . (A) Time-to-onset of phase 1 was unaltered with expression of recombinant TRPA1, whereas the time-to-onset of phase 2 was hastened with TRPA1 expression at sub-μM MeHg. Significance compared to untransfected cells is denoted by \* (p < 0.05,  $n \ge 4$ ).

at higher concentrations, such that the channels are unable to contribute to  $Ca^{2+}{}_{i}$  elevations during phase 2, or 2) the contribution of TRPA1 channels to phase 2-associcated  $Ca^{2+}{}_{i}$  increases is masked by more significant sources for  $Ca^{2+}$  entry or elevations.

# 3.4.2. Role of $Ca^{2+}_{e}$ in MeHg-induced $Ca^{2+}_{i}$ elevations in TRPA1-HEK

To assess the contribution of Ca<sup>2+</sup><sub>e</sub> in the times-to-onset of phase 1 and phase 2, Ca<sup>2+</sup><sub>e</sub> was removed from the perfusion buffer. In the absence of Ca<sup>2+</sup>e, the rate of onset of phase 1 was unaltered (Fig. 3.4A), further suggesting an intracellular source is primarily responsible for this early elevation in Ca<sup>2+</sup><sub>i</sub>. In contrast, the time-to-onset of phase 2 was slowed in TRPA1-HEK at all concentrations of MeHg when Ca<sup>2+</sup><sub>e</sub> was eliminated from the treatment buffer (Fig. 3.4B). While these results indicate Ca<sup>2+</sup> influx is critical in mediating phase 2, I thought to investigate whether it is indeed Ca<sup>2+</sup> influx through the TRPA1 channel. For this, a comparison of the timesto-onset of phases 1 and 2 between untransfected and TRPA1-HEK was made. In the absence of Ca<sup>2+</sup>e, the times-to-onset of phases 1 and 2 (Fig. 3.5A–B) are both hastened in TRPA1-HEK at 0.5 μM MeHg. Onset of either phase of Ca<sup>2+</sup><sub>i</sub> dysregulation is unaffected at higher MeHg concentrations regardless of TRPA1 expression. These results suggest the contribution of TRPA1 to phase 2 Ca<sup>2+</sup><sub>i</sub> disturbances may be mediated by release of Ca<sup>2+</sup> from an intracellular source rather than  $Ca^{2+}$  influx. Because this effect is only observed at sub- $\mu M$  concentrations, it may be that TRPA1 serves as a pathway of entry into the cell for MeHg. At lower MeHg concentrations, MeHg entry via TRPA1 may expedite release of Ca<sup>2+</sup><sub>i</sub> from the mitochondria and IP<sub>3</sub>-sensitive stores, whereas a concentration-dependent block of the channel may explain the unaltered onset of Ca<sup>2+</sup><sub>i</sub> disturbances at MeHg concentrations.

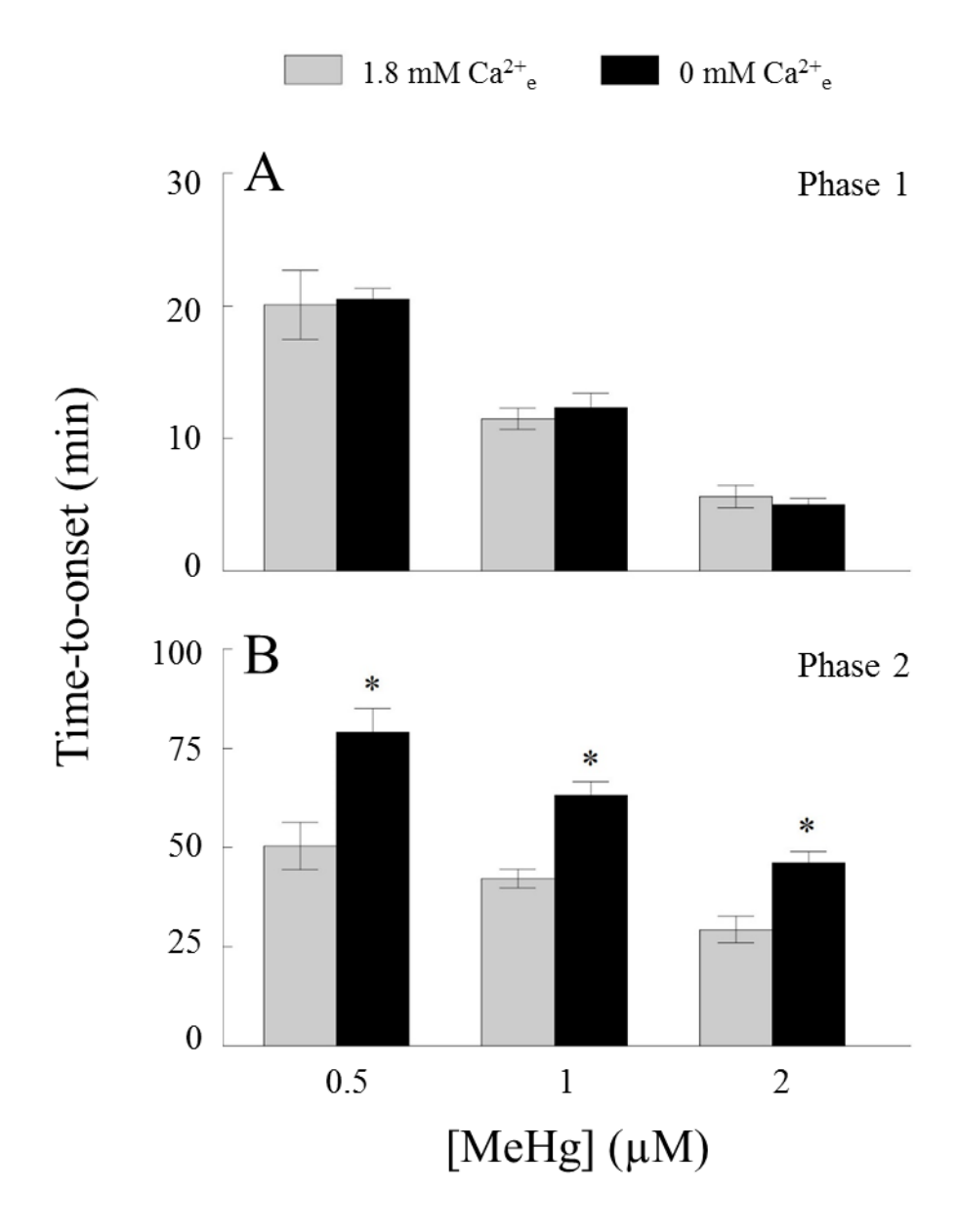


Figure 3.4. Removal of  $Ca^{2+}_e$  slows the time-to-onset of phase 2 in TRPA1-HEK. TRPA1-transfected HEK cells were superfused with MeHg in either standard HBS (1.8 mM  $Ca^{2+}_e$ ) or EGTA-HBS (0 mM  $Ca^{2+}_e$ ) while simultaneously monitoring changes in  $F_{340/380}$ . (A) Time-to-onset of phase 1 in TRPA1-HEK exposed to MeHg remained unaltered in  $Ca^{2+}_e$ -free conditions. (B) In contrast, the time-to-onset of phase 2 in TRPA1-HEK was slowed in a concentration-dependent manner upon removal of  $Ca^{2+}_e$ . Significance compared to 1.8 mM  $Ca^{2+}_e$  is denoted by \*  $(p < 0.05, n \ge 4)$ .

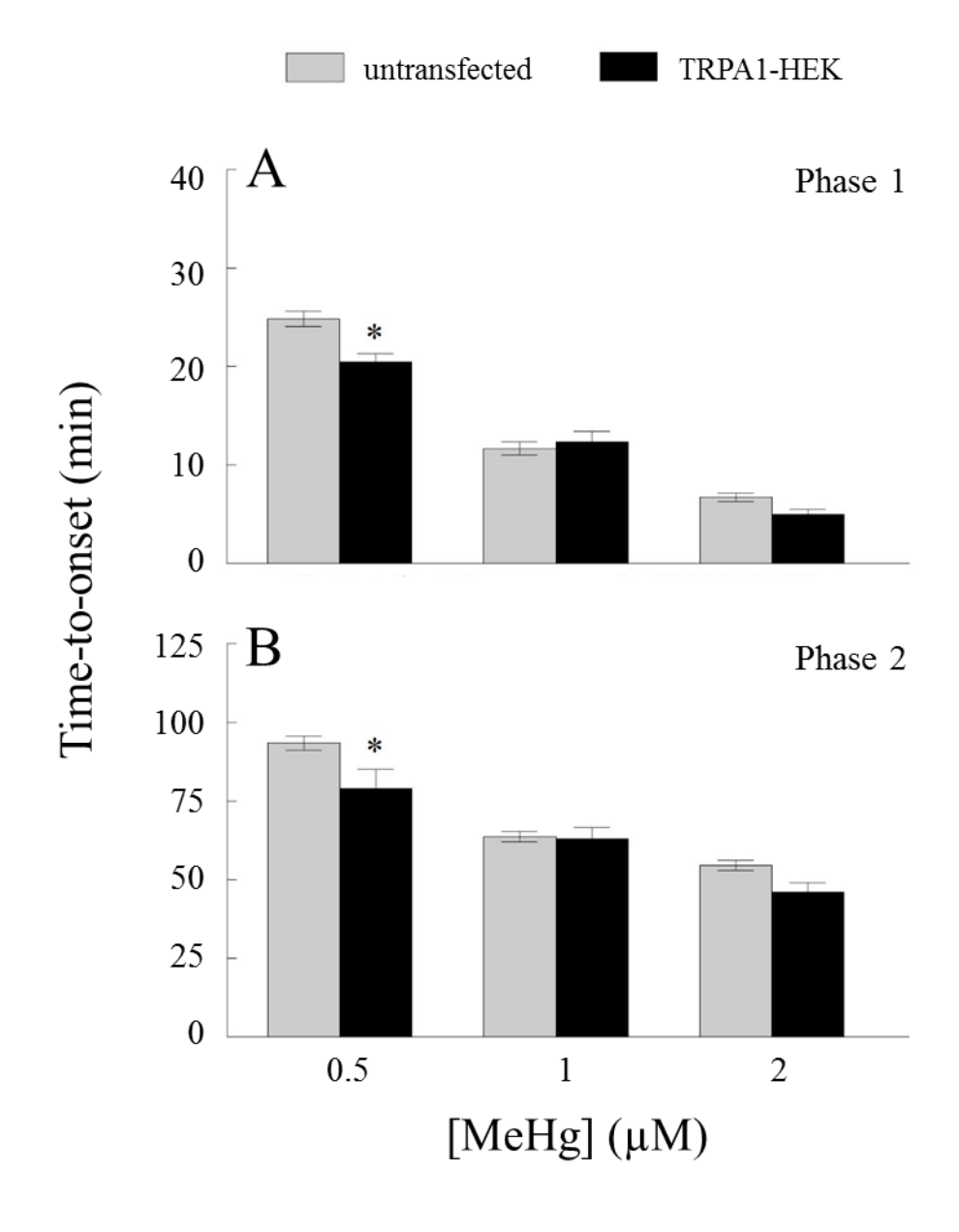


Figure 3.5. In the absence of  $Ca^{2+}_e$ , TRPA1 expression hastens the times-to-onset of phases 1 and 2 at sub-μM MeHg. Untransfected and TRPA1-HEK were superfused with MeHg in EGTA-HBS and changes in  $F_{340/380}$  were continuously monitored. Times-to-onset of (A) phase 1 and (B) phase 2 were quickened in TRPA1-HEK in  $Ca^{2+}_e$ -free conditions at sub-μM MeHg. Onset of either phase was unaffected at higher MeHg concentrations. Significance compared to the untransfected cells is denoted by \* (p < 0.05,  $n \ge 4$ ).

3.4.3. Comparative contribution of endogenous and recombinant TRPA1 to MeHg-induced  $Ca^{2+}{}_{i}$  dysregulation

To better understand the roles of both endogenous and recombinant TRPA1 channels, the channel antagonist A-967079 was used (Gauvin et al., 2009). A-967079 is a highly selective and potent antagonist which interacts with TRPA1 at two amino acid residues, serine 873 and tyrosine 874, residing on the fifth transmembrane segment (Nakatsuka et al., 2013, Banzawa et al., 2014). Predictive modeling places this region of the protein within the channel's vestibule, thus the antagonistic actions of A-967079 appear to be due to direct block of the TRPA1 channel (Klement et al., 2013). Pretreatment with 100 nM A-967079 was sufficient to block a subsequent AITCinduced rise in Ca<sup>2+</sup><sub>i</sub> (Fig. 3.6); this concentration is in line with the reported IC<sub>50</sub> of A-967079 on human TRPA1 (Chen et al., 2011), and thus block of recombinant TRPA1 was presumed under these conditions. Although untransfected HEK did not respond to AITC with a detectable rise in F<sub>340/380</sub>, the contribution of endogenous TRPA1 channels was investigated under the same A-967079 exposure conditions. Pretreatment with the antagonist did not alter the time-to-onset of phase 1 in untransfected HEK (Fig. 3.7A), however it was effective in slowing the time-to-onset of phase 2 (Fig. 3.7B). In contrast, A-967079 did not alter the time-to-onset of phase 1 (Fig. 3.8A) nor phase 2 (Fig. 3.8B) in TRPA1-HEK. When directly compared, the time-to-onset of phase 1 is hastened in TRPA1-HEK treated with A-967079 and 0.5 µM, as compared to untransfected HEK (Fig. 3.9A); phase 2 is initiated more rapidly in TRPA1-HEK across all MeHg concentrations, despite application of A-967079 (Fig. 3.9B). These results present an apparent discrepancy in the efficacy of A-967079 on endogenous versus recombinant TRPA1 channels which may be explained, in part, by the difference in receptor density among the two model cells and the potential for competition at the channel. Because application of A-967079 did not extend into the MeHg

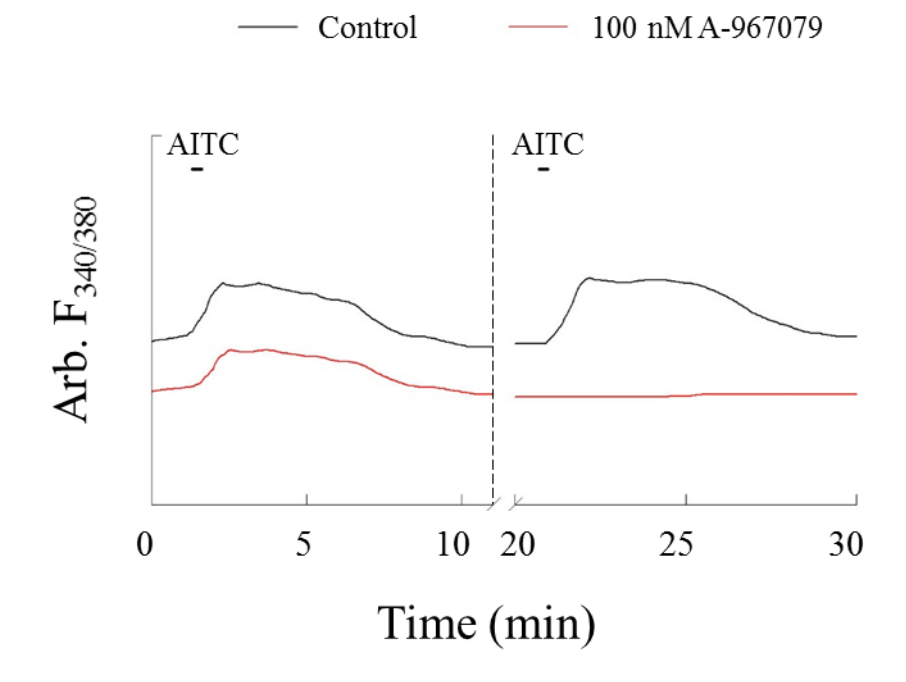


Figure 3.6. AITC-induced  $Ca^{2+}_{i}$  elevations in TRPA1-HEK is blocked by pretreatment with 100 nM A-967079. Application of 10  $\mu$ M AITC (40 s) induced a reversible elevation in  $Ca^{2+}_{i}$  in TRPA1-HEK. AITC, when applied at a later timepoint, was equally efficacious in inducing a  $Ca^{2+}_{i}$  response in naïve TRPA1-HEK (black). The response to the second pulse of AITC was blocked when cells were pretreated with 100 nM A-967079 for 10 min (red). The hashed line indicates where the recording was paused and incubation with A-967079 began.

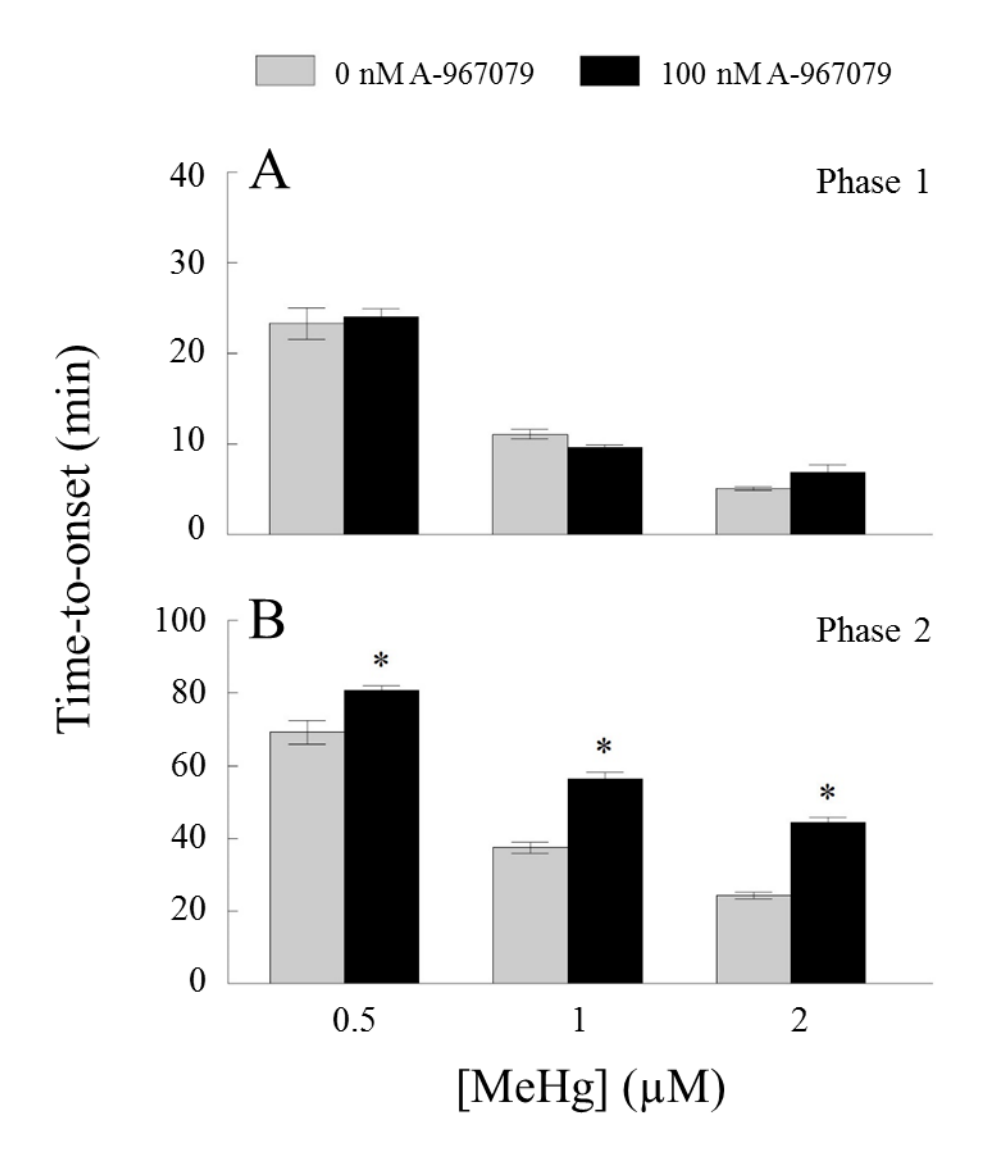


Figure 3.7. Block of endogenous TRPA1 channels slows the time-to-onset of phase 2 in untransfected HEK. Untransfected HEK cells were incubated in 100 nM A-967079 10 min prior to superfusion with MeHg while simultaneously monitoring changes in  $F_{340/380}$ . (A) Pretreatment with A967079 did not alter the time-to-onset of phase 1, however (B) the time-to-onset of phase 2 was slowed. Significance compared to the concentration-matched untransfected control is denoted by \*  $(p < 0.05, n \ge 4)$ .

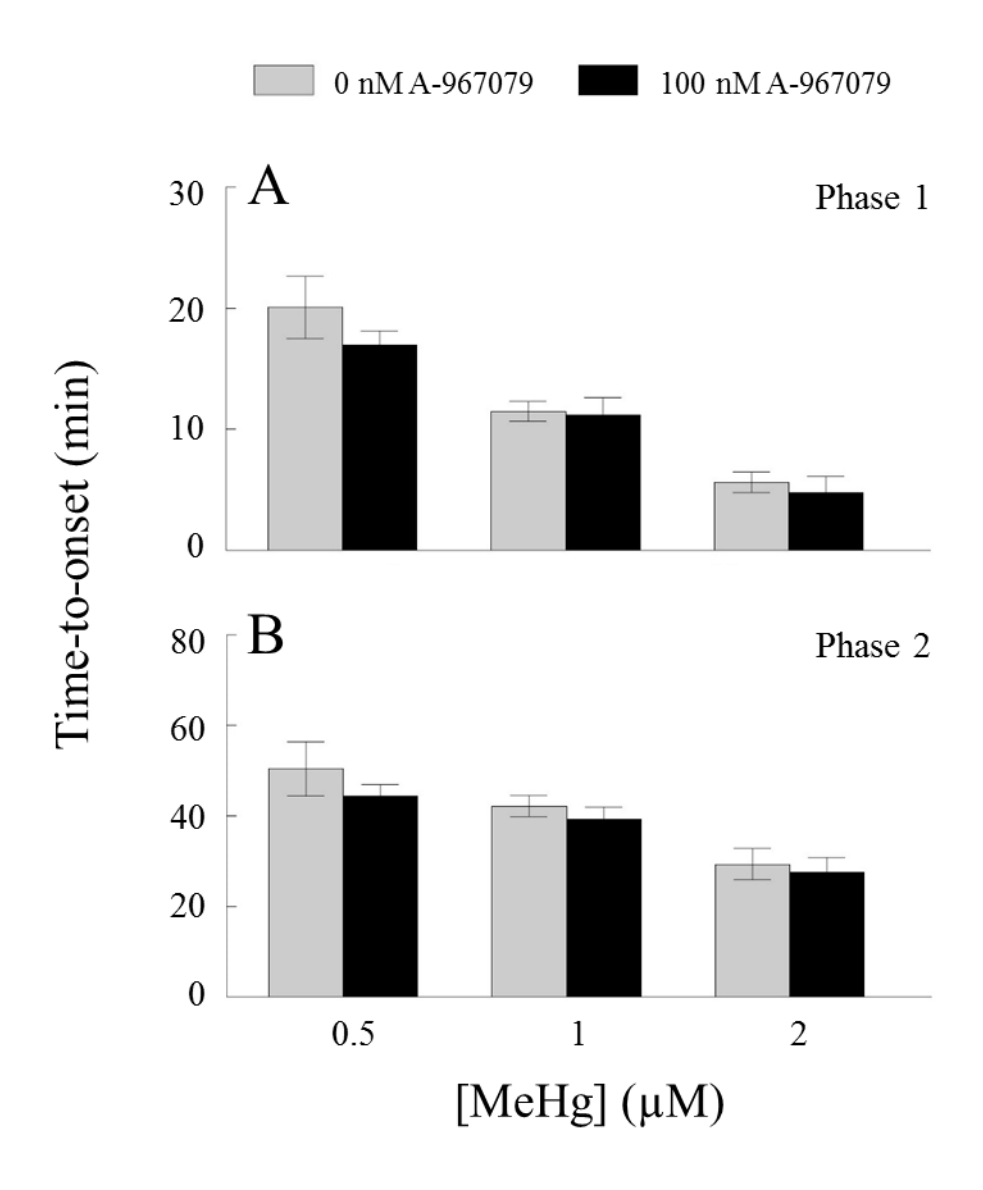


Figure 3.8. Block of recombinant TRPA1 does not alter the time-to-onset of phase 1 nor 2 in TRPA1-HEK. TRPA1-transfected HEK cells were incubated in 100 nM A-967079 10 min prior to superfusion with MeHg while simultaneously monitoring changes in  $F_{340/380}$ .. Times-to-onset of phases (A) 1 and (B) 2 were not altered with the block of recombinant channels in TRPA1-HEK. Significance compared to the concentration-matched untransfected control is denoted by \* (p < 0.05,  $n \ge 4$ ).

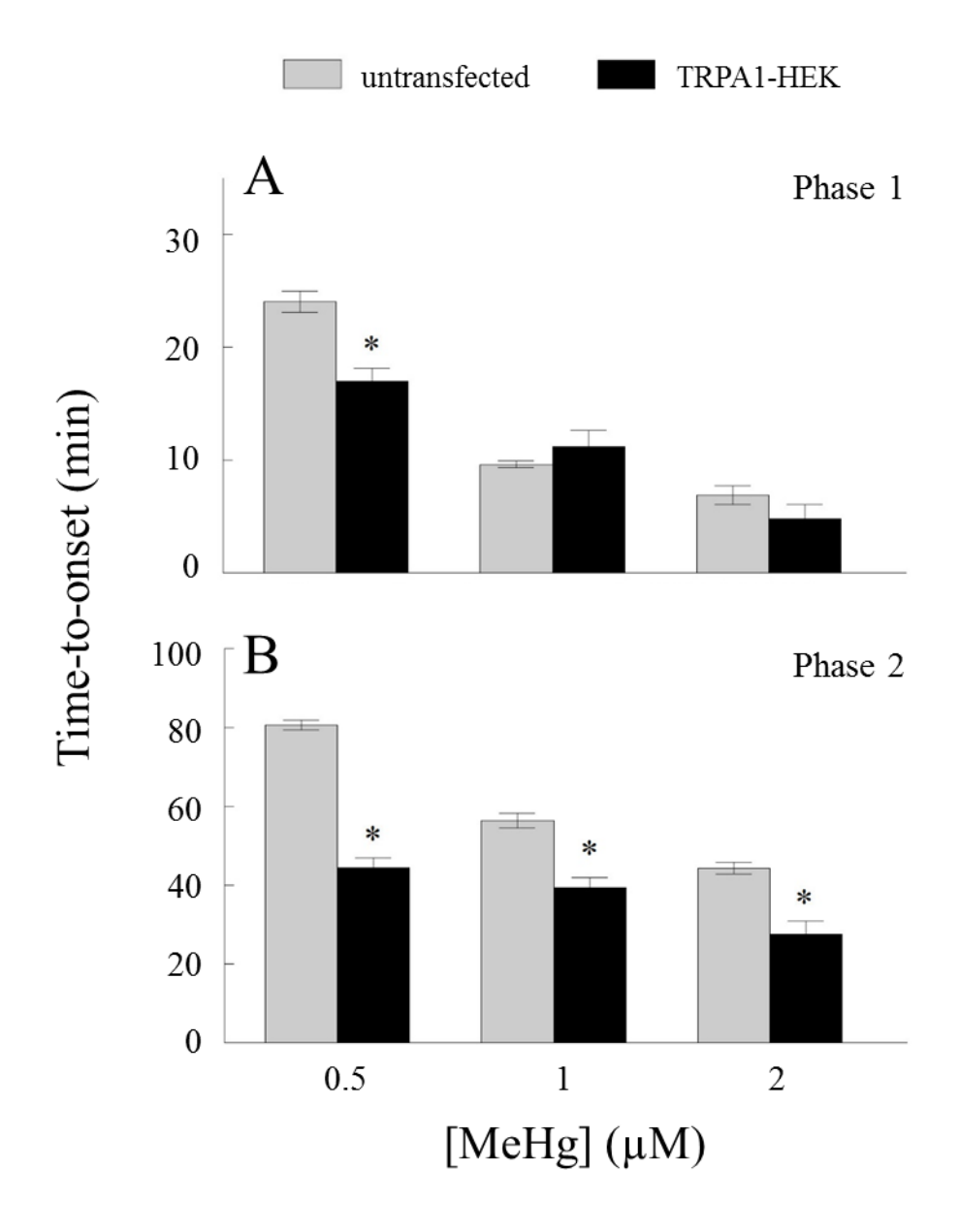


Figure 3.9. Recombinant TRPA1 expression hastens the time-to-onset of phase 2 despite pretreatment with A-967079. Untransfected HEK and TRPA1-HEK were incubated in 100 nM A-967079 10 min prior to superfusion with MeHg; changes in  $F_{340/380}$  were monitored continuously throughout exposure. (A) Time-to-onset of phase 1  $Ca^{2+}$  dysregulation was hastened only at 0.5  $\mu$ M MeHg when cells were pretreated with A-967079. (B) Although untransfected and TRPA1-HEK were both pretreated with A-967079, the phase 2 time-to-onset remained hastened in cells expressing the recombinant channel. Significance compared to the concentration-matched untransfected control is denoted by \* (p < 0.05,  $n \ge 4$ ).

exposure, it is plausible that competition for binding sites on the TRPA1 channel was incited, and the interaction of MeHg with TRPA1 may be more favorable. Alternatively, because TRPA1 channels have numerous cysteine residues that are targets for channel activation by chemical irritants (Macpherson et al., 2007, Sadofsky et al., 2011), it may be that actions of MeHg at alternative residues overcome any effect of the antagonist. In either instance, the heightened receptor density of TRPA1 in the transfected cells would presumably confer the greater sensitivity of TRPA1-HEK observed despite presence of A-967079.

## 3.4.4. Characterization of phase 0 in AITC-sensitive TRPA1-HEK

A subpopulation of AITC-sensitive TRPA1-HEK presented with an early and rapid rise in the fluorescence signal within minutes of beginning MeHg application (Fig. 3.10A). This early response has been termed "phase 0," as it precedes the canonical Ca<sup>2+</sup>e-indepdendent phase 1 response. After returning to baseline from phase 0 perturbations, an erratic and apparently protracted phase 1 response is observed. Although this response is atypical in other cell types, this feature has been characterized as phase 1 because the time-to-onset roughly corresponds to that of phase 1 in AITC-insensitive TRPA1-HEK (Fig. 3.10B). The observation of phase 0 in the TRPA1-HEK response to MeHg was concentration-dependent, where presence of the early Ca<sup>2+</sup>i disruption was reduced as MeHg concentration increased (Fig. 3.11). Pretreatment with A-967079 did not alter the occurrence of this response, though phase 0 was abolished at all MeHg concentrations when Ca<sup>2+</sup>e was removed from the treatment solution (data not shown). While the application of A-967079 did not eliminate the occurrence of phase 0, it did slow the time-to-onset of the response in TRPA1-HEK exposed to 2 μM MeHg (Fig. 3.12). The Ca<sup>2+</sup>e- and TRPA1-dependence of phase

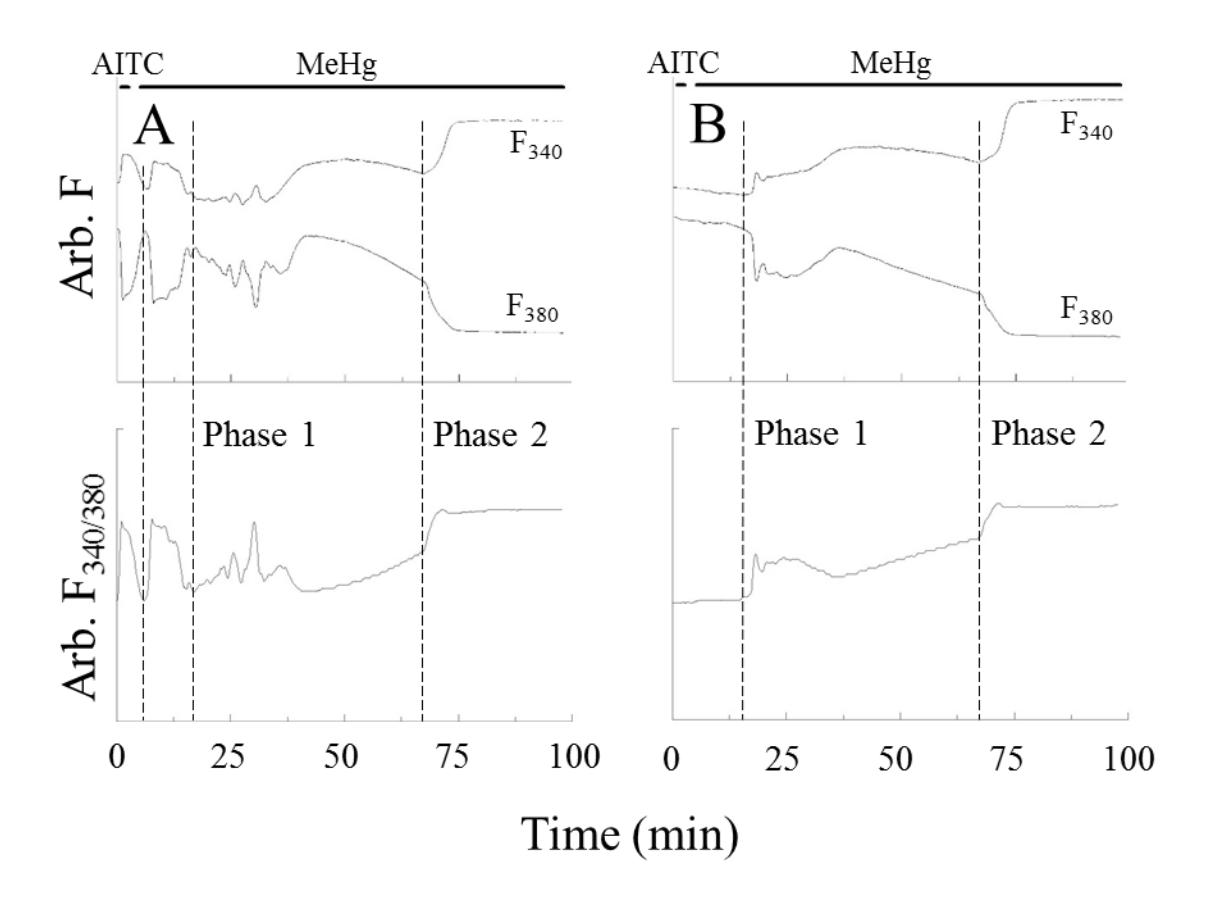


Figure 3.10. Representative tracings of TRPA1-HEK illustrating occurrence of phase 0 coincides with response to AITC. TRPA1-HEK were pulsed with 40 s 10  $\mu$ M AITC to confirm TRPA1 function prior to exposure to MeHg. (A) AITC-sensitive cells displayed a rapid rise in  $F_{340/380}$  which preceded the onset of phase 1. Following this early perturbation, erratic changes in  $F_{340/380}$  were observed. This irregular phase response corresponded with the onset of phase 1 in (B) AITC-insensitive cells. Intermediate and phase 2 Fura-2 responses were comparable regardless of AITC response. Tracings above are from the same field of cells in a single experiment in which cells were exposed to 0.5  $\mu$ M MeHg. Phases 1 and 2 are delineated at the same timepoints in both panels for ease of comparison.

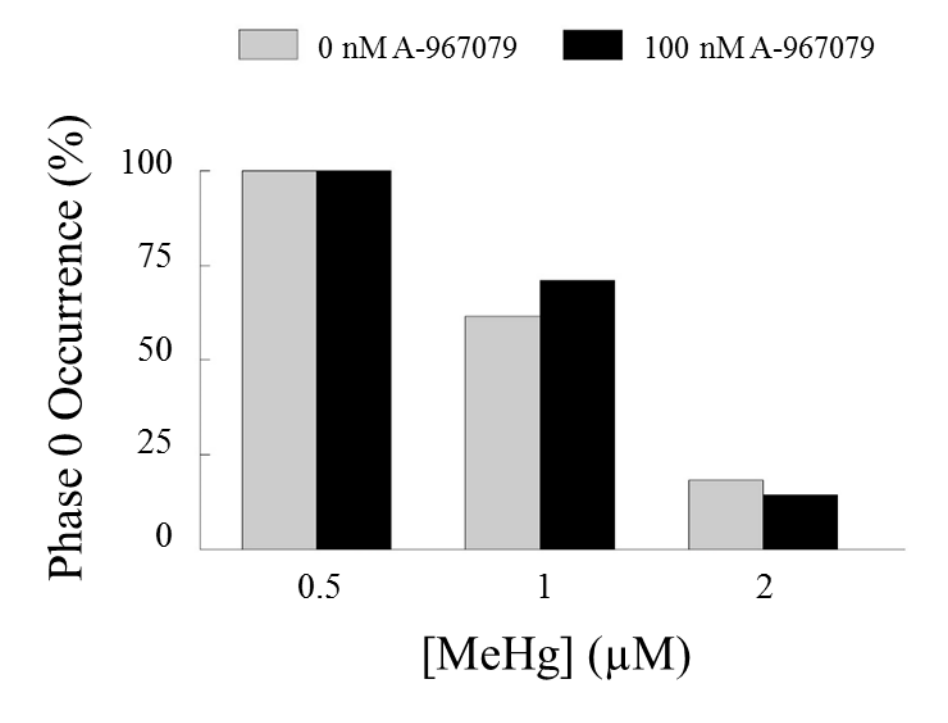


Figure 3.11. The presence of phase 0 in AITC-sensitive TRPA1-HEK is inversely related to MeHg concentration and occurrence is unaltered with block of TRPA1. MeHg application induced phase 0 in TRPA1-expressing cells in a concentration-dependent manner, where more TRPA1-HEK displayed this early phase at lower MeHg concentrations. Block of recombinant channels did not alter the rate of occurrence, although phase 0 was abolished at all MeHg concentrations with the removal of  $Ca^{2+}_{e}$  (not shown) ( $n \ge 4$ ).

0 suggests that the occurrence of this phase may be attributed to Ca<sup>2+</sup> influx through the TRPA1 channel.

## 3.4.5. Assessment of viability of TRPA1-HEK following acute in vitro MeHg exposure

Cell viability was assessed following 1 h MeHg exposure to determine whether TRPA1 expression confers sensitivity to MeHg-induced cell death. MeHg-induced cytotoxicity occurred in a concentration-dependent manner (Fig. 3.13). TRPA1-HEK viability was significantly reduced at 1 and 2  $\mu$ M MeHg, as compared to untransfected cells. Viability of TRPA1-HEK was restored to near-control levels when Ca<sup>2+</sup><sub>e</sub> was removed from the treatment solution. Thus, Ca<sup>2+</sup><sub>e</sub> is a critical mediator of MeHg-induced cytotoxicity in TRPA1-HEK.

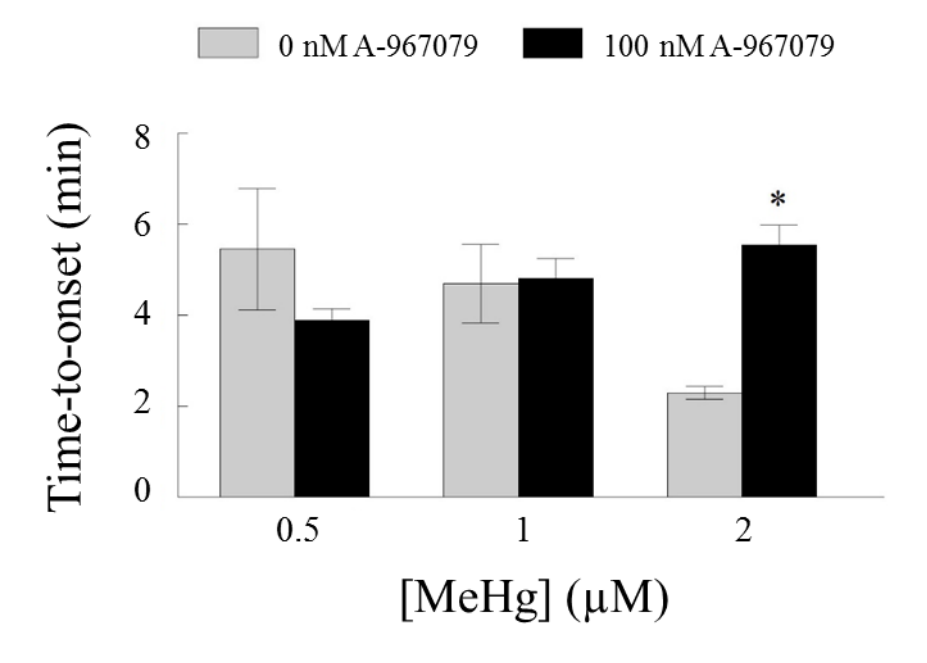


Figure 3.12. Pretreatment with A-967079 slows the time-to-onset of phase 0 in TRPA1-HEK exposed to 2  $\mu$ M MeHg. AITC-sensitive TRPA1-HEK elicited an early phase 0 in the Ca<sup>2+</sup><sub>i</sub> response to *in vitro* MeHg exposure. The onset of this phase was slowed with application of A-967079 at higher MeHg concentrations. Significance compared to the concentration-matched TRPA1-HEK control is denoted by \* (p < 0.05,  $n \ge 4$ ).

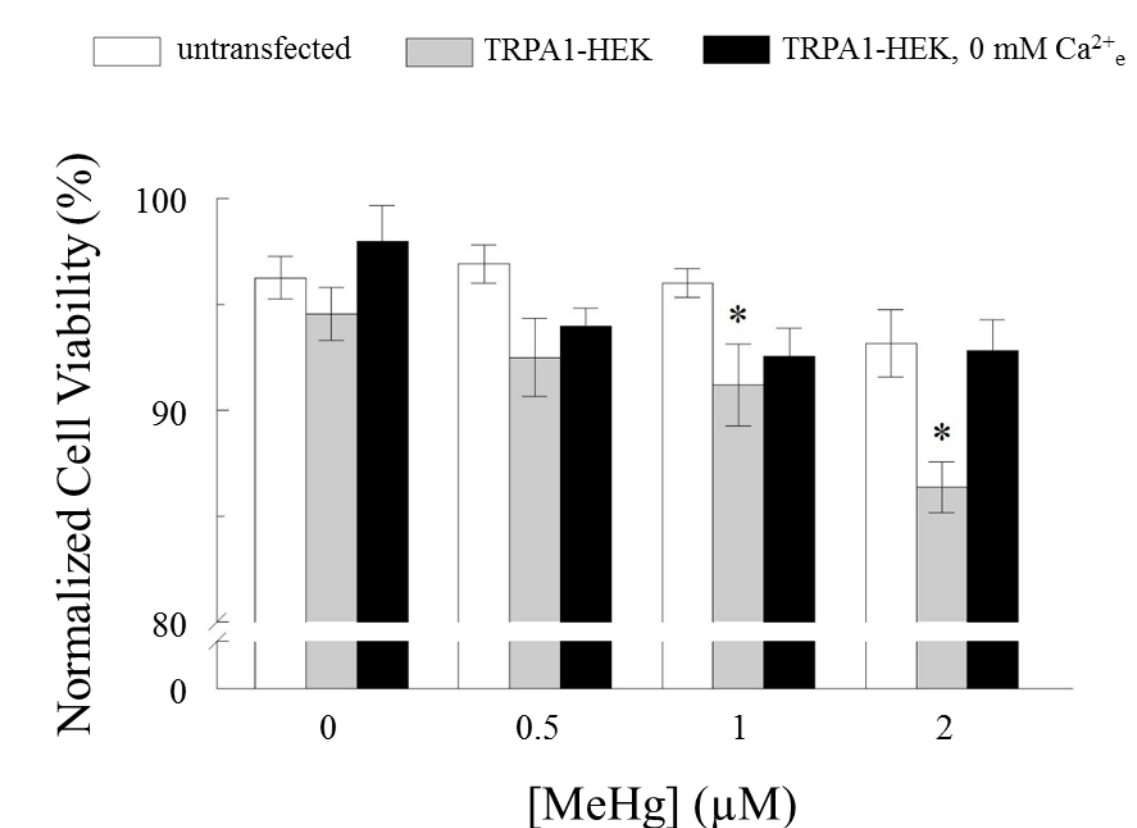


Figure 3.13. TRPA1 expression increases MeHg-mediated cytotoxicity in a  $Ca^{2+}e$ -dependent manner at 1 h post-exposure. Untransfected HEK and TRPA1 HEK were exposed to MeHg for 1 h, and cell viability was assessed 1 h immediately thereafter; TRPA1-HEK were exposed to MeHg both in standard HBS (1.8 mM  $Ca^{2+}e$ ) and EGTA-HBS (0 mM  $Ca^{2+}e$ ). Cells expressing recombinant TRPA1 exhibited a significant reduction in cytotoxicity 1 h following acute *in vitro* exposure to either 1 or 2  $\mu$ M MeHg. Removal of  $Ca^{2+}e$  from the treatment solution restored TRPA1-HEK viability under the same conditions. Significance compared to the concentration-matched untransfected control is denoted by \* (p < 0.05, n  $\geq$  4).

#### 3.5. Discussion

The results of this study demonstrate the sensitivity of TRPA1 expression confers on a cell exposed to MeHg. The actions of mercurials on TRP channels are poorly defined. Study of recombinant TRP channels demonstrated a differential susceptibility of at least 6 distinct isoforms of TRPC, TRPV, and TRPM ion channels to MeHg and  $HgCl_2$  (Xu et al., 2012). However, endogenous distribution of these isoforms does not suggest they would be responsible for mediating MeHg-induced neurotoxicity in A $\beta$  DRG (Vennekens et al., 2002, Liedtke and Heller, 2007, Pingle et al., 2007). Experiments were designed to better understand the role of TRPA1 and  $Ca^{2+}_e$  in mediating MeHg-induced  $Ca^{2+}_i$  dysregulation and cytotoxicity.

Expression of TRPA1 hastened the time-to-onset of phase 2 at 0.5 μM MeHg, as compared to untransfected cells, regardless of presence or absence of Ca<sup>2+</sup><sub>e</sub>. Because phase 2 has been attributed to Ca<sup>2+</sup> influx through Ca<sup>2+</sup>-permeable ion channels (Hare and Atchison, 1995b, Marty et al., 1997, Ramanathan and Atchison, 2011), and MeHg blocks Ca<sup>2+</sup> current in a concentration-dependent manner (Shafer and Atchison, 1991, Sirois and Atchison, 2000, Peng et al., 2002, Hajela et al., 2003, Tarabová et al., 2006), it is not improbable that TRPA1 is blocked at higher MeHg concentrations. However, because this does not resolve the observation made under Ca<sup>2+</sup><sub>e</sub>-free conditions, it is more likely that this apparently concentration-dependent effect of MeHg is mediated by a cytosolic mechanism. While TRPA1 expression conferred hastened Ca<sup>2+</sup><sub>i</sub> increases at 0.5 μM MeHg, this perturbation was not sufficient to reduce cell viability. Since cytotoxicity occurring in TRPA1-HEK at higher MeHg concentrations was dependent upon Ca<sup>2+</sup><sub>e</sub> and the kinetics of Ca<sup>2+</sup><sub>i</sub> dysregulation were unaltered, Ca<sup>2+</sup> influx and intracellular signaling pathways may converge to produce cytotoxicity. Both Ca<sup>2+</sup><sub>i</sub> and IP<sub>3</sub> are mediators of TRPA1 current activation and potentiation in TRPA1-transfected HeLa cells, TRPA1-HEK, and rat trigeminal

neurons (Cavanaugh et al., 2008, Wang et al., 2008b). It is possible that at sub-µM MeHg, these mechanisms prevail to potentiate current in TRPA1-HEK, whereas at higher concentrations of MeHg other sources contribute more significantly to Ca<sup>2+</sup><sub>i</sub> dysregulation.

When compared to TRPA1-HEK in 1.8 mM Ca<sup>2+</sup>e, phase 2 of TRPA1 HEK exposed to MeHg in the absence of Ca<sup>2+</sup>e was slowed at all concentrations. This result was unexpected since TRPA1 expression alone does not significantly alter phase 2 time-to-onset at 1 and 2 μM MeHg concentrations. Thus the role of Ca<sup>2+</sup>e in this effect is important. The involvement of Ca<sup>2+</sup>e in regulating the kinetics of TRPA1-mediated currents has been well characterized; studies demonstrate TRPA1 agonist-induced current is potentiated by permeating Ca<sup>2+</sup> ions (Andersson et al., 2008, Wang et al., 2008b, Salas et al., 2009). Furthermore, Ca<sup>2+</sup>e is critical in regulating agonist-induced TRPA1 pore dilation. Conditions of low Ca<sup>2+</sup>e (approximately 20 μM) promote TRPA1 dilation, allowing greater access to the channel pore for more efficient block of the channel (Chen et al., 2009, Banke, 2011). The Ca<sup>2+</sup>e-free conditions used in my studies were based on a protocol described by Marty et al. (1997), in which actual [Ca<sup>2+</sup>]e was estimated to be 60 nM. It is unclear to what extent the pore of TRPA1 may be dilated under the conditions of these studies. Though, it may be that pore dilation as a result of low Ca<sup>2+</sup>e enhances block of the channel by MeHg.

In the presence of A-967079, phase 2 of TRPA1-HEK is hastened, as compared to untransfected cells, suggesting either: 1) a stimulatory effect of TRPA1, or 2) poor efficacy of A-967079 in the presence of MeHg. Because pretreatment with A-967079 readily slowed phase 2 in untransfected HEK cells, presumably through block of endogenous TRPA1, and was efficacious in blocking AITC-induced Ca<sup>2+</sup><sub>i</sub> elevations, the latter conclusion is more plausible. Given the affinity of MeHg for thiol groups (Kostyniak and Clarkson, 1981, Harris et al., 2003), I have

hypothesized MeHg may activate TRPA1 through interaction with cysteine residues in a manner similar to other reactive irritants (Macpherson et al., 2007, Takahashi et al., 2008, Sadofsky et al., 2011). Thus, if the efficacy of A-967079 is lost in the presence of MeHg, there may exist competition near active sites on the channel. A-967079 binds to serine and tyrosine residues located on the fifth transmembrane segment of TRPA1 in a region identified as the putative ionic filter within the channel pore (Klement et al., 2013, Nakatsuka et al., 2013, Banzawa et al., 2014). Cysteine residues within the same pore-forming region have been identified as critical components for activation of some TRPC isoforms (Xu et al., 2012), however there is no report of conserved cysteine residues at this location on TRPA1 (Wang et al., 2012). Rather, cysteines which are covalently modified in the activation of TRPA1 are located mainly on the N- and C-termini (Karashima et al., 2010, Nilius et al., 2012, Wang et al., 2012). Combined, these studies would suggest that competition between A-967079 and MeHg for the same binding site is not likely, though this does not preclude physical obstruction due to close proximity of active sites. This, combined with the increased TRPA1 density in TRPA1-HEK may serve to rectify the hastened onset of phase 2.

While several studies in heterologous expression systems and primary cultures report a rise in Ca<sup>2+</sup><sub>i</sub> following agonist-induced activation of TRPA1 (Bandell et al., 2004, Jordt et al., 2004, Andersson et al., 2008, Wang et al., 2008b, Karashima et al., 2010, Barabas et al., 2012), the observation of phase 0 in these studies was unique. Because characteristics of TRPA1 current are agonist-dependent (Cavanaugh et al., 2008, Nilius et al., 2012), the occurrence of phase 0 may be attributable to an interaction with MeHg. The Ca<sup>2+</sup><sub>e</sub>-dependence of phase 0 seems to indicate Ca<sup>2+</sup> influx via TRPA1 when exposed to MeHg, thus supporting the hypothesis that TRPA1 mediates MeHg-induced Ca<sup>2+</sup><sub>i</sub> dysregulation. At higher MeHg concentrations, the reduction in frequency

with which phase 0 is observed may be attributed to inactivation via elevated Ca<sup>2+</sup><sub>i</sub> (Wang et al., 2008b, Nilius et al., 2012) or direct block of the channel pore. A triphasic elevation in Ca<sup>2+</sup><sub>i</sub> throughout MeHg is unique, and has only been reported in type II cerebellar astrocytes (Marty et al., 1997, Lundback et al., 2002). However, in astrocytes, the time-to-onset of each phase was unaltered by the removal of Ca<sup>2+</sup><sub>e</sub>, and the initial phase was attributed to Ca<sup>2+</sup> release from mitochondria. While this contrasts my initial findings, further pharmacologic manipulation should be performed to thoroughly identify the contributing sources of Ca<sup>2+</sup> in each phase response. Furthermore, it remains to be understood how these perturbations in Ca<sup>2+</sup><sub>i</sub> ultimately lead to disruption of electrical properties reported in MeHg-exposed DRG.

# CHAPTER FOUR

TRANSIENT RECEPTOR POTENTIAL ANKYRIN 1 CHANNEL AS A PROBABLE MEDIATOR OF METHYLMERCURY-INDUCED CALCIUM DYSREGULATION AND CYTOTOXICITY IN JUVENILE MOUSE DORSAL ROOT GANGLIA NEURONS

#### 4.1. Abstract

Recombinant expression of TRPA1 in HEK cells results in hastened elevation of Ca<sup>2+</sup><sub>i</sub> at sub-µM MeHg and marked reduction in cell viability, as compared to untransfected HEK. Because these effects were Ca<sup>2+</sup>e-dependent, Ca<sup>2+</sup> entry through the TRPA1 channel appears to be an important mechanism in mediating MeHg-induced cell death. TRPA1 channels are endogenously expressed in visceral tissues and neurons throughout the body, with expression being particularly abundant in DRG. MeHg neurotoxicity in DRG selectively reduces the size and number of large diameter mechanoreceptive AB DRG while smaller diameter nociceptive DRG are relatively unaffected. I hypothesize that the mechanosensitive TRPA1 channel may be a molecular target for MeHg and mediate selective degeneration of Aβ DRG as a result of exposure. To determine whether TRPA1 expression confers sensitivity to AB DRG, neurons were acutely dissociated from juvenile mice and plated as heterogeneous populations for comparative studies. Immunological labeling revealed TRPA1 co-expressed with heavy-chain neurofilament (200 kDa, NF-200), a marker for Aβ DRG, in addition to being expressed in smaller diameter DRG lacking NF-200. Viability of the acutely dissociated DRG was assessed at either 1 or 4 h following 30 min in vitro exposure to MeHg (200 nM  $- 2 \mu M$ ). Marked cytotoxicity was observed at 1 and 2  $\mu M$  MeHg 4 h following exposure, an effect which was improved with either the removal of Ca<sup>2+</sup><sub>e</sub> or treatment with A-967079, a TRPA1 antagonist. The potential for TRPA1 to contribute to MeHg-induced Ca<sup>2+</sup><sub>i</sub> dysregulation was then probed through the use of Fura-2 based microfluorimetry. AITC, a TRPA1 agonist, was used to confirm TRPA1 function prior to beginning any experimental treatments. The time-to-onset of phase 1 in AITC-sensitive cells was not affected by Ca<sup>2+</sup><sub>e</sub>-free conditions nor the application of A-967079; time-to-onset of phase 2 was slowed only by removal of Ca<sup>2+</sup><sub>e</sub>. Similar responses of phase 1 and 2 times-to-onset were measured in AITC-insensitive

cells. Whole-cell current recordings found  $Na^+$  to be the primary charge carrier in the agonist-induced activation of TRPA1 in A $\beta$  DRG. Reducing extracellular  $Na^+$  ( $Na^+_e$ ) in microfluorimetric studies resulted in a slowing of the time-to-onset of phase 2. These results suggest  $Na^+_e$  influx through TRPA1 elicits secondary effects which lead to  $Ca^{2+}_e$  influx and, subsequently, cell death.

#### 4.2. Introduction

The preeminent clinical sign of MeHg poisoning is distal paresthesia (Takaoka et al., 2008). MeHg-induced paresthesia manifests from degeneration of DRG (Eto, 1997, Eto et al., 2002a), though dysfunction and degeneration of DRG is not equal among the subclasses of neurons. At low concentrations of MeHg, there is a marked reduction in the number and mean soma volume of Aβ DRG, whereas the C and Aδ subtypes are relatively spared (Schiønning et al., 1998). Events leading to degeneration of Aβ neurons include morphologic alterations and swelling of cisternal organelles (Cavanagh and Chen, 1971, Delio et al., 1992), microtubule disruption (Abe et al., 1975, Miura et al., 2000), and suppression of protein synthesis (Omata et al., 1982, Kasama et al., 1989). Aβ DRG also display alterations in electrical properties as a consequence of exposure to MeHg; effects include ectopic firing (Delio et al., 1992), reduction in action potential firing threshold (Világi et al., 2000), block of voltage-activated cation channels (Leonhardt et al., 1996a, Leonhardt et al., 1996b), and reduction of GABA-induced currents (Arakawa et al., 1991, Narahashi et al., 1994).

Given that Aβ DRG are selectively affected by MeHg, it has been postulated that a molecular feature of this class of neuron may be involved in events preceding and contributing to degeneration. A potential target for MeHg-mediated toxicity in DRG is the TRP family of ion channels due to their permeability to Ca<sup>2+</sup>, distribution throughout sensory organs, and polymodal means of activation (Liedtke and Heller, 2007, Islam, 2011). Studies of TRPCs in a heterologous expression system revealed the potential for MeHg to interact with TRPC4 and TRPC5 at cysteine residues residing in the pore, resulting in Ca<sup>2+</sup> influx (Xu et al., 2012). Experiments presented in Chapter 3 describe similar findings for cells expressing recombinant TRPA1, though the site for interaction with MeHg was not elucidated.

While the studies from Xu et al. (2012) and the results presented in Chapter 3 suggest members of the TRP family of ion channels may be susceptible to MeHg when recombinantly expressed in isolation, these systems are artificially simplistic. In addition to mediating current upon chemical (Bandell et al., 2004, Jordt et al., 2004, Macpherson et al., 2007) or mechanical activation (Walker et al., 2000, Kindt et al., 2007, Kwan et al., 2009), intracellular protein kinases and phospholipases provide another mode through which TRPA1 activity can be modulated (Dai et al., 2007, Wang et al., 2008a, Mandadi et al., 2011). Since MeHg reduces the enzymatic activity of PKA and PKC (Saijoh et al., 1993, Rajanna et al., 1995), and causes Ca<sup>2+</sup>i dysregulation through phospholipase C (PLC)-linked pathways (Limke et al., 2004, Kang et al., 2006), it may be that the action of MeHg on the intracellular side of the DRG neuron may play an important role in understanding neurotoxicity. While this intracellular machinery is endogenously expressed in HEK cells (Lin et al., 2014), it is unclear the extent to which they would associate with the recombinant TRPA1 used in Chapter 3. Additionally, in physiologic conditions, TRP channels are often co-expressed and interact with one another. TRPV1 and TRPM5, in particular, confer unique pharmacologic (Buber et al., 2010, Sadofsky et al., 2014) and biophysical (Salas et al., 2009, Patil et al., 2010, Fischer et al., 2014, Spahn et al., 2014) properties to TRPA1 when co-expressed. Thus, it is of paramount importance to consider the contribution of these factors when assessing the sensitivity of TRPA1 to MeHg.

The aim of this study was two-fold: to determine 1) the sensitivity of acutely dissociated juvenile DRG to MeHg, and 2) whether TRPA1 expression confers a heightened susceptibility of A $\beta$  DRG to MeHg. A juvenile (7 – 8 weeks old) murine model was selected as the source of primary neurons. At this age, DRG function as defined by TRP expression is comparable to that of the adult mouse (Hjerling-Leffler et al., 2007, Zhu and Oxford, 2011), yet the yield of primary

neurons from a single isolation was higher than that obtained from an older animal. DRG were plated as heterogeneous populations because appropriate cell surface markers to adequately isolate Aβ from Aδ and C neurons have not been described. Characterization of the functional subtype by soma diameter also is limited in its predictive power, potentially leading to overestimation of DRG size (Moraes et al., 2014). Viability of acutely dissociated DRG was first assessed over a range of MeHg concentrations to better understand the sensitivity of the neurons. MeHg-induced neurotoxicity of rodent DRG is well characterized following *in vivo* exposures (Cavanagh and Chen, 1971, Delio et al., 1992, Schiønning et al., 1998, Eto et al., 2002b, Cao et al., 2013), but not following *in vitro* exposures of primary DRG neurons.

Studies investigating distribution of TRPA1 throughout DRG subtypes have been somewhat contradictory. While some suggest that TRPA1 is a mechanoreceptive channel located in Aβ DRG (Walker et al., 2000, Kwan et al., 2009), many implicated TRPA1 as a noxious nociceptive channel found only in smaller diameter DRG (Kobayashi et al., 2005, Ji et al., 2008, Brierley et al., 2011, Barabas et al., 2012). Thus, after characterization of the sensitivity of a heterogeneous population of DRG, the expression of TRPA1 among subtypes was assessed by dual-fluorescence immunocytochemistry. Subsequent electrophysiologic recordings and Fura-2-based Ca<sup>2+</sup> imaging employed a moderately specific TRPA1 agonist (Ohta et al., 2007, Gees et al., 2013) for functional assessment of the channel. Because the cation permeability of TRPA1 has been reported to change upon agonist activation (Chen et al., 2009, Karashima et al., 2010), some experiments were conducted in reduced Na<sup>+</sup>e conditions.

#### 4.3. Methods

#### 4.3.1. Materials

Materials were obtained from sources and solutions prepared as described in Chapters 2.3.1 and 3.3.1, unless otherwise described here. AITC and A-967079 were diluted from stocks and prepared as 1 mM and 500 nM solutions in HBS, respectively. Papain, dispase II, L-cysteine, poly-D-lysine, laminin, TTX, and Triton-X were purchased from Sigma-Aldrich. Normal goat serum (NGS) was purchased from Vector Laboratories.

#### 4.3.2. *Animals*

All studies in this chapter were conducted in accordance with the National Institutes of Health Guide for the Care and Use of Laboratory Animals and approved by the Michigan State University Institutional Animal Care and Use Committee.

### 4.3.3. Isolation of primary dorsal root ganglia

DRG (T12 – L5) were collected from 7 – 8 week old C57BL/6J mice of either gender in a laminectomy procedure derived from Malin et al. (2007); these DRG correspond with the levels in which lumbosacral enlargement of spinal gray matter was reported (Pinto et al., 2002), and serve to innervate the hindlimbs (Rigaud et al., 2008, Harrison et al., 2013). Mice were anesthetized with isoflurane (Abbott Laboratories, Abbott Park, IL) and decapitated. A longitudinal incision was made along the dorsal side to expose the vertebral column and the column was removed through a series of parallel, bilateral incisions. The tissue was placed in a Sylgard (Dow Corning Corporation, Auburn, MI)-coated petri dish and kept moist in Ca<sup>2+</sup>- and Mg<sup>2+</sup>-free HBS (CMF-HBS) containing (in mM): 135 NaCl, 5 KCl, 20 HEPES, and 20 D-glucose (pH to 7.3 with Tris).

Laminae were removed to expose the spinal cord, and DRG were collected and pooled in a separate petri dish containing ice-cold CMF-HBS. DRG were then cleared of excess nerve fiber and transferred to a conical tube containing 20 U/mL papain, 2.8 mM L-cysteine, and 1.2 mM NaHCO<sub>3</sub> in CMF-HBS. DRG were incubated in the papain solution for 20 min in a 37°C water bath with gentle agitation, at which time the solution was aspirated from the DRG and replaced with 500 U/mL collagenase II (Worthington Biochemical, Lakewood, NJ) and 2.5 U/mL dispase II. Ganglia were incubated in collagenase/dispase II for 20 min at 37°C with gentle agitation. The collagenase/dispase II solution was carefully aspirated, DRG were rinsed twice with CMF-HBS, and were then triturated in DMEM/F-12 culture medium supplemented with 10% (v/v) FBS using a fire-polished Pasteur pipette. Cells were plated at high density  $(8 \times 10^5 \text{ cells/mL})$  and low volume (40 μL) onto borosilicate glass coverslips coated with 2% (w/v) poly-D-lysine and 2% (w/v) laminin, and incubated at 37°C and 5% CO<sub>2</sub> for 2 h. Following incubation, dishes containing the DRG were flooded with DMEM/F-12 and returned to incubator until used in experiments. All experiments were conducted within 24 h of plating DRG to avoid significant alterations in electrical properties associated with culture conditions (Scott and Edwards, 1980). A single animal was used for each isolation, yielding a heterogeneous population of approximately 400,000 cells. Experiments were conducted using DRG from a minimum of three mice, where one mouse is defined as n = 1.

## 4.3.4. Single-cell microfluorimetry

Microfluorimetric measurements were made, as previously described in Chapters 2.3.3 and 3.3.4, with the few modifications. DRG were rinsed three times with HBS and incubated in 3  $\mu$ M Fura-2 AM with 3  $\mu$ M pluronic acid for 30 min at 37°C. Cells were then transferred to a heated

perfusion system (37°C, 2 mL/min) and perfused with HBS for 5 min. Experiments began with a 60 s pulse of 1 mM AITC to verify TRPA1 expression and cell viability. Once a stable baseline was reestablished, the perfusion buffer was changed to 500 nM MeHg and perfusion continued at 2 mL/min for the duration of the experiment. In experiments performed with the TRPA1 antagonist, DRG were first pulsed with 1 mM AITC in standard HBS and, upon return to baseline, were incubated with 500 nM A-967079 for 10 min. Fura-2 recordings resumed and perfusion with MeHg began immediately following this incubation period. A-967079 was not included in the MeHg perfusion buffer. For experiments conducted in low Na<sup>+</sup><sub>e</sub>, a modified HBS (choline-HBS) was used and consisted of (in mM): 110 Choline-Cl, 40 NaCl, 5.4 KCl, 2.4 CaCl<sub>2</sub>, 1.6 MgSO<sub>4</sub>, 20 HEPES, 20 D-glucose, and 0.0001 TTX (pH to 7.3 with Tris). Na<sup>+</sup> was not entirely removed from the perfusion buffer due to the noted importance of the Na<sup>+</sup>-Ca<sup>2+</sup> exchanger in regulating resting membrane potential and Ca<sup>2+</sup> extrusion in DRG (Scheff et al., 2014, Estacion et al., 2015). In these studies, TRPA1 activity was first confirmed with AITC in standard HBS before the perfusion buffer was changed to choline-HBS; cells were perfused with choline-HBS for 5 min to ensure complete buffer exchange in the perfusion chamber prior to exposure to MeHg prepared in choline-HBS. Time-to-onset was calculated for each cell responding to AITC within the experimental field, then mean times-to-onset of phases 1 and 2 were calculated for that population of cells. For each condition, a minimum of three experiments were conducted using cells from a single DRG isolation (n = 1)

#### 4.3.5. *Measurement of cell viability*

Viability of acutely dissociated DRG was assessed following *in vitro* exposure to MeHg, as described in Chapter 2.3.4. DRG were exposed to  $200 \text{ nM} - 2 \mu\text{M}$  MeHg for 30 min at  $37^{\circ}\text{C}$ .

DRG were exposed to the toxicant in standard HBS or EGTA-HBS. In a separate set of experiments, DRG were pretreated with 500 nM A-967079 for 10 min prior to MeHg exposure. Cells were labeled with 0.2 µM calcein AM and 0.1 µM EthD-1 at either 1 or 4 h following exposure to MeHg. Mean percent viabilities from triplicate wells (n = 1) were then normalized to the viability of DRG which were not exposed to MeHg, but underwent all the experimental manipulations in standard DMEM/F-12 to account for changes in viability attributed to culture conditions.

## 4.3.6. Double-fluorescence immunocytochemistry

DRG were sequentially immunolabeled to determine TRPA1 expression in Aβ DRG; procedures deviated only slightly from those described in Chapter 3.3.3. Within 12 –14 h of plating, DRG were rinsed three times in ice-cold PBS and fixed in 4% (w/v) paraformaldehyde for 10 min at room temperature. Cells were rinsed three more times with PBS prior to incubation in 0.3% (v/v) Triton-X prepared with 1% (w/v) BSA and 10% (v/v) NGS in PBS (1 h, room temperature). Following permeabilization and block, cells were rinsed three times with PBS in preparation for labeling with primary antibodies. All antibody dilutions were prepared in 1% (w/v) BSA and 10% (v/v) NGS in PBS, and cells were rinsed three times with PBS in between each sequential step. DRG were incubated in rabbit anti-TRPA1 (1:50; Thermo Fisher Scientific) overnight at 4°C, followed by fluorescein isothiocyanate (FITC)-conjugated goat anti-rabbit (1:50; Thermo Fisher Scientific) for 2 h at room temperature to first label TRPA1-expressing cells. DRG were then incubated in chicken anti-neurofilament 200 (1:1000; Abcam, Cambridge, MA) overnight at 4°C, followed by goat anti-chicken conjugated to AlexaFluor 594 (1:100; Abcam) for 2 h at room temperature. NF-200 is a component of the cytoskeleton found in subsets of neurons

including DRG, and has been used to immunologically distinguish Aβ from other DRG subtypes (Lawson et al., 1993, Ishii et al., 2004). DRG were washed a final three times in PBS before coverslips were mounted on glass microscope slides with aqueous hard-set mounting medium containing 4',6-diamidino-2-phenylindole (DAPI) (Vector Laboratories. Representative images were collected under a Nikon Eclipse fluorescence microscope equipped with a CoolSNAP EZ CCD camera and Nikon NIS-Elements software.

### 4.3.7. Whole-cell voltage-clamp

Recordings of AITC-induced currents were made to determine TRPA1 channel function in A $\beta$  DRG. All recordings were performed 3 – 8 h following plating to avoid concerns of flattening of cells and space clamp (Rall and Segev, 1985, Armstrong and Gilly, 1992). Prior to recording, coverslips containing DRG were rinsed three times with an extracellular recording solution containing (in mM): 140 TEACl, 2.5 CsCl, 2.5 CaCl<sub>2</sub>, 1 MgCl<sub>2</sub>, 10 D-glucose, 10 HEPES, and 0.0001 TTX (pH to 7.2 with CsOH, 330  $\pm$  mOsm with sucrose). For some experiments, an equimolar exchange of TEACl for NaCl was made to determine the importance of Na<sup>+</sup> as a charge carrier in AITC-induced currents. Approximately 1 mL of extracellular solution was placed in the recording chamber, and extracellular solution was gravity perfused over the coverslip at a rate of approximately 1 mL/min throughout recordings. Patch electrodes were pulled from borosilicate glass capillary tubing (inner diameter 0.84 mm, outer diameter 1.5 mm; World Precision Instruments, Sarasota, FL) using a Flaming/Brown pipette puller (Sutter Instrument Co, Novato, CA), and fire polished to a resistance of  $2-5 \text{ M}\Omega$  using a Narishige (Japan) microforge. The internal pipette solution contained (in mM): 120 CsCl, 2 MgCl<sub>2</sub>, 5 Na<sub>2</sub>ATP, 10 EGTA, and 10 HEPES (pH to 7.2 with CsOH,  $285 \pm \text{mOsm}$  with sucrose). Recordings were made in the wholecell configuration using a patch clamp circuit consisting of a CV-203 BU head stage and Axopatch 200B amplifier (Axon Instruments, Sunnyvale, CA). Data were acquired on a computer with pCLAMP software (Axon Instruments) via a Digidata 1320A interface (Axon Instruments). The whole-cell configuration was obtained by applying gentle negative pressure from a holding potential (V<sub>h</sub>) of -80 mV, and series resistances and membrane capacitances were compensated. Only cells with a membrane capacitance (C<sub>m</sub>) of 55 – 75 pF were recorded from, as they corresponded with the Aβ subtype (Pearce and Duchen, 1994). Current responses were filtered at 100 kHz using an 8-pole low-pass Bessel filter and digitized at 20 kHz. A 20 s pulse of 1 mM AITC was applied to the cell via gravity perfusion into the bath at a rate of approximately 1 mL/min. Coverslips were discarded once cells had been exposed to AITC to avoid desensitization or prolonged agonist exposure. Thus recordings were made from a maximum of one cell per coverslip, and a minimum of three cells from a single dissociation were used for each treatment condition.

#### 4.3.8. Statistics

Each experiment was performed using primary cells from a minimum of three animals, where one animal is n = 1; data are presented as mean  $\pm$  SEM. Data were analyzed using the GraphPad Prism® statistical program. A two-way ANOVA was performed to compare cell viability of DRG at the timepoints and MeHg concentrations tested. A *post hoc* Bonferroni test was used when significant differences between sample means were detected (Steel and Torrie, 1960). Microfluorimetry results were analyzed with either a one-way ANOVA and Tukey's post hoc test, or student's T-test. Values of p < 0.05 were considered to be statistically significant.

## 4.4. Results

## 4.4.1. Assessing the viability of DRG following acute in vitro MeHg exposure

Viability of acutely dissociated DRG was assessed following 30 min MeHg exposure to determine relative sensitivity. A marked reduction in cell viability was measurable at 1 h post-exposure only at 2 µM MeHg (Fig. 4.1). At 4 h post-exposure, cell viability was significantly reduced in both the 1 and 2 µM MeHg treatment groups. MeHg-induced cytotoxicity was not apparently concentration-dependent at either timepoint assessed. However, a time-dependent reduction in DRG viability was measured at 200 nM MeHg. These results indicate a high sensitivity of DRG to MeHg. While any early effects of toxicant exposure may not immediately be cytotoxic, acute exposure to low µM MeHg elicits severe cytotoxicity within a matter of hours.

To determine the role of  $Ca^{2+}_e$  in mediating MeHg-induced cytotoxicity,  $Ca^{2+}_e$  was removed from the extracellular treatment solution. At 1 h post-exposure, DRG viability was not reduced at any concentration of MeHg, but was also not improved when compared to the viability of those neurons exposed in standard 1.8 mM  $Ca^{2+}$  HBS. (Fig. 4.2). In contrast, removal of  $Ca^{2+}_e$  improved cell viability at all concentrations of MeHg 4 h following the acute exposure, as compared to their counterparts exposed in standard HBS.  $Ca^{2+}_e$  alone does not apparently incite cell death at 4 h post-exposure; cells treated with 2  $\mu$ M MeHg in EGTA-HBS displayed a reduction in viability, as compared to controls, despite having an improved viability over those treated with 2  $\mu$ M MeHg in 1.8 mM  $Ca^{2+}$  HBS. These results suggest that the MeHg-induced cytotoxicity of DRG elicited shortly after exposure is  $Ca^{2+}_e$ -independent. Conversely, later stages of MeHg-induced cytotoxicity seem to be largely  $Ca^{2+}_e$ -dependent, though intracellularly-based mechanisms may also contribute. This supports previous hypotheses and findings that MeHg may traverse the cell membrane and act upon intracellular targets prior to any changes in  $Ca^{2+}$  influx

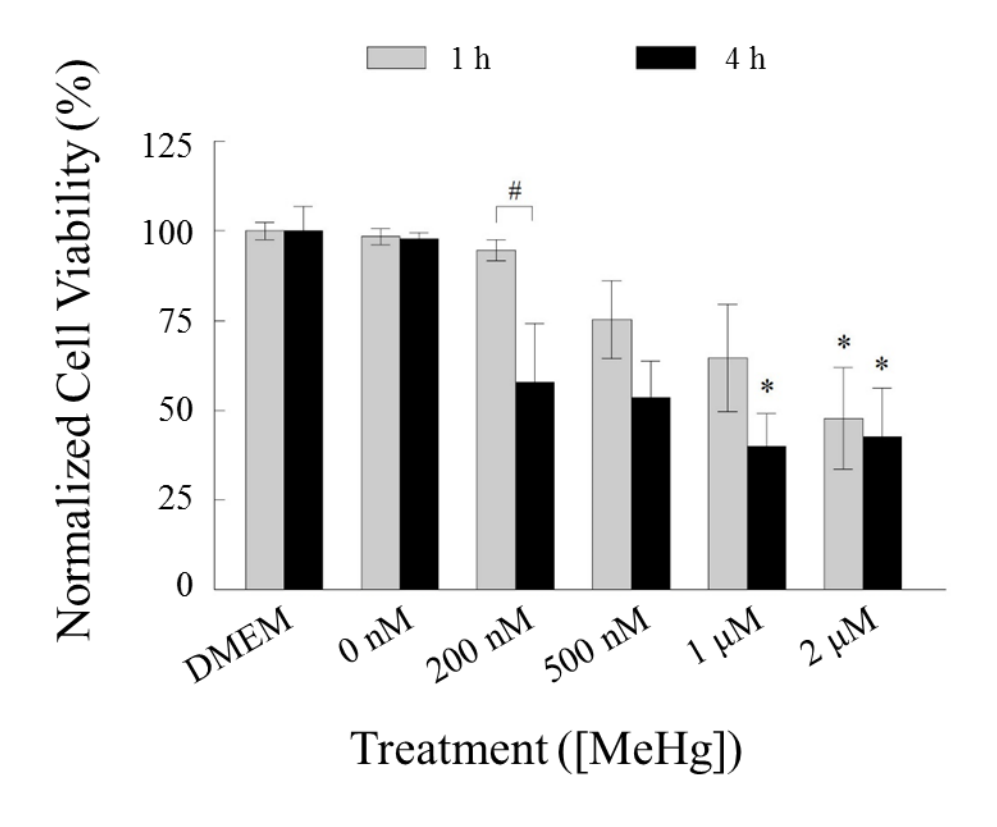


Figure 4.1. Viability of DRG is reduced within 4 h of *in vitro* exposure to low  $\mu$ M MeHg. Acutely dissociated DRG were exposed to MeHg in standard HBS (1.8 mM Ca<sup>2+</sup><sub>e</sub>) for 30 min, and viability was assessed at either 1 or 4 h immediately following. Viability was reduced at 1 h only with 2  $\mu$ M MeHg treatment; 4 h following exposure, DRG viability was reduced at both 1 and 2  $\mu$ M MeHg. A time-dependent reduction in DRG viability was observed only at 200 nM MeHg, where viability was significantly reduced at 4 h, as compared to the earlier timepoint. Values are presented as mean cell viability  $\pm$  SEM, normalized to cell viability in standard DMEM for the indicated timepoint. A significant difference from time-matched DMEM controls is denoted by \*; # denotes significance between timepoints for the indicated concentration (p < 0.05, n = 3).

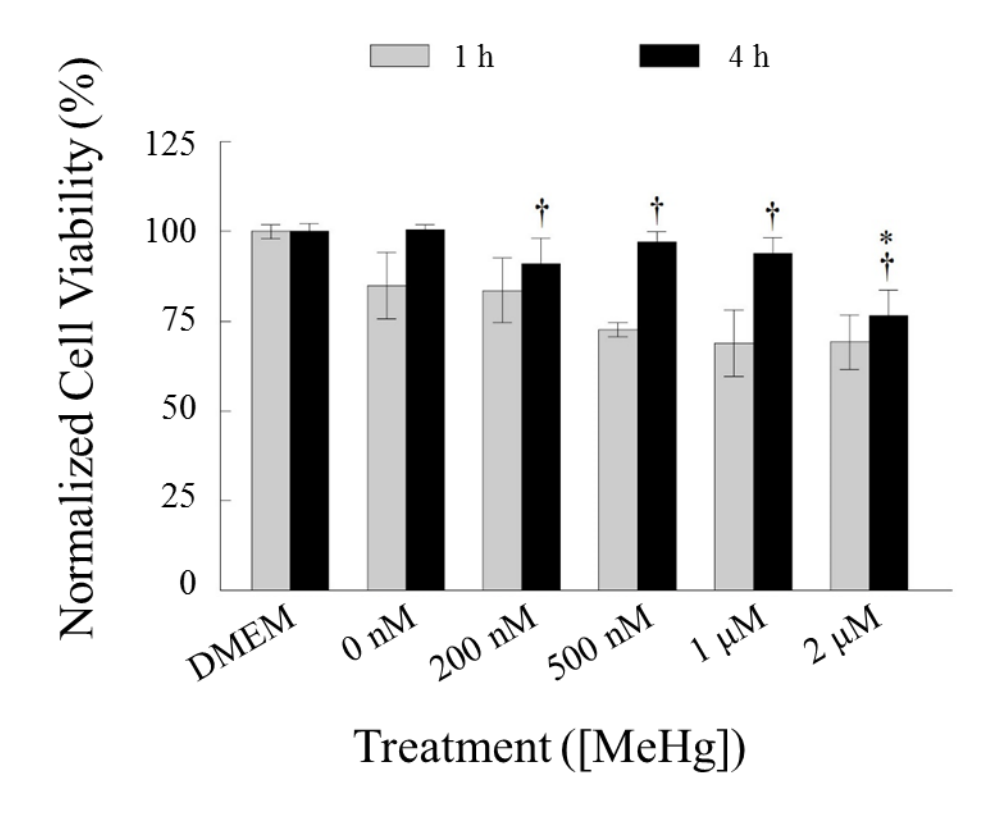


Figure 4.2. DRG viability is restored 4 h following *in vitro* MeHg exposure under  $Ca^{2+}_e$ -free conditions. Acutely dissociated DRG were exposed to MeHg in EGTA-HBS (0 mM  $Ca^{2+}_e$ ) for 30 min, and viability was assessed at either 1 or 4 h immediately following. DRG cytotoxicity elicited by exposure to MeHg was limited 4 h following treatment, as compared to standard 1.8 mM  $Ca^{2+}_e$  conditions. Viability 4 h after exposure to 2µM MeHg was still significantly reduced when compared to DMEM controls, yet was also improved over treatment with MeHg in 1.8 mM  $Ca^{2+}_e$  HBS. Values are presented as mean cell viability  $\pm$  SEM, normalized to cell viability in standard DMEM for the indicated timepoint. A significant difference from time-matched DMEM controls is denoted by \*; † denotes significance from 1.8 mM  $Ca^{2+}_e$  conditions (p < 0.05, p = 3).

(Hare and Atchison, 1995a, Marty and Atchison, 1997, Edwards et al., 2002, Limke et al., 2003, Limke et al., 2004).

To determine whether TRPA1 contributes to MeHg-induced cytotoxicity, cells were treated with A-967079 prior to MeHg exposure. Pretreatment with 500 nM A-967079 was found to be sufficient to block an increase in Ca<sup>2+</sup><sub>i</sub> induced by application of 1 mM AITC (Fig. 4.3), and thus block of endogenous TRPA1 was presumed under these conditions for cytotoxicity assessment. DRG pretreated with the TRPA1 antagonist still exhibited a marked reduction in viability at both 1 and 4 h following exposure to 2 µM MeHg (Fig. 4.4). The poor efficacy of A-967079 at 2 µM MeHg could indicate that either: 1) A-967079 and MeHg compete around the A-967079 binding site, and the antagonist is being outcompeted at higher concentrations, or 2) TRPA1 is not involved in mediating MeHg cytotoxicity. Results obtained with the blocker at lower MeHg concentrations would suggest that the latter is not likely. The antagonist was more efficacious at moderate MeHg concentrations at the 1 h timepoint; viability improved at 500 nM and 1 µM MeHg as compared to 0 mM and 1.8 mM Ca<sup>2+</sup><sub>e</sub> conditions, respectively, when A-967079 was applied. Similar results were obtained 4 h post-exposure, where pretreatment with A-967079 resulted in improvement in DRG viability for all MeHg concentrations, as compared to those exposed in standard HBS without the antagonist. It is notable that at the 4 h timepoint, there is no significant difference between the 0 mM Ca<sup>2+</sup><sub>e</sub> condition and that with the antagonist in 1.8 mM Ca<sup>2+</sup><sub>e</sub>. This may be because Ca<sup>2+</sup> influx through TRPA1 is important in mediating MeHg-induced cell death, particularly at later timepoints.

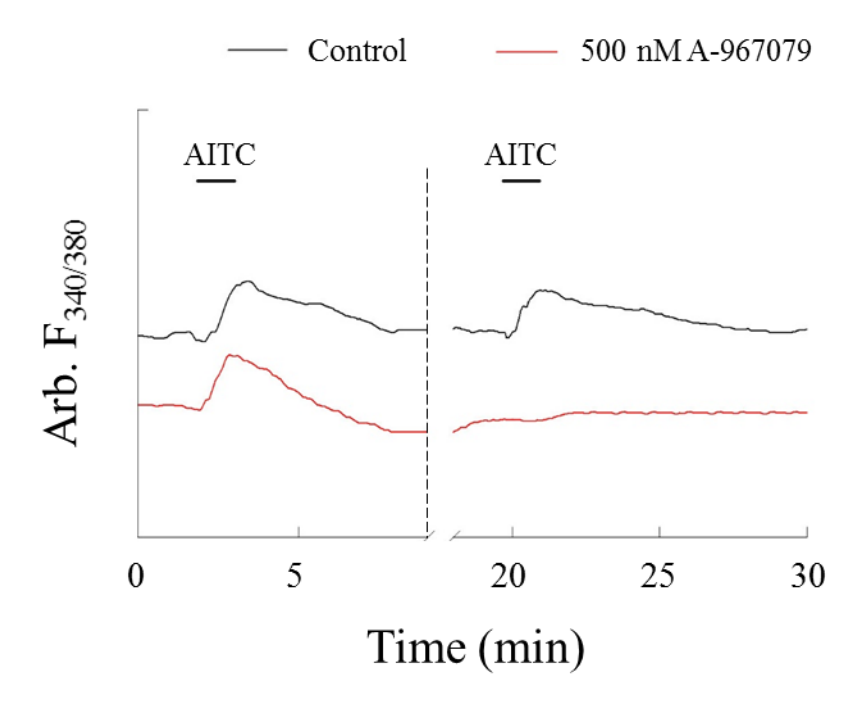


Figure 4.3. AITC-induced  $Ca^{2+}_i$  elevations in acutely dissociated DRG is blocked by pretreatment with 500 nM A-967079. Application of 1 mM AITC (60 s) induced a reversible elevation in  $Ca^{2+}_i$  in DRG, as indicated by the rise in  $F_{340/380}$ . When applied at a later timepoint, AITC elicited a similar effect in naïve DRG (black). The response to the second pulse of AITC was abolished when cells are pretreated with 500 nM A-967079 for 10 min (red). The hashed line indicates where the recording was paused and incubation with A-967079 began.

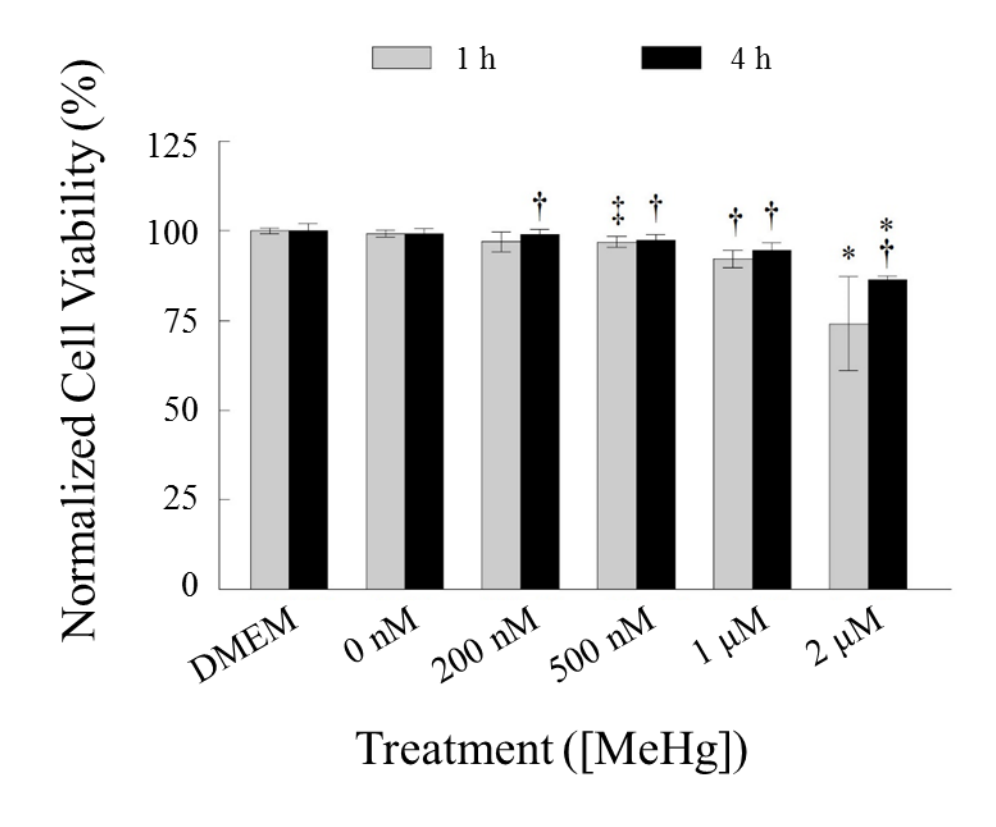


Figure 4.4. Block of TRPA1 improves DRG viability 4 h following in vitro MeHg exposure.

DRG were treated with 500 nM A-967079 10 min prior to MeHg exposure (30 min) and viability was assessed at either 1 or 4 h immediately thereafter. Pretreatment with A-967079 improved DRG viability 4 h post-exposure for all MeHg concentrations tested. This effect of A-967079 was consistent with results obtained under  $Ca^{2+}_{e}$ -free conditions. Exposure to 2  $\mu$ M MeHg reduced viability at both the 1 and 4 h timepoints, as compared to DMEM controls; application of A-967079 only partially restored DRG viability at this high MeHg concentration. 1 h following exposure to 500 nM MeHg, cell viability was when compared to  $Ca^{2+}_{e}$ -free conditions. Values are presented as mean cell viability  $\pm$  SEM, normalized to cell viability in standard DMEM for the indicated timepoint. A significant difference from time-matched DMEM controls is denoted by \*; † denotes significance from 1.8 mM  $Ca^{2+}$  conditions, ‡ denotes significant from  $Ca^{2+}_{e}$ -free conditions. (p < 0.05, n = 4).

#### 4.4.2. Distribution of TRPA1 in heterogeneous populations of acutely dissociated DRG

Expression of TRPA1 in A $\beta$  DRG has been reported with contradictory results (Walker et al., 2000, Kobayashi et al., 2005, Ji et al., 2008, Kwan et al., 2009), thus immunocytochemistry was used to elucidate channel distribution in the current model. TRPA1 expression was found in cells of various sizes and at various intensities, though not all nucleated cells expressed TRPA1 (Fig. 4.5). Immunoreactivity was detected in cell somas and, in those cells which were extending processes, neurites and nerve terminals. NF-200 was detected in neurons which neared 50  $\mu$ m in diameter. Cells immunolabeled with NF-200 were not at all abundant, as a given field of cells would only produce 1 – 2 cells positively labeled with this marker for A $\beta$  neurons. Merged micrographs revealed TRPA1 expression in NF-200-containing DRG, as well in some cells lacking NF-200 immunoreactivity. All cells which were positively labeled with NF-200 were also positively labeled with TRPA1, suggesting TRPA1 is reliably expressed in A $\beta$  DRG in this murine model and under these isolation conditions.

# 4.4.3. Contribution of $Ca^{2+}_{e}$ and TRPA1 to MeHg-induced $Ca^{2+}_{I}$ dysregulation in DRG

Application of 500 nM MeHg induced a gradual and irreversible rise in F<sub>340/380</sub>, designated as phase 1; in addition to being irreversible, the apparently protracted phase 1 response was unique when comparing acutely dissociated DRG and TRPA1-HEK. A second gradual and irreversible increase in the fluorescence signal, phase 2, followed shortly after phase 1 (Fig. 4.6A). There was no apparent intermediate phase between the onset of phase 1 and phase 2. Treatment with A-967079 prior to MeHg exposure did not alter any characteristics of the F<sub>340/380</sub> response (Fig. 4.6B). DRG exposed to MeHg in EGTA-HBS had a well-defined phase 1, where the rise in F<sub>340/380</sub> was less gradual and partially reversible (Fig.4.6C). An intermediate rising phase followed the

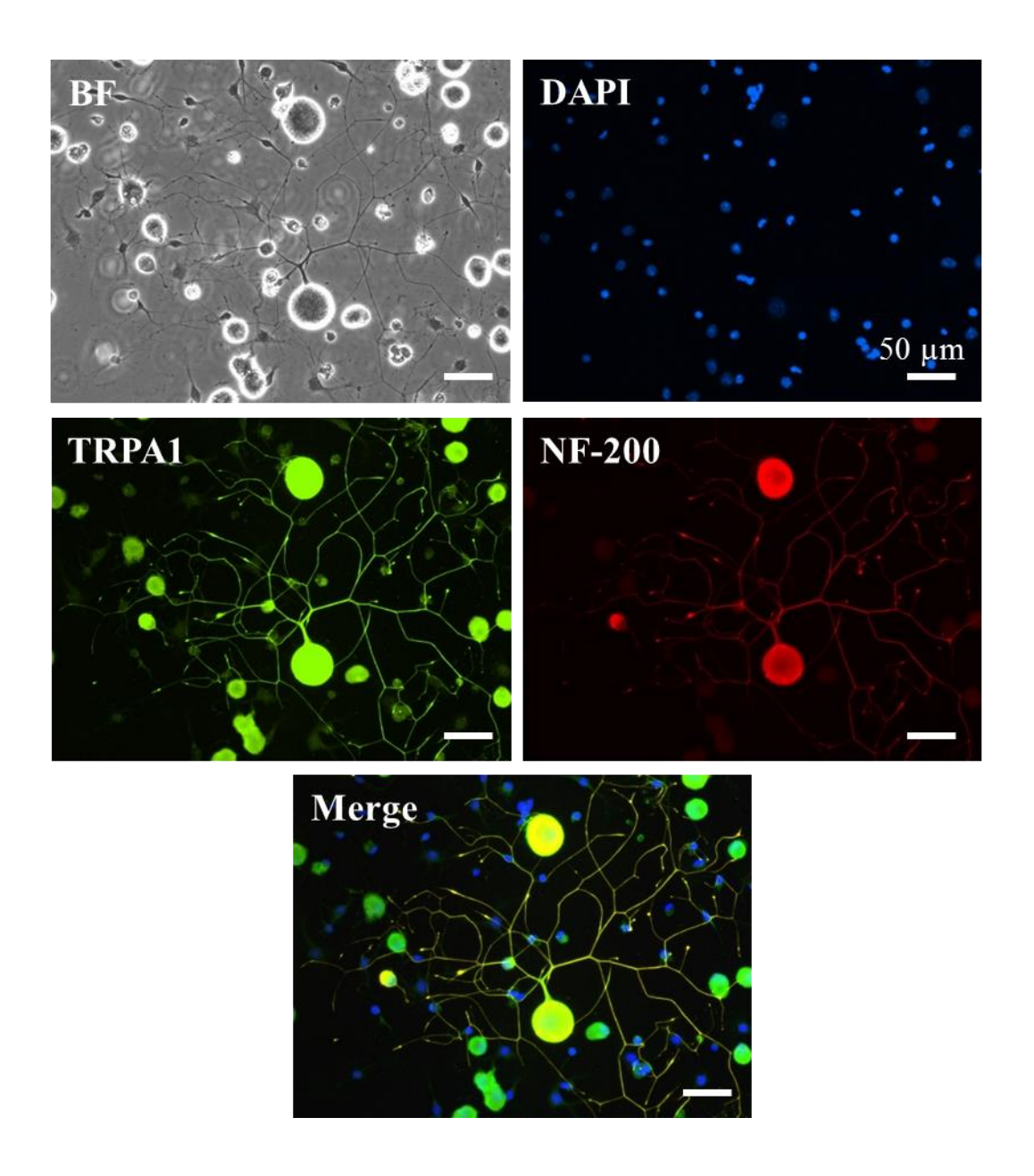


Figure 4.5. TRPA1 immunoreactivity is detected in Aβ DRG. The bright field (BF) image shows the heterogeneous acute dissociations includes DRG neurons of varying sizes and non-neuronal cells. Cells were fixed for immunolabeling at 12 - 14 h following plating, at which time extensive neurite outgrowth could already be observed. All nucleated cells were labeled with DAPI. TRPA1-expressing cells were labeled with a murine TRPA1 rabbit polyclonal antibody and detected with a goat anti-rabbit antibody conjugated to FITC; Aβ DRG containing were labeled with polyclonal chicken anti-NF-200 and detected with an AlexaFluor 594-conjugated goat anti-chicken secondary antibody. Merged fluorescence micrographs revealed TRPA1 was co-expressed with NF-200 in Aβ DRG. Images taken under  $20 \times$  magnification from the same field of cells.

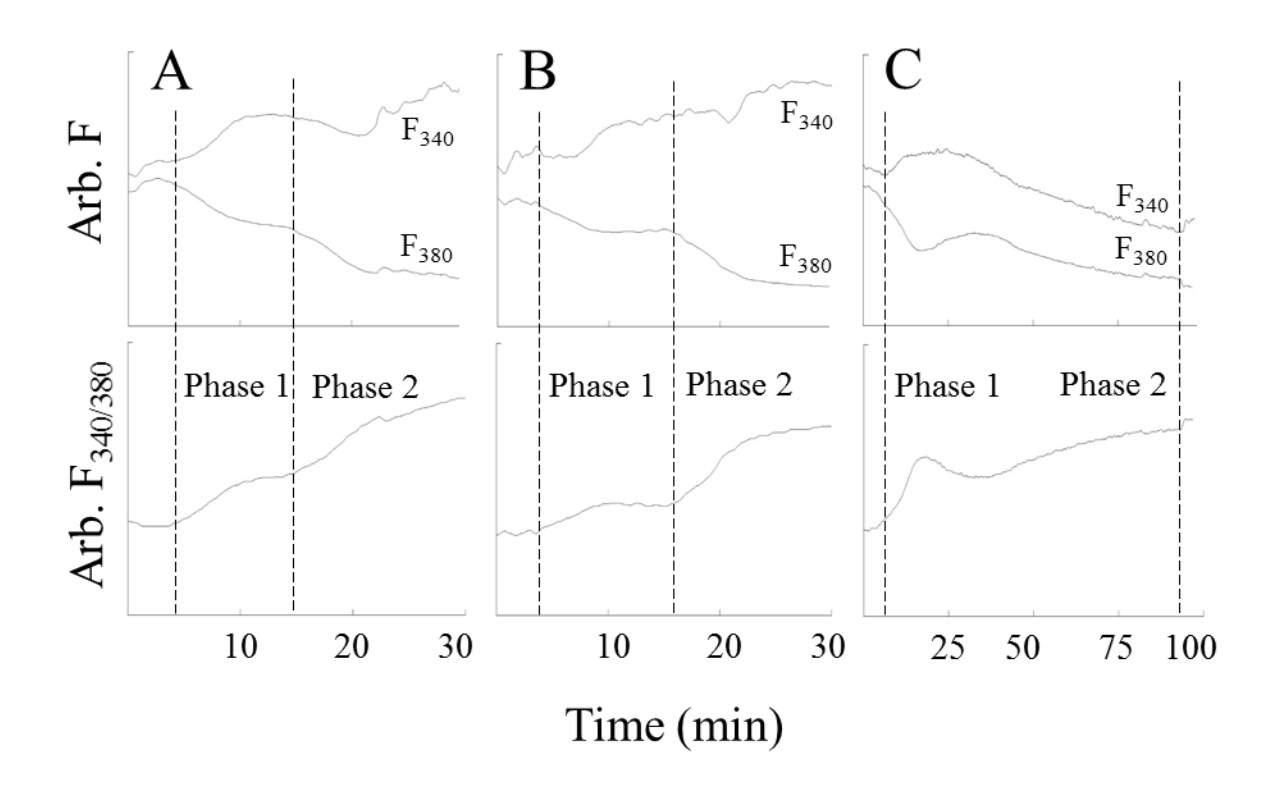


Figure 4.6. DRG exposed to MeHg display a multiphasic elevation in  $Ca^{2+}$  that is insensitive to block of TRPA1, but dependent upon  $Ca^{2+}$  (A) A multiphasic increase in  $F_{340/380}$  was observed in DRG with a functional TRPA1 response when exposed to MeHg in 1.8 mM  $Ca^{2+}$  (B) DRG pretreated with 500 nM A-967079 for 10 min also presented with two readily identifiable phases as a result of MeHg exposure. (C) The multiphasic response to MeHg exposure persisted in DRG when  $Ca^{2+}$  was removed from the superfusion solution. While a steadily rising intermediate phase was more distinguishable under this condition, the onset of phase 2 was more difficult to discern. Prior to MeHg exposure, cells were pulsed with 1 mM AITC for 60 s, and only those which displayed a rise in  $F_{340/380}$  in response to the TRPA1 agonist were included in the analysis. Hashed lines indicate where the times-to-onset of phases 1 and 2 were lineated. All representative tracings are from cells which were AITC-sensitive and exposed to 500 nM MeHg, with application of MeHg beginning at t = 0.

partial recovery from phase 1; phase 2 was difficult to discern at times, and in some cases, was not reached prior to the end of the experiment. AITC was pulsed onto the cells prior to MeHg to determine TRPA1 functionality. There was no apparent difference in the features of the microfluorimetry tracings throughout MeHg exposure in DRG regardless of sensitivity to AITC. Subsequent analyses were performed using data obtained from only those cells which responded to the AITC stimulus. The time-to-onset of phase 1 was not altered with either A-967079 pretreatment nor removal of Ca<sup>2+</sup><sub>e</sub> (Fig. 4.7A). Thus, the source of phase 1 Ca<sup>2+</sup><sub>i</sub> increases is not extracellular, nor is MeHg using TRPA1 as a means of entry into DRG. Removal of Ca<sup>2+</sup><sub>e</sub> effectively slowed the time-to-onset of phase 2, while A-967079 elicited no effect (Fig. 4.7B). This indicated phase 2 is mediated, in part, by Ca<sup>2+</sup><sub>e</sub> influx through Ca<sup>2+</sup>-permeable channels other than TRPA1. Comparison of DRG responding to AITC versus those which did not revealed no significance between the times-to-onset of the groups under any of the three experimental conditions (not shown). Together, these results suggest TRPA1 is not involved in MeHg-induced Ca<sup>2+</sup><sub>i</sub> elevations.

# 4.4.4. Involvement of Na<sup>+</sup><sub>e</sub> in MeHg-induced elevation of Ca<sup>2+</sup><sub>i</sub> in AITC-sensitive DRG

Results from viability and microfluorimetric assessment of MeHg-exposed DRG were contradictory, and so I thought to further explore the effect MeHg has on TRPA1 function via patch-clamp electrophysiology. Given the interest in understanding the heightened susceptibility of A $\beta$  DRG, only those with  $C_m$  55 – 75 pF were studied. Characterization of DRG based upon  $C_m$  has been described by Pearce and Duchen (1994), and the ability to discern discrete subtypes using this method is explored in the Appendix. Recordings were first made in a TEACl-based extracellular solution with  $Ca^{2+}$  as the primary charge carrier. When AITC was applied to DRG

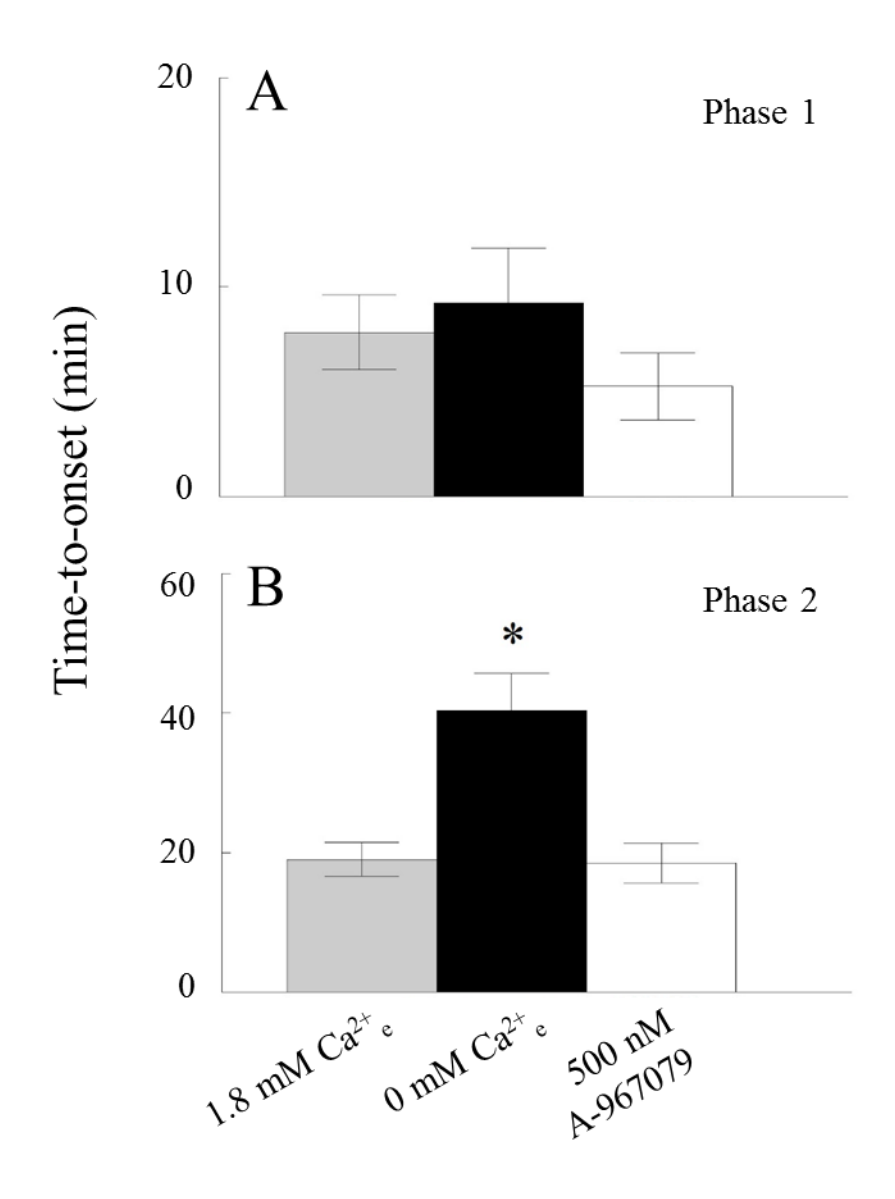


Figure 4.7. Removal of  $Ca^{2+}_e$  delays time-to-onset of phase 2, while block of TRPA1 has no effect on phase 1 nor phase 2. DRG were superfused with 500 nM MeHg in in either standard HBS (1.8 mM  $Ca^{2+}_e$ ) or EGTA-HBS (0 mM  $Ca^{2+}_e$ ) while simultaneously monitoring changes in  $F_{340/380}$ . In some experiments, cells were incubated in 500 nM A-967079 for 10 min prior to MeHg exposure in standard HBS. (A) There was no change in the time-to-onset of phase 1 in the absence of  $Ca^{2+}_e$  or with application of the TRPA1 antagonist, compared to 1.8 mM  $Ca^{2+}_e$  HBS. (B) However, removal of  $Ca^{2+}_e$  delayed the onset of phase 2, compared to standard HBS. Treatment with the TRPA1 antagonist did not affect the time-to-onset of phase 2. Values are presented as mean  $\pm$  SEM, and a significant difference from 1.8 mM  $Ca^{2+}_e$  controls is denoted by \* (p < 0.05, n = 3).

under this condition, an agonist-induced inward current was not detected (Fig. 4.8A). An equimolar substitution of NaCl for TEACl in the external solution resulted in a large, inward agonist-induced current in A $\beta$  cells (Fig. 4.8B). In some cases, the induced current was not reversible, as is the case when the concentration of cysteine-reactive agonist is too great (Raisinghani et al., 2011). The number of A $\beta$  obtained through a single isolation was limited, and thus it was implausible to perform quantitative analyses on the action of MeHg on the AITC-induced current waveform. However, these preliminary findings through whole-cell current recordings revealed the importance of Na<sup>+</sup> in mediating TRPA1 currents in DRG.

To determine the importance of Na<sup>+</sup> in the onset of MeHg-induced Ca<sup>2+</sup><sub>i</sub> dysregulation, microfluorimetry was performed in a reduced Na<sup>+</sup><sub>e</sub> choline-HBS. DRG pulsed with AITC and then perfused with choline-HBS for 1 h had a F<sub>340/380</sub> signal which remained stable (not shown). When exposed to MeHg in choline-HBS, AITC-insensitive DRG responded with a marked elevation in F<sub>340/380</sub> with two clearly identifiable phases (Fig. 4.9A). In AITC-sensitive cells, the first increase in F<sub>340/380</sub>, phase 1, was nearly indiscernible under the same low [Na<sup>+</sup>]<sub>e</sub> conditions (Fig. 4.9B). As described in previous experiments, DRG did not readily return to baseline following phase 1 elevations in Ca<sup>2+</sup><sub>i</sub> regardless of AITC response. Despite altering the shape of the F<sub>340/380</sub> response, exposure to MeHg in choline-HBS did not alter the time-to-onset of phase 1 (Fig. 4.10A). The time-to-onset of phase 2 was slowed in AITC-sensitive DRG, as compared to those which were AITC-insensitive (Fig. 4.10B). These results indicate the importance of Na<sup>+</sup><sub>e</sub> in contributing to the MeHg-induced Ca<sup>2+</sup><sub>i</sub> elevations; because a slowing of phase 2 was only observed in DRG which demonstrated a TRPA1 response, it is possible that Na<sup>+</sup> entry through the TRPA1 channel may sufficiently depolarize the cell and trigger activation of voltage-sensitive ion channels.

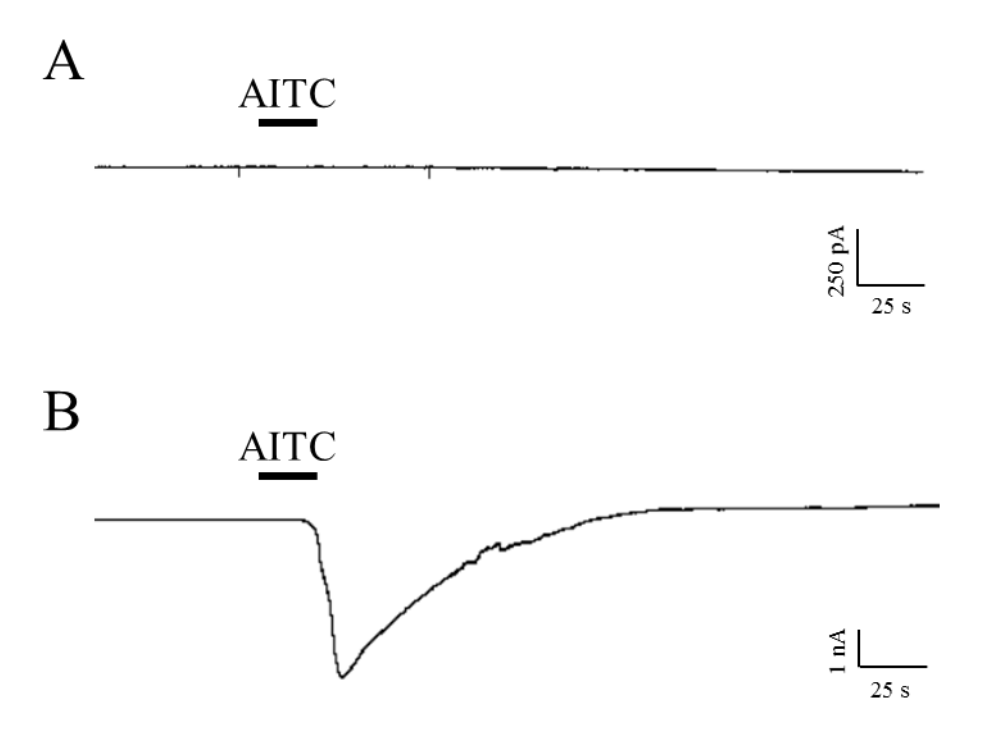
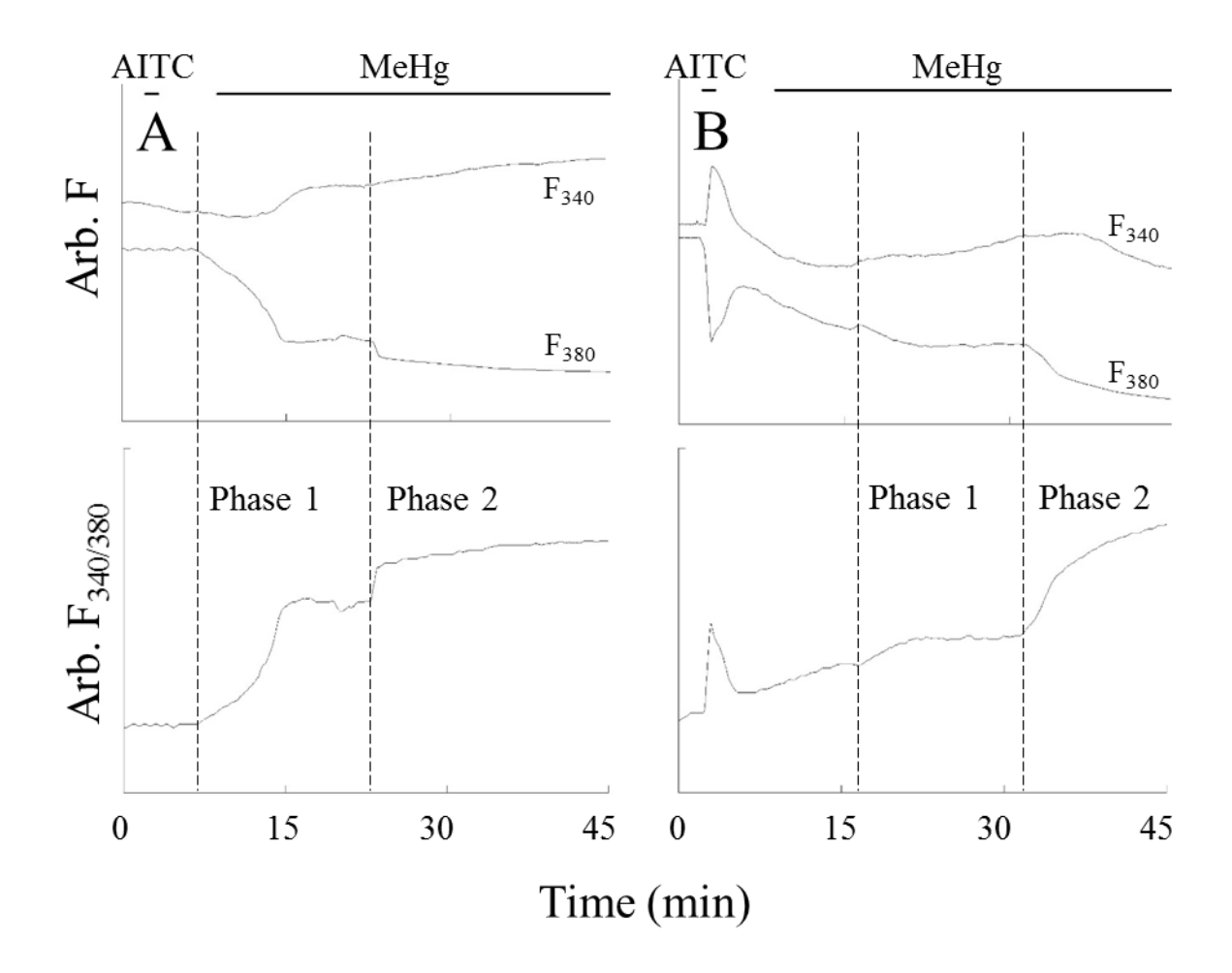


Figure 4.8. Na $^+$  is the primary charge carrier in AITC-induced current in A $\beta$  DRG. A $\beta$  DRG were patched in the whole-cell voltage clamp configuration, a V<sub>h</sub> of -80 mV was applied, and 1 mM AITC was superfused over the cells for 20 s. (A) No measurable agonist-induced current was observed in A $\beta$  DRG when the extracellular recording solution contained 140 mM TEACl as a surrogate for NaCl. (B) Equimolar exchange of NaCl for TEACl resulted in a large, inward current stimulated by AITC application. A constant 2.5 mM CaCl<sub>2</sub> was included in both the TEACl- and NaCl-containing extracellular solutions. Representative currents are from cells with  $C_m = 55 - 75$  pF.



**Figure 4.9.** The MeHg-induced multiphasic elevation in Ca<sup>2+</sup>i in AITC-sensitive DRG is diminished with the reduction of Na<sup>+</sup>e. DRG were exposed to a 60 s pulse of 1 mM AITC in standard HBS (150 mM NaCl) to determine TRPA1 response, followed by 500 nM MeHg in choline-HBS (40 mM NaCl) where indicated. (A) Cells which were insensitive to AITC displayed a prominent phase 1 and 2. (B) AITC-sensitive DRG also had two identifiable phases, though phase 1 was much less pronounced and difficult to discern in some instances. Regardless of response to AITC, DRG did not recover as readily from the rise in F<sub>340/380</sub> associated with phase 1 nor was the steadily-rising intermediate phase observed under reduced Na<sup>+</sup>e conditions. Hashed lines indicate where the time-to-onset of phase 1 and phase 2 were determined. Representative tracings are from two cells in a single experiment.

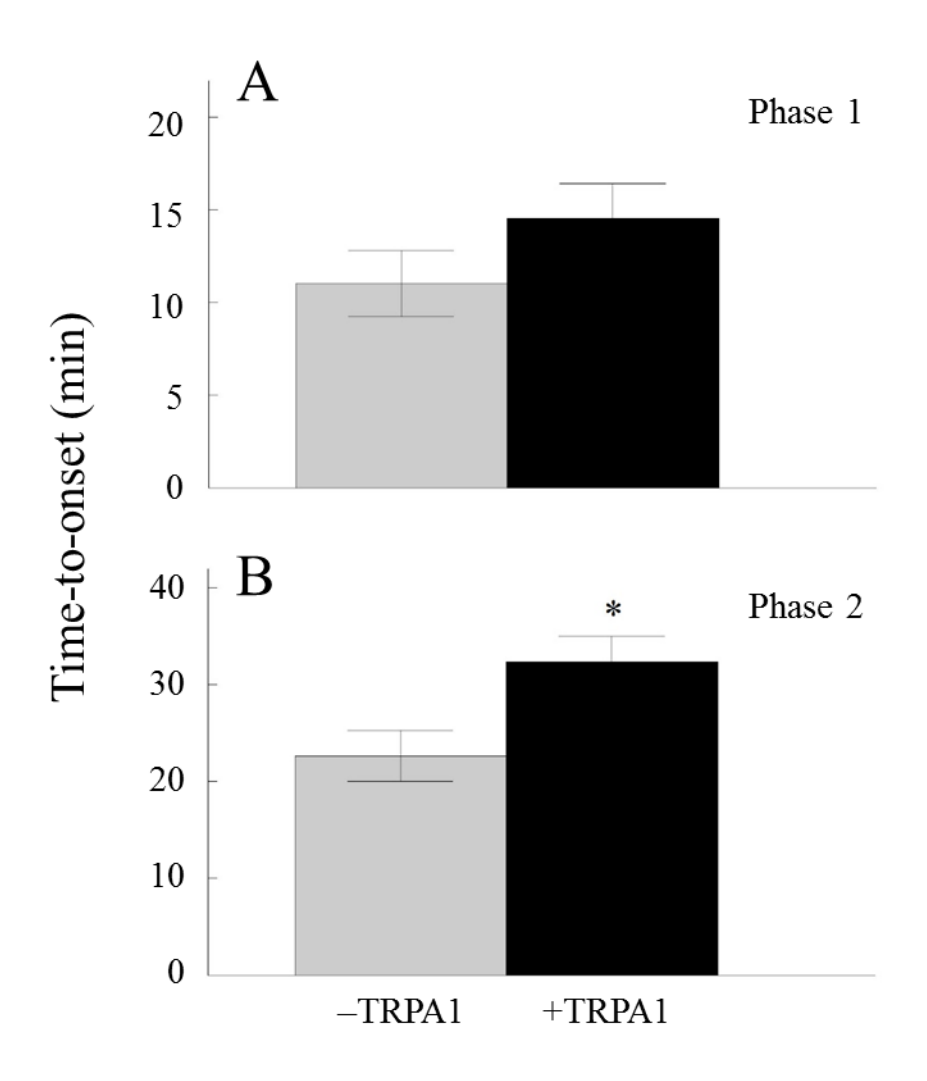


Figure 4.10. Low Na<sup>+</sup><sub>e</sub> delays the time-to-onset of phase 2 in AITC-sensitive DRG, while AITC-insensitive DRG are unaffected. DRG were superfused with MeHg in choline-HBS while simultaneously monitoring changes in  $F_{340/380}$ . (A) Time-to-onset of phase 1 Ca<sup>2+</sup><sub>i</sub> disturbances did not differ between DRG that express and those which lack TRPA1, though (B) the time-to-onset of phase 2 was slowed in cells expressing functional TRPA1 under reduced Na<sup>+</sup><sub>e</sub> conditions. Values are presented as mean  $\pm$  SEM, and a significant difference from DRG lacking functional TRPA1 is denoted by \* (p < 0.05, n = 3).

#### 4.5. Discussion

The results of this study demonstrate the sensitivity of DRG to MeHg in juvenile mouse DRG. Few studies exist which aim to define the mechanisms of MeHg neurotoxicity in DRG. Those which have been conducted commonly utilized embryonic or neonatal primary cultures (Arakawa et al., 1991, Leonhardt et al., 1996a, Leonhardt et al., 1996b, Huang and Narahashi, 1997a, b), thus obviating the adult phenotype from TRP-family ion channels which develops over approximately the first 30 days (Hjerling-Leffler et al., 2007, Zhu and Oxford, 2011). Experiments were designed to explore the role of TRPA1 and Ca<sup>2+</sup><sub>e</sub> in mediating MeHg-induced Ca<sup>2+</sup><sub>i</sub> elevations and cytotoxicity in DRG.

The sensitivity of DRG to MeHg cytotoxicity was largely  $Ca^{2+}_{e}$ -dependent, though significant cytotoxicity was only measurable at later assessment timepoints and at 1 and 2  $\mu$ M concentrations of MeHg. In comparison, primary cerebellar granule cells exposed to 500 nM and 1  $\mu$ M MeHg under a similar paradigm displayed marked cytotoxicity 3.5 h following exposure (Marty and Atchison, 1998). This result was surprising since degeneration of DRG has been described prior to any morphologic changes or degeneration in the central nervous system in adult rats treated with 2 mg/kg MeHg for 8 weeks (Yip and Chang, 1981). This discrepancy in rank-order sensitivity of primary cells following *in vitro* versus *in vivo* MeHg exposure may be attributed to the use of a heterogeneous population of DRG. The majority of DRG neurons are classified as either A $\delta$ - or C-fiber (Boron and Boulpaep, 2009), and are predominantly insensitive to the ravaging effects of MeHg neurotoxicity (Cavanagh and Chen, 1971, Delio et al., 1992, Schiønning et al., 1998). Thus, with less than 25% of DRG neurons being characterized as A $\beta$  (Meyer et al., 2005), the susceptibility of large-diameter DRG may be masked by less-sensitive subtypes in a heterogeneous population of cells. Additionally, it was observed that not as many

cells were counted in assessment of viability at 1 h, as compared to 4 h, despite keeping the density of cells constant. Cell detachment throughout *in vitro* MeHg has been reported in multiple cell types (Wasteneys et al., 1988, Aschner, 2000, Stummann et al., 2009), and can be used a marker of cytotoxicity (Ekwall et al., 1990). While care was taken during each experimental manipulation in the viability assay, it is not implausible that 30 min *in vitro* MeHg exposure was sufficient to loosen adherent DRG; when cells were assessed at 1 h post-exposure, less adherent cells could have been easily been disturbed during wash steps, whereas cells assessed 4 h post-exposure may have re-adhered to the substrate.

Block of TRPA1 improved DRG viability to a capacity comparable to that of Ca<sup>2+</sup><sub>e</sub> removal, leading to the hypothesis that Ca<sup>2+</sup> entry through TRPA1 is a critical mechanism in MeHg-induced cytotoxicity. While expression and distribution of TRPA1 in Aβ DRG has not been thoroughly studied, expression has been inferred through functional studies demonstrating the loss of mechanoreception in TRPA1 knockout and mutant animal models (Walker et al., 2000, Kindt et al., 2007, Kwan et al., 2009). In contrast, TRPA1 expression has been extensively characterized in smaller diameter DRG (Kobayashi et al., 2005, Ji et al., 2008, Barabas et al., 2012) and functionally defined as a receptor for noxious stimuli in these cells (Bandell et al., 2004, Mizushima et al., 2006, Macpherson et al., 2007, Takahashi et al., 2008, Sadofsky et al., 2011). In this study, TRPA1 immunoreactivity was detected in Aβ DRG, as determined by co-reactivity with NF-200. However, TRPA1 was also detected in other DRG subtypes in the heterogeneous neuronal population. This finding does not necessarily refute the hypothesis that TRPA1 expression may make Aβ DRG more susceptible to MeHg. Smaller diameter DRG express TRPV1, the noxious channel which is activated by capsaicin (Caterina et al., 1997, Aoki et al., 2005). Coimmunoprecipitation has revealed a close association between TRPA1 and TRPV1 channels when

co-expressed (Patil et al., 2010). This association comes with a functional consequence of suppression of TRPA1 activation through TRPV1-mediated channel internalization (Akopian et al., 2007, Patil et al., 2010). Additionally, when co-expressed, TRPA1 and TRPV1 form functional heterodimers with a pharmacologic and biophysical profile that differs from either homodimer, including hastened desensitization; the formation of the TRPA1-TRPV1 heterodimer is  $Ca^{2+}$ -dependent (Fischer et al., 2014), thus assembly may be favored more so following MeHg exposure when  $Ca^{2+}$  is elevated. This means TRPA1 channels in A $\delta$  and C DRG, through association with TRPV1, may actually provide a protective effect in the presence of MeHg.

While assessment of DRG viability following MeHg exposure implicated a role for TRPA1 as a probable mediator Ca<sup>2+</sup>e-dependent cell death, microfluorimetry studies produced apparently conflicting results. Block of TRPA1 prior to MeHg exposure was ineffective in slowing MeHginduced Ca<sup>2+</sup><sub>i</sub> dysregulation. This result was unexpected, as Ca<sup>2+</sup><sub>i</sub> has been demonstrated as an agonist for TRPA1-mediated Ca<sup>2+</sup> current (Cavanaugh et al., 2008, Nilius et al., 2012, Zaytas et al., 2013). Questions arose regarding the efficacy of the TRPA1 antagonist, however A-967079 has a reported IC<sub>50</sub> of approximately 100 nM in rodent models and is more than 1000 times selective for TRPA1 over any other TRP channel (Gauvin et al., 2009, Chen et al., 2011). A more probable explanation could be physical occlusion around the A-967079 and MeHg interaction sites, as A-967079 was not continually perfused throughout MeHg exposure. Since A-967079 binds to serine and tyrosine residues within the pore of TRPA1 (Klement et al., 2013, Nakatsuka et al., 2013, Banzawa et al., 2014), and MeHg is hypothesized to interact with cysteine residues (Kostyniak and Clarkson, 1981, Harris et al., 2003), it is not likely there is direct competition. Rather, irreversible interaction of MeHg with cysteine residues near the pore of the channel may physically occlude the binding of A-967079. Cysteine residues within the pore of TRPC4 and

TRPC5 channels have been identified as putative sites for interaction with MeHg (Xu et al., 2012), however no such studies have been performed on other TRP channel subtypes. Thus, it is unclear whether MeHg could use TRPA1 as a means of entry into the cell or interact with the channel to either block or induce currents.

An additional concern when assessing the efficacy of A-967079 was the availability of functional TRPA1 channels for activation by elevated Ca<sup>2+</sup>i, as it is probable that experimental conditions have altered the functional properties of TRPA1. Concerns initially arose in characterizing the DRG response to AITC. Whereas in TRPA1-HEK application of 10 µM AITC was sufficient to elicit a rise in Ca<sup>2+</sup>i, primary DRG required 1 mM AITC for a comparable effect. Differences in agonist sensitivity between human and murine isoforms of the TRPA1 have been described (Nagatomo and Kubo, 2008), thus differences in agonist potency is not unexpected. However, the higher concentration of AITC remained a concern due to reports of large, irreversible inward currents (Raisinghani et al., 2011) and promiscuity (Ohta et al., 2007, Gees et al., 2013) at concentrations near or exceeding 1 mM. It is unclear whether A-967079 would have efficacy under these conditions in which irreversible covalent modification have taken place. Though this does not necessarily obviate involvement of TRPA1, it underscores the complexity of the model system.

Na<sup>+</sup> was identified as the primary charge carrier in AITC-induced currents, and onset of MeHg-induced  $Ca^{2+}_{i}$  elevation was Na<sup>+</sup><sub>e</sub>-dependent. While TRPA1 is more permeable to  $Ca^{2+}$  ( $P_{Ca}/P_{Na} \approx 9$ ) (Karashima et al., 2010, Nilius et al., 2012), the relative permeability of the channel to Na<sup>+</sup> increases in the presence of specific agonists, including AITC (Chen et al., 2009, Karashima et al., 2010); dilation of the TRPA1 channel pore has been identified as the causative event for changes in ion permeability (Chen et al., 2009). It is unclear to what extent this dilation and increase in Na<sup>+</sup> permeability is reversible following removal of the agonist. It is also unknown

whether MeHg elicits a comparable conformational change in TRPA1 structure and shift in ionic currents. However, this may provide an explanation to the significant contribution of Na<sup>+</sup> in mediating phase 2 MeHg-induced Ca<sup>2+</sup> dysregulation; depolarization of the plasma membrane via TRPA1-mediated Na<sup>+</sup> current may result in activation of VGCCs. VGCCs are a well-defined contributor to phase 2 Ca<sup>2+</sup> influx (Hare and Atchison, 1995b, Marty and Atchison, 1997, Ramanathan and Atchison, 2011) and Ca<sup>2+</sup> current carried through these channels is unaltered under these exposure conditions. In addition to the study of TRP channels, the direct or indirect interaction of these channels with VGCCs should be further explored to better understand MeHg neurotoxicity in DRG.

# CHAPTER FIVE

# SUMMARY AND CONCLUSIONS

### 5.1. Summary of experiments

Prior work has begun to elucidate the mechanisms of MeHg neurotoxicity which includes the release of Ca<sup>2+</sup> from storage organelles (Levesque and Atchison, 1991, Hare and Atchison, 1995a, Limke and Atchison, 2002, Limke et al., 2003, Limke et al., 2004), Ca<sup>2+</sup> influx (Hare et al., 1993, Marty and Atchison, 1997, Ramanathan and Atchison, 2011), and disruption of VGCC function (Shafer et al., 1990, Shafer and Atchison, 1991, Sirois and Atchison, 2000). However, the putative targets of MeHg described in these studies are ubiquitously distributed throughout the nervous system, thus failing to explain the apparent sensitivity of discrete neuronal populations, such as DRG, following *in vivo* exposure to MeHg. The studies presented in this dissertation were designed to classify the contribution of Ca<sup>2+</sup>-permeable ion channels in mediating MeHg-induced [Ca<sup>2+</sup>]<sub>i</sub> dysregulation and cell death. The central hypothesis of these studies is that nonspecific, Ca<sup>2+</sup>-permeable ion channels highly expressed in DRG are sensitive molecular targets of MeHg and mediate cellular events precursory to MeHg neurotoxicity. Results from these in vitro studies implicate TRPA1 as a molecular target for MeHg. Though it was posited TRPA1 would directly mediate Ca<sup>2+</sup> influx upon exposure to MeHg, results suggest an indirect relationship between TRPA1 and Ca<sup>2+</sup><sub>i</sub> dysregulation which is Na<sup>+</sup><sub>e</sub>-dependent. Whereas prior studies have described a role for TTX-sensitive voltage-gated Na<sup>+</sup> channels in MeHg-induced Ca<sup>2+</sup> perturbations (Atchison, 1987, Traxinger and Atchison, 1987, Shafer and Atchison, 1992, Hare and Atchison, 1995b, Marty and Atchison, 1997, Ramanathan and Atchison, 2011), this work is the first to highlight the potentially important contribution of a TTX-resistant Na<sup>+</sup> component to the MeHg response, presumably mediated through TRP channels.

## 5.1.1. Differential VGCC expression does not alone confer unique sensitivity to MeHg

Chapter 2 aimed to characterize the susceptibility of cells expressing discrete VGCC isoforms to MeHg-induced elevations in  $[Ca^{2+}]_i$  and cells death. The interaction of MeHg with VGCCs is well characterized (see Chapter 1.1.5.) and appears to occur in a subtype-specific manner (Peng et al., 2002, Hajela et al., 2003, Tarabová et al., 2006). Although VGCCs are not uniquely expressed in DRG, subclasses of DRG fibers carry distinct  $Ca^{2+}$  currents (Scroggs and Fox, 1992a, b) which corresponds to differential distribution of VGCCs among the neuronal population (Scroggs and Fox, 1991). This pattern of VGCC distribution has been postulated to subserve the sensory modalities, and consequentially may also underlie the differential sensitivity of DRG neurons to MeHg. Chapter 2, therefore, was working under the hypothesis that unique sensitivity of A $\beta$  DRG may not necessarily be attributed to a distinct molecular entity, but rather a unique composition of ion channels contributing to the macroscopic  $Ca^{2+}$  current.

In the first set of experiments, changes in  $Ca^{2+}_i$  in VGCC-HEK were continuously monitored throughout exposure to MeHg. The onset of  $[Ca^{2+}]_i$  dysregulation was found to be VGCC subtype- and phase-dependent. A hastened time-to-onset of phase 1 was consistently observed in P/Q-type-expressing HEK across all concentrations of MeHg, whereas expression of the N-type VGCC conferred a more rapid time-to-onset of phase 2. However, electrophysiologic-based studies of VGCC current in the same heterologous expression model belie the conclusion that these microfluorimetry are directly attributed to  $Ca^{2+}$  influx through each respective channel. Hajela et al. (2003) and Peng et al. (2002) demonstrated MeHg (0.125 – 5  $\mu$ M) reliably blocks N-and R-type VGCCs with reported IC50 values of 1.3  $\mu$ M and 1.1  $\mu$ M, respectively. Block of N-and R-type currents occurred biphasically, with an initial rapid component in the first 100 – 150 s of MeHg exposure, and complete block within approximately 300 s. Similar results were obtained

in HEK expressing the L-type VGCC, however a fraction of L-type current was resistant to block by MeHg (Peng et al., 2002, Hajela et al., 2003). Because the microfluorimetry results indicate the onset of phase 1 in VGCC-HEK occurs at the approximate time which complete current block is expected, it is not likely VGCC expression alone would confer MeHg sensitivity upon a cell. A similar conclusion was reached in the study of differential susceptibility of native VGCCs in cerebellar granule cells when antagonists for distinct VGCC isoforms each failed to attenuate MeHg-induced block of VGCC current (Sirois and Atchison, 2000).

Subsequent studies on untransfected cells made use of endogenously-expressed T-type VGCCs to determine sensitivity of this subtype to MeHg. Whereas microfluorimetry and viability results from recombinantly-expressed VGCCs could not be reconciled with electrophysiologic recordings, studies of T-type channels are well-aligned. Block of endogenous T-type channels slows phase 2  $\text{Ca}^{2+}_{i}$  increases and improves viability. Theoretically, T-type channels should be available to conduct current under these experimental conditions; Tarabová et al. (2006) reported a T-type VGCCs are blocked by MeHg with an IC50 of 13.0  $\mu$ M. However, T-type channels are characterized by their small and transient conductance, and MeHg (1 – 100  $\mu$ M) further accelerates inactivation of T-type currents (Tarabová et al., 2006). Thus, it is also unlikely T-type VGCCs would confer MeHg sensitivity upon a cell.

Both untransfected and VGCC-HEK, irrespective of VGCC subtype, responded to MeHg with a triphasic elevation in Ca<sup>2+</sup><sub>i</sub>. This response was congruent with Ca<sup>2+</sup><sub>i</sub> dysregulation observed in rat cerebellar type II astrocytes (Marty et al., 1997, Lundback et al., 2002), though overall, a multiphasic response atypical. Similar studies conducted in primary neuronal cultures (Marty and Atchison, 1997, Ramanathan and Atchison, 2011) and a neuroblastoma-derived cell line (Hare et al., 1993) consistently demonstrate MeHg elicits a biphasic elevation in Ca<sup>2+</sup><sub>i</sub>. The intermediate

rising phase observed in HEK was, unlike cerebellar type II astrocytes, Ca<sup>2+</sup>e-dependent. Whereas this phase of Ca<sup>2+</sup>i disruption in astrocyte cultures was attributed to Ca<sup>2+</sup> buffering or Fura-2 binding non-Ca<sup>2+</sup> divalent cations (Marty et al., 1997), the intermediate phase is apparently due to an endogenous Ca<sup>2+</sup> influx pathway in HEK cells. TRPA1 was a putative target which arose when considering these findings, as it is one of few endogenously-expressed Ca<sup>2+</sup>-permeable ion channels (Tanner et al., 2007, Buber et al., 2010, Lin et al., 2014). Recently, TRPA1 has been described to play an integral role in maintaining basal Ca<sup>2+</sup>i and generating spontaneous Ca<sup>2+</sup>i spikes in hippocampal astrocytes (Shigetomi et al., 2011, Jackson and Robinson, 2015). Though Marty et al. (1997) did not determine Ca<sup>2+</sup>e entry to contribute significantly to the multiphasic response in cerebellar type II astrocytes, as determined in HEK cells, this difference may be simply attributed to differences in TRPA1 density between the examined cell types.

The model used in this study was the heterologous expression of VGCCs described by Hajela et al. (2003) and Peng et al. (2002). HEK were co-transfected with GFP as a marker for transfection efficiency, and a transfection efficiency of approximately 70 – 80% was routinely obtained. Though prior studies demonstrated functional expression of the recombinant VGCCs through measurement of whole-cell currents (Peng et al., 2002, Hajela et al., 2003), there was no such functional assessment coinciding with the fluorometric analyses conducted here. To ensure VGCC-HEK are in fact expressing the recombinant channels, immunocytochemistry may be performed. Without first permeabilizing the membrane, this would serve to identify the VGCCs which have translocated to the cell's surface. Alternatively, functional assessment of the channel may be conducted using microfluorimetry. A depolarizing pulse of KCl could be applied to induce an increase in [Ca<sup>2+</sup>]<sub>i</sub> and, thus, in F<sub>340/380</sub>. Subsequent application of a VGCC antagonist and delivery of a second KCl pulse would presumably result in a reduced or abolished change in

[Ca<sup>2+</sup>]<sub>i</sub>, indirectly establishing presence of a functional ion channel population. If the antagonists selected were irreversible, this study could presumably be conducted at the onset of each experiment prior to MeHg exposure. However, because some of the most widely used and potent VGCC antagonists are peptide toxins that produce either poorly reversible or irreversible channel block (McCleskey et al., 1987, Bourinet et al., 2001, Botana, 2014), functional assessment preceding each recording may not be possible.

Though this study demonstrates that differential expression of VGCC isoforms does not alone confer a cell with heightened susceptibility to MeHg, it did not directly address the hypothesis in DRG. A model of heterologous expression was selected to simplify the biologic system and control the auxiliary subunits with which the recombinant  $\alpha_1$  associated. This model, then, presumes the interaction site for MeHg and VGCCs lies on the  $\alpha_1$  subunit. Indeed, there is evidence to suggest that MeHg alters VGCC function through direct action on the pore-forming subunit, specifically through direct interaction with the VGCC selectivity filter residing near the mouth of the pore; in PC12 cells and rat brain synaptosomes, MeHg  $(10 - 100 \,\mu\text{M})$  alters cationic selectivity and permeation rates to Ca<sup>2+</sup>, Sr<sup>2+</sup>, and Ba<sup>2+</sup> (Shafer et al., 1990, Shafer and Atchison, 1991). However, the potential for MeHg to interact with VGCC auxiliary subunits has not been explored. Future work may aim to determine whether varying the individual auxiliary subunits, while keeping  $\alpha_1$  constant, alters the actions of MeHg. The role of auxiliary subunits, particularly β, in modulating the kinetics of VGCC activation and inactivation suggests MeHg disruption at this locale has great potential for altering VGCC function. Of course, primary DRG may be used as a model to more accurately elucidate the contribution of discrete VGCC subtypes in mediating MeHg-induced [Ca<sup>2+</sup>]<sub>i</sub> dysregulation. Though if this approach were selected, knockdown of VGCC expression through the use of siRNA would be preferential; pharmacologic manipulation

introduces the possibility for competition at the ion channel, and efficacy of VGCC antagonists in the presence of MeHg would be a concern (Sirois and Atchison, 2000).

## 5.1.2. TRPA1 contributes to $[Ca^{2+}]_i$ dysregulation at sub- $\mu$ M MeHg

Chapter 3 aimed to determine the sensitivity of TRPA1-expressing cells to MeHg, and characterize the role of the recombinant channel in mediating Ca<sup>2+</sup><sub>i</sub> disruptions. In contrast to VGCCs, localization of TRPA1 is restricted to somatosensory neurons and visceral tissues (Story et al., 2003, Liedtke and Heller, 2007); its function in mechanoreception (Walker et al., 2000, Kindt et al., 2007, Kwan et al., 2009) indicates expression in Aβ DRG is probable. Though the function of TRPA1 when exposed to MeHg has not been investigated, activation of the channel following application of cysteine-reactive chemical irritants results in elevated [Ca<sup>2+</sup>]<sub>i</sub> (Bandell et al., 2004, Jordt et al., 2004, Macpherson et al., 2007, Sadofsky et al., 2011, Komatsu et al., 2012). Chapter 3 was working under the hypothesis that MeHg-induced Ca<sup>2+</sup> influx is mediated, in part, through TRPA1, and results in subsequent cytotoxicity.

Changes in  $Ca^{2+}_{i}$  in TRPA1-HEK were continuously monitored throughout exposure to MeHg. Expression of recombinant TRPA1 was found to hasten the time-to-onset of phase 2 in a  $Ca^{2+}_{e}$ -dependent manner, though only at 0.5  $\mu$ M MeHg. This indicates the contribution of TRPA1 to mediating  $Ca^{2+}$  influx during phase 2. The potential for the channel to be blocked by MeHg at higher concentrations is unclear, though the data suggest alternative mechanisms to elevate  $[Ca^{2+}]_{i}$  may contribute more significantly at 1 and 2  $\mu$ M MeHg. Studies in rat cerebellar granule cells demonstrates release of mitochondrial  $Ca^{2+}$  occurs within approximately 15 min when exposed to 0.5  $\mu$ M MeHg, and block of this release slows only the time-to-onset of phase 1 (Limke and Atchison, 2002); moreover, the onset of phase 2 in these cells has been attributed to depletion of

ATP and  $Ca^{2+}_{e}$  influx (Marty and Atchison, 1997, Limke et al., 2003). Thus, the source of  $Ca^{2+}$  which is potentially masking a TRPA1 component of phase 2 at 1 and 2  $\mu$ M MeHg may be attributed to influx of  $Ca^{2+}_{e}$  through another unidentified ion channel or an increase in the plasma membrane permeability to  $Ca^{2+}$  (Denny and Atchison, 1996).

Though TRPA1 does minimally contribute to phase 2, the apparently prominent role for the channel in mediating MeHg-induced [Ca<sup>2+</sup>]<sub>i</sub> disruption occurs at more immediate timepoints following the onset of exposure. A distinctive phase preceding phase 1 was observed in a subset of cells which expressed functional TRPA1 channels. The Ca<sup>2+</sup><sub>e</sub>-dependence of phase 0 indicates that Ca<sup>2+</sup> influx via TRPA1 occurs within minutes of MeHg application. Similar rapid changes in Ca<sup>2+</sup><sub>i</sub> were observed in recombinantly-expressed TRPC5 channels; MeHg (0.1 – 10  $\mu$ M) increased Fluo3 fluorescence shortly following application (EC<sub>50</sub> = 2.03  $\mu$ M). Though timecourse studies were not reported in this model, the authors did correlate the rapid increase in Ca<sup>2+</sup> with inward currents mediated through TRPC5 (Xu et al., 2012). MeHg-induced activation of TRPC5 currents required the two critical cysteine resides residing near the pore of the channel, highlighting the potential for MeHg to rapidly activate TRPA1 via a comparable mechanism.

In each instance in which phase 0 was observed, the succeeding phase 1 was particularly aberrant and resembled Ca<sup>2+</sup> bursting. This pattern of [Ca<sup>2+</sup>]<sub>i</sub> dysregulation in response to MeHg has not been reported in the NG108-15 cell line (Hare et al., 1993) nor in primary neuronal culture (Marty and Atchison, 1997, Edwards et al., 2005, Ramanathan and Atchison, 2011). A similar bursting pattern has been reported in co-cultures of rat hippocampal neurons and astrocytes. Bursting activity was reported to be mediated by TRPA1, Ca<sup>2+</sup><sub>e</sub>-dependent, and co-localized with mitochondria (Shigetomi et al., 2011, Jackson and Robinson, 2015). Although Ca<sup>2+</sup> bursts in these

hippocampal co-cultures were not induced by MeHg, these studies highlight the potential for interaction between internal storage organelles and TRPA1-mediated  $Ca^{2+}_{e}$  influx.

The comparison between untransfected cells and TRPA1-HEK permitted identification of a contribution of recombinant TRPA1 in MeHg-induced [Ca<sup>2+</sup>]<sub>i</sub> disruption, yet this effect was not readily reversible with the application of the TRPA1 antagonist A-967079. A significant limitation of investigating TRPA1 as described in Chapter 3 is the application of A-967079; although A-967079 is a highly potent and specific TRPA1 antagonist (Gauvin et al., 2009), it is extremely cost-prohibitive to include the antagonist in the perfusion buffer throughout the duration of MeHg exposure. Despite pretreatment with the antagonist and a demonstrated reduction of TRPA1 Ca<sup>2+</sup> response, A-967079 does not effectively slow the time-to-onset of phase 0 or phase 2, nor does it reduce the frequency with which phase 0 is observed. Channel antagonists have been reported to perform poorly in the presence of MeHg, citing possible competition (Sirois and Atchison, 2000). While it is possible MeHg outcompetes A-967079 at the TRPA1 channel, the fact that the antagonist is rendered ineffective in altering phase 0 would suggest MeHg has a high affinity for TRPA1. Displacement of A-967079 by MeHg could be confirmed via a radioligand biding assay, assuming a radiolabeled form of A-967079 could be obtained or constructed.

Patch-clamp electrophysiology would be particularly advantageous to continue the investigation of TRPA1 function in the presence of MeHg. Because microfluorimetry studies indicated an early role for TRPA1 in MeHg-induced [Ca<sup>2+</sup>]<sub>i</sub> dysregulation, recordings could presumably be shorter in duration, thus permitting continuous application of A-967079. The use of an outside-out patch configuration would effectively isolate the channel from the cytosolic constituents, effectively removing any membrane-delimited means through which TRPA1 function could be altered. These studies could be instrumental in identifying causation of the Ca<sup>2+</sup>

bursting activity observed in the phase 1  $Ca^{2+}_i$  response in TRPA1-HEK. Because TRPA1 is inactivated by elevated  $[Ca^{2+}]_i$  (Wang et al., 2008b), it is unclear as to why TRPA1 expression did not significantly alter the  $Ca^{2+}_i$  response upon exposure to 1 and 2  $\mu$ M MeHg; outside-out patch recording could also serve to rectify this question by identifying whether TRPA1 is being blocked by MeHg or inactivated as a consequence of MeHg-induced  $[Ca^{2+}]_i$  elevations.

## 5.1.3. Na<sup>+</sup><sub>e</sub> influx contributes to phase 2 Ca<sup>2+</sup><sub>i</sub> disruption in AITC-sensitive DRG

Chapter 4 aimed to determine whether TRPA1 expression confers DRG with sensitivity to MeHg. Numerous studies have investigated MeHg-induced neurotoxicity in DRG, but most fail to discern between fiber types when interpreting the findings (see Chapter 1.1.6). Because  $A\beta$  are most prominently affected in MeHg poisoning (Eto, 1997, Schiønning et al., 1998), the mechanistic studies in primary DRG sought to characterize the cellular response to MeHg by fiber type. TRPA1 have been implicated to be involved in mechanotransduction (Walker et al., 2000, Kindt et al., 2007, Kwan et al., 2009), therefore focus was directed at understanding the function of this ion channel in  $A\beta$  DRG when exposed to MeHg. Chapter 4 worked under the hypothesis that TRPA1 is abundantly expressed in  $A\beta$  DRG, and mediates  $Ca^{2+}$  current upon activation by MeHg.

In the first set of studies in primary DRG, relative sensitivity of the cells to MeHg was assessed through cell viability assays and microfluorimetry. In comparison to rat cerebellar granule cells exposed to the same concentration of MeHg (Marty and Atchison, 1997, 1998), DRG exhibit comparable times-to-onset of phase 1 and 2 [Ca<sup>2+</sup>]<sub>i</sub> elevations. Despite the apparently similar pattern of Ca<sup>2+</sup> dysregulation, the viability of DRG is reduced more so than that of cerebellar granule cells under similar exposure conditions (Marty and Atchison, 1998). While Fura-2

provides an indication of relative changes in [Ca<sup>2+</sup>]<sub>i</sub> allowing for a comparison of kinetics, the magnitude of Ca<sup>2+</sup> accumulation within each phase cannot be determined from these studies alone. Thus, these results may be rectified through the distinction between the rate versus magnitude of [Ca<sup>2+</sup>]<sub>i</sub> elevations. In assessment of the function of TRPA1, cell viability results revealed block of TRPA1 could improve viability of MeHg-exposed cells, however A-967079 was not effective in slowing the rise in [Ca<sup>2+</sup>]<sub>i</sub>. The contradictory findings between recombinant versus native TRPA1 channels could suggest is a more complex Ca<sup>2+</sup><sub>i</sub> response underlies MeHg toxicity in DRG. This is not the first instance in which two distinct cell types responded to MeHg in a different manner; Ca<sup>2+</sup> contributing to phase 1 originates from IP<sub>3</sub>-sensitive stores in NG108-15 cells (Hare and Atchison, 1995a), whereas mitochondrial Ca<sup>2+</sup> is the primary source in rat cerebellar granule cells (Limke and Atchison, 2002, Limke et al., 2003). It has been posited by Limke et al. (2003) that there is a correlation between MeHg-induced release of mitochondrial Ca<sup>2+</sup> and neuronal damage. however this has not been explored in DRG. To fully understand MeHg neurotoxicity in DRG, the precise sources which readily contribute to cytosolic Ca<sup>2+</sup> need to be identified. The complexity of the MeHg-induced [Ca<sup>2+</sup>]<sub>i</sub> response in DRG is not limited to internal sources of Ca<sup>2+</sup>. The ability of TRP channels to interact with one another and intracellular Ca2+ stores is well documented (Liedtke and Heller, 2007, Salas et al., 2009, Staruschenko et al., 2010). Of particular note, TRPA1 activation has been described as a trigger to induce current through other Ca<sup>2+</sup>-dependent channels, including TRPM5 (Buber et al., 2010).

To overcome the apparently complex Ca<sup>2+</sup><sub>i</sub> response induced by MeHg in DRG, whole-cell patch-clamp electrophysiology was used. AITC elicited large, inward currents only when Na<sup>+</sup> was the predominant charge carrier. The ability of TRPA1 to conduct Na<sup>+</sup> is agonist-dependent and results from pore dilation and shift in relative ion permeability (Chen et al., 2009, Karashima

et al., 2010, Nilius et al., 2012). MeHg-induced [Ca<sup>2+</sup>]<sub>i</sub> dysregulation in AITC-sensitive DRG was dependent upon the presence of Na<sup>+</sup><sub>e</sub>; the Ca<sup>2+</sup><sub>e</sub>-dependent phase 2 was slowed when Na<sup>+</sup><sub>e</sub> was reduced. This suggests Na<sup>+</sup><sub>e</sub> influx through TRPA1 may initiate or potentiate the Ca<sup>2+</sup> component of phase 2 through depolarization of the plasma membrane. This finding is in line with that reported in NG108-15 cells; cells exposed to 2 μM MeHg in the presence of TTX or reduced Na<sup>+</sup><sub>e</sub> (14.5 mM) slowed the time-to-onset of phase 2 (Hare and Atchison, 1995b). Similar observations in mammalian neuromuscular junctions also support a role for Na<sup>+</sup> in mediating the effects of MeHg (Atchison, 1987, Traxinger and Atchison, 1987, Shafer and Atchison, 1992). However, in contrast to prior studies, the inclusion of TTX in the choline-HBS used in these studies would suggest involvement of a TTX-resistant Na<sup>+</sup> component to the MeHg response.

In a separate set of studies, the effect of MeHg on VGCC current in DRG was assessed. Surprisingly, results showed whole-cell  $Ca^{2+}$  current was unaltered when exposed to 500 nM MeHg for 5 min. This contrasts recordings in PC12 (Shafer and Atchison, 1991), cerebellar granule cells (Sirois and Atchison, 2000), and neonatal DRG (Leonhardt et al., 1996a, Leonhardt et al., 1996b) where application of MeHg (0.25 – 10  $\mu$ M) was found to rapidly reduced whole-cell Ba<sup>2+</sup> currents. Even at the lowest MeHg concentration assessed (1  $\mu$ M), PC12 cell Ba<sup>2+</sup> current was reduced by more than 20% after 5 min. The sensitivity of recombinant VGCC isoforms to block by MeHg (0.125 – 10  $\mu$ M) has also been reliably demonstrated when expressed in isolation (Peng et al., 2002, Hajela et al., 2003, Tarabová et al., 2006). One possible explanation for this discrepancy may also be explained by a primary limitation of these recordings, which is that whole-cell  $Ca^{2+}$  currents in juvenile DRG were found to rundown rapidly despite the addition of cyclic nucleotides in the internal pipette solution. Because of this, the frequency with which cells were stimulated was maintained at 0.05 Hz. The use-dependence of MeHg current block (Shafer and

Atchison, 1991, Leonhardt et al., 1996b, Sirois and Atchison, 2000) suggests that application of a higher stimulation frequency would result in a hastened rate and magnitude of block. However, MeHg block of VGCC current does not require cells to be electrically stimulated, nor is it state dependent (Shafer and Atchison, 1991, Sirois and Atchison, 2000). The apparent insensitivity of whole-cell Ca<sup>2+</sup> current in juvenile DRG to block by MeHg may indicate a more sensitive molecular target within this model.

Based upon the findings presented in Chapter 4, it is posited that in MeHg activates TRPA1 and elicits a Na<sup>+</sup> current, resulting in membrane depolarization and activation of VGCCs. Whereas TRPA1 activity is co-expressed with and inactivated by TRPV1 in small-diameter DRG (Salas et al., 2009, Patil et al., 2010), there is no evidence to suggest TRP-mediated modulation of TRPA1 in A\beta DRG. Thus, this mechanism may underlie the observed sensitivity of A\beta DRG to MeHg. Further work needs to be performed to support this hypothesis. Foremost, it remains to be determined whether MeHg acts as a TRPA1 agonist to effectively induce Na<sup>+</sup> current. To test this, whole-cell voltage clamp may be used to measure the current which results from application of MeHg. Assuming MeHg is found to elicit Na<sup>+</sup><sub>e</sub> influx, subsequent studies could employ currentclamp recording to determine whether this effect is sufficient to depolarize the membrane and lead to activation of VGCCs. These studies could not be completed with efficiency under the present model. To facilitate identification of TRPA1-expressing Aβ DRG in recordings, a GFP-TRPA1 transgenic mouse model could be used as the source of primary neurons. Alternatively, comparative studies of A\beta DRG in response to MeHg may be conducted using cells isolated from wildtype and TRPA1 knockout animals. The advantage to electrophysiological approach to future studies is the ability to discern between DRG fiber types by C<sub>m</sub>, as an immunologic marker which permits the separation of AB DRG remains to be identified. While these recommended studies

utilize the whole-cell configuration, it may be preferred to use the perforated-patch to overcome the marked rundown observed in whole-cell recordings of DRG.

## 5.2. Proposed mechanism of TRPA1-mediated MeHg neurotoxicity

The results presented in this dissertation implicate a contribution of TRPA1 in MeHg neurotoxicity through a Na<sup>+</sup>e-dependent elevation of [Ca<sup>2+</sup>]<sub>i</sub>. I propose the following mechanism for TRPA1-mediated neurotoxicity of DRG throughout exposure to sub µM MeHg (Fig. 5.1):

MeHg-induced [Ca<sup>2+</sup>]<sub>i</sub> dysregulation in DRG is multiphasic; the onset of phase 1 is Ca<sup>2+</sup>e-independent, and thus may be attributed to release of Ca<sup>2+</sup> from storage organelles. Despite being highly permeable to Ca<sup>2+</sup> (Karashima et al., 2010, Nilius et al., 2012), the relative ion permeability of TRPA1 appears to shift to favor Na<sup>+</sup> in the presence of MeHg, as reported with other agonists (Chen et al., 2009, Karashima et al., 2010). MeHg activates TRPA1, perhaps through covalent modification of cysteine residues (Macpherson et al., 2007, Takahashi et al., 2008, Wang et al., 2012), to induce inward Na<sup>+</sup> current. Sufficient depolarization of the plasma membrane activates VGCCs; the relative expression of VGCC isoforms differs among DRG subtypes, and thus may contribute to the differential susceptibility of DRG to MeHg (Scroggs and Fox, 1992b). Additional unidentified Ca<sup>2+</sup>-permeable ion channels are also critical mediators of MeHg-induced Ca<sup>2+</sup>e influx, as block of TRPA1 alone does not confer protection.

Similarly, the expression of TRPA1 alone does not confer sensitivity to MeHg; TRPA1 expression and function has been extensively characterized in small-diameter DRG (Gold et al., 1996, Numazaki and Tominaga, 2004, Kobayashi et al., 2005, Anand et al., 2008) and visceral tissues (Du et al., 2007, Liedtke and Heller, 2007, Streng et al., 2008, Mukhopadhyay et al., 2011, Nassini et al., 2012, Nilius et al., 2012). However, TRPV1 is also expressed in these cells (Caterina et al., 1997, Aoki et al., 2005) and alters TRPA1 kinetics (Salas et al., 2009, Spahn et al., 2014), pharmacologic properties (Buber et al., 2010, Sadofsky et al., 2014), and channel internalization (Akopian et al., 2007, Patil et al., 2010). TRPA1-TRPV1 heteromers may also be found in cells

where TRPA1 and TRPV1 are co-expressed (Fischer et al., 2014), however the heteromeric channel likely would be insensitive to MeHg; TRPA1-TRPV1 heteromers maintain pharmacologic and kinetic properties of the homomeric TRPV1 channel (Fischer et al., 2014), which is insensitive to MeHg when heterologously-expressed (Xu et al., 2012). Close association between TRPA1 and TRPV1 may serve a protective role in MeHg-exposed small diameter DRG (Fig. 5.2). Upon activation by MeHg, TRPA1 co-expressed with TRPV1 may have a reduced Na<sup>+</sup> conductance or hastened inactivation. As a result, VGCCs may not be activated to mediate phase 2 [Ca<sup>2+</sup>]<sub>i</sub> elevations. Other unidentified Ca<sup>2+</sup>-permeable ion channels, such as other TRP isoforms, may mediate phase 2 of MeHg-induced [Ca<sup>2+</sup>]<sub>i</sub> elevations, though the kinetics and magnitude of these responses remains to be elucidated.

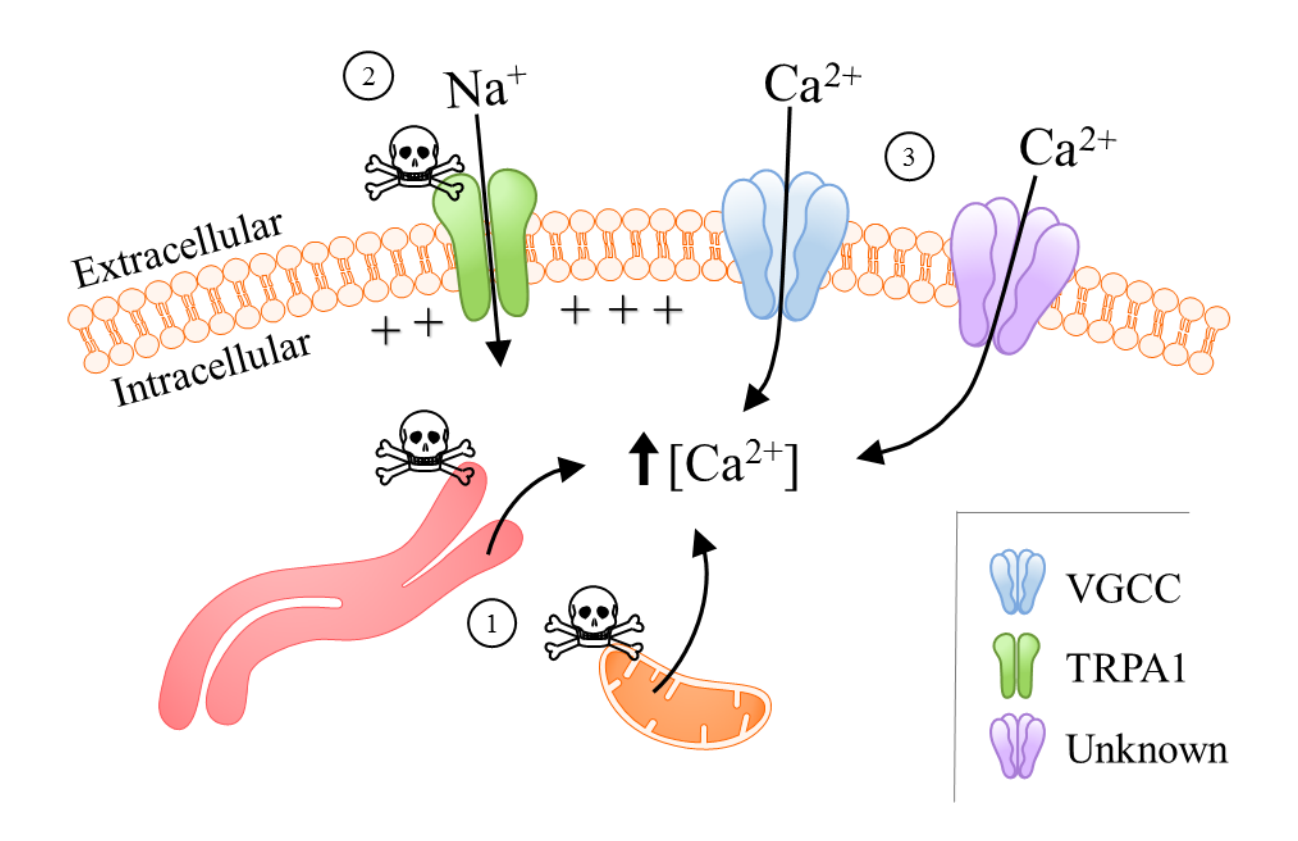


**Figure 5.1. Proposed mechanism of TRPA1-mediated MeHg toxicity in Aβ DRG.** Expression of TRPA1 in Aβ DRG may hasten MeHg-induced  $[Ca^{2+}]_i$  dysregulation.  $[Ca^{2+}]_i$  disruption is initiated with the release of  $Ca^{2+}$  from intracellular storage organelles, perhaps the endoplasmic reticulum or mitochondria. TRPA1 is activated by MeHg, resulting in an inward Na<sup>+</sup> current and, consequentially, membrane depolarization; this membrane depolarization is sufficient to activate VGCCs.  $Ca^{2+}$  entry via VGCCs and other unidentified  $Ca^{2+}$ -permeable ion channels mediate phase 2 of MeHg-induced  $[Ca^{2+}]_i$  elevations.

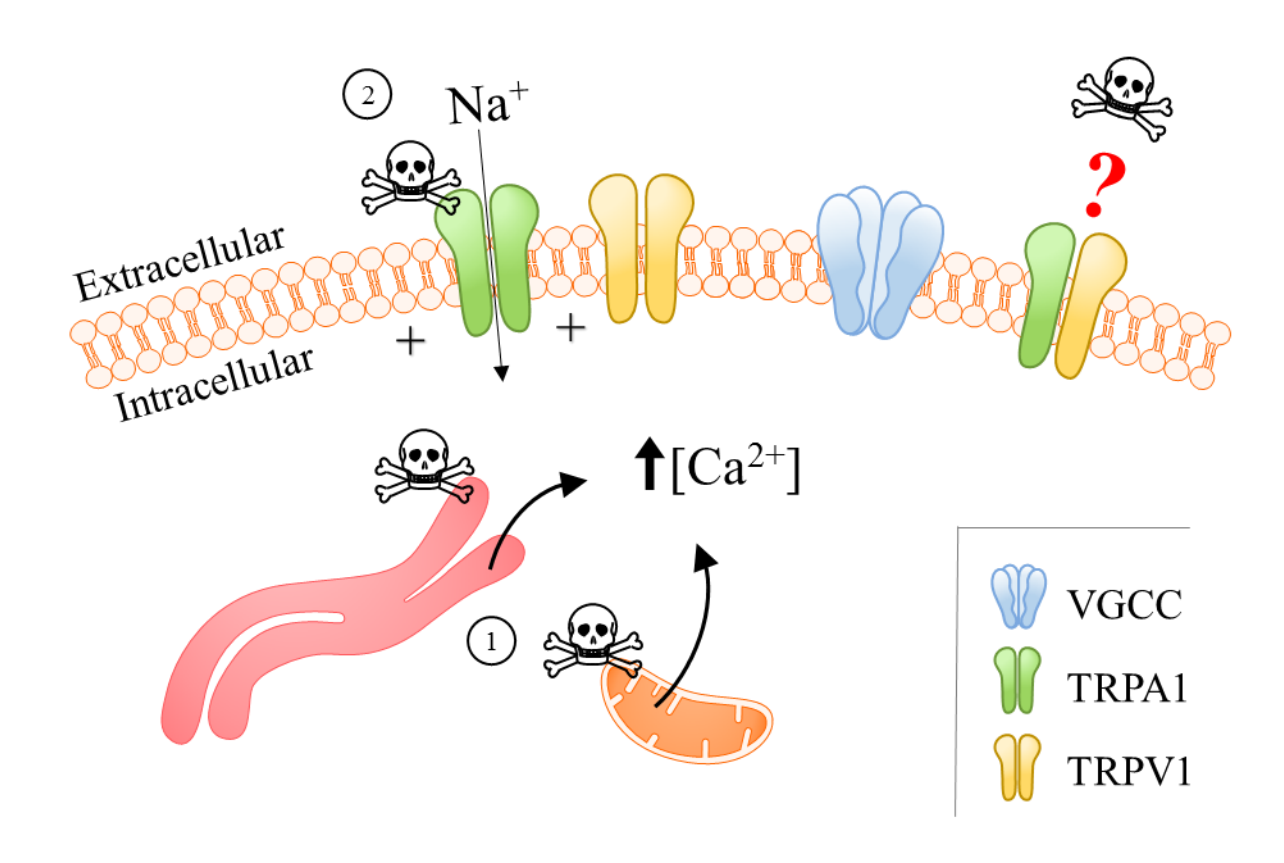


**Figure 5.2.** Hypothesized protection from TRPA1-mediated MeHg toxicity in small-fiber DRG. Although TRPA1 is expressed in other cells, including small-diameter DRG, MeHg-induced [Ca<sup>2+</sup>]<sub>i</sub> dysregulation is not necessarily imminent. MeHg-induced [Ca<sup>2+</sup>]<sub>i</sub> disruption is initiated with the release of Ca<sup>2+</sup> from intracellular storage organelles, perhaps the endoplasmic reticulum or mitochondria. TRPA1 is activated by MeHg. However, co-expression and close association with TRPV1, results in a current with potentially reduced Na<sup>+</sup> conductance or increased inactivation kinetics. The resulting membrane depolarization may not be sufficient to activate VGCCs. Other unidentified Ca<sup>2+</sup>-permeable ion channels, such as other TRP isoforms, may mediate phase 2 of MeHg-induced [Ca<sup>2+</sup>]<sub>i</sub> elevations, though the kinetics and magnitude of these responses remains to be elucidated; TRPA1-TRPV1 likely are not involved.

### 5.3. Concluding remarks

In summary, this dissertation shows that differential expression of VGCC isoforms does not alone confer a cell with MeHg sensitivity. In fact, native voltage-activated Ca<sup>2+</sup> currents in DRG are unaltered when cells are acutely exposed to sub-uM MeHg. The central hypothesis of this study was supported in a heterologous expression system; recombinant TRPA1 contributes to [Ca<sup>2+</sup>]<sub>i</sub> dysregulation at sub-µM MeHg, notably with a distinctive Ca<sup>2+</sup><sub>e</sub>-dependent phase 0. The role of TRPA1 in MeHg-induced [Ca<sup>2+</sup>]<sub>i</sub> dysregulation in DRG is more unclear, though Na<sup>+</sup><sub>e</sub> is apparently important in regulating the time-to-onset of the Ca<sup>2+</sup><sub>e</sub>-dependent in AITC-sensitive DRG. The results of this study are novel in that they sought a mechanistic understanding of the interaction between MeHg and TRPA1, and is the first to highlight the contribution of Na<sup>+</sup><sub>e</sub> in MeHg neurotoxicity in DRG, presumably via influx through TRPA1. At the time of defense of this dissertation, only one published study explores the relationship between mercurials and TRP function, with a particular focus on TRPC isoforms (Xu et al., 2012). Furthermore, results presented in Chapter 4 and the Appendix were obtained through the unique application of C<sub>m</sub>based size sorting in MeHg-exposed cells for comparative electrophysiological analyses. Though the results of this dissertation do not directly support the central hypothesis, the role of TRPA1 in mediating MeHg-induced neurotoxicity cannot be fully discarded without further mechanistic study of the Na<sup>+</sup>e-dependent pathway to disrupt [Ca<sup>2+</sup>]<sub>i</sub>.

This work highlights the need to further explore interactions between MeHg and TRP channels to fully understand the complexity of MeHg neurotoxicity in DRG. However, application of the concepts gleaned from the study of such interactions would extend beyond a mechanistic understanding of MeHg-associated paresthesia. Environmental exposure to MeHg has been postulated to incite the development of Alzheimer's disease through mechanisms which include

elevated [Ca<sup>2+</sup>]<sub>i</sub> and increased expression of amyloid precursor protein (Monnet-Tschudi et al., 2006, Chin-Chan et al., 2015). Evidence for TRP involvement in Alzheimer's pathogenesis is mounting (Yamamoto et al., 2007), thus extending the studies presented in this dissertation may have broad impact.

**APPENDIX** 

# EFFECTS OF METHYLMERCURY ON VOLTAGE-ACTIVATED CALCIUM CURRENTS IN ACUTELY DISSOCIATED DORSAL ROOT GANGLIA NEURONS OF THE JUVENILE MOUSE

MeHg (0.125 –100 μM) block of current through VGCCs has been described in multiple models (Shafer and Atchison, 1991, Leonhardt et al., 1996a, Sirois and Atchison, 2000, Peng et al., 2002, Hajela et al., 2003, Yuan et al., 2005, Tarabová et al., 2006). The sensitivity of DRG to MeHg-induced cytotoxicity and Ca<sup>2+</sup><sub>i</sub> dysregulation was previously described in Chapter 4, and the decision to use 500 nM MeHg in preliminary electrophysiological recordings was based upon those results. This study was conducted to investigate the effect of 500 nM MeHg on currents mediated by VGCCs expressed in DRG.

DRG were isolated as described in Chapter 4.3.3. Whole-cell patch clamp electrophysiology was used, as described by Murali et al. (2015) and in Chapter 4.3.7. The whole-cell configuration was obtained by applying gentle negative pressure from  $V_h$  of -80 mV, and series resistances and membrane capacitances were compensated.  $Ca^{2+}$  currents were activated from  $V_h$  of -80 mV using a step protocol that applied 140 ms test pulses from -90 to +60 mV in 10 mV and 20 s increments. Peak current ( $I_{Peak}$ ) at each step potential was measured to generate a current-voltage relationship for each cell;  $I_{Peak}$  was defined as the maximum current measured within the first 20 ms of the test potential. DRG subtype was identified by  $C_m$ , a membrane property indicative of cell size (Taylor, 2012), according to (Pearce and Duchen, 1994). Data for each subtype were transformed to median  $C_m$  prior to generating mean current-voltage relationships for C,  $A\delta$ , and  $A\beta$  (Fig. A.1A–C). Current-voltage relationships were similar among all DRG subtypes, where currents were first measurable near -30 mV and increased in magnitude until

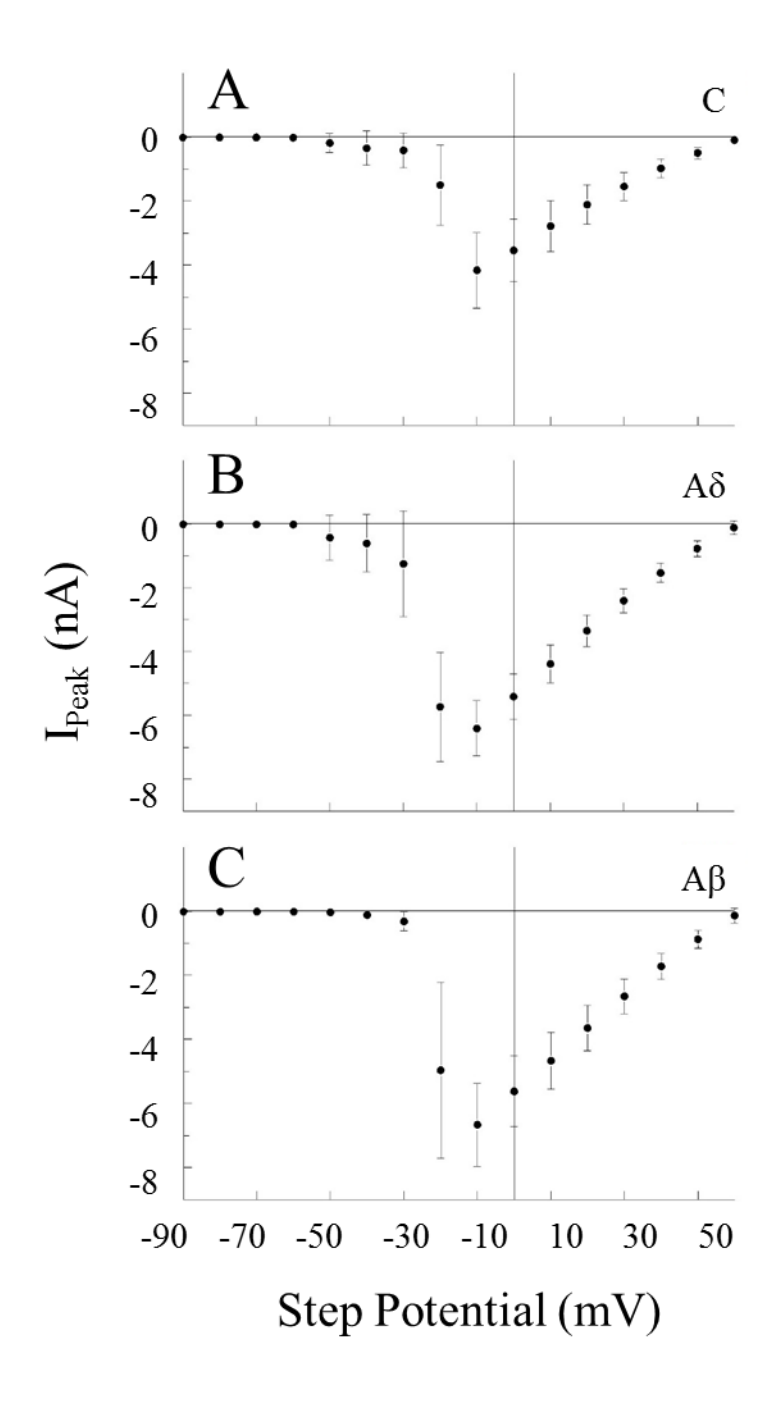


Figure A.1. Mean current-voltage relationships are similar among DRG subtypes. Whole-cell currents were obtained from DRG via voltage clamp. A  $V_h$  of -80 mV was applied to DRG before a 140 ms voltage step at 10 mV intervals (-90 – +60 mV). Current-voltage relationships among the three DRG subtypes were similar in shape, but differed in magnitude; amplitude of  $I_{Peak}$  in (A) C-fiber DRG was lower than that of (B) A $\delta$  and (C) A $\beta$ . Maximum current was reached at the step potential of -10 mV in each of the fiber types. Currents were transformed to the median membrane capacitance for each subtype, and are presented as mean  $\pm$  SEM (n = 3).

maximizing at -10 mV. The amplitude of  $I_{Peak}$  decreased with each subsequent test pulse until reaching the reversal potential at approximately +60 mV.

Timecourse studies were conducted using a step protocol that applied a single test potential;  $Ca^{2+}$  currents were elicited by stepping from  $V_h$  of -80 mV to +10 mV (140 ms) at a sweep interval of 20 s. The step potential of +10 mV was selected to ensure the change in voltage was sufficient to activate the population of VGCCs, yet minimize rundown that could be associated with eliciting maximum Ca<sup>2+</sup> currents by stepping to -10 mV (Scott et al., 1991). In C-fiber DRG, this voltage step produced an inward current which inactivated slightly (Fig. A.2A), whereas the inactivating component was much more prominent in Aδ DRG currents (Fig. A.2B). The non-inactivating current which remained in the final 20 ms of the voltage step was termed I<sub>End</sub>, and was used in later analyses. Ca<sup>2+</sup> currents from Aβ were largest in magnitude and relatively non-inactivating (Fig. A.2C). Currents from DRG, regardless of subtype, also had a characteristic tail (I<sub>Tail</sub>) component which remained following return to V<sub>h</sub>. Tail currents have been attributed to Cl<sup>-</sup> influx through Ca<sup>2+</sup>-activated Cl<sup>-</sup> channels (Currie and Scott, 1992, Scott et al., 1995). Occasionally, Aβ had tail currents with protracted duration (Fig. A.2D); the significance of this event is unknown, as it was difficult to correlate longer duration tail current with AB size or culture conditions. Measurements of I<sub>Peak</sub>, I<sub>End</sub>, I<sub>Tail</sub>, and I<sub>Tail</sub> duration were made, and values were transformed to the median C<sub>m</sub> for each subtype. Characterization of DRG subtype by C<sub>m</sub>, as described by Pearce and Duchen (1994), separated the cells into three distinct categories with unique characteristics of voltage-activated Ca<sup>2+</sup> currents (Table A.1) in which I<sub>Peak</sub> roughly corresponded to C<sub>m</sub> (Fig. A.3.). Thus, this method of sorting DRG subtypes was deemed appropriate for our studies.

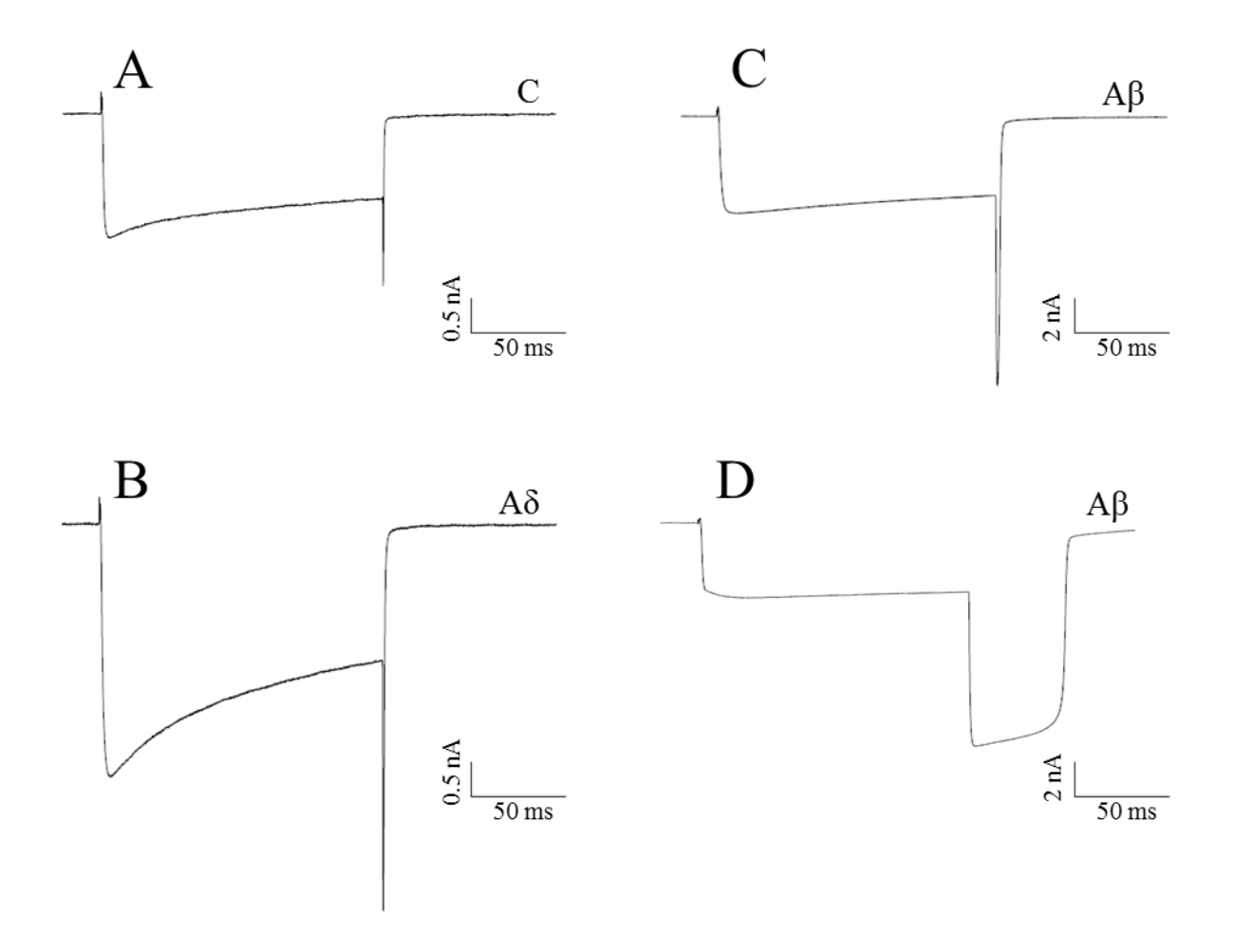


Figure A.2. Representative current tracings in naïve DRG. Whole-cell currents were obtained from DRG via voltage clamp. A  $V_h$  of -80 mV was applied before a 140 ms step to +10 mV. (A) C-fiber DRG had the smallest  $I_{Peak}$ , and current inactivated slightly to  $I_{End}$ . An  $I_{Tail}$  component remained following return to  $V_h$ . (B) Aδ DRG had a larger inactivating current component between  $I_{Peak}$  and  $I_{End}$ . (C)  $I_{Peak}$  was less defined in Aβ DRG, as the currents of these cells inactivated very slowly. (D)  $I_{Tail}$  was occasionally broader in Aβ DRG for an unidentifiable reason.

Fiber type (Capacitance, pF)

|                        | C<br>(10 – 29.9) | $A\delta \ (30-54.9)$ | $A\beta \\ (55-75)$ |
|------------------------|------------------|-----------------------|---------------------|
| $C_{m}(pF)$            | $25.9 \pm 1.7$   | $41.0 \pm 6.0$        | $67.0 \pm 4.4$      |
| I <sub>Peak</sub> (nA) | $-1.8 \pm 0.4$   | $-3.1 \pm 0.3$        | $-5.1 \pm 0.3$      |
| I <sub>End</sub> (nA)  | -1.3 ± 0.3       | $-2.2 \pm 0.2$        | $-4.3 \pm 0.2$      |
| I <sub>Tail</sub> (nA) | $-3.6 \pm 1.0$   | $-6.8 \pm 0.9$        | $-13.9 \pm 0.5$     |
| Tail duration (ms)     | $2.6 \pm 0.4$    | $3.4 \pm 0.4$         | $19.1\pm8.0$        |

Table A.1. Classification of DRG subtypes by  $C_m$  and characteristics of whole-cell current. Whole-cell currents were obtained from DRG via voltage clamp. A  $V_h$  of -80 mV was applied before a 140 ms step to +10 mV. DRG subtypes were defined by  $C_m$ , and measurements of  $I_{Peak}$ ,  $I_{End}$ , and  $I_{Tail}$  were made. Values were transformed to the median membrane capacitance for each subtype, and are presented as mean  $\pm$  SEM (n = 3).

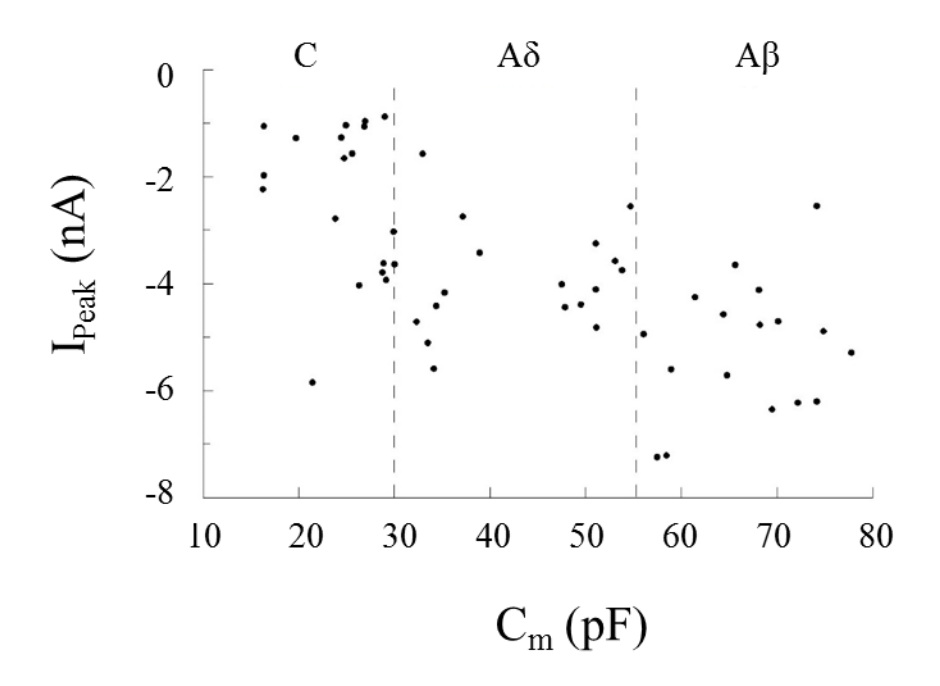


Figure A.3. Relationship between  $I_{Peak}$  roughly corresponds with  $C_m$  and, in turn, cell size. Whole-cell voltage clamp was performed on acute dissociations of DRG.  $I_{Peak}$  elicited by a 140 ms step to +10 mV was measured as extracellular solution was perfused over the cells. Lower  $I_{Peak}$  values were primarily measured in cells with lower  $C_m$ ; as  $C_m$  increased,  $I_{Peak}$  generally increased as well. Hashed lines denote  $C_m$  cutoffs for each DRG subtype.

In timecourse studies of naïve DRG, current rundown was observed after approximately 2 min of applying the step protocol and continued throughout the duration of the recording, about 10 min. Rundown of I<sub>Peak</sub>, I<sub>End</sub>, and I<sub>Tail</sub> followed a similar timecourse and, while it was more apparent in AB DRG carrying larger currents, rundown was observed in cells of all sizes (Fig. A.4A-C). In a separate set of experiments, DRG were exposed to 500 nM MeHg to assess the timecourse of the effects of MeHg on voltage-activated Ca<sup>2+</sup> currents. Because electrical disturbances in DRG following in vivo MeHg exposure were only reported in Aδ and Aβ (Delio et al., 1992, Világi et al., 2000), currents from C-fiber DRG were not included in my assessment. Characteristics of Ca<sup>2+</sup> current were measured following 5 min exposure to MeHg, normalized to controls to account for inherent rundown, and transformed to median C<sub>m</sub> for each subtype. Longer timecourse exposures were not performed due to rundown of cells after several minutes of recording. Magnitude of I<sub>Peak</sub>, I<sub>End</sub>, and I<sub>Tail</sub> were all unaffected by MeHg treatment in both Aδ (Fig. A.5A) and Aβ DRG (Fig. A.5B). The duration of the tail current was also unaffected in both fiber types (Fig. A.6A–B). No noticeable change in current waveform was observed as a result of MeHg exposure (not shown). These results suggest VGCCs function is not impaired at the earliest timepoints following exposure to 500 nM MeHg. Thus, the channels may contribute to early effects of MeHg, including Ca<sup>2+</sup><sub>i</sub> dysregulation.

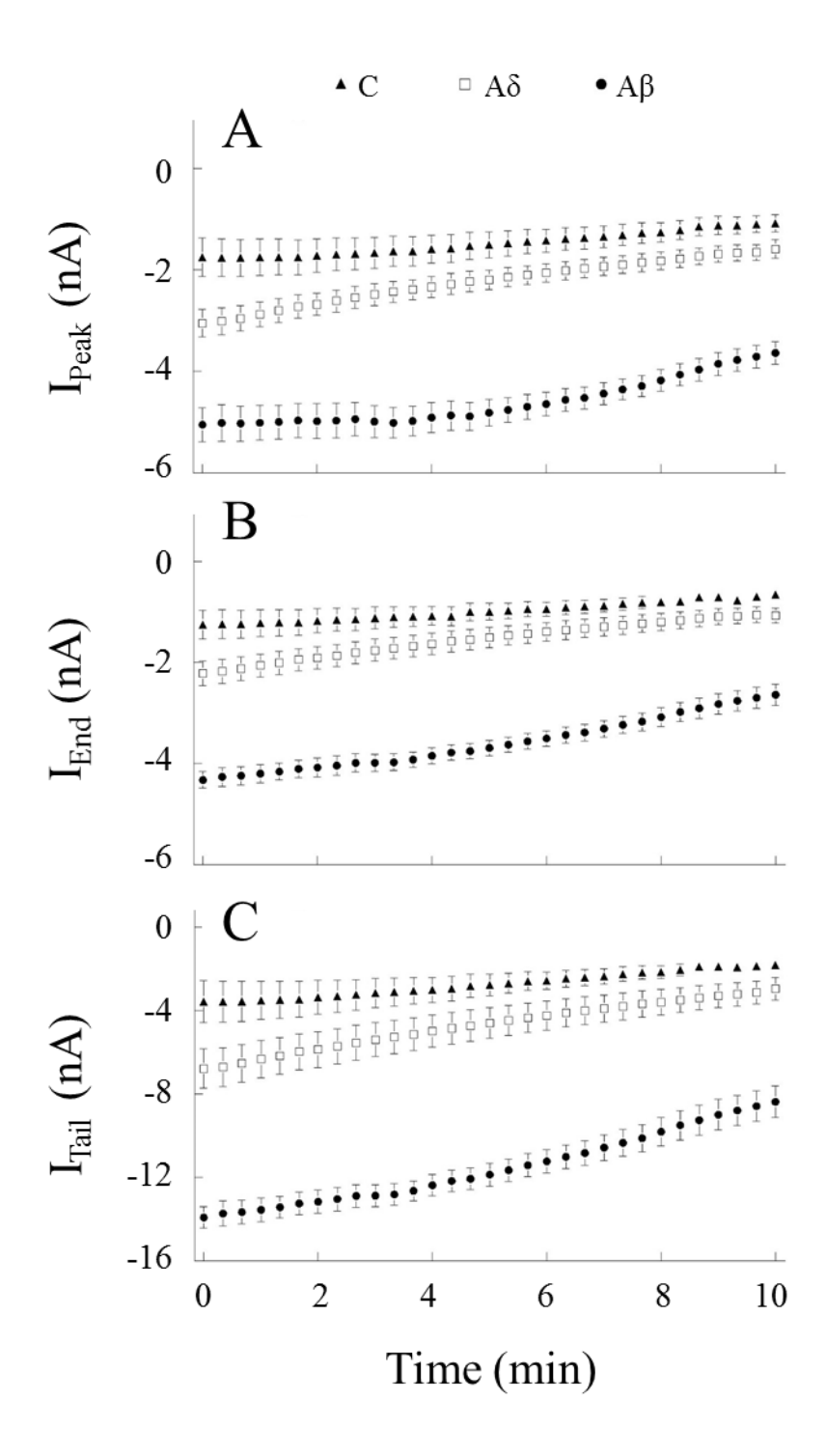


Figure A.4. Timecourse of reduction in the amplitude of  $I_{Peak}$ ,  $I_{End}$ , and  $I_{Tail}$  in all DRG subtypes under standard recording conditions. DRG were depolarized to +10 mV from a  $V_h$  of -80 mV every 20 s. Extracellular solution was continually perfused over cells throughout recordings. Rundown of (A)  $I_{Peak}$ , (B)  $I_{End}$ , and (C)  $I_{Tail}$  occurred in each DRG subtype over the 10 min recording period. Values were transformed to the median membrane capacitance for each subtype, and are presented as mean  $\pm$  SEM (n = 3).

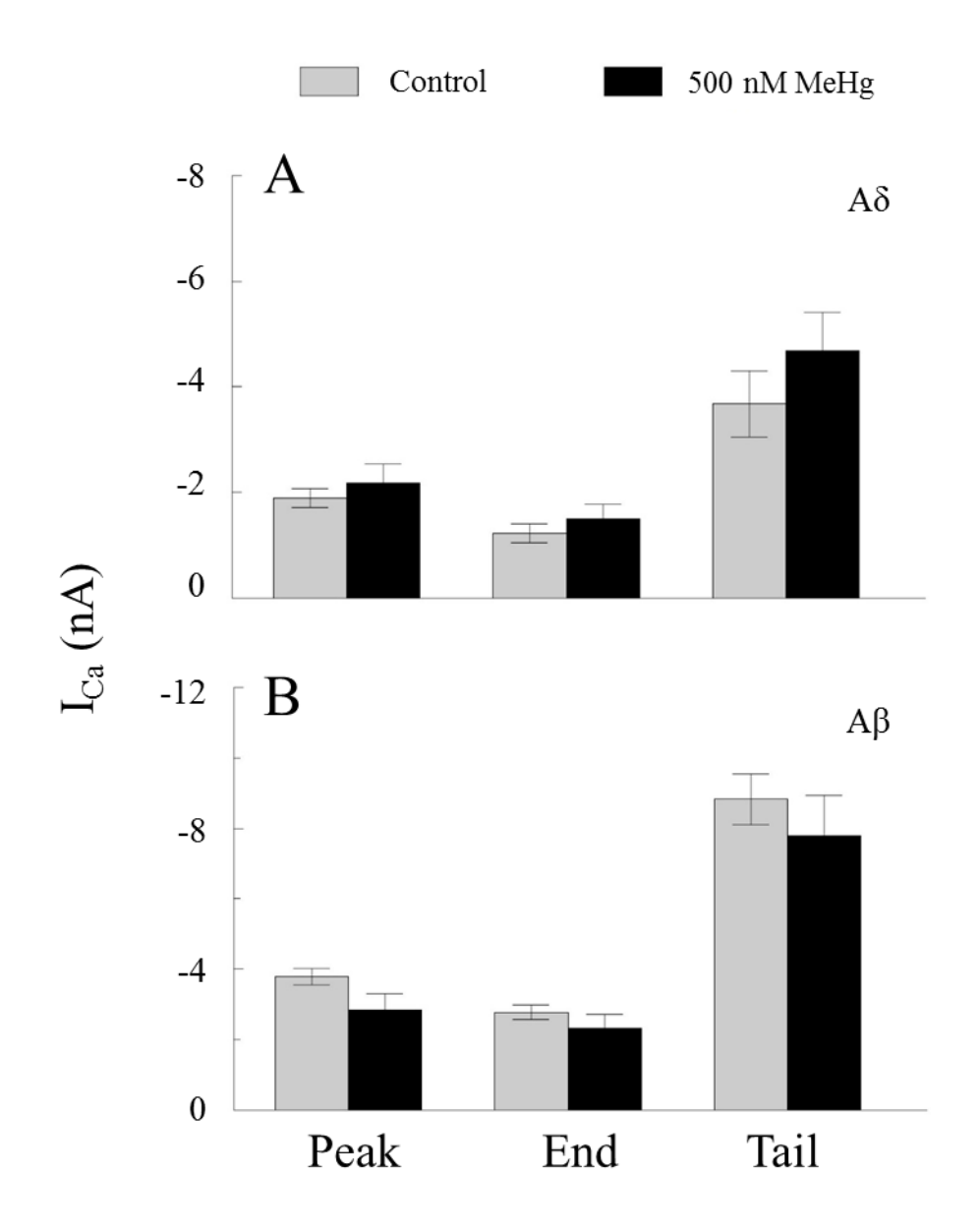


Figure A.5. Whole-cell  $Ca^{2+}$  currents in Aδ and Aβ DRG are unaffected by exposure to 500 nM MeHg. DRG were depolarized to +10 mV from a  $V_h$  of -80 mV every 20 s. Extracellular solution was continually perfused over cells throughout recording. 500 nM MeHg was added to the perfusion after 4 min, and the effects of MeHg on characteristics of  $Ca^{2+}$  currents ( $I_{Ca}$ ) were assessed after 5 min of exposure. (A)  $I_{Peak}$ ,  $I_{End}$ , and  $I_{Tail}$  were not altered in Aδ nor (B) Aβ DRG following MeHg exposure. Values were transformed to the median membrane capacitance for each subtype. Data from MeHg-exposed cells were normalized to controls to account for rundown which occurs throughout recording. Data are presented as mean ± SEM (n = 3).

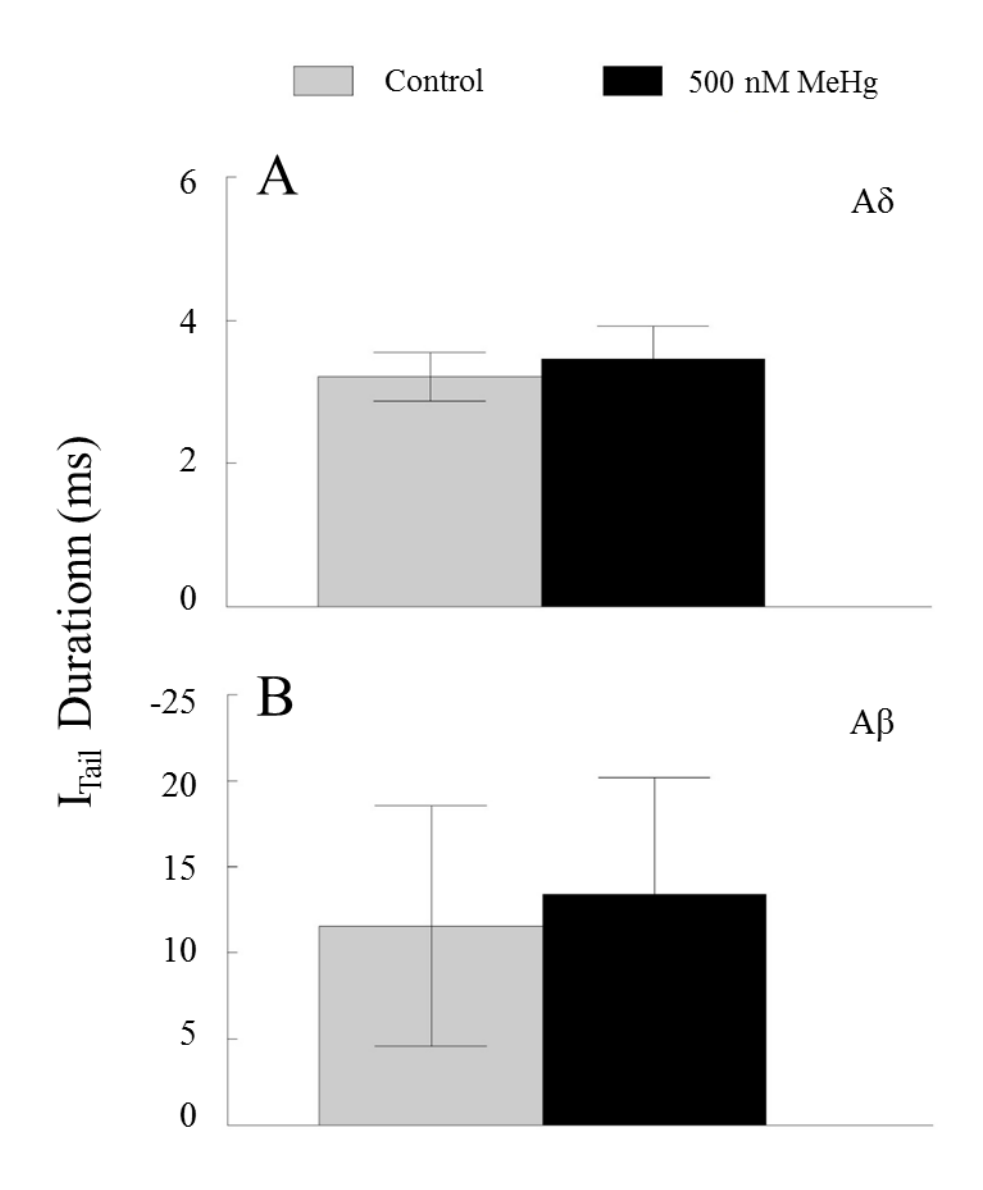


Figure A.6.  $I_{Tail}$  duration in both Aδ and Aβ DRG is unaltered with exposure to 500 nM MeHg. DRG were depolarized to +10 mV from a  $V_h$  of -80 mV every 20 s. Extracellular solution was perfused over cells continuously throughout recording. 500 nM MeHg was added to the perfusion after 4 min, and the effects of MeHg on characteristics of  $I_{Ca}$  were assessed after 5 min of exposure. The duration of  $I_{Tail}$  was not affected in (A) Aδ nor (B) Aβ DRG. Values were transformed to the median membrane capacitance for each subtype. Data from MeHg-exposed cells were normalized to controls to account for rundown which occurs throughout recording. Data are presented as mean  $\pm$  SEM (n = 3).

REFERENCES

## REFERENCES

- Abe T, Haga T, Kurokawa M (1975) Blockage of axoplasmic transport and depolymerisation of reassembled microtubules by methyl mercury. Brain Res 86:504-508.
- Akopian AN (2011) Regulation of nociceptive transmission at the periphery via TRPA1-TRPV1 interactions. Curr Pharm Biotechnol 12:89-94.
- Akopian AN, Ruparel NB, Jeske NA, Hargreaves KM (2007) Transient receptor potential TRPA1 channel desensitization in sensory neurons is agonist dependent and regulated by TRPV1-directed internalization. J Physiol (Lond) 583:175-193.
- Al-saleem T (1976) Levels of mercury and pathological changes in patients with organomercury poisoning. Bull World Health Organ 53 Suppl:99-104.
- Anand U, Otto WR, Facer P, Zebda N, Selmer I, Gunthorpe MJ, Chessell IP, Sinisi M, Birch R, Anand P (2008) TRPA1 receptor localisation in the human peripheral nervous system and function studies in cultured human and rat sensory neurons. Neurosci Lett 438:221-227.
- Ancora S, Rossi R, Simplicio PD, Lusini L, Leonzio C (2002) *In vitro* study of methylmercury in blood of bottlenose dolphins (*Tursiops truncatus*). Arch Environ Contam Toxicol 42:348-353.
- Andersson DA, Gentry C, Moss S, Bevan S (2008) Transient receptor potential A1 is a sensory receptor for multiple products of oxidative stress. J Neurosci 28:2485-2494.
- Aoki Y, Ohtori S, Takahashi K, Ino H, Douya H, Ozawa T, Saito T, Moriya H (2005) Expression and co-expression of VR1, CGRP, and IB4-binding glycoprotein in dorsal root ganglion neurons in rats: differences between the disc afferents and the cutaneous afferents. Spine 30:1496-1500.
- Arakawa O, Nakahiro M, Narahashi T (1991) Mercury modulation of GABA-activated chloride channels and non-specific cation channels in rat dorsal root ganglion neurons. Brain Res 551:58-63.
- Armstrong CM, Gilly WF (1992) Access resistance and space clamp problems associated with whole-cell patch clamping. Methods Enzymol 207:100-122.

- Aschner M (2000) Possible mechanisms of methylmercury cytotoxicity. In: Molecular Biology Today, vol. 1, pp 43-48 Poole: Caister Academic Press.
- Atchison WD (1986) Extracellular calcium-dependent and -independent effects of methylmercury on spontaneous and potassium-evoked release of acetylcholine at the neruomuscular junction. J Pharmacol Exp Ther 237:672-680.
- Atchison WD (1987) Effects of activation of sodium and calcium entry on spontaneous release of acetylcholine induced by methylmercury. J Pharmacol Exp Ther 241:131-139.
- Atchison WD (2003) Effects of toxic environmental contaminants on voltage-gated calcium channel function: from past to present. J Bioenerg Biomembr 35:507-532.
- Atchison WD, Joshi U, Thornburg JE (1986) Irreversible suppression of calcium entry into nerve terminals by methylmercury. J Pharmacol Exp Ther 238:618-624.
- Atchison WD, Narahashi T (1982) Methylmercury-induced depression of neuromuscular transmission in the rat. Neurotoxicology 3:37-50.
- Audesirk G (1993) Electrophysiology of lead intoxication: effects on voltage-sensitive ion channels. Neurotoxicology 14:137-147.
- Bahr GF, Moberger G (1954) Methyl-mercury-chloride as a specific reagent for protein-bound sulfhydryl groups. Exp Cell Res 6:506-518.
- Bakir F, Damluji SF, Amin-Zaki L, Murtadha M, Khalidi A, al-Rawi NY, Tikriti S, Dhahir HI, Clarkson TW, Smith JC, Doherty RA (1973) Methylmercury poisoning in Iraq. Science 181:230-241.
- Ballatori N, Clarkson TW (1985) Biliary secretion of glutathione and of glutathione-metal complexes. Fundam Appl Toxicol 5:816-831.
- Ballatori N, Gatmaitan Z, Truong AT (1995) Impaired biliary excretion and whole body elimination of methylmercury in rats with congenital defect in biliary glutathione excretion. Hepatology 22:1469-1473.

- Bandell M, Story GM, Hwang SW, Viswanath V, Eid SR, Petrus MJ, Earley TJ, Patapoutian A (2004) Noxious cold ion channel TRPA1 is activated by pungent compounds and bradykinin. Neuron 41:849-857.
- Bangalore R, Mehrke G, Gingrich K, Hofmann F, Kass RS (1996) Influence of L-type Ca channel α2/δ-subunit on ionic and gating current in transiently transfected HEK 293 cells. Am J Physiol Heart Circ Physiol 270:H1521-1528.
- Banke TG (2011) The dilated TRPA1 channel pore state is blocked by amiloride and analogues. Brain Res 1381:21-30.
- Banzawa N, Saito S, Imagawa T, Kashio M, Takahashi K, Tominaga M, Ohta T (2014) Molecular basis determining inhibition/activation of nociceptive receptor TRPA1 protein: a single amino acid dictates species-specific actions of the most potent mammalian TRPA1 antagonist. J Biol Chem 289:31927-31939.
- Barabas ME, Kossyreva EA, Stucky CL (2012) TRPA1 is functionally expressed primarily in IB4-binding, non-peptidergic mouse and rat sensory neurons. PLoS One 7:e47988.
- Baxter GJ, Smith RA (1998) Changes in neuropeptide immunoreactivity in cultured adult mouse sensory neurons following methylmercury chloride treatments. Neurosci Lett 246:13-16.
- Benarroch EE (2010) Neuronal voltage-gated calcium channels: brief overview of their function and clinical implications in neurology. Neurology 74:1310-1315.
- Berjukow S, Döring F, Froschmayr M, Grabner M, Glossmann H, Hering S (1996) Endogenous calcium channels in human embryonic kidney (HEK293) cells. Br J Pharmacol 118:748-754.
- Berk AJ (2005) Recent lessons in gene expression, cell cycle control, and cell biology from adenovirus. Oncogene 24:7673-7685.
- Bernhoft RA (2012) Mercury toxicity and treatment: a review of the literature. J Environ Public Health 2012:460508.
- Berridge MJ (1998) Neuronal calcium signaling. Neuron 21:13-26.

- Bezprozvanny I, Tsien RW (1995) Voltage-dependent blockade of diverse types of voltage-gated Ca<sup>2+</sup> channels expressed in *Xenopus* oocytes by the Ca<sup>2+</sup> channel antagonist mibefradil (Ro 40-5967). Mol Pharmacol 48:540-549.
- Bobkov YV, Corey EA, Ache BW (2011) The pore properties of human nociceptor channel TRPA1 evaluated in single channel recordings. Biochim Biophys Acta 1808:1120-1128.
- Boron WF, Boulpaep EL (2009) Medical Physiology. Philadelphia: Saunders.
- Botana LM (2014) Seafood and Freshwater Toxins: Pharmacology, Physiology, and Detection. Boca Raton: CRC Press.
- Bourinet E, Stotz SC, Spaetgens RL, Dayanithi G, Lemos J, Nargeot J, Zamponi GW (2001) Interaction of SNX482 with domains III and IV inhibits activation gating of  $\alpha_{1E}$  (Ca<sub>v</sub>2.3) calcium channels. Biophys J 81:79-88.
- Brierley SM, Castro J, Harrington AM, Hughes PA, Page AJ, Rychkov GY, Blackshaw LA (2011) TRPA1 contributes to specific mechanically activated current and sensory neuron mechanical hypersensitivity. J Physiol (Lond) 589:3575-3593.
- Brust PF, Simerson S, McCue AF, Deal CR, Schoonmaker S, Williams ME, Veliçelebi G, Johnson EC, Harpold MM, Ellis SB (1993) Human neuronal votlage-depedent calcium channels: studies on subunit structure and role in channel assembly. Neuropharmacology 32:1089-1102.
- Buber MT, Cerne R, Cortés RY, Bryant RW, Lee SP (2010) Overexpression of human transient receptor potential M5 upregulates endogenous human transient receptor potential A1 in a stable HEK cell line. Assay Drug Dev Technol 8:695-702.
- Cao B, Lv W, Jin S, Tang J, Wang S, Zhao H, Guo H, Su J, Cao X (2013) Degeneration of peripheral nervous system in rats experimentally induced by methylmercury intoxication. Neurol Sci 34:663-669.
- Castellano A, Wei X, Birnbaumer L, Perez-Reyes E (1993a) Cloning and expression of a neuronal calcium channel β subunit. J Biol Chem 268:12359-12366.
- Castellano A, Wei X, Birnbaumer L, Perez-Reyes E (1993b) Cloning and expression of a third calcium channel β subunit. J Biol Chem 268:3450-3455.

- Caterina MJ, Schumacher MA, Tominaga M, Rosen TA, Levine JD, Julius D (1997) The capsaicin receptor: a heat-activated ion channel in the pain pathway. Nature 389:816-824.
- Catterall WA (1998) Structure and function of neuronal Ca<sup>2+</sup> channels and their role in neurotransmitter release. Cell Calcium 24:307-323.
- Catterall WA (2000) Structure and regulation of voltage-gated Ca<sup>2+</sup> channels. Annu Rev Cell Dev Biol 16:521-555.
- Catterall WA, Striessnig J, Snutch TP, Perez-Reyes E (2003) International Union of Pharmacology. XL. Compendium of voltage-gated ion channels: calcium channels. Pharmacol Rev 55:579-581.
- Cavanagh JB, Chen FC (1971) The effects of methyl-mercury-dicyandiamide on the peripheral nerves and spinal cord of rats. Acta Neuropathol 19:208-215.
- Cavanaugh EJ, Simkin D, Kim D (2008) Activation of transient receptor potential A1 channels by mustard oil, tetrahydrocannabinol and Ca<sup>2+</sup> reveals different functional states. Neuroscience 154:1467-1476.
- Cernichiari E, Brewer R, Myers GJ, Marsh DO, Lapham LW, Cox C, Shamlaye CF, Berlin M, Davidson PW, Clarkson TW (1995a) Monitoring methylmercury during pregnancy: maternal hair predicts fetal brain exposure. Neurotoxicology 16:705-710.
- Cernichiari E, Toribara TY, Liang L, Marsh DO, Berlin M, Myers GJ, Cox C, Choisy O, Davidson PW, Clarkson TW (1995b) The biological monitoring of mercury in the Seychelles study. Neurotoxicology 16:613-628.
- Cesare P, McNaughton P (1996) A novel heat-activated current in nociceptive neurons and its sensitization by bradykinin. Proc Natl Acad Sci USA 93:15435-15439.
- Chang LW, Hartmann HA (1972) Ultrastructural studies of the nervous system after mercury intoxication. II. Pathological changes in the nerve fibers. Acta Neuropathol 20:316-334.
- Chen J, Joshi SK, DiDomencio S, Perner RJ, Mikusa JP, Gauvin DM, Segreti JA, Han P, Zhang XF, Niforatos W, Bianchi BR, Baker SJ, Zhong C, Simler GH, McDonald HA, Schmidt RG, McGaraughty SP, Chu KL, Faltynek CR, Kort ME, Reilly RM, Kym PR (2011) Selective blockade of TRPA1 channel attenuates pathological pain without altering noxious cold sensation or body temperature regulation. Pain 152:1165-1172.

- Chen J, Kim D, Bianchi BR, Cavanaugh EJ, Faltynek CR, Kym PR, Reilly RM (2009) Pore dilation occurs in TRPA1 but not in TRPM8 channels. Mol Pain 5:3.
- Cheung M, Verity MA (1981) Methyl mercury inhibition of synaptosome protein synthesis: role of mitochondrial dysfunction. Environ Res 24:286-298.
- Chin-Chan M, Navarro-Yepes J, Quintanilla-Vega B (2015) Environmental pollutants as risk factors for neurodegenerative disorders: Alzheimer and Parkinson diseases. Front Cell Neurosci 9:124.
- Chouabe C, Drici MD, Romey G, Barhanin J, Lazdunski M (1998) HERG and KvLQT1/IsK, the cardiac K<sup>+</sup> channels involved in long QT syndromes, are targets for calcium channel blockers. Mol Pharmacol 54:695-703.
- Clarkson TW (1995) Environmental contaminants in the food chain. Am J Clin Nutr 61:682S-686S.
- Clarkson TW, Magos L (2006) The toxicology of mercury and its chemical compounds. Crit Rev Toxicol 36:609-662.
- Cook MJ (1965) The Anatomy of the Laboratory Mouse. London: Academic Press.
- Corey DP, García-Añoveros J, Holt JR, Kwan KY, Lin SY, Vollrath MA, Amalfitano A, Cheung EL, Derfler BH, Duggan A, Géléoc GS, Gray PA, Hoffman MP, Rehm HL, Tamasauskas D, Zhang DS (2004) TRPA1 is a candidate for the mechanosensitive transduction channel of vertebrate hair cells. Nature 432:723-730.
- Currie KP, Scott RH (1992) Calcium-activated currents in cultured neurones from rat dorsal root ganglia. Br J Pharmacol 106:593-602.
- Cvetkov TL, Huynh KW, Cohen MR, Moiseenkova-Bell VY (2011) Molecular architecture and subunit organization of TRPA1 ion channel revealed by electron microscopy. J Biol Chem 286:38168-38176.
- Dai Y, Wang S, Tominaga M, Yamamoto S, Fukuoka T, Higashi T, Kobayashi K, Obata K, Yamanaka H, Noguchi K (2007) Sensitization of TRPA1 by PAR2 contributes to the sensation of inflammatory pain. J Clin Invest 117:1979-1987.

- Davis LE, Kornfeld M, Mooney HS, Fiedler KJ, Haaland KY, Orrison WW, Cernichiari E, Clarkson TW (1994) Methylmercury poisoning: long-term clinical, radiological, toxicological, and pathological studies of an affected family. Ann Neurol 35:680-688.
- De Koninck P, Carbonetto S, Cooper E (1993) NGF induces neonatal rat sensory neurons to extend dendrites in culture after removal of satellite cells. J Neurosci 13:577-585.
- Delio DA, Reuhl KR, Lowndes HE (1992) Ectopic impulse generation in dorsal root ganglion neurons during methylmercury intoxication: an electrophysiological and morphological study. Neurotoxicology 13:527-539.
- Denny MF, Atchison WD (1994) Methylmercury-induced elevations in intrasynaptosomal zinc concentrations: an <sup>19</sup>F-NMR study. J Neurochem 63:383-386.
- Denny MF, Atchison WD (1996) Mercurial-induced alterations in neuronal divalent cation homeostasis. Neurotoxicology 17:47-61.
- Denny MF, Hare MF, Atchison WD (1993) Methylmercury alters intrasynaptosomal concentrations of endogenous polyvalent cations. Toxicol Appl Pharmacol 122:222-232.
- Djouhri L, Bleazard L, Lawson SN (1998) Association of somatic action potential shape with sensory receptive properties in guinea-pig dorsal root ganglion neurones. J Physiol (Lond) 513:857-872
- Dodd J, Jahr CE, Hamilton PN, Heath MJ, Matthew WD, Jessell TM (1983) Cytochemical and physiological properties of sensory and dorsal horn neurons that transmit cutaneous sensation. Cold Spring Harb Symp Quant Biol 48:685-695.
- Doerner JF, Gisselmann G, Hatt H, Wetzel CH (2007) Transient receptor potential channel A1 is directly gated by calcium ions. J Biol Chem 282:13180-13189.
- Du S, Araki I, Yoshiyama M, Nomura T, Takeda M (2007) Transient receptor potential channel A1 involved in sensory transduction of rat urinary bladder through C-fiber pathway. Urology 70:826-831.
- Dutczak WJ, Ballatori N (1992) γ-Glutamyltransferase-dependent biliary-hepatic recycling of methyl mercury in the guinea pig. J Pharmacol Exp Ther 262:619-623.

- Dutczak WJ, Ballatori N (1994) Transport of the glutathione-methylmercury complex across liver canalicular membranes on reduced glutathione carriers. J Biol Chem 269:9746-9751.
- Dutczak WJ, Clarkson TW, Ballatori N (1991) Biliary-hepatic recycling of a xenobiotic: gallbladder absorption of methyl mercury. Am J Physiol 260:G873-880.
- Dyer D, Tigyi G, Miledi R (1992) The effect of active serum albumin on PC12 cells: II. Intracellular Ca<sup>2+</sup> transients and their role in neurite retraction. Brain Res Mol Brain Res 14:302-309.
- Early S (2012) TRPA1 channels in the vasculature. Br J Pharmacol 167:13-22.
- Eberhard M, Miyagawa K, Hermsmeyer K, Erne P (1995) Effects of mibefradil on intracellular Ca<sup>2+</sup> release in cultured rat cardiac fibroblasts and human platelets. Naunyn Schmiedebergs Arch Pharmacol 353:94-101.
- Edwards JR, Cobbett P, Atchison WD (2002) Comparative disruption of intracellular calcium regulation by methylmercury in PC12 and PC18 cells. Soc Neurosci Abstr 833.5.
- Edwards JR, Marty MS, Atchison WD (2005) Comparative sensitivity of rat cerebellar neurons to dysregulation of divalent cation homeostasis and cytotoxicity caused by methylmercury. Toxicol Appl Pharmacol 208:222-232.
- Ekwall B, Silano V, Paganuzzi-Stammati A, Zucco F (1990) Toxicity tests with mammalian cell cultures. In: Short-term Toxicity Tests for Non-genotoxic Effects (Bourdeau, P. et al., eds), pp 75-97 Chichester: Wiley.
- Ellinor PT, Yang J, Sather WA, Zhang JF, Tsien RW (1995) Ca<sup>2+</sup> channel selectivity at a single locus for high-affinity Ca<sup>2+</sup> interactions. Neuron 15:1121-1132.
- Ellinor PT, Zhang JF, Randall AD, Zhou M, Schwarz TL, Tsien RW, Horne WA (1993) Functional expression of a rapidly inactivating neuronal calcium channel. Nature 363:455-458.
- Ertel EA, Campbell KP, Harpold MM, Hofmann F, Mori Y, Perez-Reyes E, Schwartz A, Snutch TP, Tanabe T, Birnbaumer L, Tsien RW, Catterall WA (2000) Nomenclature of voltage-gated calcium channels. Neuron 25:533-535.

- Estacion M, Vohra BP, Liu S, Hoeijmakers J, Faber CG, Merkies IS, Lauria G, Black JA, Waxman SG (2015) Ca<sup>2+</sup> toxicity due to reverse Na<sup>+</sup>/Ca<sup>2+</sup> exchange contributes to degeneration of neurites of DRG neurons induced by a neuropathy-associated Nav1.7 mutation. J Neurophysiol 114:1554-1564.
- Eto K (1997) Pathology of Minamata disease. Toxicol Pathol 25:614-623.
- Eto K, Tokunaga H, Nagashima K, Takeuchi T (2002a) An autopsy case of Minamata disease (methylmercury poisoning)- pathological viewpoints of peripheral nerves. Toxicol Pathol 30:714-722.
- Eto K, Yasutake A, Korogi Y, Akima M, Shimozeki T, Tokunaga H, Kuwana T, Kaneko Y (2002b) Methylmercury poisoning in common marmosets- MRI findings and peripheral nerve lesions. Toxicol Pathol 30:723-734.
- Fang X, McMullan S, Lawson SN, Djouhri L (2005) Electrophysiological differences between nociceptive and non-nociceptive dorsal root ganglion neurones in the rat *in vivo*. J Physiol (Lond) 565:927-943.
- Fariñas I, Cano-Jaimez M, Bellmunt E, Soriano M (2002) Regulation of neurogenesis by neurotrophins in developing spinal sensory ganglia. Brain Res Bull 57:809-816.
- Fischer MJ, Balasuriya D, Jeggle P, Goetze TA, McNaughton PA, Reeh PW, Edwardson JM (2014) Direct evidence for functional TRPV1/TRPA1 heteromers. Pflugers Arch 466:2229-2241.
- Fitzgerald WF, Clarkson TW (1991) Mercury and monomethylmercury: present and future concerns. Environ Health Perspect 96:159-166.
- Freire MA, Oliveira RB, Picanço-Diniz CW, Pereira A, Jr (2007) Differential effects of methylmercury intoxication in the rat's barrel field as evidenced by NADPH diaphorase histochemistry. Neurotoxicology 28:175-181.
- Gauvin DM, Mikusa J, Baker S, Zhong C, Simler G, Zhang X, Bianchi B, Didomencio S, Perner R, Reilly R, Kort M, Jacobson P, Honore M, Chen J, Joshi S, Kym P (2009) A-967079, a potent and selective TRPA1 antagonist, is efficacious in rat preclinical pain models. Soc Neurosci Abstr 761.3.

- Gees M, Alpizar YA, Boonen B, Sanchez A, Everaerts W, Segal A, Xue F, Janssens A, Owsianik G, Nilius B, Voets T, Talavera K (2013) Mechanisms of transient receptor potential vanilloid 1 activation and sensitization by allyl isothiocyanate. Mol Pharmacol 84:325-334.
- Gold MS, Dastmalchi S, Levine JD (1996) Co-expression of nociceptor properties in dorsal root ganglion neurons from the adult rat *in vitro*. Neuroscience 71:265-275.
- Gomora JC, Enyeart JA, Enyeart JJ (1999) Mibefradil potently blocks ATP-activated K<sup>+</sup> channels in adrenal cells. Mol Pharmacol 56:1192-1197.
- Gomora JC, Xu L, Enyeart JA, Enyeart JJ (2000) Effect of mibefradil on voltage-dependent gating and kinetics of T-type Ca<sup>2+</sup> channels in cortisol-secreting cells. J Pharmacol Exp Ther 292:96-103.
- Graham FL, Smiley J, Russell WC, Nairn R (1977) Characteristics of a human cell line transformed by DNA from human adenovirus type 5. J Gen Virol 36:59-74.
- Grynkiewicz G, Poenie M, Tsien RY (1985) A new generation of Ca<sup>2+</sup> indicators with greatly improved fluorescence properties. J Biol Chem 260:3440-3450.
- Hajela RK, Peng SQ, Atchison WD (2003) Comparative effects of methylmercury and Hg<sup>2+</sup> on human neuronal N- and R-type high-voltage activated calcium channels transiently expressed in human embryonic kidney 293 cells. J Pharmacol Exp Ther 306:1129-1136.
- Hamdy MK, Noyes OR (1975) Formation of methyl mercury by bacteria. Appl Microbiol 30:424-432.
- Hamill OP, Marty A, Neher E, Sakmann B, Sigworth FJ (1981) Improved patch-clamp techniques for high-resolution current recording from cells and cell-free membrane patches. Pflugers Arch 391:85-100.
- Hannon HE, Atchison WD (2011)  $Ca^{2+}$  channel  $\alpha_1$  subunits differentially modulate methylmercury-induced  $Ca^{2+}$  dysregulation in HEK-293 cells in a concentration- and phase-dependent manner. Soc Neurosci Abstr 867.05.
- Hans M, Urrutia A, Deal C, Brust PF, Stauderman K, Ellis SB, Harpold MM, Johnson EC, Williams ME (1999) Structural elements in domain IV that influence biophysical and pharmacological properties of human α<sub>1A</sub>-containing high-voltage-activated calcium channels. Biophys J 76:1384-1400.

- Harada M (1995) Minamata disease: methylmercury poisoning in Japan caused by environmental pollution. Crit Rev Toxicol 25:1-24.
- Hare MF, Atchison WD (1992) Comparative action of methylmercury and divalent inorganic mercury on nerve terminal and intraterminal mitochondrial membrane potentials. J Pharmacol Exp Ther 261:166-172.
- Hare MF, Atchison WD (1995a) Methylmercury mobilizes Ca<sup>++</sup> from intracellular stores sensitive to inositol 1,4,5-trisphosphate in NG108-15 cells. J Pharmacol Exp Ther 272:1016-1023.
- Hare MF, Atchison WD (1995b) Nifedipine and tetrodotoxin delay the onset of methylmercury-induced increase in [Ca<sup>2+</sup>]<sub>i</sub> in NG108-15 cells. Toxicol Appl Pharmacol 135:299-307.
- Hare MF, McGinnis KM, Atchison WD (1993) Methylmercury increases intracellular concentrations of Ca<sup>++</sup> and heavy metals in NG108-15 cells. J Pharmacol Exp Ther 266:1626-1635.
- Harper AA, Lawson SN (1985) Electrical properties of rat dorsal root ganglion neurones with different peripheral nerve conduction velocities. J Physiol (Lond) 359:47-63.
- Harris HH, Pickering IJ, George GN (2003) The chemical form of mercury in fish. Science 301:1203.
- Harrison M, O'Brien A, Adams L, Cowin G, Ruitenberg MJ, Sengul G, Watson C (2013) Vertebral landmarks for the identification of spinal cord segments in the mouse. Neuroimage 68:22-29.
- Heinemann SH, Schlief T, Mori Y, Imoto K (1994) Molecular pore structure of voltage-gated sodium and calcium channels. Braz J Med Biol Res 27:2781-2802.
- Hewett SJ, Atchison WD (1992) Effects of charge and lipophilicity on mercurial-induced reduction of <sup>45</sup>Ca<sup>2+</sup> uptake in isolated nerve terminals of the rat. Toxicol Appl Pharmacol 113:267-273.
- Hjerling-Leffler J, AlQatari M, Ernfors P, Koltzenburg M (2007) Emergence of functional sensory subtypes as defined by transient receptor potential channel expression. J Neurosci 27:2435-2443.

- Hodgkin AL, Huxley AF (1945) Resting and action potentials in single nerve fibres. J Physiol (Lond) 104:176-195.
- Hodgkin AL, Huxley AF (1952) A quantitative description of membrane current and its application to conduction and excitation in nerve. J Physiol (Lond) 117:500-544.
- Hökfelt T, Elde R, Johansson O, Luft R, Nilsson G, Arimura A (1976) Immunohistochemical evidence for separate populations of somatostatin-containing and substance P-containing primary afferent neurons in the rat. Neuroscience 1:131-136.
- Hong DH, Yang D, Choi IW, Son YK, Jung WK, Kim DJ, Han J, Na SH, Park WS (2012) The T-type Ca<sup>2+</sup> channel inhibitor mibefradil inhibits voltage-dependent K<sup>+</sup> channels in rabbit coronary arterial smooth muscle cells. J Pharmacol Sci 120:196-205.
- Huang CS, Narahashi T (1996) Mercury chloride modulation of the GABA<sub>A</sub> receptor-channel complex in rat dorsal root ganglion neurons. Toxicol Appl Pharmacol 140:508-520.
- Huang CS, Narahashi T (1997a) The role of G proteins in the activity and mercury modulation of GABA-induced currents in rat neurons. Neuropharmacology 36:1623-1630.
- Huang CS, Narahashi T (1997b) The role of phosphorylation in the activity and mercury modulation of GABA-induced currents in rat neurons. Neuropharmacology 36:1631-1640.
- Hullin R, Singer-Lahat D, Freichel M, Biel M, Dascal N, Hofmann F, Flockerzi V (1992) Calcium channel β subunit heterogeneity: functional expression of cloned cDNA from heart, aorta and brain. EMBO J 11:885-890.
- Imura N, Miura K, Inokawa M, Nakada S (1980) Mechanisms of methylmercury cytotoxicity: by biochemical and morphological experiments using cultured cells. Toxicology 17:241-254.
- Inoue M, Fujita T, Goto M, Kumamoto E (2012) Presynaptic enhancement by eugenol of spontaneous excitatory transmission in rat spinal substantia gelatinosa neurons is mediated by transient receptor potential A1 channels. Neuroscience 210:403-415.
- Irukayama K (1977) Case history of Minamata. In: Minamata Disease: Methylmercury Poisoning in Minamata and Niigata (Tsubaki, T. and Irukayama, K., eds), pp 1-56 Japan: Kodansha.

- Ishii M, Miyashita T, Tsuchiya K, Ueda K, Umemura A, Honda T (2004) Histological distribution and ultrastructural features of immunoreactive terminals against RT97, a monoclonal antibody to a 200 kD neurofilament, in the spinal dorsal horn of a rat. Fukushima J Med Sci 50:65-74.
- Islam MS (2011). New York: Springer.
- Jackson JG, Robinson MB (2015) Reciprocal regulation of mitochondrial dynamics and calcium signaling in astrocyte processes. J Neurosci 35:15199-15213.
- Jeftinija S, Jeftinija K (1990) Calcitonin gene-related peptide immunoreactivity in neuronal perikarya in dorsal root. Brain Res 519:324-328.
- Jensen S, Jernelöv A (1969) Biological methylation of mercury in aquatic organisms. Nature 223:753-754.
- Jernelöv A (1969) Conversion of mercury compounds. In: Chemical Fallout (Miller, M. W. and Berg, G. G., eds), pp 68-74 Springfield: Charles C. Thomas.
- Ji G, Zhou S, Carlton SM (2008) Intact Aδ-fibers up-regulate transient receptor potential A1 and contribute to cold hypersensitivity in neuropathic rats. Neuroscience 154:1054-1066.
- Jones LP, Patil PG, Snutch TP, Yue DT (1997) G-protein modulation of N-type calcium channel gating current in human embryonic kidney cells (HEK 293). J Physiol 498:601-610.
- Jordt SE, Bautista DM, Chuang HH, McKemy DD, Zygmunt PM, Högestätt ED, Meng ID, Julius D (2004) Mustard oils and cannabinoids excite sensory nerve fibres through the TRP channel ANKTM1. Nature 427:260-265.
- Juang MS (1976) An electrophysiological study of the action of methylmercuric chloride and mercuric chloride on the sciatic nerve-sartorius muscle preparation of the frog. Toxicol Appl Pharmacol 37:339-348.
- Kang MS, Jeong JY, Seo JH, Jeon HJ, Jung KM, Chin MR, Moon CK, Bonventre JV, Jung SY, Kim DK (2006) Methylmercury-induced toxicity is mediated by enhanced intracellular calcium through activation of phosphatidylcholine-specific phospholipase C. Toxicol Appl Pharmacol 216:206-215.

- Karashima Y, Prenen J, Talavera K, Janssens A, Voets T, Nilius B (2010) Agonist-induced changes in Ca<sup>2+</sup> permeation through the nociceptor cation channel TRPA1. Biophys J 98:773-783.
- Kasama H, Itoh K, Omata S, Sugano H (1989) Differential effects of methylmercury on the synthesis of protein species in dorsal root ganglia of the rat. Arch Toxicol 63:226-230.
- Kauppinen RA, Komulainen H, Taipale H (1989) Cellular mechanisms underlying the increase in cytosolic free calcium concentration induced by methylmercury in cerebrocortical synaptosomes from guinea pig. J Pharmacol Exp Ther 248:1248-1254.
- Kavalali ET (2015) The mechanisms and functions of spontaneous neurotransmitter release. Nat Rev Neurosci 16:5-16.
- Kerper LE, Ballatori N, Clarkson TW (1992) Methylmercury transport across the blood-brain barrier by an amino acid carrier. Am J Physiol 262:R761-765.
- Kim MS, Morii T, Sun LX, Imoto K, Mori Y (1993) Structural determinants of ion selectivity in brain calcium channel. FEBS Lett 318:145-148.
- Kindt KS, Viswanath V, Macpherson L, Quast K, Hu H, Patapoutian A, Schafer WR (2007) *Caenorhabditis elegans* TRPA-1 functions in mechanosensation. Nat Neurosci 10:568-577.
- Klement G, Eisele L, Malinowsky D, Nolting A, Svensson M, Terp G, Weigelt D, Dabrowski M (2013) Characterization of a ligand binding site in the human transient receptor potential ankyrin 1 pore. Biophys J 104:798-806.
- Kobayashi K, Fukuoka T, Obata K, Yamanaka H, Dai Y, Tokunaga A, Noguchi K (2005) Distinct expression of TRPM8, TRPA1, and TRPV1 mRNAs in rat primary afferent neurons with  $A\delta/C$ -fibers and colocalization with trk receptors. J Comp Neurol 493:596-606.
- Koch M, Kreutz S, Böttger C, Grabiec U, Ghadban C, Korf HW, Dehghani F (2011) The cannabinoid WIN 55,212-2-mediated protection of dentate gyrus granule cells is driven by CB1 receptors and modulated by TRPA1 and Cav2.2. Hippocampus 21:554-564.
- Komatsu T, Uchida K, Fujita F, Zhou Y, Tominaga M (2012) Primary alcohols activate human TRPA1 channel in a carbon chain length-dependent manner. Pflugers Arch 463:549-559.

- Komulainen H, Bondy SC (1987) Increased free intrasynaptosomal Ca<sup>2+</sup> by neurotoxic organometals: distinctive mechanisms. Toxicol Appl Pharmacol 88:77-86.
- Kong HK, Wong MH, Chan HM, Lo SC (2013) Chronic exposure of adult rats to low doses of methylmercury induced a state of metabolic deficit in the somatosensory cortex. J Proteome Res 12:5233-5245.
- Kostyniak PJ, Clarkson TW (1981) Role of chelating agents in metal toxicity. Fundam Appl Toxicol 1:376-380.
- Kosugi M, Nakatsuka T, Fujita T, Kuroda Y, Kumamoto E (2007) Activation of TRPA1 channel facilitates excitatory synaptic transmission in substantia gelatinosa neurons of the adult rat spinal cord. J Neurosci 27:4443-4451.
- Kwan KY, Glazer JM, Corey DP, Rice FL, Stucky CL (2009) TRPA1 modulates mechanotransduction in cutaneous sensory neurons. J Neurosci 29:4808-4819.
- Lacerda AE, Kim HS, Ruth P, Perez-Reyes E, Flockerzi V, Hofmann F, Birnbaumer L, Brown AM (1991) Normalization of current kinetics by interaction between the  $\alpha_1$  and  $\beta$  subunits of the skeletal muscle dihydropyridine-sensitive Ca<sup>2+</sup> channel. Nature 352:527-530.
- Lawson SN (2002) Phenotype and function of somatic primary afferent nociceptive neurones with C-, Aδ- or  $A\alpha/\beta$ -fibres. Exp Physiol 87:239-244.
- Lawson SN, Biscoe TJ (1979) Development of mouse dorsal root ganglia: an autoradiographic and quantitative study. J Neurocytol 8:265-274.
- Lawson SN, Perry MJ, Prabhakar E, McCarthy PW (1993) Primary sensory neurones: neurofilament, neuropeptides, and conduction velocity. Brain Res Bull 30:239-243.
- Lee KH, Chung K, Chung JM, Coggeshall RE (1986) Correlation of cell body size, axon size, and signal conduction velocity for individually labelled dorsal root ganglion cells in the cat. J Comp Neurol 243:335-346.
- Leonhardt R, Haas H, Büsselberg D (1996a) Methyl mercury reduces voltage-activated currents of rat dorsal root ganglion neurons. Naunyn Schmiedebergs Arch Pharmacol 354:532-538.

- Leonhardt R, Pekel M, Platt B, Haas HL, Büsselberg D (1996b) Voltage-activated calcium channel currents of rat DRG neurons are reduced by mercuric chloride (HgCl<sub>2</sub>) and methylmercury (CH<sub>3</sub>HgCl). Neurotoxicology 17:85-92.
- Levesque PC, Atchison WD (1991) Disruption of brain mitochondrial calcium sequestration by methylmercury. J Pharmacol Exp Ther 256:236-242.
- Levesque PC, Hare MF, Atchison WD (1992) Inhibition of mitochondrial Ca<sup>2+</sup> release diminishes the effectiveness of methyl mercury to release acetylcholine from synaptosomes. Toxicol Appl Pharmacol 115:11-20.
- Liedtke WB, Heller S (2007) TRP Ion Channel Function in Sensory Transduction and Cellular Signaling Cascades. Boca Raton: CRC Press.
- Liem LK, Simard JM, Song Y, Tewari K (1995) The patch clamp technique. Neurosurgery 36:382-392.
- Limke TL, Atchison WD (2002) Acute exposure to methylmercury opens the mitochondrial permeability transition pore in rat cerebellar granule cells. Toxicol Appl Pharmacol 178:52-61.
- Limke TL, Atchison WD (2009) Application of single-cell microfluorimetry to neurotoxicology assays. Curr Protoc Toxicol 42:12.15:12.15.11-12.15.13.
- Limke TL, Bearss JJ, Atchison WD (2004) Acute exposure to methylmercury causes Ca<sup>2+</sup> dysregulation and neuronal death in rat cerebellar granule cells through an M3 muscarinic receptor-linked pathway. Toxicol Sci 80:60-68.
- Limke TL, Otero-Montañez JKL, Atchison WD (2003) Evidence for interactions between intracellular calcium stores during methylmercury-induced intracellular calcium dysregulation in rat cerebellar granule neurons. J Pharmacol Exp Ther 304:949-958.
- Lin YC, Boone M, Meuris L, Lemmens I, Van Roy N, Soete A, Reumers J, Moisse M, Plaisance S, Drmanac R, Chen J, Speleman F, Lambrechts D, Van de Peer Y, Tavernier J, Callewaert N (2014) Genome dynamics of the human embryonic kidney 293 lineage in response to cell biology manipulations. Nat Commum 5:4767.
- Lindberg A, Björnberg KA, Vahter M, Berglund M (2004) Exposure to methylmercury in non-fish-eating people in Sweden. Environ Res 96:28-33.

- Liu JH, Bijlenga P, Occhiodoro T, Fischer-Lougheed J, Bader CR, Bernheim L (1999) Mibefradil (Ro 40-5967) inhibits several Ca<sup>2+</sup> and K<sup>+</sup> currents in human fusion-competent myoblasts. Br J Pharmacol 126:245-250.
- Louis N, Evelegh C, Graham FL (1997) Cloning and sequencing of the cellular-viral junctions from the human adenovirus type 5 transformed 293 cell line. Virology 233:423-429.
- Lu SG, Zhang X, Gold MS (2006) Intracellular calcium regulation among subpopulations of rat dorsal root ganglion neurons. J Physiol (Lond) 577:169-190.
- Lundback SS, Musetti VM, Marty MS, Atchison WD (2002) Methylmercury-induced alterations in calcium homeostasis in rat cerebellar type II astrocytes. Soc Neurosci Abstr 436.17.
- Macpherson LJ, Dubin AE, Evans MJ, Marr F, Schultz PG, Cravatt BF, Patapoutian A (2007) Noxious compounds activate TRPA1 ion channels through covalent modification of cysteines. Nature 445:541-545.
- Magos L, Brown AW, Sparrow S, Bailey E, Snowden RT, Skipp WR (1985) The comparative toxicology of ethyl- and methylmercury. Arch Toxicol 57:260-267.
- Maher M, Ao H, Banke T, Nasser N, Wu NT, Breitenbucher JG, Chaplan SR, Wickenden AD (2008) Activation of TRPA1 by farnesyl thiosalicylic acid. Mol Pharmacol 73:1225-1234.
- Malin SA, Davis BM, Molliver DC (2007) Production of dissociated sensory neuron cultures and considerations for their use in studying neuronal function and plasticity. Nat Protoc 2:152-160.
- Mandadi S, Armati PJ, Roufogalis BD (2011) Protein kinase C modulation of thermo-sensitive transient receptor potential channels: implications for pain signaling. J Nat Sci Biol Med 2:13-25.
- Marrero-Rosado B, Fox SM, Hannon HE, Atchison WD (2013) Effects of mercury and lead on voltage-gated calcium channel function. In: Encylcopedia of Metalloproteins (Kretsinger, R. H. et al., eds), pp 1336-1346 New York: Springer.
- Martin RL, Lee JH, Cribbs LL, Perez-Reyes E, Hanck DA (2000) Mibefradil block of cloned T-type calcium channels. J Pharmacol Exp Ther 295:302-308.

- Marty MS, Atchison WD (1997) Pathways mediating Ca<sup>2+</sup> entry in rat cerebellar granule cells following *in vitro* exposure to methyl mercury. Toxicol Appl Pharmacol 147:319-330.
- Marty MS, Atchison WD (1998) Elevations of intracellular Ca<sup>2+</sup> as a probable contributor to decreased viability in cerebellar granule cells following acute exposure to methylmercury. Toxicol Appl Pharmacol 150:98-105.
- Marty MS, Master S, Atchison WD (1997) Methylmercury induces elevations in intracellular Ca<sup>2+</sup> concentration in rat cerebellar type II astrocyte cultures. The Toxicologist 36:297.
- Mason RP, Abbott ML, Bodaly RA, Bullock OR, Jr., Driscoll CT, Evers D, Lindberg SE, Murray M, Swain EB (2005) Monitoring the response to changing mercury deposition. Environ Sci Technol 39:14A-22A.
- McAlpine D, Araki S (1958) Minamata disease: an unusual neurological disorder caused by contaminated fish. Lancet 2:629-631.
- McCarter GC, Reichling DB, Levine JD (1999) Mechanical transduction by rat dorsal root ganglion neurons *in vitro*. Neurosci Lett 273:179-182.
- McCleskey EW, Fox AP, Feldman DH, Cruz LJ, Olivera BM, Tsien RW, Yoshikami D (1987) ω-Conotoxin: direct and persistent blockade of specific types of calcium channels in neurons but not muscle. Proc Natl Acad Sci USA 84:4327-4331.
- McCool BA, Harpold MM, Stauderman KA, Brust PF, Lovinger DM (1997) Relative contributions of G protein, channel, and receptor to voltage-dependent inhibition of neuronal N-type and P/Q-type calcium channels in HEK 293 cell lines. Neurosci Lett 239:89-92.
- Mergler D, Anderson HA, Chan LHM, Mahaffey KR, Murray M, Sakamoto M, Stern AH (2007) Methylmercury exposure and health effects in humans: a worldwide concern. *AMBIO* 36:3-11.
- Meyer RA, Ringkamp M, Campbell JN, Raja SN (2005) Peripheral mechanisms of cutaneous nociception. In: Wall and Melzack's Textbook of Pain (McMahon, S. B. and Koltzenburg, M., eds), pp 3-34 Edinburgh: Churchill Livingstone.

- Miura K, Himeno S, Koide N, Imura N (2000) Effects of methylmercury and inorganic mercury on the growth of nerve fibers in cultured chick dorsal root ganglia. Tohoku J Exp Med 192:195-210.
- Mizushima T, Obata K, Katsura H, Yamanaka H, Kobayashi K, Dai Y, Fukuoka T, Tokunaga A, Mashimo T, Noguchi K (2006) Noxious cold stimulation induces mitogen-activated protein kinase activation in transient receptor potential (TRP) channels TRPA1- and TRPM8-containing small sensory neurons. Neuroscience 140:1337-1348.
- Monnet-Tschudi F, Zurich MG, Boschat C, Corbaz A, Honegger P (2006) Involvement of environmental mercury and lead in the etiology of neurodegenerative diseases. Rev Environ Health 21:105-117.
- Moraes ER, Kushmerick C, Naves LA (2014) Characteristics of dorsal root ganglia neurons sensitive to substance P. Mol Pain 10:73.
- Mori Y, Friedrich T, Kim MS, Mikami A, Nakai J, Ruth P, Bosse E, Hofmann F, Flockerzi V, Furuichi T, Mikoshiba K, Imoto K, Tanabe T, Numa S (1991) Primary structure and functional expression from complementary DNA of a brain calcium channel. Nature 350:398-402.
- Mukhopadhyay I, Gomes P, Aranake S, Shetty M, Karnik P, Damle M, Kuruganti S, Thorat S, Khairatkar-Joshi N (2011) Expression of functional TRPA1 receptor on human lung fibroblast and epithelial cells. J Recept Signal Transduct Res 31:350-358.
- Murali SS, Napier IA, Mohammadi SA, Alewood PF, Lewis RJ, Christie MJ (2015) High-voltage-activated calcium current subtypes in mouse DRG neurons adapt in a subpopulation-specific manner after nerve injury. J Neurophysiol 113:1511-1519.
- Nagatomo K, Kubo Y (2008) Caffeine activates mouse TRPA1 channels but suppresses human TRPA1 channels. Proc Natl Acad Sci USA 105:17373-17378.
- Nakada S, Saito H, Imura N (1981) Effect of methylmercry and inorganic mercury on the nerve growth factor-induced neurite outgrowth in chick embryonic sensory ganglia. Toxicol Lett 8:23-28.
- Nakatsuka K, Gupta R, Saito S, Banzawa N, Takahashi K, Tominaga M, Ohta T (2013) Identification of molecular determinants for a potent mammalian TRPA1 antagonist by utilizing species differences. J Mol Neurosci 51:754-762.

- Narahashi T, Ma JY, Arakawa O, Reuveny E, Nakahiro M (1994) GABA receptor-channel complex as a target site of mercury, copper, zinc, and lanthanides. Cell Mol Neurobiol 14:599-621.
- Nassini R, Pedretti P, Moretto N, Fusi C, Carnini C, Facchinetti F, Viscomi AR, Pisano AR, Stokesberry S, Brunmark C, Svitacheva N, McGarvey L, Patacchini R, Damholt AB, Geppetti P, Materazzi S (2012) Transient receptor potential ankyrin 1 channel localized to non-neuronal airway cells promotes a non-neurogenic inflammation. PLoS One 7:e42454.
- Neher E, Sakmann B (1976) Single-channel currents recorded from membrane of denervated frog muscle fibres. Nature 260:799-802.
- Nilius B, Appendino G, Owsianik G (2012) The transient receptor potential channel TRPA1: from gene to pathophysiology. Pflugers Arch 464:425-458.
- Nilius B, Owsianik G (2011) The transient receptor potential family of ion channels. Genome Biol 12:218.
- Nilius B, Prenen J, Kamouchi M, Viana F, Voets T, Droogmans G (1997) Inhibition by mibefradil, a novel calcium channel antagonist, of Ca<sup>2+</sup>- and volume-activated Cl<sup>-</sup> channels in macrovascular endothelial cells. Br J Pharmacol 121:547-555.
- Nilius B, Prenen J, Owsianik G (2011) Irritating channels: the case of TRPA1. J Physiol (Lond) 589:1543-1549.
- Ninomiya T, Imamura K, Kuwahata M, Kindaichi M, Susa M, Ekino S (2005) Reappraisal of somatosensory disorders in methylmercury poisoning. Neurotoxicol Teratol 27:643-653.
- Numazaki M, Tominaga M (2004) Nociception and TRP channels. Curr Drug Targets CNS Neurol Disord 3:479-485.
- Ohta T, Imagawa T, Ito S (2007) Novel agonistic action of mustard oil on recombinant and endogenous porcine transient receptor potential V1 (pTRPV1) channels. Biochem Pharmacol 73:1646-1656.
- Omata S, Momose Y, Ueki H, Sugano H (1982) *In vivo* effect of methylmercury on protein synthesis in peripheral nervous tissues of the rat. Arch Toxicol 49:203-214.

- Otten U, Goedert M, Mayer N, Lembeck F (1980) Requirement of nerve growth factor for development of substance P-containing sensory neurones. Nature 287:158-159.
- Papadopoulos NG, Dedoussis GVZ, Spanakos G, Gritzapis AD, Baxevanis CN, Papamichail M (1994) An improved fluorescence assay for the determination of lymphocyte-mediated cytotoxicity using flow cytometry. J Immunol Methods 177:101-111.
- Park SH, Suh YS, Kim H, Rhyu IJ, Kim HL (1997) Chromosomal localization and neural distribution of voltage dependent calcium channel β<sub>3</sub> subunit gene. Mol Cells 7:200-203.
- Patil MJ, Jeske NA, Akopian AN (2010) Transient receptor potential V1 regulates activation and modulation of transient receptor potential A1 by Ca<sup>2+</sup>. Neuroscience 171:1109-1119.
- Pearce RJ, Duchen MR (1994) Differential expression of membrane currents in dissociated mouse primary sensory neurons. Neuroscience 63:1041-1056.
- Peng SQ, Hajela RK, Atchison WD (2002) Effects of methylmercury on human neuronal L-type calcium channels transiently expressed in human embryonic kidney cells (HEK-293). J Pharmacol Exp Ther 302:424-432.
- Pérez-García MT, Kamp TJ, Marbán E (1995) Functional properties of cardiac L-type calcium channels transiently expressed in HEK 293 cells: roles of  $\alpha_1$  and  $\beta$  subunits. J Gen Physiol 105:289-305.
- Perez-Reyes E (2003) Molecular physiology of low-voltage-activated T-type calcium channels. Physiol Rev 83:117-161.
- Pickhardt PC, Fisher NS (2007) Accumulation of inorganic and methylmercury by freshwater phytoplankton in two contrasting water bodies. Environ Sci Technol 41:125-131.
- Pingle SC, Matta JA, Ahern GP (2007) Capsaicin receptor: TRPV1 a promiscuous TRP channel. Handb Exp Pharmacol 179:155-171.
- Pinto FC, Fontes RB, Leonhardt MC, Amodio DT, Porro FF, Machado J (2002) Anatomic study of the filum terminale and its correlations with the tethered cord syndrome. Neurosurgery 51:725-729.

- Powers PA, Liu S, Hogan K, Gregg RG (1992) Skeletal muscle and brain isoforms of a β-subunit of human voltage-dependent calcium channels are encoded by a single gene. J Biol Chem 267:22967-22972.
- Pozsgai G, Bodkin JV, Graepel R, Bevan S, Andersson DA, Brain SD (2010) Evidence for the pathophysiological relevance of TRPA1 receptors in the cardiovascular system *in vivo*. Cardiovasc Res 87:760-768.
- Quandt FN, Kato E, Narahashi T (1982) Effects of methylmercury on electrical responses of neuroblastoma cells. Neurotoxicology 3:205-220.
- Rabenstein DL, Isab AA, Reid RS (1982) A proton nuclear magnetic resonance study of the binding of methylmercury in human erythrocytes. Biochim Biophys Acta 720:53-64.
- Raisinghani M, Zhong L, Jeffry JA, Bishnoi M, Pabbidi RM, Pimentel F, Cao DS, Evans MS, Premkumar LS (2011) Activation characteristics of transient receptor potential ankyrin 1 and its role in nociception. Am J Physiol Cell Physiol 301:C587-600.
- Rajanna B, Chetty CS, Rajanna S, Hall E, Fail S, Yallapragada PR (1995) Modulation of protein kinase C by heavy metals. Toxicol Lett 81:197-203.
- Rall W, Segev I (1985) Space clamp problems when voltage clamping branched neurons with intracellular microelectrodes. In: Voltage and Patch Clamping with Microelectrodes (Smith, T. G. et al., eds), pp 191-215 New York: Springer.
- Ramanathan G, Atchison WD (2011) Ca<sup>2+</sup> entry pathways in mouse spinal motor neurons in culture following *in vitro* exposure to methylmercury. Neurotoxicology 32:742-750.
- Randall A, Tsien RW (1995) Pharmacological dissection of multiple types of Ca<sup>2+</sup> channel currents in rat cerebellar granule neurons. J Neurosci 15:2995-3012.
- Ranson SW, Clark SL (1953) The Anatomy of the Nervous System: Its Development and Function. Philadelphia: WB Saunders.
- Reid G, Babes A, Pluteanu F (2002) A cold- and menthol-activated current in rat dorsal root ganglion neurones: properties and role in cold transduction. J Physiol (Lond) 545:595-614.

- Rexed B (1952) The cytoarchitectonic organization of the spinal cord in the cat. J Comp Neurol 96:414-495.
- Rexed B (1954) A cytoarchitectonic atlas of the spinal cord in the cat. J Comp Neurol 100:297-379.
- Rice DC, Schoeny R, Mahaffey K (2003) Methods and rationale for derivation of a reference dose for methylmercury by the U.S. EPA. Risk Anal 23:107-115.
- Rigaud M, Gemes G, Barabas ME, Chernoff DI, Abram SE, Stucky CL, Hogan QH (2008) Species and strain differences in rodent sciatic nerve anatomy: implications for studies of neuropathic pain. Pain 136:188-201.
- Rowland IR, Mallett AK, Flynn J, Hargreaves RJ (1986) The effect of various dietary fibres on tissue concentration and chemical form of mercury after methylmercury exposure in mice. Arch Toxicol 59:94-98.
- Rowland IR, Robinson RD, Doherty RA (1984) Effects of diet on mercury metabolism and excretion in mice given methylmercury: role of gut flora. Arch Environ Health 39:401-408.
- Sadofsky LR, Boa AN, Maher SA, Birrell MA, Belvisi MG, Morice AH (2011) TRPA1 is activated by direct addition of cysteine residues to the N-hydroxysuccinyl esters of acrylic and cinnamic acids. Pharmacol Res 63:30-36.
- Sadofsky LR, Sreekrishna KT, Lin Y, Schinaman R, Gorka K, Mantri Y, Haught JC, Huggins TG, Isfort RJ, Bascom CC, Morice AH (2014) Unique responses are observed in transient receptor potential ankyrin 1 and vanilloid 1 (TRPA1 and TRPV1) co-expressing cells. Cells 3:616-626.
- Saijoh K, Fukunaga T, Katsuyama H, Lee MJ, Sumino K (1993) Effects of methylmercury on protein kinase A and protein kinase C in the mouse brain. Environ Res 63:264-273.
- Sakamoto M, Ikegami N, Nakano A (1996) Protective effects of Ca<sup>2+</sup> channel blockers against methyl mercury toxicity. Pharmacol Toxicol 78:193-199.
- Salas MM, Hargreaves KM, Akopian AN (2009) TRPA1-mediated responses in trigeminal sensory neurons: interaction between TRPA1 and TRPV1. Eur J Neurosci 29:1568-1578.

- Sarafian TA (1993) Methyl mercury increases intracellular Ca<sup>2+</sup> and inositol phosphate levels in cultured cerebellar granule neurons. J Neurochem 61:648-657.
- Scheff NN, Yilmaz E, Gold MS (2014) The properties, distribution and function of Na<sup>+</sup>-Ca<sup>2+</sup> exchanger isoforms in rat cutaneous sensory neurons. J Physiol (Lond) 592:4969-4993.
- Schiønning JD, Larsen JO, Tandrup T, Brændgaard H (1998) Selective degeneration of dorsal root ganglia and dorsal nerve roots in methyl mercury-intoxicated rats: a stereological study. Acta Neuropathol 96:191-201.
- Scott BS, Edwards BA (1980) Electric membrane properties of adult mouse DRG neurons and the effect of culture duration. J Neurobiol 11:291-301.
- Scott RH, Pearson HA, Dolphin AC (1991) Aspects of vertebrate neuronal voltage-activated calcium currents and their regulation. Prog Neurobiol 36:485-520.
- Scott RH, Sutton KG, Griffin A, Stapleton SR, Currie KP (1995) Aspects of calcium-activated chloride currents: a neuronal perspective. Pharmacol Ther 66:535-565.
- Scroggs RS, Fox AP (1991) Distribution of dihydropyridine and ω-conotoxin-sensitive calcium currents in acutely isolated rat and frog sensory neuron somata: diameter-dependent L channel expression in frog. J Neurosci 11:1334-1346.
- Scroggs RS, Fox AP (1992a) Calcium current variation between acutely isolated adult rat dorsal root ganglion neurons of different sizes. J Physiol (Lond) 445:639-658.
- Scroggs RS, Fox AP (1992b) Multiple Ca<sup>2+</sup> currents elicited by action potential waveforms in acutely isolated adult rat dorsal root ganglion. J Neurosci 12:1789-1801.
- Sha J, Ghosh MK, Zhang K, Harter ML (2010) E1A interacts with two opposing transcriptional pathways to induce quiescent cells into S phase. J Virol 84:4050-4059.
- Shafer TJ, Atchison WD (1989) Block of  $^{45}$ Ca uptake into synaptosomes by methylmercury: Ca<sup>++</sup>- and Na<sup>+</sup>-dependence. J Pharmacol Exp Ther 248:696-702.
- Shafer TJ, Atchison WD (1991) Methylmercury blocks N- and L-type Ca<sup>++</sup> channels in nerve growth factor-differentiated pheochromocytoma (PC12) cells. J Pharmacol Exp Ther 258:149-157.

- Shafer TJ, Atchison WD (1992) Effects of methylmercury on perineurial Na<sup>+</sup> and Ca<sup>2+</sup>-dependent potentials at neuromuscular junctions of the mouse. Brain Res 595:215-219.
- Shafer TJ, Contreras ML, Atchison WD (1990) Characterization of interactions of methylmercury with Ca<sup>2+</sup> channels in synaptosomes and pheochromocytoma cells: radiotracer flux and binding studies. Mol Pharmacol 38:102-113.
- Shaw G, Morse S, Ararat M, Graham FL (2002) Preferential transformation of human neuronal cells by human adenoviruses and the origin of HEK 293 cells. FASEB J 16:869-871.
- Shigetomi E, Tong X, Kwan KY, Corey DP, Khakh BS (2011) TRPA1 channels regulate astrocyte resting calcium and inhibitory synapse efficacy through GAT-3. Nat Neurosci 15:70-80.
- Sigworth FJ, Neher E (1980) Single Na<sup>+</sup> channel currents observed in cultured rat muscle cells. Nature 287:447-449.
- Simmons-Willis TA, Koh AS, Clarkson TW, Ballatori N (2002) Transport of a neurotoxicant by molecular mimicry: the methylmercury-L-cysteine complex is a substrate for human L-type large neutral amino acid transporter (LAT) 1 and LAT2. Biochem J 367:239-246.
- Sirois JE, Atchison WD (2000) Methylmercury affects multiple subtypes of calcium channels in rat cerebellar granule cells. Toxicol Appl Pharmacol 167:1-11.
- Skryma R, Prevarskaya N, Gkika D, Shuba Y (2011) From urgency to frequency: facts and controversies of TRPs in the lower urinary tract. Nat Rev Urol 8:617-630.
- Smith JC, Allen PV, Turner MD, Most B, Fisher HL, Hall LL (1994) The kinetics of intravenously administered methyl mercury in man. Toxicol Appl Pharmacol 128:251-256.
- Snider WD, Silos-Santiago I (1996) Dorsal root ganglion neurons require functional neurotrophin receptors for survival during development. Philos Trans R Soc Lond B Biol Sci 351:395-403.
- Soong TW, Stea A, Hodson CD, Dubel SJ, Vincent SR, Snutch TP (1993) Structure and functional expression of a member of the low voltage-activated calcium channel family. Science 260:1133-1136.

- Spahn V, Stein C, Zöllner C (2014) Modulation of transient receptor vanilloid 1 activity by transient receptor potential ankyrin 1. Mol Pharmacol 85:335-344.
- Staruschenko A, Jeske NA, Akopian AN (2010) Contribution of TRPV1-TRPA1 interaction to the single channel properties of the TRPA1 channel. J Biol Chem 285:15167-15177.
- Stea A, Tomlinson WJ, Soong TW, Bourinet E, Dubel SJ, Vincent SR, Snutch TP (1994) Localization and functional properties of a rat brain  $\alpha_{1A}$  calcium channel reflect similarities to neuronal Q- and P-type channels. Proc Natl Acad Sci USA 91:10576-10580.
- Steel RGD, Torrie JH (1960) Principles and Procedures of Statistics. New York, NY: McGraw-Hill.
- Story GM, Peier AM, Reeve AJ, Eid SR, Mosbacher J, Hricik TR, Earley TJ, Hergarden AC, Andersson DA, Hwang SW, McIntyre P, Jegla T, Bevan S, Patapoutian A (2003) ANKTM1, a TRP-like channel expressed in nociceptive neurons, is activated by cold temperatures. Cell 112:819-829.
- Streng T, Axelsson HE, Hedlund P, Andersson DA, Jordt SE, Bevan S, Andersson KE, Högestätt ED, Zygmunt PM (2008) Distribution and function of the hydrogen sulfide-sensitive TRPA1 ion channel in rat urinary bladder. Eur Urol 53:391-399.
- Stummann TC, Hareng L, Bremer S (2009) Hazard assessment of methylmercury toxicity to neuronal induction in embryogenesis using human embryonic stem cells. Toxicology 257:117-126.
- Suda I, Hirayama K (1992) Degradation of methyl and ethyl mercury into inorganic mercury by hydroxyl radical produced from rat liver microsomes. Arch Toxicol 66:398-402.
- Suda I, Suda M, Hirayama K (1993) Phagocytic cells as a contributor to *in vivo* degradation of alkyl mercury. Bull Environ Contam Toxicol 51:394-400.
- Szücs A, Angiello C, Salánki J, Carpenter DO (1997) Effects of inorganic mercury and methylmercury on the ionic currents of cultured rat hippocampal neurons. Cell Mol Neurobiol 17:273-288.
- Takahashi N, Mizuno Y, Kozai D, Yamamoto S, Kiyonaka S, Shibata T, Uchida K, Mori Y (2008) Molecular characterization of TRPA1 channel activation by cysteine-reactive inflammatory mediators. Channels (Austin) 2:287-298.

- Takahashi N, Mori Y (2011) TRP channels as sensors and signal integrators of redox status changes. Front Pharmacol 2:58.
- Takaoka S, Kawakami Y, Fujino T, Oh-ishi F, Motokura F, Kumagai Y, Miyaoka T (2008) Somatosensory disturbance by methylmercury exposure. Environ Res 107:6-19.
- Takeuchi T, Morikawa N, Matsumoto H, Shiraishi Y (1962) A pathological study of Minamata disease in Japan. Acta Neuropathol 2:40-57.
- Takumida M, Ishibashi T, Hamamoto T, Hirakawa K, Anniko M (2009) Expression of transient receptor potential channel melastin (TRPM) 1-8 and TRPA1 (ankyrin) in mouse inner ear. Acta Otolaryngol 129:1050-1060.
- Tanaka O, Sakagami H, Kondo H (1995) Localization of mRNAs of voltage-dependent  $Ca^{2+}$ -channels: four subtypes of  $\alpha_1$  and  $\beta$ -subunits in developing and mature rat brain. Brain Res Mol Brain Res 30:1-16.
- Tanner S, Shen Z, Ng J, Florea L, Guigó R, Briggs SP, Bafna V (2007) Improving gene annotation using peptide mass spectrometry. Genome Res 17:231-239.
- Tarabová B, Kurejová M, Sulová Z, Drabová M, Lacinová L (2006) Inorganic mercury and methylmercury inhibit the Ca<sub>v</sub>3.1 channel expressed in human embryonic kidney 293 cells by different mechanisms. J Pharmacol Exp Ther 317:418-427.
- Tasaki I, Singer I, Watanabe A (1967) Cation interdiffusion in squid giant axons. J Gen Physiol 50:989-1007.
- Taylor AL (2012) What we talk about when we talk about capacitance measured with the voltage-clamp step method. J Comput Neurosci 32:167-175.
- Thomas P, Smart TG (2005) HEK293 cell line: a vehicle for the expression of recombinant proteins. J Pharmacol Toxicol Methods 51:187-200.
- Traxinger DL, Atchison WD (1987) Reversal of methylmercury-induced block of nerve-evoked release of acetylcholine at the neuromuscular junction. Toxicol Appl Pharmacol 90:23-33.
- Tsien RW, Ellinor PT, Horne WA (1991) Molecular diversity of voltage-dependent Ca<sup>2+</sup> channels. Trends Pharmacol Sci 12:349-354.

- Uddenberg N (1966) Studies on modality segregation and second-order neurones in the dorsal funiculus. Experientia 22:441-442.
- Uddenberg N (1968) Differential localization in dorsal funiculus of fibres originating from different receptors. Exp Brain Res 4:367-376.
- Uta D, Furue H, Pickering AE, Rashid MH, Mizuguchi-Takase H, Katafuchi T, Imoto K, Yoshimura M (2010) TRPA1-expressing primary afferents synapse with a morphologically identified subclass of substantia gelatinosa neurons in the adult rat spinal cord. Eur J Neurosci 31:1960-1973.
- Vahter ME, Mottet NK, Friberg LT, Lind SB, Charleston JS, Burbacher TM (1995) Demethylation of methyl mercury in different brain site of Macaca fascicularis monkes during long-term subclinical methyl mercury exposure. Toxicol Appl Pharmacol 134:273-284.
- Vennekens R, Voets T, Bindels RJ, Droogmans G, Nilius B (2002) Current understanding of mammalian TRP homologues. Cell Calcium 31:253-264.
- Verity MA, Brown WJ, Cheung M (1975) Organic mercurial encephalopathy: *in vivo* and *in vitro* effects of methyl mercury on synaptosomal respiration. J Neurochem 25:759-766.
- Vidal V, Fox SM, Atchison WD (2011) Different susceptibilities to MeHg-induced cell death between non-neuronal and neuronal cells. The Toxicologist 120:296.
- Világi I, Dóczi J, Banczerowski-Pelyhe I (2000) Altered electrophysiological characteristics of developing rat cortical neurones after chronic methylmercury chloride treatment. Int J Dev Neurosci 18:493-499.
- Villière V, McLachlan EM (1996) Electrophysiological properties of neurons in intact rat dorsal root ganglia classified by conduction velocity and action potential duration. J Neurophysiol 76:1924-1941.
- Vogel DG, Margolis RL, Mottet NK (1985) The effects of methyl mercury binding to microtubules. Toxicol Appl Pharmacol 80:473-486.
- Volsen SG, Day NC, McCormack AL, Smith W, Craig PJ, Beattie R, Ince PG, Shaw PJ, Ellis SB, Gillespie A, Harpold MM, Lodge D (1995) The expression of neuronal voltage-dependent calcium channels in human cerebellum. Brain Res Mol Brain Res 34:271-282.

- Walker RG, Willingham AT, Zuker CS (2000) A *Drosophila* mechanosensory transduction channel. Science 287:2229-2234.
- Wall PD, Dubner R (1972) Somatosensory pathways. Annu Rev Physiol 34:315-336.
- Wang L, Cvetkov TL, Chance MR, Moiseenkova-Bell VY (2012) Identification of *in vivo* disulfide conformation of TRPA1 ion channel. J Biol Chem 287:6169-6176.
- Wang S, Dai Y, Fukuoka T, Yamanaka H, Kobayashi K, Obata K, Cui X, Tominaga M, Noguchi K (2008a) Phospholipase C and protein kinase A mediate bradykinin sensitization of TRPA1: a molecular mechanism of inflammatory pain. Brain 131:1241-1251.
- Wang YY, Chang RB, Waters HN, McKemy DD, Liman ER (2008b) The nociceptor ion channel TRPA1 is potentiated and inactivated by permeating calcium ions. J Biol Chem 283:32691-32703.
- Wasteneys GO, Cadrin M, Reuhl KR, Brown DL (1988) The effects of methylmercury on the cytoskeleton of murine embryonal carcinoma cells. Cell Biol Toxicol 4:41-60.
- Watson C, Paxinos G, Kayalioglu G (2009) The Spinal Cord: A Christopher and Dana Reeve Foundation Text and Atlas. Cambridge: Academic Press.
- WHO (1976) Environmental Health Criteria 101: Mercury. In: International Program on Chemical Safety Geneva: World Health Organization.
- WHO (1990) Environmental Health Criteria 101: Methylmercury. In: International Program on Chemical Safety Geneva: World Health Organization.
- Wilke RA, Kolbert CP, Rahimi RA, Windebank AJ (2003) Methylmercury induces apoptosis in cultured rat dorsal root ganglion neurons. Neurotoxicology 24:369-378.
- Williams ME, Brust PF, Feldman DH, Patthi S, Simerson S, Maroufi A, McCue AF, Veliçelebi G, Ellis SB, Harpold MM (1992a) Structure and functional expression of an ω-conotoxin-sensitive human N-type calcium channel. Science 257:389-395.
- Williams ME, Feldman DH, McCue AF, Brenner R, Veliçelebi G, Ellis SB, Harpold MM (1992b) Structure and functional expression of  $\alpha_1$ ,  $\alpha_2$ , and  $\beta$  subunits of a novel human neuronal calcium channel subtype. Neuron 8:71-84.

- Williams ME, Marubio LM, Deal CR, Hans M, Brust PF, Philipson LH, Miller RJ, Johnson EC, Harpold MM, Ellis SB (1994) Structure and functional characterization of neuronal α<sub>1E</sub> calcium channel subtypes. J Biol Chem 269:22347-22357.
- Willis WD, Jr., Coggeshall RE (2004) Sensory Mechanisms of the Spinal Cord. New York: Springer.
- Wood JN, Winter J, James IF, Rang HP, Yeats J, Bevan S (1988) Capsaicin-induced ion fluxes in dorsal root ganglion cells in culture. J Neurosci 8:3208-3220.
- Wu Y, Wang WX (2011) Accumulation, subcellular distribution and toxicity of inorganic mercury and methylmercury in marine phytoplankton. Environ Pollut 159:3097-3105.
- Xu SZ, Zeng B, Daskoulidou N, Chen GL, Atkin SL, Lukhele B (2012) Activation of TRPC cationic channels by mercurial compounds confers the cytotoxicity of mercury exposure. Toxicol Sci 125:56-68.
- Yamamoto S, Wajima T, Hara Y, Nishida M, Mori Y (2007) Transient receptor potential channels in Alzheimer's disease. Biochim Biophys Acta 1772:958-967.
- Yan CH, Atchison WD (1996) Characterization of interaction of methylmercury with Ca<sup>2+</sup> channels of rat cerebellar synaptosomes. The Toxicologist 30:187.
- Yang J, Ellinor PT, Sather WA, Zhang JF, Tsien RW (1993) Molecular determinants of Ca<sup>2+</sup> selectivity and ion permeation in L-type Ca<sup>2+</sup> channels. Nature 366:158-161.
- Yip RK, Chang LW (1981) Vulnerability of dorsal root neurons and fibers toward methylmercury toxicity: a morphological evaluation. Environ Res 26:152-167.
- Yip RK, Riley DA (1987) Effects of methylmercury on the motor and sensory innervation of the rat extensor digitorum longus muscle. Environ Res 43:85-96.
- Yokoyama T, Ohbuchi T, Saito H, Sudo Y, Fujihara H, Minami K, Nagamoto T, Uezono Y, Ueta Y (2011) Allyl isothiocyanates and cinnamaldehyde potentiate miniature excitatory postsynaptic inputs in the supraoptic nucleus in rats. Eur J Pharmacol 655:31-37.

- Yuan Y, Atchison WD (2003) Methylmercury differentially affects GABA<sub>A</sub> receptor-mediated spontaneous IPSCs in Purkinje and granule cells of rat cerebellar slices. J Physiol (Lond) 550:191-204.
- Yuan Y, Atchison WD (2005) Methylmercury induces a spontaneous, transient slow inward chloride current in Purkinje cells of rat cerebellar slices. J Pharmacol Exp Ther 313:751-764.
- Yuan Y, Atchison WD (2007) Methylmercury-induced increase of intracellular Ca<sup>2+</sup> increases spontaneous synaptic current frequency in rat cerebellar slices. Mol Pharmacol 71:1109-1121.
- Yuan Y, Otero-Montañez JKL, Yao A, Herden CJ, Sirois JE, Atchison WD (2005) Inwardly rectifying and voltage-gated outward potassium channels exhibit low sensitivity to methylmercury. Neurotoxicology 26:439-454.
- Zaytas V, Samad A, Minofar B, Roelofs KE, Stockner T, Ettrich R (2013) Regulation of the transient receptor potential channel TRPA1 by its N-terminal ankyrin repeat domain. J Mol Model 19:4689-4700.
- Zhu W, Oxford GS (2011) Differential gene expression of neonatal and adult DRG neurons correlates with the differential sensitization of TRPV1 responses to nerve growth factor. Neurosci Lett 500:192-196.
- Zigmond MJ, Bloom FE, Landis SC, Roberts JL, Squire LR (1999) Fundamental Neuroscience. Cambridge, MA: Academic Press.